Polysaccharide Nanovesicles for Combination and Targeted Drug Delivery in Cancer Cells

A THESIS

SUBMITTED IN PARTIAL FULFILMENT OF THE REQUIREMENTS

OF THE DEGREE OF

DOCTOR OF PHILOSOPHY

BY

Nilesh Umakantrao Deshpande

Reg No: 20133263

DEPARTMENT OF CHEMISTRY

INDIAN INSTITUTE OF SCIENCE EDUCATION AND

RESEARCH PUNE – 411 008

October 2018

Dedicated to

My Parents

भारतीय विज्ञान शिक्षा एवं अनुसंधान संस्थान पुणे
INDIAN INSTITUTE OF SCIENCE EDUCATION AND RESEARCH PUNE
(An Autonomous Institution of Ministry of Human Resource Development, Govt. of India)
Dr. Homi Bhabha Road, Pune - 411 008.

Prof. Manickam Jayakannan
Department of Chemistry

CERTIFICATE

Certified that the work incorporated in the thesis entitled ***"Polysaccharide Nanovesicles for Combination and Targeted Drug Delivery in Cancer Cells"*** submitted by **Mr. Nilesh Umakantrao Deshpande** was carried out by the candidate under my supervision. The work presented here or any part of it has not been included in any other thesis submitted previous for the award of any degree or diploma from any other University or Institution

Date: 24th October 2018
Pune, Maharashtra, India

Professor M. Jayakannan
(Thesis Supervisor)
24/10/2018.

DECLARATION

I declare that this written submission represents my ideas in my own words and where others' ideas have been included; I have adequately cited and referenced the original sources. I also declare that I have adhered to all principles of scientific honesty and integrity and have not misrepresented or fabricated or falsified any idea/data/fact/source in my submission. I understand that violation of the above will be cause for disciplinary action by the institute and can also evoke penal action from the sources which have thus not been properly cited or from whom proper permission has not been taken when needed.

Date: 24th October 2018

Pune (MH) India

Deshpande Nilesh Umakantrao

Roll No: 20133263

ACKNOWLEDGEMENTS

I would like to take this opportunity to thank all the people who helped me during my PhD journey. First of all I wish to thank my thesis supervisor **Prof. M. Jayakannan**, for his excellent guidance, enthusiastic encouragement, and all kind of help during my PHD tenure. His constructive criticism and valuable suggestions helped me to build excellent scientific contribution during past five years. It had been always a fruitful discussion with him which gave me a liberty to plan and execute my ideas in research without any pressure. It's been a wonderful experience to work with such an energetic person.

I am very much thankful to **Dr. Asha S. K.** for her constant support and for extending research facilities in her laboratory. I would like to thank **Dr. Nagaraj Balasubramanian (NB)** for valuable scientific discussion and for allowing me to work in his lab. I specially thank to Siddhi Inchanalkar for providing me experimental hand on training for tissue culture protocols and for her time to time help. I would also like to thank **Dr. Sandanaraj Britto** and **Dr. Shanmuganathan Kadhiravan** for being my research advisory committee members and providing me valuable suggestions during the meetings. I would like to express my sincere thanks to **Prof. K.N. Ganesh**, Former Director, IISER-Pune and **Prof. Jayant Udgaonkar** Director IISER-Pune for providing world class research facility at IISER Pune. I would like to thank all the faculty members in the department of chemistry, IISER Pune for interactive scientific discussions.

Special thanks to my former lab members Dr.Smita, Dr.Pramod, Dr.Anantharaj, Dr. Bapurao, Dr.Rajendra, Dr.Narasimha for their excellent guidance and cooperation which made my life memorable at IISER, Pune. I would also like to thank former MS students Vikas, Thameez, Maitreyee, Khushboo, Abhishek, Anu and sharafu. I would like to take this opportunity to extend my great appreciation to my current lab members Dr. Sonashree, Bhagyashree, Mehak, Dheeraj, Ruma, Mishika, Mohammed Khuddus, Utreshwar, Pranav, Rasika, Sharada, carrroline for keeping healthy environment in the lab and for their valuable scientific discussions. I take this opportunity to say my heartfelt thanks to Sonashree and Mehak for their help in bioimaging studies.

I would like to thank all instruments technicians of IISER Pune for their suppo0rt: Deepali (NMR), Swati (MALDI), Megha (AFM), Anil, Yatish (FE-SEM), I thank National Chemical Laboratory (NCL) Pune for HR TEM and SLS facilities. Special thanks to Nitin and Mahesh for their valuable support.

I would like to thanks all my friends who have been always there in all my up and downs. I extend my sincere appreciation to Dr. Nagesh Kolhe, Dr. Chinmay Nardele, Dr. Pradip Pachfule, Dr. Shekhar Shinde, Dr.Nagesh Khupase, Dr. Sandip Agalave, Dr. Arun Nikam, Dr. Shrikant Khake, Satej Deshmukh, Shahaji Gaikwad, Durgaprasand Shinde, Pravin Shinde, Rahul Jagtap, Rameshwar Swami, Nilesh Mote, Mahendra Wagh, Ravi Swami, Bhagyashree Gadgil, Suwarna, Sheetal, Megha,Yogesh, Vijay, Manik, Satej Dharmapurikar, Balasaheb Jawale, Aslam Shaikh and there are so many... I would like to acknowledge all my IISER friends, batchmates, Chemphilic team members.

I would also like to thank my brother sandip for his constant support and help. Also I would like to take this opportunity to thank all my childhood friends Avinash, Prashant, Shrikant, Pravin, Ravi, Avinsh chakrawar, Vinayak, Yogesh, Swaraj.....

Finally I would like to thank my family members (especially Bhakti) for their extensive support and blessings.

Nilesh Umakantrao Deshpande

Synopsis

Design and development of polymer drug delivery system is emerging as an important area of research to target specific organ or host location in the cancer treatment. Among the various challenges, delivering multiple anticancer drugs based on single polymer nano-carrier is particularly emerging as challenging task to enhance the tumor resistance and enhance drug therapeutic efficacies in cancer cells. Polymer vesicles are important classes of nano-carriers for drug delivery applications due to their unique ability to delivery both water soluble and water insoluble drugs from single nano-platform. The present thesis work is aimed to make new classes of enzyme and GSH-responsive polysaccharide (dextran) nano-vesicles using renewable resource amphiphiles and employ the vesicles successfully as nanocarriers to cancer cells. The capabilities of polysaccharide nano-vesicles were demonstrated for the delivery of triple-drug cocktail and accomplishing synergistic effect, targeted delivery to cancer cells, and also delivery Aurora kinase A inhibitor to study the anchorage independent growth in breast cancer cells. Additionally, fluorescent dextran vesicles were also made by chemically conjugating tetraphenylethene (TPE) which is an aggregation induced emission (AIE) probe. The fluorescent vesicles were employed as *Turn-On* bioprobes as well as colour-tuneable fluorescence resonance energy transfer (FRET) probes to study the real-time drug release and bio-imaging in cancer cells. The thesis is divided into five chapters and their details are as follows:

Chapter 1: The introduction chapter gives brief account of polymer vesicles (or polymersomes) in the drug delivery applications, polymer design aspects of making vesicular nano-assemblies, stimuli-responsive deliveries of drugs/genes in cancer treatment, polysaccharide and their vesicular assemblies, and finally put forward the concepts for the aim of this theses work.

Chapter 2: New carboxylic functionalized dextran vesicles were designed and developed and employ them triple drug delivery systems for cisplatin, doxorubicin (DOX) and camptothecin. The role of the GSH detoxification of Pt-drugs, antagonism versus synergistic delivery is discussed in detail.

Chapter 3: GSH-responsive and biotin-tagged dextrin vesicles were developed as receptor-mediated endocytosis delivery of DOX to cancer cells. Time dependent cellular

uptake studies by confocal and flow cytometry analyses were carried out to demonstrate the targeted delivery approach.

Chapter 4: Fluorescent-tagged polysaccharide vesicles were tailor-made using tetraphenylethene (TPE) as AIE probe. DOX loaded TPE-vesicles were constructed as intracellular turn-off to Turn-On probe for real-time monitoring of DOX release at the cellular level. FRET probe was constructed between TPE-vesicles and fluorophores such as Rhodeamine-B, Nile red and Rose Bengal as efficient bio-imaging tools.

Chapter 5: Polysaccharide nanovesicles were demonstrated as very good platform for delivering Aurora Kinase inhibiting water insoluble drug MLN 8237. Detail biochemical analysis was done in collaboration work to demonstrate the proof of concept in 3D breast cancer cell model.

In chapter 2, new cisplatin-stitched polysaccharide vesicular nano-carrier is developed for combination therapy of three clinical important antagonistic drugs together to accomplish synergistic cancer therapy in breast cancer treatment. Carboxylic functionalized dextran was tailor-made for the chemical conjugation of cisplatin and renewable hydrophobic unit was anchored in the backbone to inter-digitize the chains to self-assemble as cisplatin-stitched polysaccharide nanovesicles. Water soluble DNA-intercalating drug doxorubicin.HCl (DOX) and water insoluble topoisomerase type I inhibitor drug camptothecin (CPT) were encapsulated in these vesicles to produce dual or triple drug loaded vesicular nano-carrier. This unique cisplatin, DOX and CPT triple drugs loaded dextran vesicles were stable in aqueous medium and the vesicular geometry acted as a shield for Pt-polymer drug conjugate against glutathione (GSH) detoxification under physiological conditions. In vitro cytotoxicity studies revealed that free cisplatin was highly detoxified by the GSH in breast cancer cells whereas the enhanced stability of Pt-

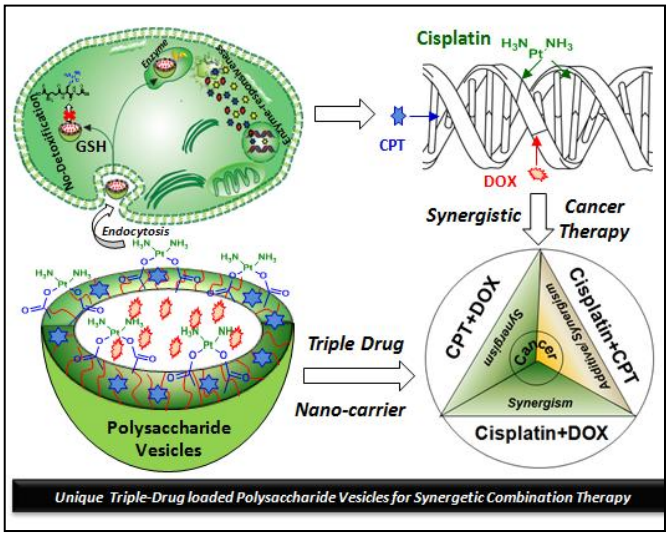

stitched dextran vesicle against GSH facilitated ~ 99 % cell killing in breast cancer cells. Combination therapy studies revealed that the free cisplatin, DOX, and CPT were found to be antagonistic to each others. Dual drug loaded vesicles exhibited synergistic cancer cell killing while delivering these antagonistic drugs from dextran vesicular platform. Remarkable synergistic cell killing was accomplished in cisplatin, DOX and CPT triple drug loaded vesicles at nanogram concentrations in breast cancer cells. The internalization of drugs and cellular uptake were confirmed by confocal microscope and flow cytometry analysis. The drugs were taken by the cancer cells in large amounts while delivering them from dextran vesicles compared to their free form.

In chapter 3, biotin-conjugated multi-stimuli-responsive polysaccharide vesicular nanocarriers are designed and developed, for the first time, to accomplish receptor-mediated endocytosis in cancer cells and to deliver anticancer drugs at the intracellular compartments. For this purpose, a new renewable hydrophobic unit was custom designed with redox-degradable disulphide and enzyme-biodegradable aliphatic ester chemical linkages and it was conjugated along with biotin on the dextran backbone. Avidin-HABA assay established the high affinity of biotin-tagged dextran vesicles towards membrane-receptors up to 25 nM concentration. Doxorubicin-hydrochloride (DOX.HCl) loaded dextran vesicles exhibited stable formulation in PBS and FBS. Redox-degradation by glutathione (GSH) showed 60 % drug release whereas lysosomal esterase enzyme enabled > 98 % drug release in 12 h. Confocal microscope and flow cytometry assisted time-dependent cellular uptake studies revealed that the biotin-receptor over expressed cervical cancer cells (HeLa) exhibited larger drug accumulation through receptor-assisted endocytosis process. This process enabled the delivery of higher amount of DOX and significantly enhanced the killing in cancer cells (HeLa) compared to wild-type mouse embryonic

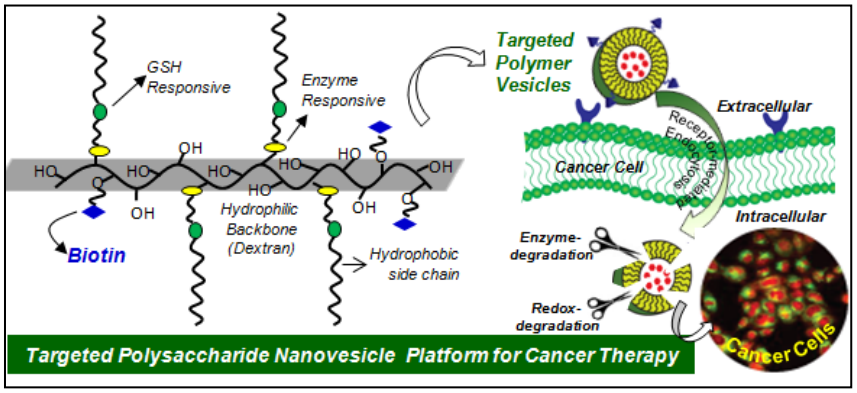

fibroblast cells (WT-MEF, normal cells). Control experiments such as biotin pre-treatment in cancer cells and energy-suppressed cellular uptake at 4°C further supported the occurrence of receptor-mediated endocytosis by the biotin-tagged polymer vesicles.

In chapter 4, enzyme responsive fluorescent polysaccharide vesicle were designed and developed as "Turn ON" probe and for bio-imaging purpose in cancer cells. To do so, a polysaccharide dextran backbone was decorated with a special aggregation induced emissive (AIE) fluorophore tetraphenylethene (TPE) along with vesicular director hydrophobic source pentadecyl phenol (PDP). These dextran-PDP-TPE derivatives are nonfluorescent in nature when dissolved in organic solvents where as gives blue colour emission in aqueous medium. These derivatives when dispers ed in water, produces vesicular structures which are subsequently used encapsulation of different water soluble and water insoluble drug and dye molecules. When these vesicles are loaded with doxorubicin drug molecule, owing to the spectral overlap and confined geometrical arrangement showed excellent fluorescence resonance energy transfer (FRET) phenomenon. This energy transfer from TPE (Donor) to the DOX molecules (acceptor) resulted in emission quenching due to the aggregation caused quenching (ACQ) effect shown by a doxorubicin. Hence, at physiological conditions these vesicles are in fluorescence off state whereas upon enzyme action, their fluorescence was regained thus, acting as a "Turn ON" probe for doxorubicin delivery to the cancer cells. This property of vesicles was studied in human breast cancer MCF 7 cells and their intracellular enzyme responsive was successfully demonstrated. Furthermore, these vesicles were loaded with three different red colure dyes namely rhodamin-B (RHB), Nile red (NR) and rose Bengal. There photophysical studies proved an efficient FRET phenomenon between TPE and these fluorophore. Time correlated single photon counting studies (TCSPC) proved the co-existence of these fluorophore within FRET distance. Intracellular FRET mechanism of these vesicles was studied in MCF 7 cells and proved that these vesicles can be used for bioimaging application.

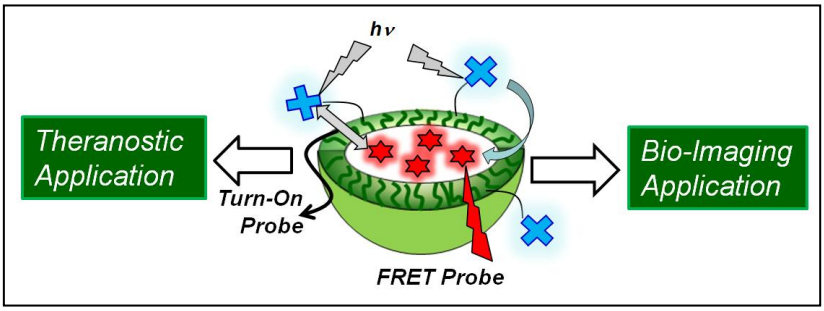

Further these designed vesicles were modified with acid functionality to produce blue luminescent acid functionalised polysaccharide vesicles. These vesicles were used for cisplatin (effective anticancer drug) conjugation and real time monitoring of drug release in MCF 7 cells. These fluorescent polysaccharide vesicles can be used as theranostics for drug delivery application in cancer cells.

In chapter 5, polymer nanovesicle platform is used for the first time to deliver and differentially inhibit Aurora kinase A (AURKA) in cancer cells. For this purpose, polysaccharide nanovesicles made from amphiphilic dextran were used as nanocarriers to successfully administer MLN8237 (V_{MLN}) in cancer cells in 2D and 3D microenvironments. These nanovesicles (<200nm) carry the drug in their intermembrane space with up to 85% of it released by the action of esterase enzyme(s). Lysotracker experiments reveal the polymer nanovesicles localize in the lysosomal compartment of the cell, where they are enzymatically targeted and MLN released in a controlled manner. Rhodamine-B fluorophore trapped in the nanovesicles hydrophilic core ($V_{MLN+RhB}$) allows us to visualize its uptake and localization in cells in a 2D and 3D microenvironment. In breast cancer, MCF-7 cells V_{MLN} inhibits AURKA significantly better than the free drug at low concentrations (0.02 to 0.04μM). This ensures that the drugs in VMLN at these concentrations can specifically inhibitup to 94% of endogenous AURKA without affecting AURKB. This targeting of AURKA causes the downstream differential inhibition of active RalA (but not RalB). Free MLN8237 at similar concentrations and conditions failed to affect RalA activation. V_{MLN} mediated inhibition of RalA, in turn, disrupts the anchorage-independent growth of MCF-7 cells supporting a role for the AURKA-RalA crosstalk in mediating the same. These studies not only identify the polysaccharide nanovesicle to be an improved way to efficiently deliver low

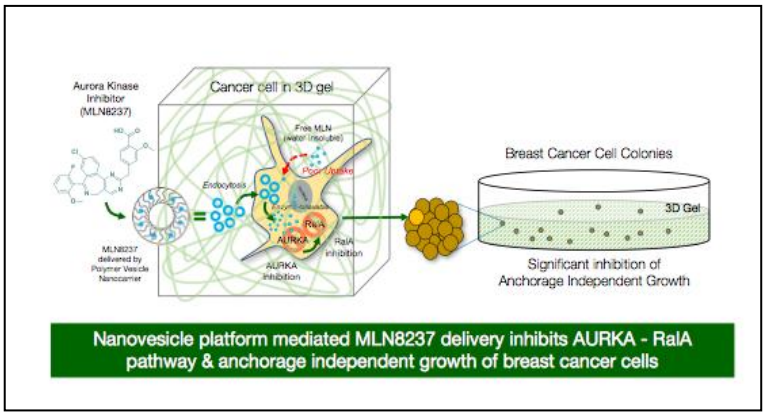

concentrations of MLN8237 to inhibit AURKA but in doing so also help reveal a role for AURKA and its crosstalk with RalA in anchorage-independent growth of MCF-7 cells.

The last chapter summarizes the thesis work and put forward the direction for future research. The new classes of polysaccharide nanovesicles designed and developed in this thesis are new entries as enzymatic-biodegradable and GSH-responsive nano-carriers in the literature; hence they would be expected to be very important for long-term application in the biomedical field. Further, the fluorescent-tagged polysaccharide vesicles are promising candidates for simultaneous delivery and direct tracking of drug and nano-carriers together the cancer cells. Thus, the work described in the thesis opens up opportunities in biomaterials arena for polymer vesicles, in general.

TABLE OF CONTENTS

Introduction

1.1 Introduction to Polymer Drug Delivery

Most of the drugs available till date exhibit poor aqueous solubility and bioavailability, thus hampering their therapeutic efficacy. For delivering such drug molecules, conventional drug delivery systems such as injection, ingestion, inhalation etc are commonly practiced in the medical field[1]Following their administration, these systems are often exposed to the several biological barriers such as sequestration by monophagocytes, renal clearance from the body, blood plasma stability, escape from endolysosomal compartment most importantly the drug efflux pumps[2,3]. Therefore to achieve better clinical results, increase in the dose frequency is commonly observed which leads to the excessive dumping of drug molecules inside the body[4,5]. Together these factors induce undesirable side effects and reduce the overall performance of the conventional drug delivery systems[6]. To overcome these issues, development of smart drug delivery systems which could achieve better therapeutic efficacy is an urgent need of biomedical field. Thus, the use of polymers in crafting the drug delivery vehicle has been the topic of interest from several decades. Polymers, being macromolecular architectures can undergo self organization to produce variety of self assembled structures which provides an opportunity for drug encapsulation and their subsequent delivery at the intracellular environment[7,8]. These drug encapsulated polymeric assemblies can prevent early renal clearance of drug molecules and protects them from undergoing the unwanted side reactions in the biological system[9]. This could assist the longer retention of drug delivery vectors in systematic circulation and facilitates the slow and controlled released of the drug molecules. A rational model for use of polymers in designing drug delivery vectors was first proposed by Helmut Ringsdorf in 1975, which is based on the use of biocompatible polymer backbone and other three major parameters as (1) use of solubalising agent which imparts water solubility to polymer backbone, (2) Conjugation of drug molecule on polymer backbone and (3) use of targeting agent which helps in achieving site specific delivery of the drug molecules[10]. The schematic illustration of this mode is shown in figure 1.1.

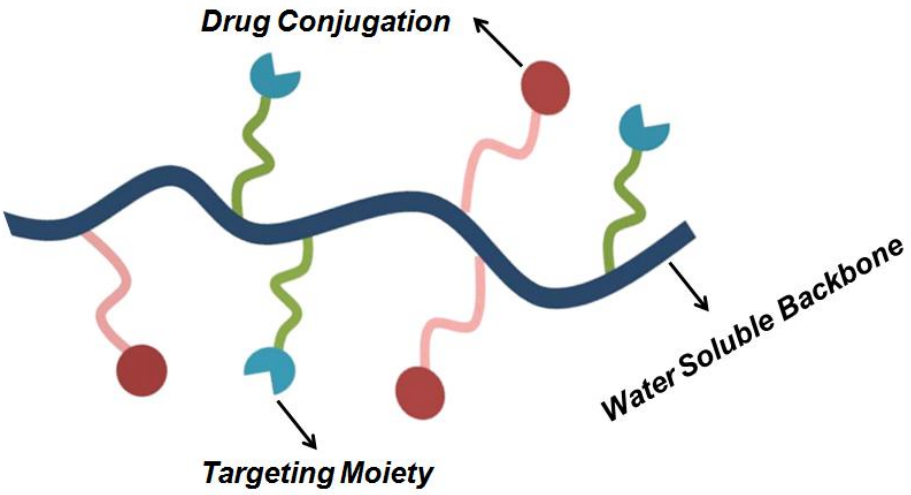

Figure 1.1: *Ringsdorf model for polymer drug delivery approach. Adapted from Pang et al. J. Control. Rel.2016, 222, 116-129.*

This Ringsdorf model formed the basis for growth of polymeric drug delivery systems and enlightens the path for making the ideal drug delivery system. Generally the polymers are high molecular weight compounds and incorporating enough hydrophilic and hydrophobic characters in them can lead to the aggregation of these polymers into self assembled structures[11]. These self assembled cargoes are of potential interest owing to their better stability in the biological systems and ability for transportation of therapeutic agents across the cell membrane. Due to slow degradation or disassembly of the polymeric systems, the drug release rate can also be tune to achieve slow and controlled release. According to Ringsdorf model, polymers can provide opportunity for the drug conjugation using variety chemical linkages which are vulnerable to cleave in the presence of certain biological stimuli related with the diseased condition[10]. For effective polymer-drug conjugate system, polymer should be non immunogenic and be able to carry the adequate amount of drug in relation to its potency. Hence fluorescent polymer drug conjugates would be the ideal candidates to track and monitor the real time intracellular release and imaging of the drug molecules. Conjugation of targeting ligand on the polymer backbone can help in active targeting by recognition of drug delivery system at the diseased regions. This will avoid the surplus toxicity caused by the drug molecules in the healthy tissues. Based on above mentioned design principle, number of polymeric drug delivery vectors has been reported and huge amount of development have

been achieved till date, still the success in terms of transformation of these vectors to the clinical trials (1 out of 1000 enters the clinical trial phase) has been limited and provides scope of development in the coming future[12]. The practical problem faced by any drug delivery vehicles in the biological system is to differentiate between the diseased region and a healthy region. This kind of problems are the major limitations in the development of drug delivery systems for a disease like cancer where the early diagnosis and differentiation between normal and tumor tissue is challenging task till date[13]. Cancer is a devastating disease and one of the major causes of increased mortality from last few decades. This disease is Charecterized by uncontrolled growth of cells which leads to the formation of malignant tumors. These tumors can be easily metastasize to the different parts of the body and demands more oxygen and energy[5-7]. To fulfil ever increasing demand of oxygen and micronutrients, the tumors are Charecterized with the leaky vasculature. This differ the tumor tissue from the normal tissues and using this property of the tumor tissues most of the drug delivery vectors known till date accumulates at the tumor site and this effect is called as enhanced permeability. Moreover the impaired lymphatic drainage system of the cancer tissues helps in retention of the foreign materials at the tumor site. Together this is called as enhanced permeability and retention effect (EPR Effect) which was first discovered by Matsumura and Maeda in 1986. This EPR effect is the only known pathway till date which is most widely used roadmap to passively target the tumor tissues[14,15]. This effect facilitates the accumulation of nanocarriers at the tumor sites. The schematic illustration of EPR effect is shown in figure 1.2, which depicts properties linked with healthy tissue and tumor tissues[16]. The leaky vasculature of the tumors works in a window of 5 - 200 nm size which allows the polymeric self assemble structure to permeate in the tumor tissue and facilitates their accumulation by impaired drainage system[15]. Thus, the formation of the different size and shape of the polymeric structures is crucial step in achieving enhanced drug accumulation at site of action. Hence it is important to have a self assembles structures which have sizes in the range of 1-200 nm which could pass these vasculature barriers and reach the site of action based on the Ringsdorf vision and Maeda's EPR principle, a number of polymeric drug conjugates have been reported, some of them have showed

promising *invitro* results while some of them could make it to clinical trials but their biocompatibility and inherent toxicity prevents them from the further development[12-13].

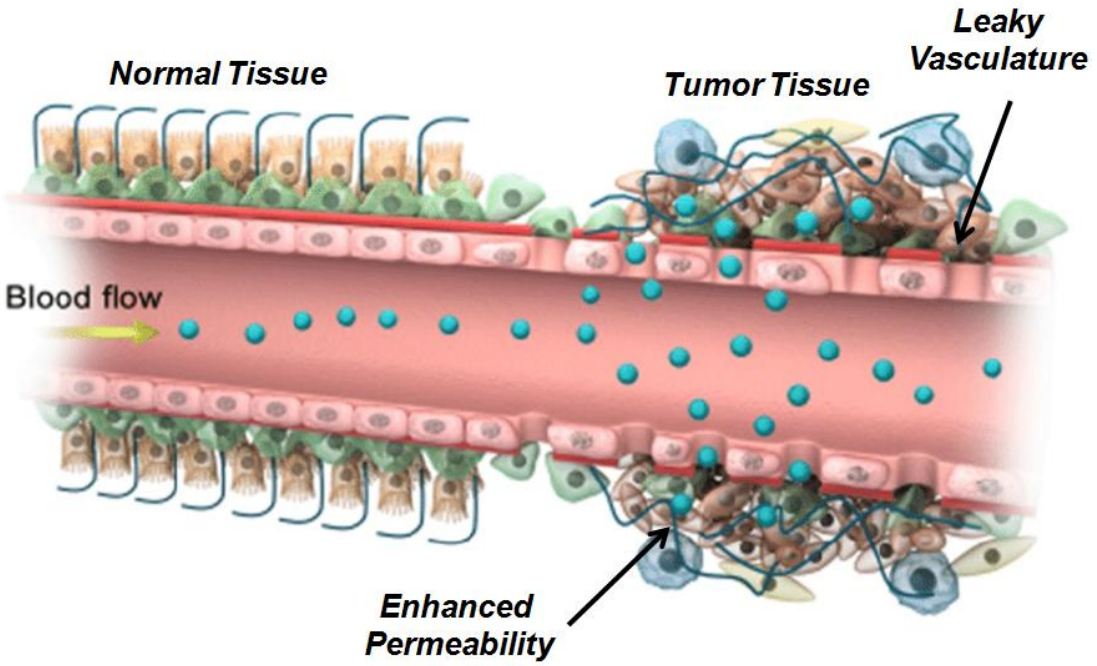

Figure 1.2: *Schematic illustration of enhanced permeability and retention effect which helps in accumulation of drug delivery vectors at tumor site. Adopted from Abdalla et al. Theranostics 2018, 8, 533-549.*

Based on the above discussion it has been observed that the polymers have played a potential role in the growth of drug delivery technology and the detailed explanation is given hereafter in this chapter. The different types of polymeric nanocarriers used for drug delivery application are given in figure 1.3. Fundamentally the micelles are considered to be the nanoaggregates of the surfactant molecules or any amphiphilic molecules which self assemble themselves in aqueous medium to form a thermodynamically stable morphology. These structures possesses ability of solubalising the hydrophobic molecules by encapsulating them in the core of the micelles. As the micellar structures are small in size (in the range of 5-200 nm) they can protect the drug molecules from rapid renal clearance and mononuclear phagocytes allowing their prolong systematic circulation in biological medium. Since the micelles are made from amphiphilic polymers which have a hydrophilic and hydrophobic segment connected by a

chemical linkage, it is indeed easy to tune these linkages synthetically and make them susceptible to cleave in the intracellular conditions of the target tissues[12].

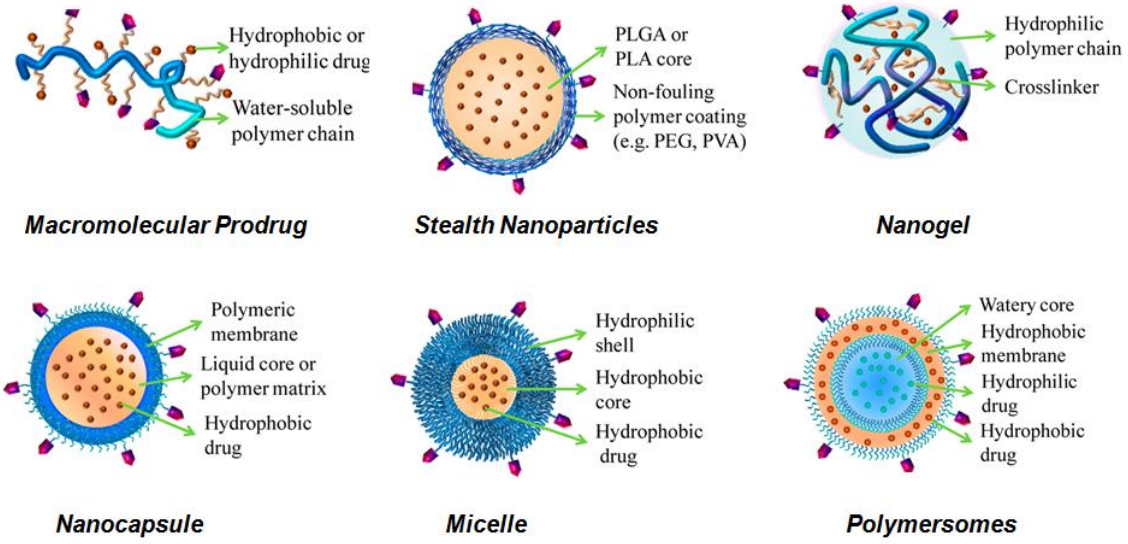

Figure 1.3: *Schematics of different types of polymeric drug delivery vectors used in biomedical field. Adopted from Zhong et al. Biomacromolecules 2014, 15, 1955-1969.*

This makes the micelles to disassemble and released the encapsulated entities at the site of action. The shape of the micelle does play an important role in sustaining the pressure exerted by the body fluid in the circulatory conditions and on their accumulation at the target site. It has been reported that spherical shape of the micelles helps in endocytosis and accumulation in the intracellular condition whereas the cylindrical or rod like shape tend move in the circulatory conditions without internalizing the cell membranes[17]. Hence it is desirable to make spherical shape micelles to have better accumulation at tumor site. Considering all these factors, different micelles have been made and reported in the literature and there has been a tremendous progress in the field from last few decades. This improvement has extended micellar nanocarriers such as Genexol[18], NK-105[19], DACH-Platin[20], Lipotecan[21] to the clinical trials amongst which Genexol is clinically approved in some of the countries. Despite the momentous progress in the field of micellar nanocarriers, the efforts to make a multiresponsive and multidrug carriers "smart micelle" is still under the process which may help in achieving the higher goals in this field. It is enviable to make micellar structure which has a multi responsiveness so as to achieve controlled and sequential delivery of the drug molecules. This sequential delivery of the therapeutics is of prime importance in case of diseased

conditions like cancer wherein due to molecular complexity and defense mechanism, drug molecules often fails to achieve the efficacy[22]. To achieve this goal numerous polymeric micelles were made using different polymers which includes poly L-lysine[23-27], polycaprolactone[28-32], polystyrene[33-37], polyaspartic acid[38-42], poly lactic acid[43-44], polylactic-co-glycolic[45-47], polyvinyl alcohol[48-52] and there are so many which includes the functionalized monomers. Most of these polymers forms the hydrophobic domain of the polymer and to bring in the hydrophilic character, a most extensively and regularly used polymer is polyethylene glycol (PEG) owing its special features[53]. So these amphiphilic polymers decorated with unique chemical linkages are used for encapsulation and delivery of the anticancer agents. Polyethylene glycol-b-polycaprolactone was made in similar way and the formed micelles were used for the delivery doxorubicin to the cancer cells[54]. The chemical structure and schematic illustration of these micelles is showed in figure 1.4. The schematic illustration showed a distinct hydrophilic and hydrophobic segments and how they have self assembled in aqueous medium taking a hydrophobic drug molecule in the core of the micelles. These block copolymers were inbuilt with the aliphatic ester linkages and are degradable in the presence of intracellular enzymes.

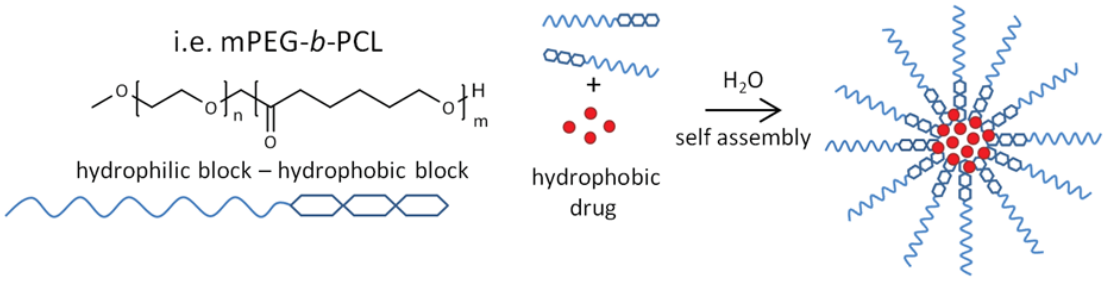

Figure 1.4: *Chemical structure PEG-b-PCL polymer and schematic illustration explaining their aqueous self assembly and drug encapsulation in micelles. Adopted from Larson et al. Chem. Mater. 2012, 24, 840-853.*

Jayakannan and coworkers synthesized a new carboxylic acid functionalized caprolactones monomer[55]. This monomer was used for synthesis of enzyme responsive polymeric micelles by structurally engineering the amide and ester side chain substituted on block copolymer of polyethylene glycol and caprolactone (PEG-b-PCL). These polymeric micelles were used for delivery of different anticancer drug molecules. When

invitro release kinetics were carried out in the presence of esterase enzyme, ester side chain substituted block copolymers exhibited fast release where as the amide substituted copolymers showed a slow and controlled release proving the effect of hydrogen bonding on the release kinetics of the drug molecules. The cellular uptake and intracellular drug release of these different drug loaded micelles were proved in cervical cancer cell lines. The chemical structure and schematic illustration is showed in figure 1.5, where the self assembly and enzymatic cleavage of diblock were depicted. It is very essential to trace the intracellular biodistributon of the nanocarriers in understanding the stability of the system, to monitor the real time drug release kinetics, to understand the degradation and clearance of the polymer following the drug delivery. Recently, a new methodology called theranostics, where imaging and drug delivery can be done simultaneously has emerged and routinely used in the biomedical field. This system involves the conjugation of polymeric backbone with fluorescent molecules and makes "visible nanocarriers" for drug delivery applications. Recently, Zhang et al. reported the fluorescent micelles using a special aggregation induced emission (AIE) probe tetraphenylethene (TPE) conjugated to PEG chain[56]. These micelles showed higher degree of doxorubicin encapsulation with efficient fluorescence resonance energy transfer (FRET), and therefore they are in fluorescence off state at physiological conditions.

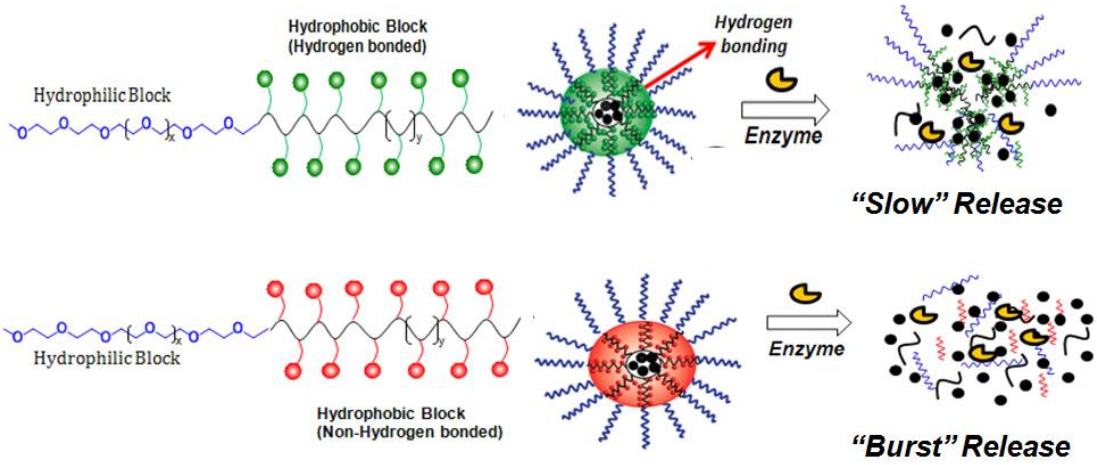

Figure 1.5: *Schematic illustration of self assembly of PEG-b-PCL polymers, subsequent drug encapsulation and their enzymatic clevage. Adopted from Bapurao et al. ACS Biomater. Sci. Eng., 2016, 2, 1926-1941.*

Upon the intracellular disassembly of these micelles, their emission property is recovered and facilitates the bio-imaging and intracellular delivery of the doxorubicin drug to the tumor tissue. The proof of concept for "Turn On" probe and delivery of doxorubicin was successfully showed in human breast cancer MCF 7 cells. The diagram explaining the self assembly and intracellular drug release was showed in figure 1.6. There are few anticancer drugs which are non-luminescent in nature and it is very difficult to track their intracellular biodistributon and release kinetics. Cisplatin, a most effective and clinically practiced anticancer drug is one amongst them and its nonfluorescent nature limits its clinical application due to inability in visualizing the drug biodistributon which leads to severe side effects. Hence in an attempt to make fluorescent nanocarriers for cisplatin, Liu and co-workers have come up with platinum (IV) conjugates (prodrug of cisplatin) modified with a AIE fluorescent probe tetraphenylsilane (TPS) for tracking biodistributon and a targeting moiety cRGD peptide for receptor mediated accumulation of these drug at the target tissues[57].

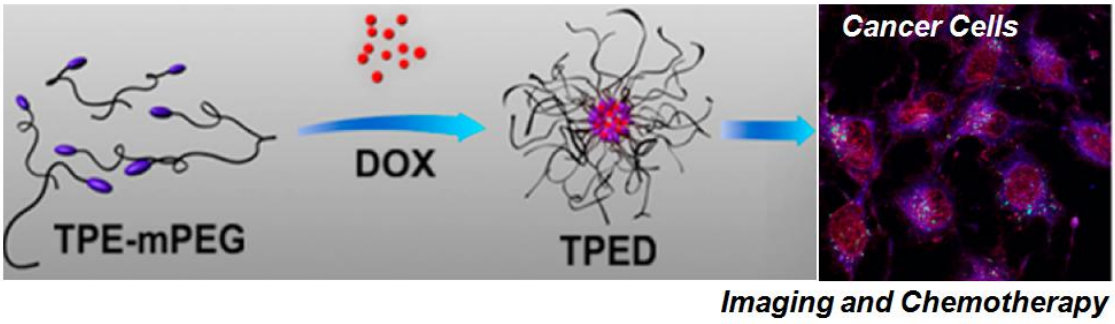

Figure 1.6: *A diagram explaining the self assembly of PEG-TPE conjugates encapsulated with doxorubicin and their intracellular drug release in MCF 7 cells. Adopted from Zhang et al. ACS Appl. Mater. Interfaces. 2014, 6, 5212-5220*

This nanocarriers were nonfluorescent at physiological conditions due to very good aqueous solubility of the fluorophore, however becomes fluorescent by the action of apoptotic caspase enzymes. This activation of apoptotic caspase enzymes was triggered by reduction of Pt (IV) conjugate to its active form Pt (II) by the ascorbic acid and this pt (II) form induces the apoptosis and activates the caspase 3 enzymes. This concept of receptor mediated targeting and real time imaging was proven in U-87 MG cells and showed a very good *invitro* cytotoxic effects due to which are better than free cisplatin

which induces severe side effects along with cell ablation in cancer cells. The structural and schematic representation of these nanocarriers is showed in figure 1.7.

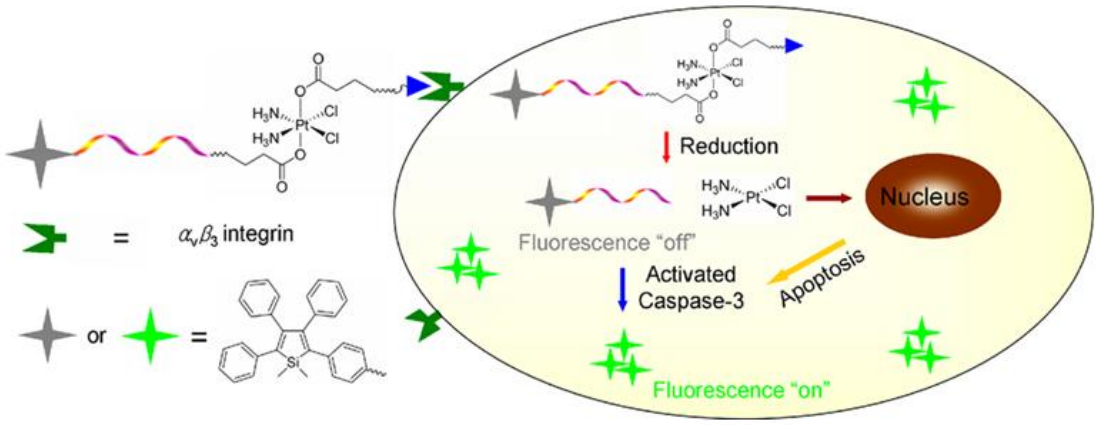

Figure 1.7: *Schematic representation of Pt (IV) prodrug modified with fluorescent probe TPS and targeting moiety cRGD peptide and their subsequent cellular internalization and fluorescence turn-on in U87-MG cells. Adopted from Yuan et al. J. Am. Chem. Soc., 2014, 136, 2546-2554.*

The above mentioned are some of the examples of polymeric micelles systems used for drug delivery application. Nonetheless these are not the only examples for polymeric micellar systems, the field has made enormous progress and the attempts to make efficient drug delivery micelles is still under process. Amongst all, self assembled structures showed in figure 1.3, vesicles being Charecterized with the hydrophobic layer and hydrophilic core are capable delivering multiple drugs together from single nanocarriers where as the micelles having hydrophobic core could deliver only water insoluble drugs. Most of the chemotherapeutic agents or molecules are water soluble and needs to be transferred across the cell membrane without hampering the activity of the drug. Hence vesicular nanocarriers are very important for transportation of such molecules across the cell membrane. There are some characteristic features by which vesicular morphology is preferred over the micellar structures. These features are discussed in table 1.0. One of the important advantage which vesicle hold is that, it can load water soluble and water insoluble drugs in the core and layer respectively and hence are very useful in drug delivery application[58].

Table 1: *Table shows polymeric self assembled structures and their features. Adopted from Grabole et al. Biomater. Sci. 2015,3, 25-40.*

Properties	***Micelle / Nanoparticles***	***Polymer Vesicles (Polymersomes)***
Morphology	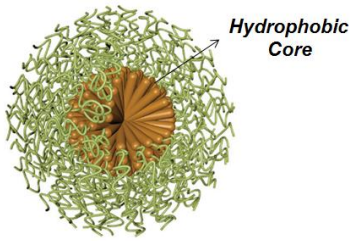	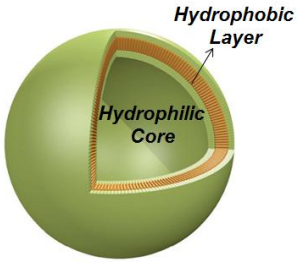
Size	10-100 nm	5 nm-500 nm
Feature	Hydrophobic core	Hydrophobic layer and Hydrophilic core
Drug/Dye Encapsulation	Stabilizes only hydrophobic drugs.	Stabilizes hydrophilic drugs in core and hydrophobic drugs in Layer. Dual drug loading carriers
Degradation	Difficult in biological medium	Relatively easy

1.2 Polymeric Vesicles

A Polymer vesicle, owing to their unique structural feature allows the encapsulation of hydrophilic and hydrophobic anticancer drug, proteins, genes etc[59]. Additionally these polymer vesicles can be structurally engineered with variety of functional groups for effective conjugation of the drugs, targeting ligands etc for enhanced accumulation of the pharmacologically active molecules. Discher and co-workers have proved that polymer vesicles have 10-fold higher thickness of the layer than the liposomes and due to higher mechanical strength they possess a very good stability needed for stable encapsulation[60,61]. The formation of the polymer vesicles is governed by several parameters and self assembly process. To understand the detailed mechanism of the polymer vesicle formation, it is important to understand the molecular self assembly of surfactants which has a vital role in the construction of artificial nanostructures used in the biomedical as well as industrial application. This process is governed by important parameters such as nature of the solvent, length of the hydrophilic and hydrophobic segment, concentration, volume of the surfactant etc and based on these conditions surfactants can form different type of self assemble structures[17,22].

Similarly the self assembly of polymeric structures was also assessed by certain polymeric properties such as molecular weight of the polymer, distribution of the polymer chains (broad and narrow), apmhiphilicity, polydispersity etc. This distinctiveness directs polymers to self assemble in variety of nanostructures such as micelles, vesicles, cylindrical micelles, inverted micelles etc[17]. There are different types of polymers generally used for the biomedical and industrial application which includes homopolymers, copolymers, star shaped polymers and these are typically made by using different polymerization techniques. The size distribution of the polymer chains can greatly vary by the technique they have made. Apart from these, the polymers also can be modified using post polymerization techniques and these cases their distribution can vary upon the degree of grafting or substitution. The variation in distribution of polymers can affect the self organization of the polymer chains undergoing the self assembly process. In general it has been observed that, the polymer with narrow distribution tends to form a uniform self assemble structures than the polymers which has a broad distribution of the

chains. Moreover the block length or the length of hydrophilic or hydrophobic domains in the polymers also imparts huge effect on the self assembly process of the polymers. In case of the graft copolymers and post polymer modifications, the degree of grafting and substitution also showed a distinct effect on the self organization of the polymers. It has also been observed that changing the block length of the same molecular weight polymers can produce different types of structures depending upon the volume fraction covered by block of a polymer[17]. Hence to determine the morphology (self assembly) of the surfactants, a critical packing parameter (CPP) can be calculated using an equation, p = V/A × L, where V denotes the volume of hydrophobic segment, A represents the area of the polar head group of the surfactant and Lrepresents the length of the hydrophobic tail. This equation was derived by Israelachvili and coworkers and showed that changing any of the above mentioned parameter can induce the change in the self assembly of the surfactant molecules[62]. The amphiphilic polymers can be considered as the mimics of surfactant molecules and can follow the similar equation to determine their morphology.

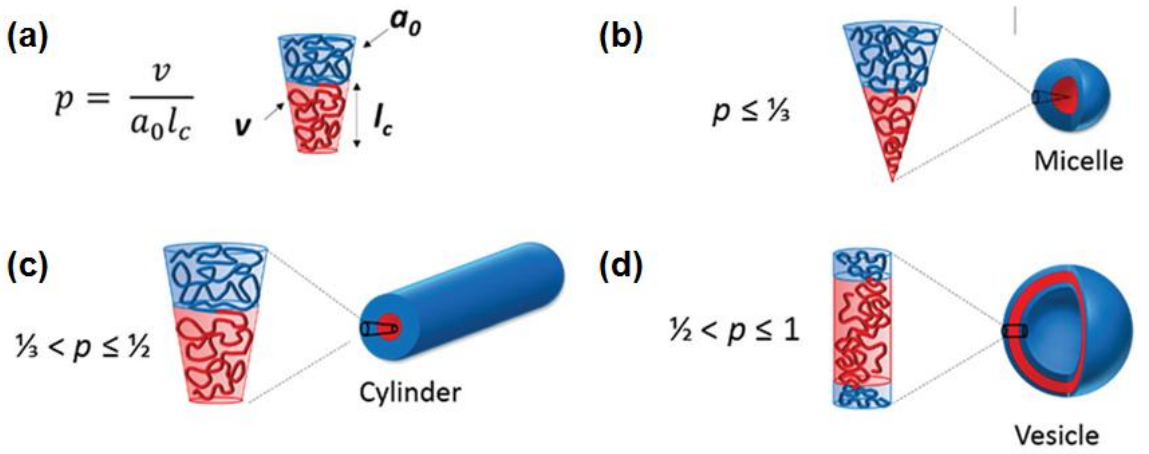

Figure 1.8: *Equation for critical packing parameter (a), Schematics showing the different types morphology obtained based on the critical packing parameter values (p) for micelles (b), cylindrical micelles (c) and vesicles (d). Adopted from the Doncom et al. Chem. Soc. Rev., 2017, 46, 4119-4134.*

One of the important points to be noted here is that, this process leads to the formation of thermodynamically stable conformation and hence this equation hold true for most of the cases in which the polymers have enough amphiphilic character and are dissolved in appropriate solvent. Based on the above equation, a spherical micelle morphology was observed for the p value p ≤ 1/3, cylindrical morphology was observed

for $1/3 < p \leq 1/2$ and vesicles were formed when $1/2 < p \leq 1$. A general observation was made and type of morphology it forms based on this values was shown in figure 1.8. Generally the formation of these structures is concentration dependent process and hence a minimum concentration is needed to form the self assembly and it is termed as critical aggregation concentration (CAC)[17]. In case of small molecule surfactants, usually the CAC values are very high and prevent their utility in biological application. On the other hand polymers which are high molecular weight structures, concentration needed for their self assembly lies in the micromolar range and hence can be good alternatives for small molecules surfactants. Each of the above mentioned morphologies have special features which can be explore for a variety of application. For instance the micellar morphologies are Charecterized by a hydrophobic core which is very good pocket for encapsulation of the hydrophobic drug molecules. Similarly the vesicles have a distinct hydrophobic layer and a hydrophilic core and provide the opportunity for encapsulation of both hydrophilic as well as hydrophobic molecules.

Recently Jayakannan and co-workers reported the mechanism of vesicles formation using diblock copolymer[63]. The formation of multivesicular bodies and unilamellar vesicles were proved by the experimental techniques such HRTEM, single crystal structure of small molecule and theoretical calculation of packing parameter. A very good correlation between the experimental results and theoretical calculations were observed. The diblock copolymer was made using a hydrophobic pentadecylphenol molecule and polyethylene glycol chain. This polymer self organizes into multivesicular bodies in aqueous medium and subsequently forms the small unilamellar vesicles. The mechanism by which this vesicular morphology was formed was discussed in detail to understand the self assembly of the polymeric structures in aqueous medium. Based on the theoretical calculations, the formation of the vesicles involves two consecutive steps as (i) the diblock copolymer with appropriate hydrophilic and hydrophobic character undergoes or rearranges themselves in water to produce disc like large diblock membrane having radius R_D and (ii) in order to reduce membrane elastic strain energy, these diblocks undergo closure to produce the large vesicles. The large vesicles often undergo shape change to produce energy minimized structures and produce vesicles or stomatocytes depending upon their inward or outward curvatures. These curvatures were

calculated using the packing parameters as discussed above. This report showed a classical example of vesicular morphology formation in case of diblock copolymers and established a very good correlation between experimental results and theoretical calculations. The schematics of detailed course of vesicle formation and the HRTEM images of the vesicles are given in figure 1.9. Formation of this kind of morphologies is a very crucial for drug delivery application since it allows the encapsulation of therapeutic agents and delivers them to the site of action. Hence molecular self assembly of the polymers extended their use in the drug delivery application and based on this, numerous polymer drug conjugates are being made and used for delivery of clinically important drug molecules[22]. To obtain the vesicular morphologies from the polymers, numerous polymeric structures were synthesized and optimized to balance the amphiphilicity in the polymer backbone. These different polymeric structures were discussed in detailed by Hu et al[64].

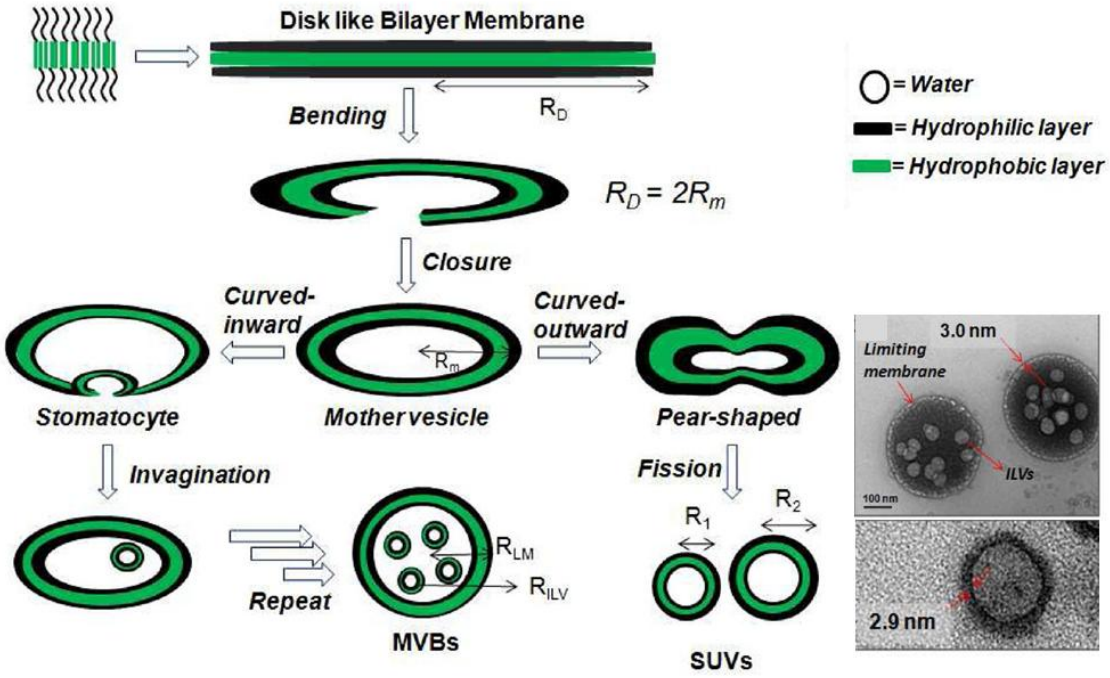

Figure 1.9: *Schematics of detailed course of vesicle e formation in case of diblock polymers and their subsequent correlation with HRTEM images. Adopted from smita et al. J. Phy. Chem. B 2012, 116, 9820-9831.*

In one such report, discher and co-workers reported the hydrolytic degradation of the block copolymers and showed the morphological transformation of the vesicles to

micelles depending upon the change in the length of the hydrophobic segment. This example clearly emphasizes the role of hydrophilic and hydrophobic segments on the self assembly of the polymeric structures[65]. This morphological transformation and ratio of hydrophobic segments was showed in figure 1.10. Apart from the polymer vesicles, liposome's are also a very good class of nanocarrier's frequently used in the drug delivery application. These are made from phospholipids and polyethylene glycols and finds suitable application in biomedical field[66]. These liposomes are easy make and can be prepared using hand held liposomal extruder as showed in figure 1.11. Based on this approach, liposomal formulation of doxorubicin (DOXIL)[67] and cisplatin (Lipoplatin)[68] have been made and regularly used in clinics for treatment of several cancers. Though these drug formulations are frequently used in the clinics, they have their own disadvantages and tend to show severe side effects. Moreover the liposome accumulates predominantly in the liver when given intravenous injection (see figure 1.12). This makes it difficult to distribute the drug in the affected region of the body[67,68]. When liposomes's are given by inhalation it mostly resides in the lungs and eliminates too early before the action of the drugs. These limitations associated with doxil shows adverse effect when used in the treatment[67].

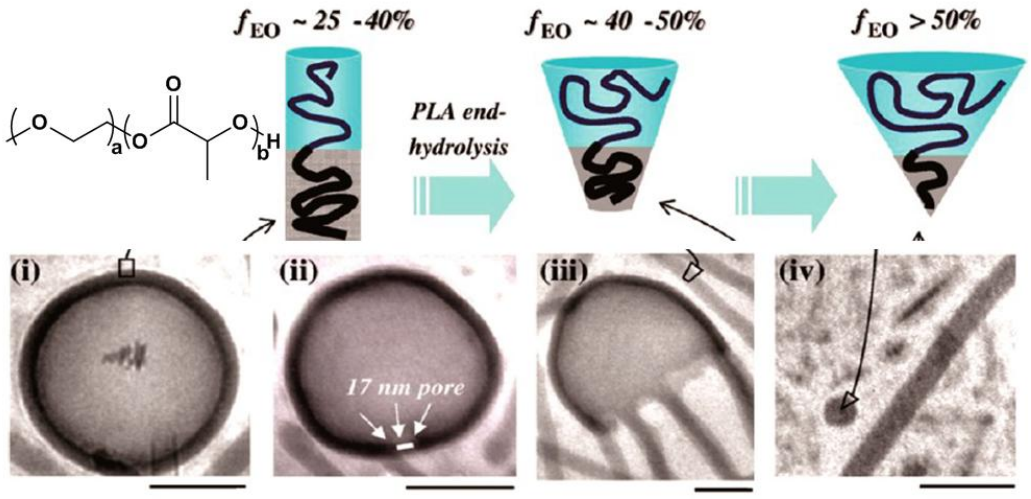

Figure 1.10: *Schematics of PEG−PLA-based polymersome self-assembly, degradation, and their Cryo-TEM images. Hydrolysis of PLA in the vesicle core triggers the growth of pores and conversion of vesicles into wormlike micelles and spheres. Adopted from Ahmad et al. J. Contrl. Rel. 2006, 116, 150-162.*

One more major limitation Doxil showed is the stability in the blood plasma. Doxil has very short half life in the plasma and it is about two hours which makes very difficult to achieve the therapeutic effects from the doxorubicin (see figure 1.12).

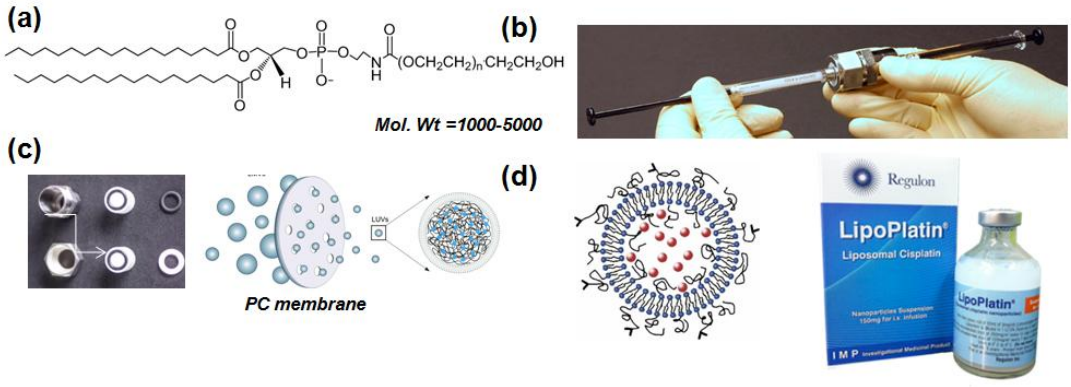

Figure 1.11: *Structure of PEG-phospholipid used for making liposomes (a), diagram of liposomal extruder (b), and mechanism of liposome formation (c), schematics and FDA approved liposomal formulations of cisplatin. Adopted from Gao et al. J. Mater. Chem. B 2013, 1, 6569-658.*

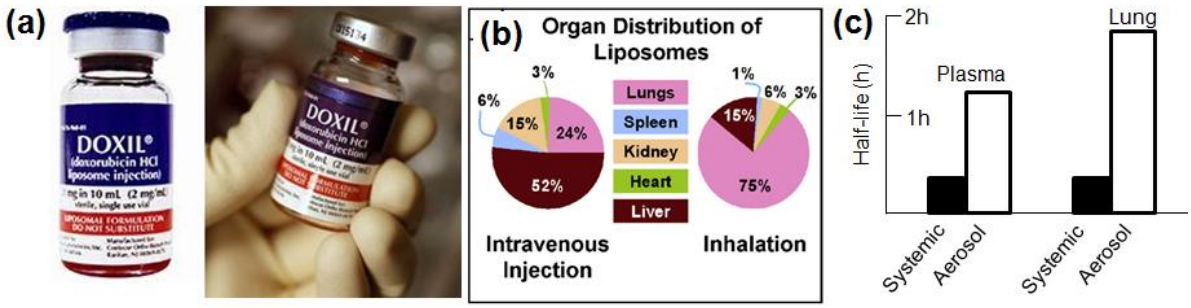

Figure 1.12: *FDA approved liposomal formulation of doxorubicin hydrochloride (a), diagram showing the biodistributon of liposome's in the body (b), and bar diagram depicting the half life of the Doxil in the blood plasma (c). Adopted from Barenholz et al. J. Contrl. Rel. 2012, 160, 117-134.*

With this detailed understanding, it has now been advisable to make nanocarriers which can deliver the multiple drugs at the cancer tissues by a new therapy called "combination therapy" which offers the means of delivering two or three drugs simultaneously from a single nanocarrier. This can greatly enhance the therapeutic efficacy by i) synergistic interaction of different drugs at intracellular environment and ii) by avoiding multidrug resistance associated with most of the tumors. To ensure the

synergistic interaction, selection of drugs which do not interfere with their mechanism of action and their release kinetics do play a vital role in combination therapy.

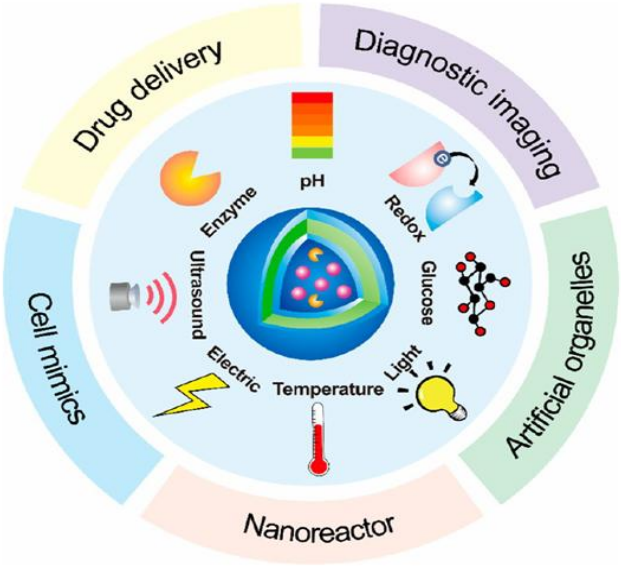

Figure 1.13: *Schematic illustration of different stimuli sensitive polymer vesicles or polymer vesicles and their application in the biomedical field. Adopted from Hu et al. Biomacrmolecules 2017, 18, 649-673.*

Thus, research in this area has made a significant progress and currently focuses towards the incorporation of different stimuli in the polymer vesicles which can be ruptured at tumor microenvironment. To date variety of polymer vesicles are reported which are sensitive to different internal and external stimuli such as pH, redox conditions, enzymatic activity, temperature (internal stimuli) etc and electric, magnetic field, ultrasound etc (external stimuli)[64]. The diagram given in figure 1.13 shows the classification of the polymer vesicles based on their stimuli and application in which they have been used.

1.3 Stimuli-Responsive Vesicles

Cellular uptake and subsequent degradation of the nanocarriers is a crucial step in a drug delivery application. Thus, it is very important for drug delivery vehicles to respond particular type of stimuli (intracellular or extracellular) to release the loaded cargoes. In case of cancer tissues, they are associated with certain characteristics which make them different from the normal tissues[22]. Using these special features, drug delivery systems can be designed with certain chemical linkages which are susceptible to cleave under intracellular conditions. For better understanding, schematics were drawn and showed in figure 1.14which explains cellular uptake and intracellular path which most of the nanocarriers follows upon their cellular internalisation. These nanocarriers upon cellular uptake, exposed to the different compartment of the cells such as early endosomes, late endosomes, lysosomes or they have to face the chemicals present in the intracellular matrix such as intracellular thiols etc. Each one of these compartment is associated with special features and hence can be used for the degradation of the nanoparticles or nanocarriers[69]. For instance, pH stimuli is one of the most extensively studied chemical linkage for the drug delivery application due to the presence of physiological pH gradient in the biological system. The pH at the tumor tissue was found to be slightly more acidic (6.5 - 7.0) compared to healthy tissue (pH = 7.2) Furthermore intracellular compartment of the cells such lysosomes and endosomes were also found to be acidic nature with pH ranging from (pH = 4.0 - 6.5). This disparity in pH at the tumor microenvironment and intracellular conditions permit the degradation of the pH responsive polymer vesicles in the biological milieu and making them potential modalities for drug delivery application. Another most widely used stimulus is the enzyme responsiveness. Enzymes play a crucial role in complex biological and metabolic processes and are significantly important for regulating the biological cycle of living organism. The up or down regulation of the enzymes is often tied with disease conditions like cancer, inflammation, infections etc. Thus, the utility of these enzymes in drug delivery progress can have profound impact on the drug release and their subsequent cytotoxic action on the tumor tissues. The lyso-endosomal compartment of the cells are filled with variety of enzyme which can chop-off a broad range of chemical linkages thus

providing an opportunity to tune polymer design to have a better biodegradation and drug release from the drug delivery systems. This enzyme responsiveness is typically more relevant since the enzyme actions are very specific and selective in their mode of action and happens at physiological conditions[64,69,70].

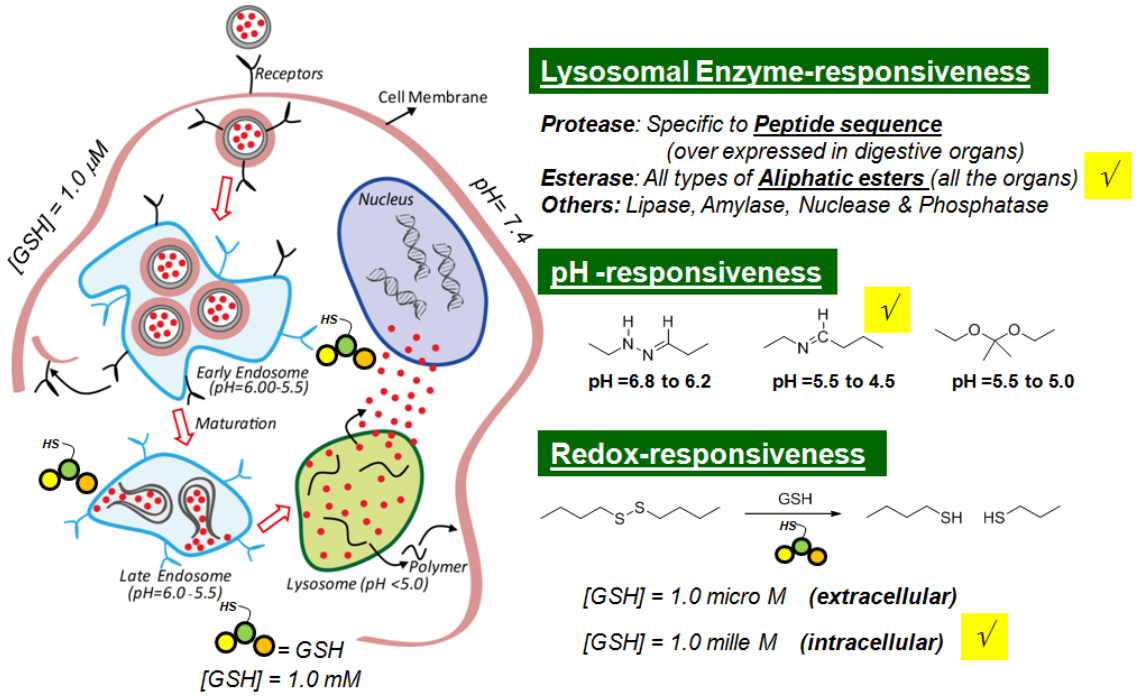

Figure 1.14: *Schematics of cell showing endocytosis of nanovesicles and different intracellular stimuli used for drug release.*

Cancer tissues are commonly distinguish from the healthy tissues by the overexpresssion of several biological factor linked with tumor microenvironment. The difference in the amount of glutathione (GSH) present in the normal cells and tumor cells offered unique opportunity to selectively disassemble the nano-vesicles in tumor environment. Generally plasma and healthy tissue have 1-2µM GSH concentration whereas the tumor tissues have 4 fold higher concentration of GSH (approximately 2-20mM)[71]. The glutathione (GSH) facilitates the cleavage of disulfide bond (-s-s-) in order to regulate several biological processes. This allows researchers to design the chemical structures to develop a "sense and act" type of drug delivery systems, wherein the tumor environment sense the presence of disulfide and triggers the release of loaded cargoes[22].

Reactive oxygen species (ROS) are produced in the living organism by various endogenous processes. They play a vital role in regulating the different biological processes such as apoptosis, cellular signaling, immune response etc. However it has been observed that, these ROS are overproduced in the cancer tissues and have been used as one of the stimuli for drug delivery application to cancer tissues[72]. The above explained are some of the intracellular responses which are commonly explored for the drug delivery application. Based on these responses, numerous nanocarriers are made till date and the development is still under progress. Some of the examples of polymer vesicles which use the above mentioned responsiveness are explained in detailed in the next section.

(a) pH Responsive Polymer Vesicles

Based on the pH gradient in biological system, various pH responsive polymer vesicles for anticancer drug delivery are reported in the literature and found to have superior impact on the cancer cell ablation. Yang and co-workers prepared the pH responsive polymer vesicles for doxorubicin delivery to the cancer tissues. To make this polymer vesicles, polyethylene glycol and doxorubicin were conjugated by a pH sensitive hydrazone linkage, their further blending with cholate grafted poly L-lysine produces a DOX encapsulated polymer vesicles[73]. These polymer vesicles showed enhanced cellular uptake and reduction in cancer cell growth following their treatment with human breast cancer MCF 7 Cells. The diagram given in figure 1.15 represents the polymer structure, morphology and their cellular uptake in MCF 7cells. To date various pH responsive linkages have been used for drug delivery which includes imine, orthoesters, acetals, ester etc. Zhong and co-workers reported acid sensitive polymer vesicles from PEG and poly(2,4,6trimethoxybenzylidenepentaerythrritol carbonate) and proved their disassembly in the mildly acidic conditions[74]. This strategy was incorporated in polymethacrylate based copolymers and formed polymer vesicles were used for delivery of hydrophobic and hydrophilic anticancer drugs. Polypeptide based polymer vesicles[75] which undergoes the disassembly in the acidic environment due to ionization of the functional groups were prepared by chen et al. PEG-poly(L-leucine)-poly(L-glutamic acid) were synthesized using NCA route and their aqueous self assembly produces the polymer vesicles[76] which are used for doxorubicin encapsulation and delivery to the breast cancer cells MCF 7.

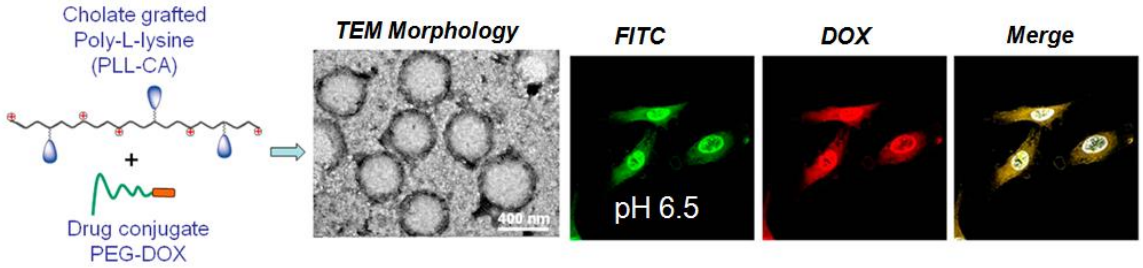

Figure 1.15: *A diagram showing the polymer structure, morphology and cellular uptake at pH 6.5 for polymer vesicles made from co assembly of PEG-DOX conjugate and cholate grafted poly L-lysine. Adopted from Zhu et al. Langmuir 2012, 28, 11988-11996.*

In the acidic condition of tumor microenvironment these polymer vesicles exhibited the DOX released following their acid sensitive swelling. This approach showed very good growth inhibition in MCF 7 cell compared to the free doxorubicin drug. Voit and co-workers reported pH sensitive photocrosslinked polymer vesicles using poly-(ethyleneglycol)-block-poly[2-(diethylamino) ethyl methacrylatestat-2-hydroxy-4-(methacryloyloxy) benzophenone] (PEG-b-P(DEAEMA-stat-BMA))[77]. Herein, 2-hydroxy-4-(methacryloyloxy) benzophenone (BMA) was used as photocrosslinking agent and the polymer vesicles with varying degree of cross linking were produced.

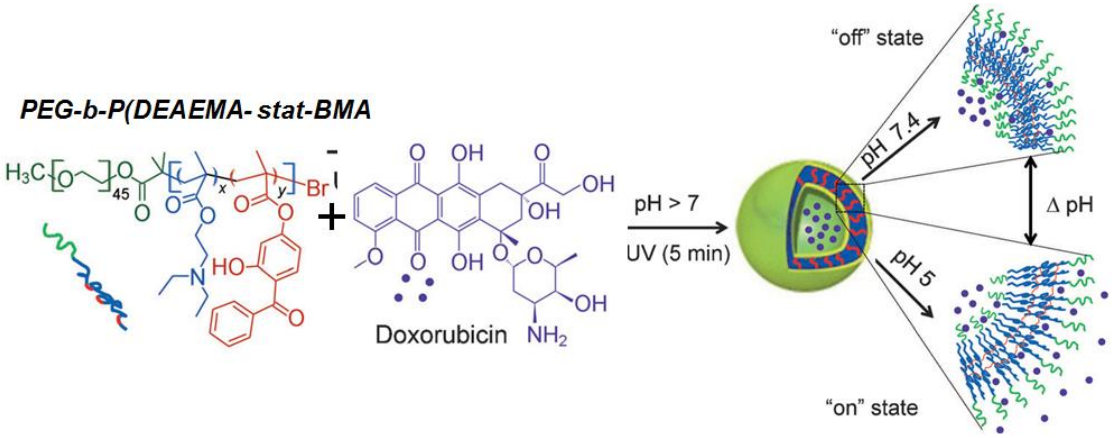

Figure 1.16: *A diagram showing the structure of the polymer and schematics of drug loading and pH responsive drug release from the polymer vesicles. Adopted from Yassin et al. Chem. Eur. J. 2012, 18, 12227-12231.*

These polymer vesicles were employed for doxorubicin encapsulation and delivery to the MCF 7 cells. Based on the degree of crosslinking, the doxorubicin to polymer ratio was tuned to achieve the higher drug encapsulation. The pH responsive disassembly exhibited the slow and controlled drug release to accomplish the better cell

killing in breast cancer MCF 7 cells. The diagram in figure 1.16 shows the structure of the polymer and schematics of drug loading and pH responsive drug release from the polymer vesicles. Liu et al. reported the synthesis of chimeric polymer vesicles using asymmetric PEG-PCL-PDEA triblock copolymer for encapsulation and delivery of exogenous proteins, cytochrome c, immunoglobulin etc[78]. The polymer vesicles showed a excellent stability even after the protein loading and does not alter the properties of the loaded cargoes. Importantly, the released cytochrome c fully maintained its activity and this has been successfully shown in RAW 646.7 cells by confocal microscopic images.

(b) Enzyme Responsive Polymer Vesicles

The enzyme rich endo-lysosomal compartment of the cells provides an opportunity to degrade the nanocarriers and hence enzyme responsive polymer vesicles made using the polymeric structures have attained much interest for delivery of pharmaceutical agents. In one such approach, Lee et al. prepared the lysosmally cleavable peptide containing polymer vesicles using the biocompatible polyethylene glycol (PEG) and Poly D/L lactide polymers[79]. These two polymers were linked by a peptide linkage Gly-Phu-Leu-Gly-Phe (GELF) which is susceptible to cleave in the presence of cathepsin B, an enzyme present in the lysosomes. Acridine orange, a model drug, was used for encapsulation and to understand the degradation of these polymer vesicles. A anti epidermal growth factor receptor (EGFR) antibody was also immobilized on these polymer vesicles to achieve active targeting of the cancer tissues. The endocytosis of these polymer vesicles was investigated by conjugating fluoroscein isothiocynate (FITC) labeled dextran onto the polymer vesicles. The effect of active targeting was studied in SKBR3 cells, which showed the enhanced uptake for EGFR labeled polymer vesicles as compared to negative control wherein the EGFR was not immobilized. The degradation of these polymer vesicles was studied at physiological condition and different pH environment (pH 7.4 and 5.0) in the presence of cathepsin B enzyme. It has been found that these polymer vesicles could be degraded in the presence of cathepsin B enzyme in the lysosomal pH conditions only and did not respond to the enzyme at physiological conditions. This proves that the polymer vesicles are only cleavable in the lysosomal

compartment of the cells. The diagram in figure 1.17 shows the structural representation of the polymer structure and schematics of the polymer vesicles.

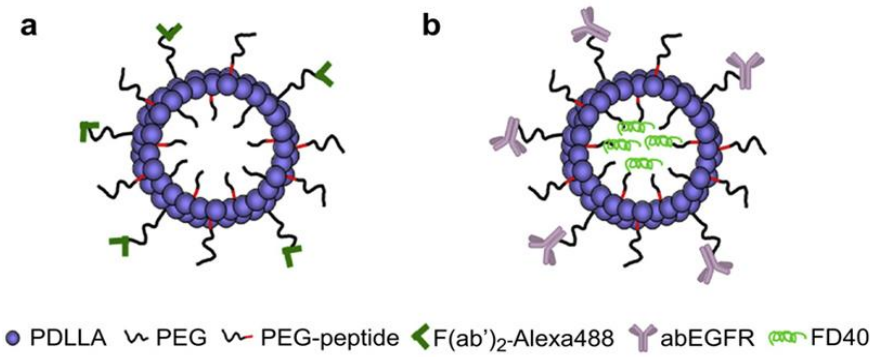

Figure 1.17: *A schematic representation of Peg-PDLLA polymer vesicles (a) labeled with alexa 488 and (b) immobilized with EGFR antibody and a fluorescent reporter dextran isothiocynate. Adopted from Lee et al. Biomaterials 2011, 32, 9144-9153.*

In another report, Liu and co-workers synthesized enzyme responsive polymer vesicles for bacterial strain selective delivery of antimicrobial agents. The antimicrobial resistance is a major challenge for the use of currently available antibacterial agents and to address this issue, penicillin G amidase and β-lactamase enzyme responsive polymer vesicles are prepared[80]. Theses enzymes are actively produced by the resistance pathogens thus, can be used as trigger for drug release in such conditions.

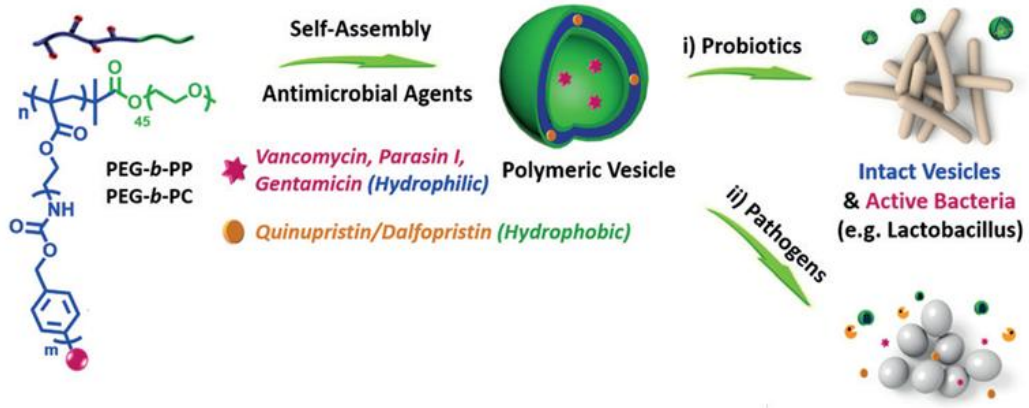

Figure 1.18: *A diagram showing the structure of polymer, schematics of polymer vesicles and encapsulation and their subsequent enzymatic degradation pathway. Adopted from Li et al. Angew. Chem. Int. Ed. 2016, 55, 1760-1764.*

Polymer vesicles were prepared by self assembly of diblock copolymer having polyethylene glycol (PEG) as hydrophilic segment and PP/ PC as hydrophobic segment

to produce PEG-b-PP and PEG-b-PC polymers. Calcein, Nile red and FITC-parasin I are used as model payloads to understand the cellular uptake and degradation process of these polymers. Chlorophenol red-β-d-galactopyranoside (CPRG) antibiotic and myoglobin, a therapeutic protein model were loaded together in these polymer vesicles to study their cytotoxic effects on the milli-Q cells. The results obtained proved that these polymer vesicles were able to take the antibiotics inside cells without causing any cytotoxic effect and without hampering the activity of the model protein. The biodegradation of these polymer vesicles were studied in the presence penicillin G amidase and β-lactamase, which confirmed the enzyme responsiveness of these polymer vesicles. This polymer design and schematics are showed in figure 1.18.

(c) Reduction Responsive Polymer Vesicles

The large difference in the amount of glutathione present at intracellular and extracellular levels in the cancer tissues makes it a one of the stimuli to be explored for drug delivery application. To utilize this property of the tumor microenvironment, Li and co-workers reported the synthesis of GSH responsive polymer vesicles using amphiphilic block copolymer of polyethylene glycol (PEG) and polyacrylates. These two polymer segments (hydrophilic and hydrophobic) were connected by a disulfide bond which can be cleaved at the tumor site[81]. Polymer vesicles were prepared by aqueous self assembly of this diblock copolymer and used for calcein encapsulation. The GSH responsive degradation of these polymer vesicles was studied by transmission electron microscopy and cumulative release of calcein dye from the self assemble structure. These polymer vesicles were found to be very stable in the presence of phosphate buffer saline (PBS). Using this diblock polymer design, the proof of concept was established for GSH responsive polymer vesicles which proved that this design can be potential candidate for drug delivery in cancer tissues. The diagram in the figure 1.19 depicts the structure and morphology of the polymer vesicles. In another attempt to use these stimuli, Zhang and co-workers prepared a triblock copolymer using polyethylene glycol, polyacrylic acid and poly-n-isopropylacrylamide. This PEG-b-PAA-b-PNIPAM was made and crosslinked using amine group of cystamine and acid group of acrylic acid to produce stable polymer vesicles in aqueous medium[82]. The presence of acrylamide group endows

these polymer vesicles with additional temperature responsiveness. To visualize the polymer vesicles intracellualrly, a FITC conjugated dextran was encapsulated. Thus, GSH and temperature dual stimuli sensitive polymer vesicles were made and used for protein delivery application.

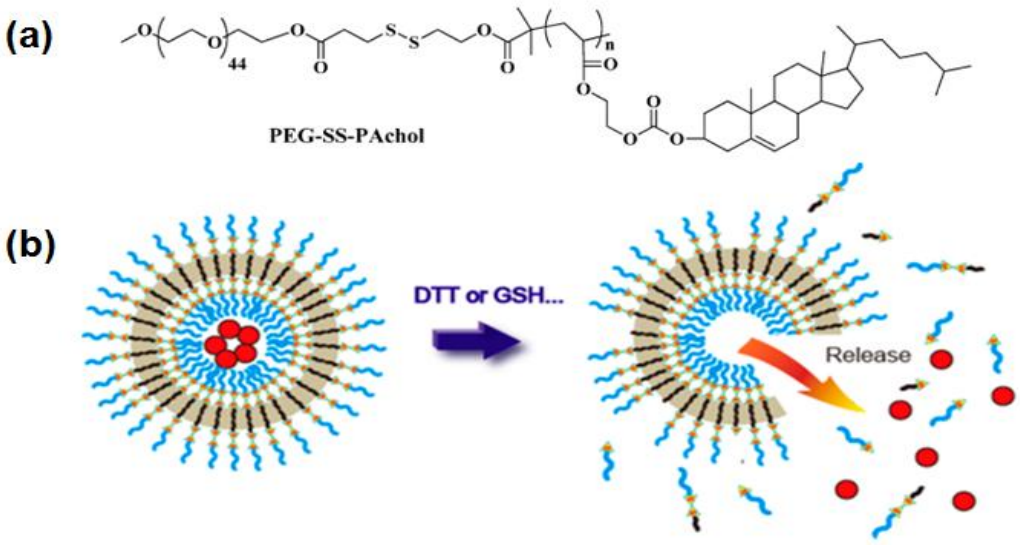

Figure 1.19: *A diagram showing the structure of polymer (a) and schematic illustration of polymer vesicles and their GSH assisted degradation. Adopted from Li et al. Biomacromolecules 2014, 15, 2206-2217.*

In another attempt, Thambi et al. reported the synthesis of polymer vesicles from a triblock copolymer using polyethylene glycol, poly-lysine and polycaprolactone. This PEG-b-poly-lysine-SS-polycaprolactone was made and their aqueous self assembly facilitates the formation of polymer vesicles[83]. These polymer vesicles were now used for encapsulation of the both hydrophilic drug in core and hydrophobic drug in the layer of the polymer vesicles. For these purpose two anticancer drugs namely camptothecin (water insoluble, goes in the layer of polymer vesicles) and doxorubicin hydrochloride (water soluble, goes in the core of polymer vesicles) were chosen which are differing in their action of mechanism as well as physical properties. This dual drug loaded polymer vesicles were then employed for combination therapy in squamous carcinoma 7 cells (SSC 7) wherein they have showed a enhance cellular uptake and better cancer cell inhibition as compared to their free drug counterparts. The structural representation and dual drug loading is showed in figure 1.20.

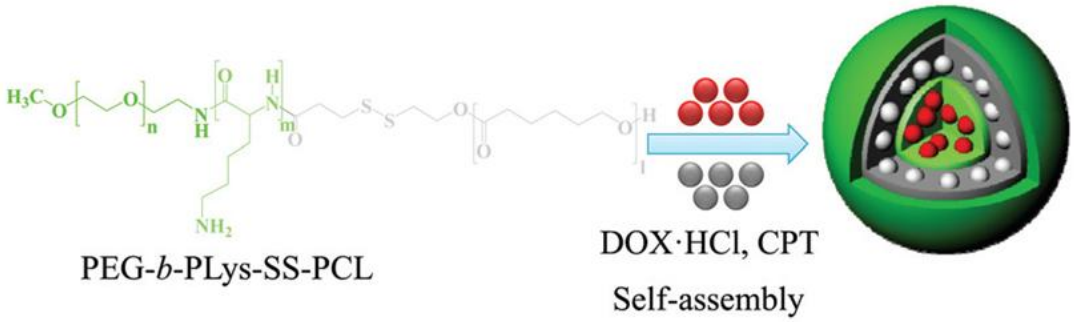

Figure 1.20: *A diagram showing the structure of polymer and schematics of dual drug encapsulation. Adopted from Thambi et al. J. Mater. Chem. 2012, 22, 22028-22036.*

(d) Oxidation Responsive Polymer Vesicles

The presence of the reactive oxygen species at the intracellular condition can be used as one of the stimuli and it has been observed that, these ROS are overproduced in the cancer tissues and have been used as one of the stimuli for drug delivery application to cancer tissues. This approach was used by Liu and co-workers and fabricated the mitochondria targeting H_2O_2 responsive polymer vesicles using the aryl boronate ester containing diblock copolymers[84]. The synthesized polymers when dispersed in water formed various self assemble structures such as micelles, vesicles, large compound vesicles. This polymer vesicles or polymer vesicles were then used for dual drug encapsulation to achieve combination therapy. Further they have also demonstrated the use of these polymer vesicles as nano-reactors and bio-probes for biomedical application. The oxidation responsive boronate ester cleavage, their cross linking and hydrophobic to hydrophilic transition of the polymer vesicles bilayer was also demonstrated. The figure 1.21 showed the structure and schematics of these polymer vesicles. In another attempt, Fu and co-workers made a ROS responsive cholesterol decorated poly L-cysteine copolymer assemblies and showed unusual micelle to vesicles transformation[85]. The cholesterol modified n-carboxy anhydride monomer of cysteine was synthesized and polymerized using ring opening polymerization (ROP) technique to produce a cholesterol modified poly l-cysteine polymer. The micellar assemblies were produced on the aqueous self assembly of this polymer, whereas upon H_2O_2 action, micelle to vesicle

transformation was observed. H_2O_2 induced oxidation of sulfur group of cysteine to sulfone group was attributed to this transformational change.

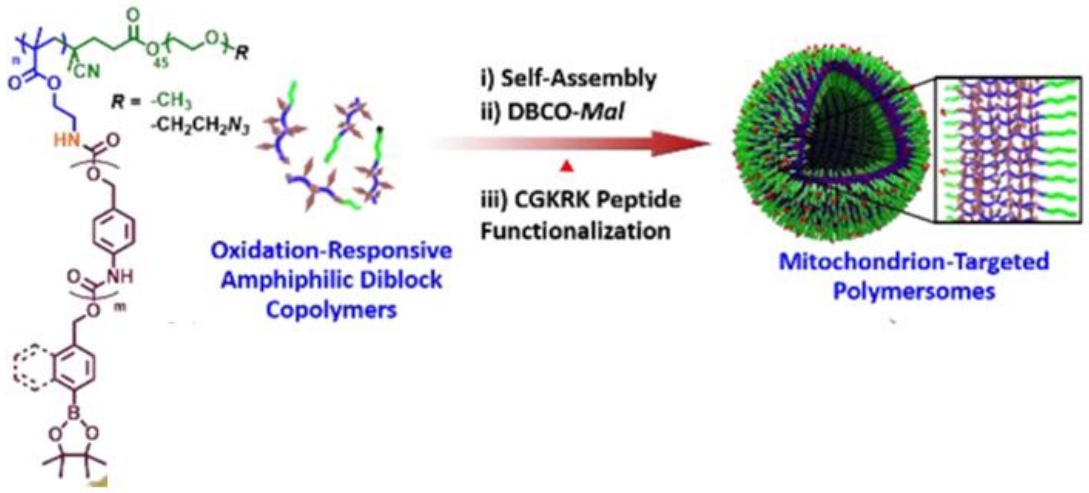

Figure 1.21: *A diagram showing the polymer structure and schematics of polymer vesicles. Adopted from Deng et al. J. Am. Chem. Soc. 2016, 138, 10452- 10460.*

It was proved that, the presence of sulfone group imparts the hydrophilicity to the polymer backbone which forces the morphological conversion. The polypeptides are prone to undergo the conformational change from β sheet to α-helix structure and this has been validated using CD studies in the current report. The cellular uptake of these polymer vesicles was also studied by encapsulation of rhodamin6G dye in the core of the polymer vesicles. The diagram showed in figure 1.22 depicts the structure of the polymer and schematics of micelle to vesicle transformation.

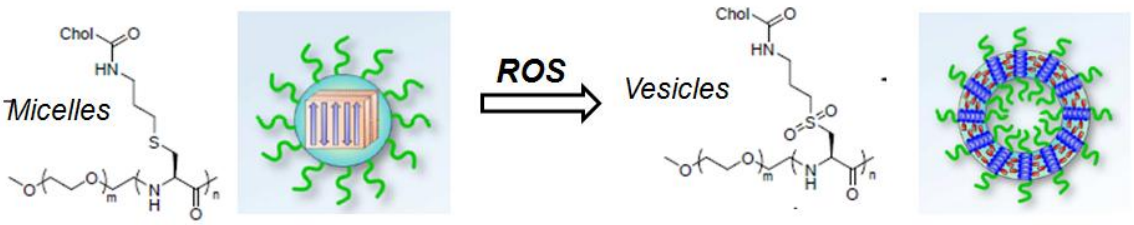

Figure 1.22: *A diagram showing the structure of the polymer and schematics of micelle to vesicles transformation. Adopted from Liu et al. J. Am. Chem. Soc. 140, 21, 6604-6610.*

Discussed until now are some the synthetic polymer assemblies used for drug delivery application. These polymers though have been explored widely for the drug delivery application, but their non biocompatible and nonbiodegradable nature limits their clinical use. Moreover the drug release rate, renal clearance and unwanted cytotoxicity produced from the synthetic polymers creates a serious concern for their biological application. Thus it is advisable to use the polymers which are biocompatible and biodegradable polymer to overcome the problems associated with synthetic polymeric systems. Hence, naturally occurring biocompatible polymers polysaccharides can be a very good alternative source to be used for this application. These polysaccharides are abundantly available or can be obtained from natural resources easily. The chapter hereafter will focus on the contribution of these polysaccharides in the drug delivery application.

1.4 Polysaccharides for Drug Delivery Application

Polysaccharides are naturally existing polymers and can be obtained from different sources such as algae origin (alginate and carrageenan), microbial origin (dextran and chitin), animal origin (hyluronan, chondroitin and heparin), and plant origin (cellulose, pectin and guar gum)[86-89]. Polysaccharides are nontoxic and biocompatible in nature and therefore unique class of polymers to be used for drug delivery application. They possess many desirable characteristics such as extremely good water solubility, enhanced stability, low cost, ease of chemical modification etc which are necessary for their utility in biomedical application[90,91]. There are many polysaccharides available which has different structural units, varying molecular weights and properties, figure 1.23 depicts the structure and chemical composition of the various polysaccharides available. From the chemical structure it can seen that the polysaccharide backbones are decorated with variety of functional groups such as acid, hydroxyl, amine etc and functional groups. These functional groups can be easily modified to tune the properties of polysaccharides so as to make them useful for this application[92-94]. These polysaccharides are higher molecular weight polymers and hence accumulated in the body for long time without causing any side effect. The prolong stay of the polysaccharides in the body helps in their biodegradation using specific enzymes in the body, where upon they are expelled from the body by renal clearance. As such the polysaccharide does not lead to the formation of any kind self assemble motifs however suitable modification of the polymer backbone facilitates their self assembly to produce various self assemble motifs such as micelles, vesicles, hydrogels, nanoparticles[94]. These polysaccharide due to their inherent properties, imparts a great amount of stability to self assemble structures and produces a suitable architectures for drug delivery application. Cellulose, chitosan, dextran, hyaluronic acid, heparin, cyclodextrin are some the polysaccharides currently being explored for drug delivery application[86]. Chitosan is one such polysaccharide, available in wide range of molecular weights and Charecterized with positive charge on the polymer backbone. This kind of positively charged polysaccharides especially important for nucleic acid and gene delivery application. Nucleic acid and genes are very sensitive in their action and should be protected before reaching the target site. Thus, negatively

charged nucleic acids and gene were hold strongly by the positively charged chitosan and makes it possible to deliver them to the target site without hampering their activity. Hyaluronic acid has a acid functionality on a polymer backbone which allows the conjugation of drug molecules, targeting moiety, peptides, etc and helps in passive as well as active targeting of the tumors for site specific drug delivery[95].

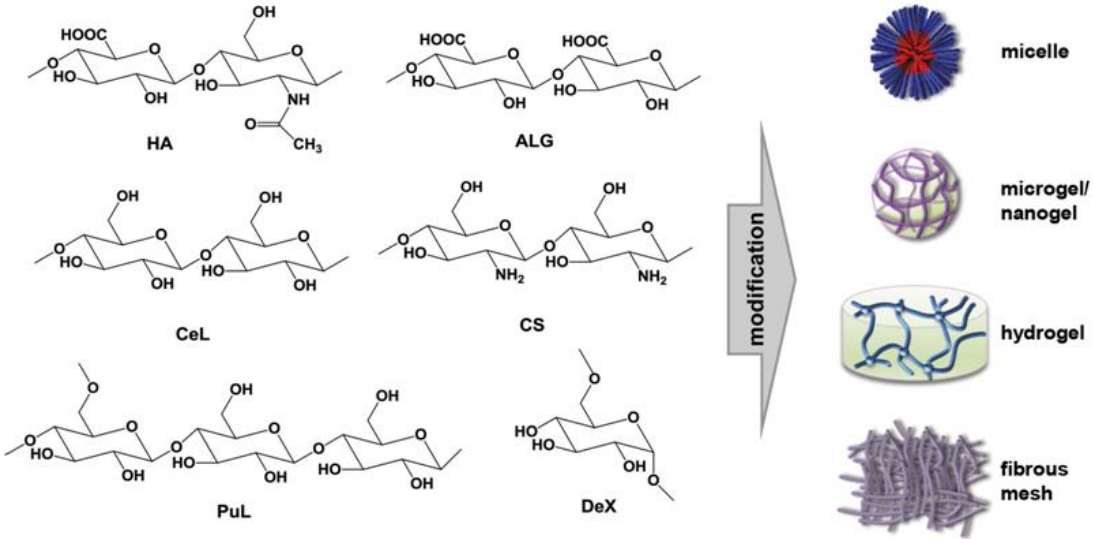

Figure 1.23: *A diagram showing the structure of different polysaccharides and schematics of their self assemble structures after suitable modification. The abbreviations used are HA: hyaluronic acid, ALG: Alginate, Cel: Cellulose, CS: Chitosan, Pul: Pullulan and DeX: Dextran. Adopted from Wen et al. Macromol. Rapid Commumn. 2014, 35, 1819-1832.*

Additionally this hyaluronic acid itself is recognized by receptors (CD 44 receptors) present on the surface of several cancer tissues and hence is a potential candidate for drug delivery application. This property of hyaluronic acid was explored by several researchers and variety of active drug delivery systems are being reported till date. Owing to the presence of acid functionality, hyaluronic acid has been extensively used for the delivery of the cisplatin drug to the tumor tissues[94]. The appropriate modification on the polysaccharide backbone and their subsequent blending may lead to the formation of hydrogels which can be used for the drug delivery application. The feasibility of introducing the appropriate stimuli on the polysaccharide backbone makes them especially important for anticancer drug delivery application[86]. Introduction of such

stimuli on the polysaccharide backbone assist slow and controlled release of the anticancer drugs which is desirable for accomplishing cancer cell growth inhibition. The different reactions involved in polysaccharides modifications are esterification, oxidation, sulfonation, reduction, amidation etc. These polysaccharides are extensively employed various application in biomaterials and biomedical field. Amongst them three extensively used polysaccharide (Chitosan, pullulan and dextran) are discussed in detail in the coming section of the chapter.

(a) Chitosan Nanocarriers

Chitosan is important class of polysaccharides, composed of β-(1,4) linked 2-deoxy-2-amino-D-glucopyranose and partially of β-(1,4) linked 2-deoxy-2-acetamido-D-glucopyranose and produced from deacetylation of chitin. Chitin is the major component of the exoskeletal in crustaceans[96]. Chitosan being nontoxic, biodegradable and biocompatible, it has been explored as biomaterial and its derivatives have been developed drug delivery application. Chitosan can also be used for various applications such as such as membrane, gene delivery, cell culture, tissue engineering, biosensors, and scaffold generation[97]. In one such report, Meng et al. prepared the pH and light dual responsive crosslinked polymeric micelles (CPM) by the self-assembly of amphiphilic glycol chitosan-o-nitrobenzyl succinate conjugates (GC-NBSCs). These conjugates were then cross-linked using glutaraldehyde (GA). This crosslinked chitosan micelles exhibited excellent biocompatibility in NIH 3T3 and MCF 7 cells[97]. Further these micelles were used for camptothecin loading and delivery to the human breast cancer cells. The pH and light dual responsive behaviour of these micelles showed a better release of the camptothecin drug and exhibited enhanced cell killing compared to the free drug. Figure 1.24 shows the newly modified chitosan structure, camptothecin encapsulation and subsequent cellular internalisation in MCF 7 cells. In another attempt, Ho et al. reported the synthesis of farnesylated glycol chitosan (FGC), an amphiphilic graft polymer which self assembles in aqueous medium to produce nanoparticles[98]. The size of FGC nanoparticles can be tuned depending upon the degree of farnesylation and pH of the aqueous solution and it has been observed that it forms the nanoparticles of size around 200-500 nm.

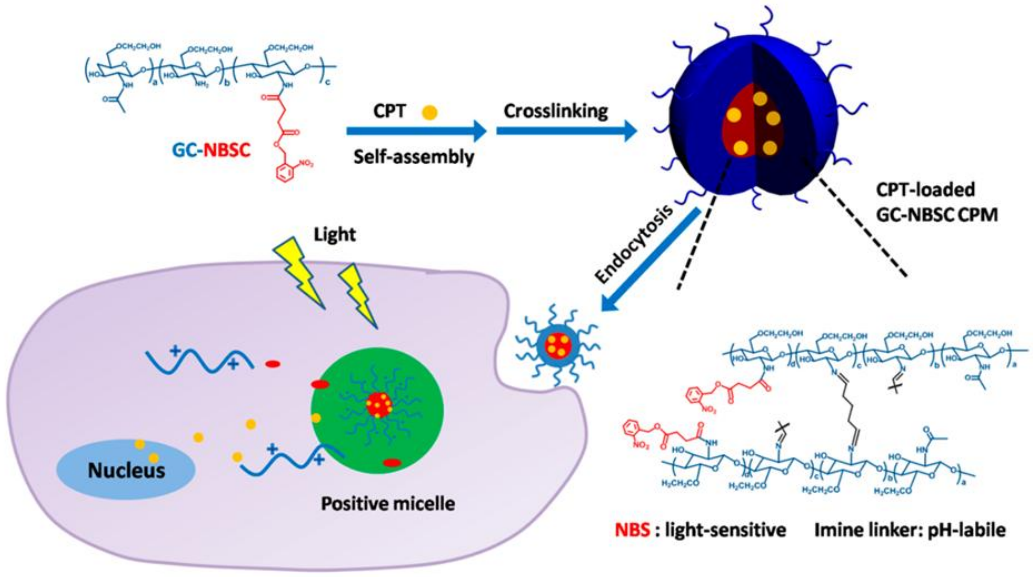

Figure 1.24: *Chemical Structure of the modified chitosan and schematics of camptothecin loading in crosslinked chitosan micelles and their cellular internalisation in MCF 7cells. Adopted from Meng et al. Biomacromolecules, 2013, 14, 2601-2610.*

These nanoparticles were found to be biocompatible and stable at physiological conditions. The interaction of these nanoparticles with human mucus was examined by multiple particle tracking and found that 80 % of the particles remain immobilized within the mucus matrix. Figure 1.25 shows the structure of the farnesylated glycol chitosan and self assembly into nanoparticles at pH 5.0

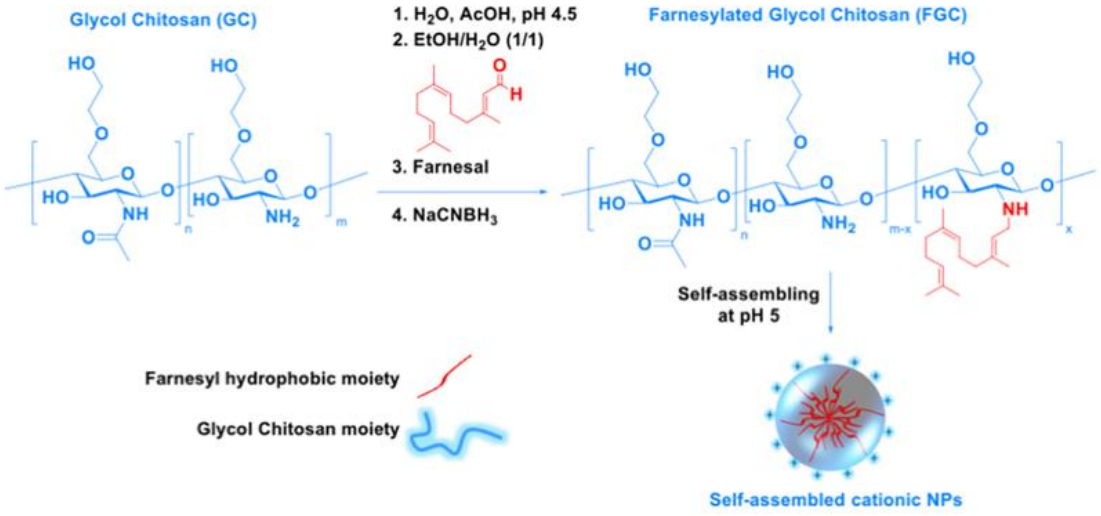

Figure 1.25: *Chemical structure of chitosan and farnesylated glycol chitosan and schematics of self assembly in aqueous medium at pH 5.0. Adopted from Ho et al. Biomacromolecules 2018, 19, 3489-3501.*

The above explained are the two examples of drug delivery application of the chitosan. Apart from this chitosan find application in various fields such as food packaging, membrane for antibacterial strains, bone regeneration, etc. This all applications have been discussed in detail by Ikram and co-workers[99]. So from the above discussion it was understood that the chitosan has played a vital role in biomedical application.

(b) Pullulan Nanocarriers

. Pullulan is a natural polysaccharide that possesses high biocompatibility, biodegradability, and poly functionality owing to the presence of nine hydroxyl groups per repeating unit for chemical decoration[100]. It is also found that pullulan has good blood compatibility, non immunogenicity, and fair solubility in water. Pullulan also shows a specific affinity towards asialoglycoprotein receptor (ASGP-R), which is specific for hepatocytes, and highly expressed on their sinusoidal membranes[101]. The explicit binding of pullulan to ASGP-Receptors provides important pathway for targeted therapy of liver tumors. To make use of this naturally occurring polysaccharide, Li et al. prepared a series of pullulan- doxorubicin conjugates and employed for delivery in hepatic carcinoma cells[102]. Doxorubicin was anchored onto the pullulan backbone with acid cleavable hydrazone bond using spacers with different alkane chain lengths. The degree of doxorubicin was archived as 50% and in the presence of acidic conditions, slow and controlled release of the drug was observed. Cytotoxicity studies proved that these pullulan dox conjugated could accomplish better cell killing in hepatic carcinoma cells. The invivo studies were carried out and it has been observed that, these Pullulan-dox nanoparticles could inhibit the growth of solid tumors and prolongs the lifetime of the animals. The figure 1.26 shows the schematics of nanoparticle formation and their subsequent effect of inhibition of solid tumor growth. Zhou et al. reported the synthesis of cationic guanidine-decorated dendronized pullulan (OGG3P) for efficient genetic photodynamic therapy[103]. This modified pullulan was able block the migration of the DNA where as the control polymer couldn't show any effect on the DNA migration.

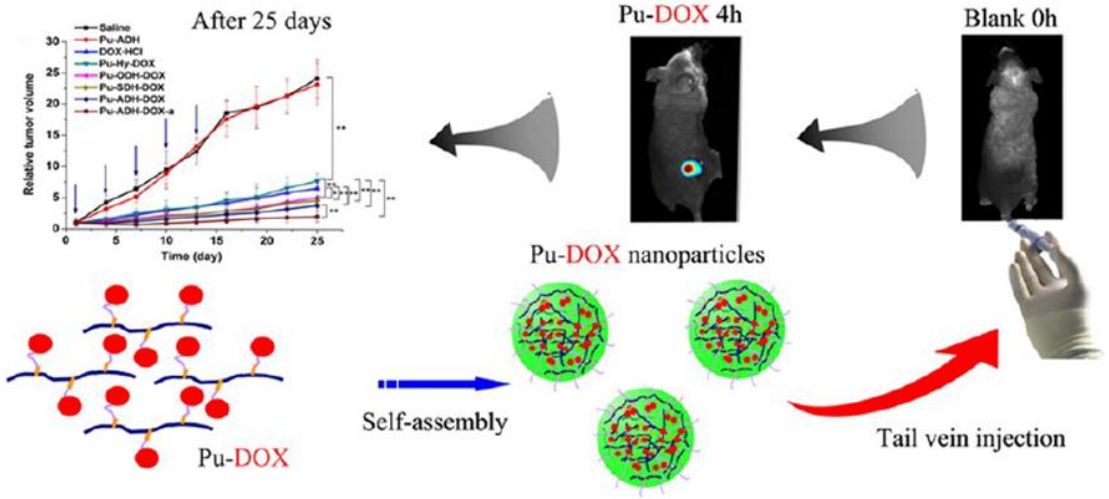

Figure 1.26: *Schematics of pullulan-dox conjugates and their self assembly into nanoparticles and their subsequent effect on the growth inhibition of solid tumors. Adopted from Li et al. ACS Appl. Mater. Interfaces, 2015, 7, 15855-5865.*

Gaunidination of the pullulan caused the changes in cellular uptake pathway and led to the macropinocytosis which could be the reason for higher trasfection efficiency. Further these derivatives were used for reactive oxygen species (ROS) induced cancer cell ablation. Figure 1.27 shows the schematics of the modified pullulan nanoparticles and their cellular uptake by different endocytosis pathways.

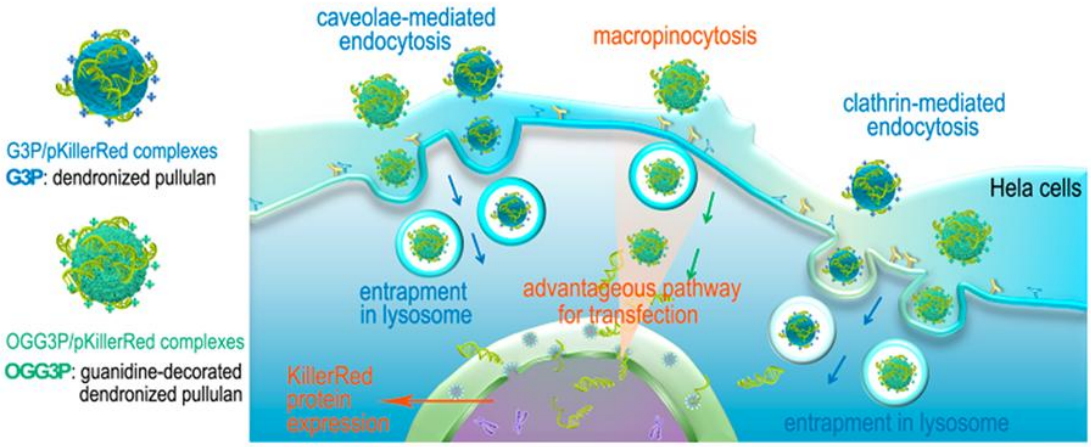

Figure 1.27: *Schemtaics of the nanoparticles formed from odified pullulan derivatives and their subsequent cellular uptake by different endocytosis pathways. Adopted from Zhou et al. Biomacromolecules 2018, 19, 2214-2226.*

These results revealed that the guanidination of the pullulan indeed interacts with the phosphate group of the DNA and stops the migration. These nanoparticles were found to be biocompatible and showed enhanced cellular uptake in HEK293T and HeLa cells.Thus, pullulan being neutral polysaccharide, with ease of modification have been explored extensively for the drug and gene delivery application. Hence, pullulan and chitosan are the two polysaccharides which have been used regularly for the biomedical application. Apart from these two there are other polysaccharides such as cellulose, hyaluronic acid, alginate, starch also have been used for the drug delivery application.

1.5 Dextran for Drug Delivery Application

Dextran is a highly water soluble polysaccharide having predominantly linear α-(1,6) glucosidic linkage (see figure 1.28) with short degree of branching from α-(1,4), α-(1,3) and α-(1,2) position of the backbone[86]. Dextran is derived from bacterial culture of lactic acid bacteria such as *Leuconostoc Mesenteroides.* The degree of branching on the dextran backbone and the molecular weights are dependent on the bacterial source from which they are derived and hence providing the choice of selection. Dextran is available in wide range of molecular weights ranging from 6 to 200 KDa[103]. More than 200 tonnes of dextran is produces annually for different biological and industrial application. From the last several decades dextran have been used in the clinics as plasma volume expander, antirhombolytic agent, peripheral blood flow promoter etc. Dextran being highly water soluble, does not produce any self assembly if used as such, but the presence of many hydroxyl groups on the polymer back bone provides an opportunity for chemical modification.

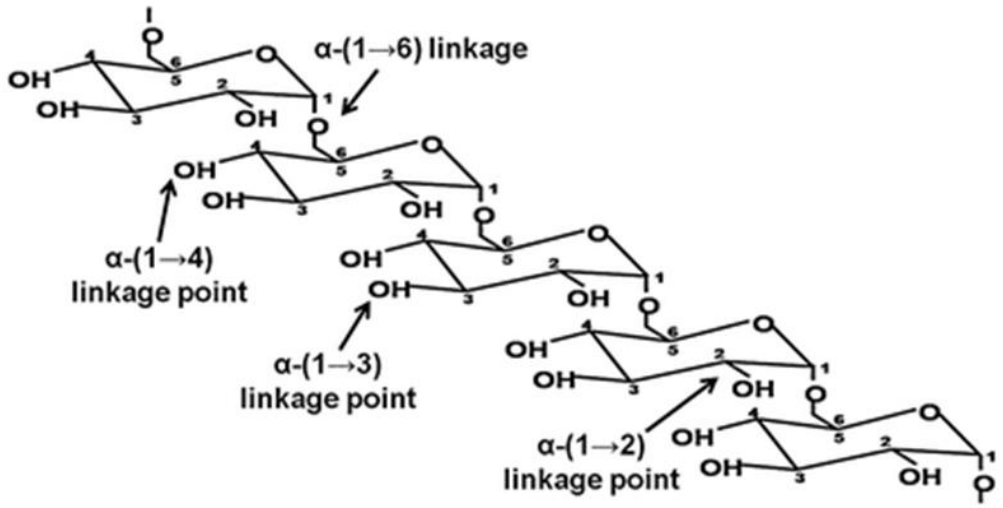

Figure 1.28 : *Chemical structure of dextran showing α-(1→6) glucose units and having branching at α-(1→4) or α-(1→3) or α-(1→2) positions depending upon type of bacterial strains used for the production. (Adopted from Kothari D., Das D., Patel S., Goyal A. (2014) Dextran and Food Application. In: Ramawat K., Mérillon JM. (eds) Polysaccharides. Springer, Cham).*

The reactivity of these hydroxyl groups has been studied and found as C_2 hydroxyl > C_4 hydroxyl > C_3 hydroxyl. Hence most of the substitution done on the

dextran backbone uses the C_2 hydroxyl group[104]. Dextran modification has been done using various chemistries such as oxidation, iminisation, esterification, etherification, etc. Out of these esterification and etherification are most commonly used techniques and based on these numerous reports have been published in the literature. Moreover the presence of dextran degradable enzymes in the body is a key factor in the development of dextran based drug delivery systems[105-108]. Thus, the dextran has been a very good alternative for the existing synthetic polymers, extensively used in the drug delivery application. Considering the benefits of the dextran, it has been extensively used in the biomedical application and recently and dextran-drug conjugates have reach the clinical trials and some of the examples are already mentioned in the polymer drug conjugates section of this chapter. Inspired from this success, various drug delivery reports have appeared in the literature and some of them are discussed in detail hereafter. In one such report, Zhong and co-workers reported the synthesis of reduction responsive reversibly crosslinked dextran nanoparticles for doxorubicin delivery to the cancer cells. The dextran backbone was substituted using lipoic acid and further cross linking was done using the small amount of dithiothreitol (DTT)[109]. These produced crosslinked dextran nanoparticles which could able to load the anticancer drug doxorubicin with higher efficiency of loading as good as 84%. These nanoparticles were treated with cervical cancer cells (HeLa) and intracellular trafficking of doxorubicin proved the enhanced uptake of drug compared to the free drug. The reduction responsiveness of these nanoparticles was studied using dynamic light scattering technique and increase in the size of the nanoparticles upon treatment DTT confirmed the decrosslinking of nanoparticles. Schematics in the figure 1.29 depict the self assembly, crosslinking and intracellular delivery of the nanoparticles in cervical cancer cells. The same group have come up with synthesis of dextran-*b*-poly(ε-caprolactone) diblock copolymer wherein the two diblock are connected via a reduction responsive disulfide bond. The formed diblock copolymer produces micellar assemblies upon the aqueous self assembly and they have been used for doxorubicin encapsulation and delivery to the cancer cells. Wang et al. made amphiphilic graft copolymer from dextran and poly l-lactide and used for effective haemoglobin encapsulation. Carboxyl terminated poly l-lactide was made and grafted on the dextran backbone to yield dextran-g-PLA[110].

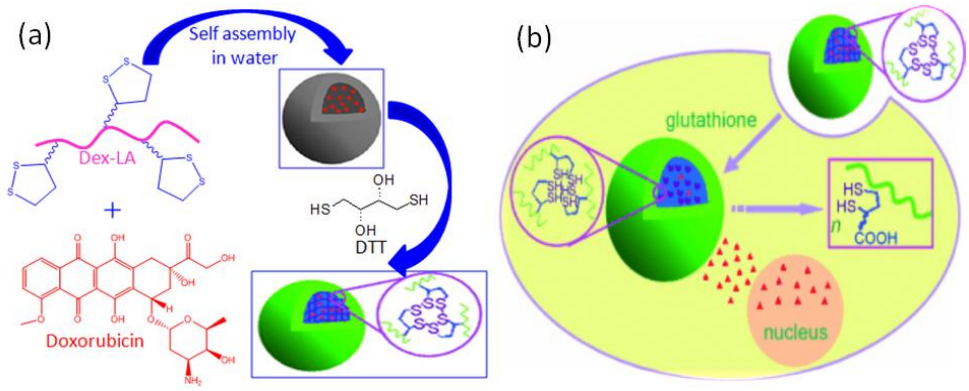

Figure 1.29: *A diagram showing the self assembly, drug encapsulation (a) and intracellular drug delivery from reversibly stabilized multifunctional dextran nanoparticles (b). Adopted from Li et al. Angew. Chem. Int. Ed. 2009, 48, 9914-9918.*

This copolymer produced the vesicle upon aqueous self assembly which are used for haemoglobin encapsulation. The oxygen affinity of haemoglobin encapsulated vesicles were calculated and found to be very close as that of free haemoglobin and proved the potential of these vesicles as blood substitute. Chen and co-workers reported the synthesis of succinic acid substituted dextran nanoparticles for active targeting of the cisplatin drug in metastatic breast cancer. In this report acid functionalized dextran was produced by ring opening of succinic anhydride by hydroxyl group of dextran backbone. Cisplatin was stitched to this acid functionalized LHRH conjugated dextran nanoparticles and used for active targeting of metastatic breast cancer[111]. Further *In vivo* studies proved that these nanoparticles could able to reduce the side effects caused by the free cisplatin. Thus, these nanoparticles can be very good candidates for active targeting of metastatic breast cancers using cisplatin as drug.

Houga *et al.* reported the synthesis of series of diblock copolymer of dextran and styrene[112]. The self assembly of dextran-b-polystyrene (DEX-b-PS) in organic solvents and water was studied and showed in figure 1.30. Polystyrene (PS) is a toxic non biodegradable material and its content in the copolymer system was varied from 7 % to 92 % w/w, while the hydrophilic dextran molar mass was kept constant at 6600 g/mol. In this study , the self assembly of different block lengths was studies and it has been shown that block copolymer with low hydrophobic content self assembled to form micelles and nanoparticles. High degree of substitution yielded vesicles as shown in the figure 1.29.

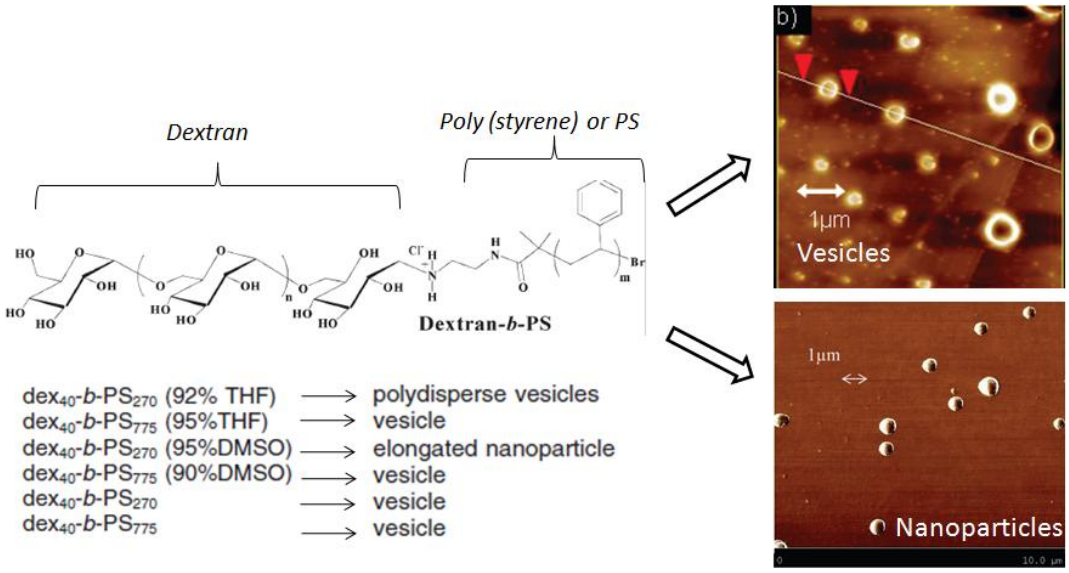

Figure 1.30: *The chemical structure of dextran-b-Polystyrene (DEX-b-PS) and AFM image of vesicles and nanoparticles formed by varying block length of hydrophobic (PS) content. Adopted from Houga et al. Biomacromolecules,* 2009, *10,* 32-40.

It has been observed that there are very few reports in the literature which investigates the vesicular morphology of the dextran. The above study revealed that in case of dextran, the balance of hydrophilic segment (dextran chain) and hydrophobic content is very crucial for determining the type of self assembled structure is produces in aqueous medium. Moreover the above given example uses a nonbiodegradable and toxic polystyrene as hydrophobic source and hence the use of this kind of self assemble structures is not advisable for the biological purpose. Thus, choice of proper hydrophobic segment (should be biocompatible) and maintaining the appropriate hydrophilic to hydrophobic balance is a difficult task when dealing with the polysaccharide dextran.

From our group, a new hydrophobic segments pentadecyl phenol based on renewable resource was anchored onto dextran backbone. The resultant dextran derivatives when dispersed in water, produces vesicular structures as showed in figure 1.31. These polymer vesicles were capable of loading water soluble guest (Rhodamine-B, RhB, water soluble dye) in its interior hydrophilic cavity and water insoluble polyaromatic anticancer drug (Camptothecin, CPT) in its unilamellar hydrophobic membrane. It was also able to protect the plasma sensitive CPT lactone pharmacophore

against the hydrolysis by ten times better than the CPT alone in PBS. The aliphatic ester linkage connecting the hydrophobic tail with dextran was found to be ruptured by esterase under physiological conditions for fast releasing of CPT or RhB. Confocal microscopic images confirmed that both RhB and CPT-loaded vesicles to be taken up by fibroblasts compared to drug/dye alone, showing a distinctly perinuclear localization in cell[113].

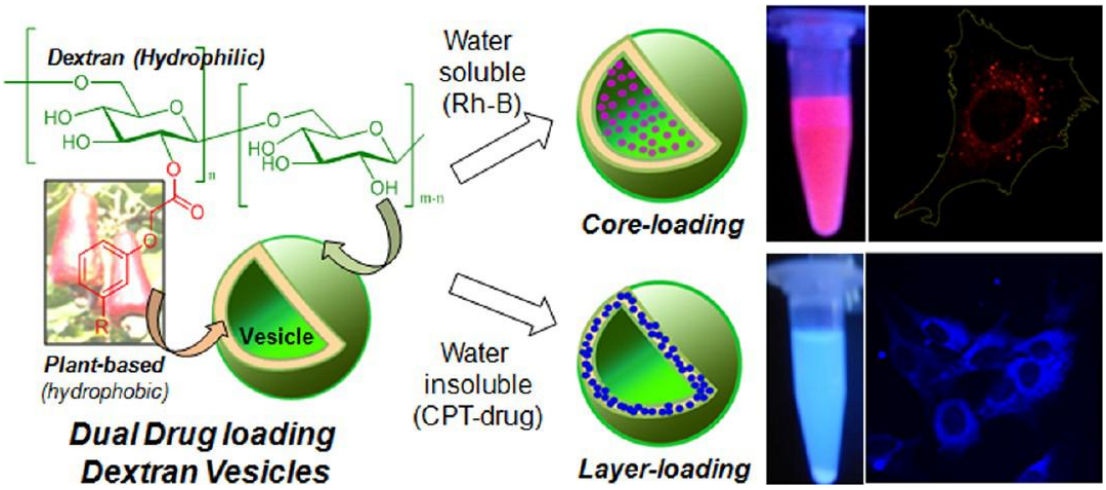

Figure 1.31: *Chemical structure of newly designed dextran derivatives, self assembly and cellular uptake Adopted from Pramod et al. Biomacromolecules 2013, 13, 3627-3640.*

Further these vesicles were used for development of multiple drug loading and sequential drug delivery of anticancer drugs DOX (topoisomerases II inhibitor) and CPT (topoisomerases I inhibitor) to achieve synergistic killing of cancer cells. This nanovesicle facilitated the investigation of dual drug loaded single-vesicle versus the cocktail of individual drug loaded nano-vesicles. Further, evaluation of the role of caveolae in endocytosis of these polymer scaffolds was also made. Endocytosis of this nano-vesicle in caveolae lacking (Cav-1 $^{-/-}$) MEFs was seen to be better (see figure 1.31). This differential uptake is also seen in caveolin-1 (and hence caveolae lacking) breast cancer (MCF7) and colon cancer (DLD1) cells[114] The dual loaded polysaccharide nanovesicles containing DOX and CPT promote synergistic effect in killing cancer cells (see figure 1.32). Cocktail of vesicles having more amount of CPT than DOX showed enhancement in the synergistic effect suggesting that both the combination of multiple anticancer drugs and their amount played a crucial role in the therapeutic effect. The

results provide significant new insights into polysaccharide loaded dual drug action of DOX: CPT drug combination in the breast and colon cancer cells[115].

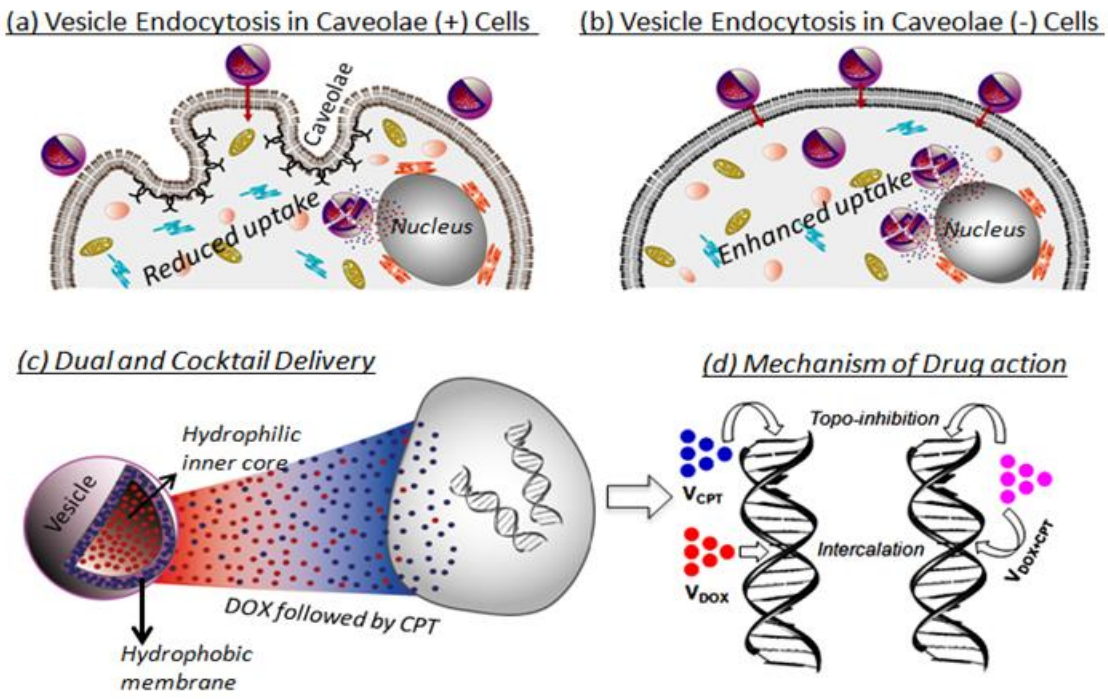

Figure 1.32: *Schematics showing the cellular uptake of dextran vesicles in caveolae (+) cells (a), caveolae (-) cells (b), dual and cocktail delivery of the drugs (c) and mechanism of action of the drugs (d). Adopted from Pramod et al. Nanoscale 2014, 6, 11841-11855.*

Further, pH and enzyme dual responsive polysaccharide vesicular nano-scaffolds were designed for the delivery of doxorubicin both physical loading and chemical drug conjugation. Dextran was suitably modified with renewable resource 3-pentadecyl phenol via imine and aliphatic ester linkages that act as pH and esterase enzyme stimuli for delivering drugs (see figure 1.33). These dual responsive polysaccharide derivatives self-organized as nano-vesicles in water[116]. A doxorubicin anticancer drug was used for chemical conjugation through imine linkage and also physically loaded in these vesicles. The disruption of these vesicles in acidic environment proved the acid sensitive delivery of these drugs. In MCF7 cells, DOX loaded vesicles exhibited better cell killing efficiency than free drug and drug conjugated vesicles and the confocal microscopic images confirmed that DOX in nano-vesicles were taken up better by cells compared to free DOX molecules.

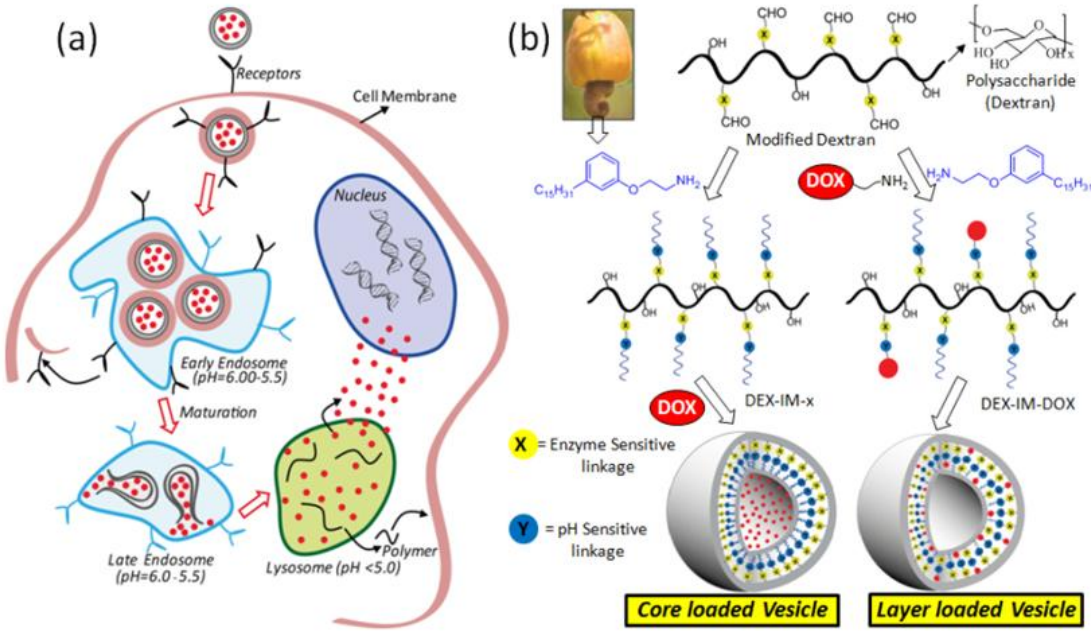

Figure 1.33: *Schematics dictating the path of the nanovesicles followed in intracellular milieu (a) and the chemical structure of the modified dextran derivatives and their self assembly (b). Adopted from Pramod et al. Nanoscale 2015, 7, 6636-6652.*

Further these polymer vesicles were used to estimate real time drug release parameters from enzyme responsive polysaccharide vesicles using time resolved fluorescence technique[117]. Remarkably, a significant difference was observed in the TCSPC life time of free RhB and RhB loaded in the vesicles. The limitations of normal absorbance, emission and dynamic dialysis method to distinguish the species such as drug/dye bound to polymer (loaded) and released into PBS was successfully overcome using time resolved fluorescent (TCSPC) technique (see figure 1.34). The fractional contribution of the dye loaded in the vesicles and released into solution (PBS) after esterase enzyme treatment was meticulously estimated using TCSPC method, without any additional treatment such as dialysis, centrifugation etc. Moreover, the ability of enzyme to rupture the polysaccharide vesicles was investigated using docking studies. The peculiar positioning of the molecules in active site of enzyme and the binding energy data generated using AUTODOCK programme supported its capability to attack the ester linkage on polysaccharide based vesicles.

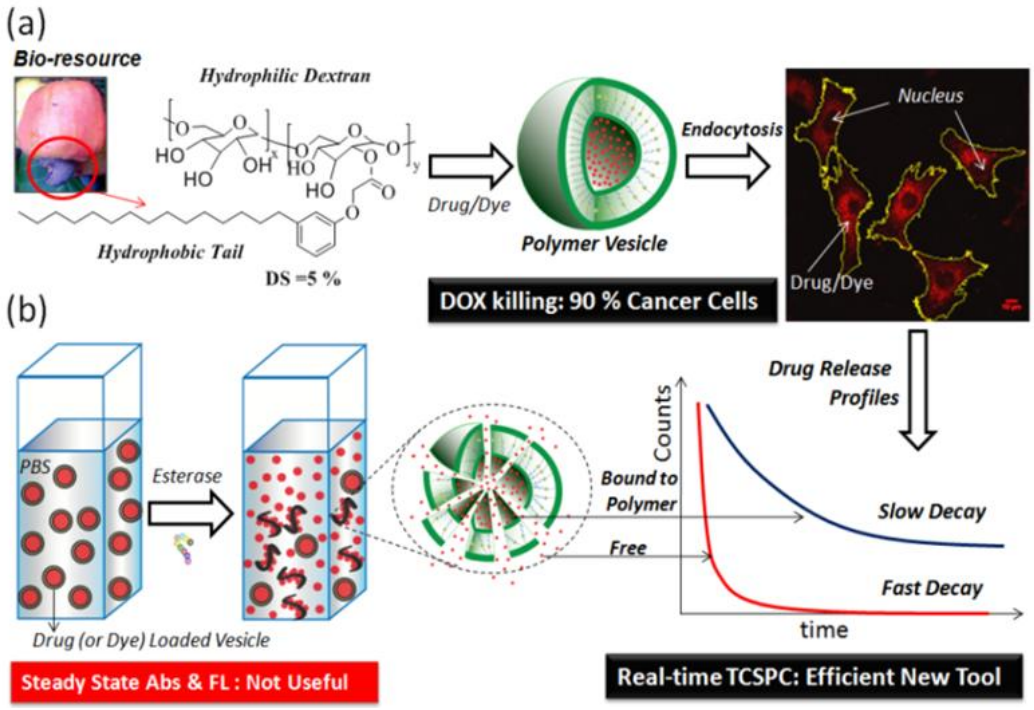

Figure 1.34: *Chemical structure of the newly designed dextran derivatives, their self assembly and cellular uptake (a) and schematics explaining the use of these vesicles for monitoring the real time drug release using TCSPC technique (b). Adopted from Pramod et al. J. Phy. Chem. B 2015, 119, 10511-10523.*

From the above discussion it was confirmed that though the polysaccharide and other synthetic polymers have been widely used for drug delivery application but the transition of these motifs to the clinical trials has not been achieved. This emphasizes the need for the development of the better drug delivery vehicles to accomplish the goal of tumor growth inhibition.

1.6 Aim of the thesis work

The detail literature survey indicates that polysaccharide nanovesicles are very unique since they are capable of encapsulating both water soluble and water insoluble anticancer drugs at the layer and core, respectively, and provide unique single polymer platform for multiple drug delivery applications. Though, many efforts have been put to study the structural aspects of the polymer vesicles; only few reports are known for their biomedical applications, more specifically in the area of drug delivery to cancers. Further, polysaccharide vesicles are one of the least explored areas due the limited availability of appropriate vesicular directors for the highly ordered sugar backbone. Earlier work from our group (by Pramod et al.) has demonstrated the usage of renewable resource 3-pendadecyl phenol derivative from cashew nut liquid as excellent choice for making dextran vesicles. In the present thesis work, the dextran vesicles were appropriately designed to address many important questions in drug delivery to cancers. The different problems addressed in the thesis and the new concepts are schematically shown in figure 1.35

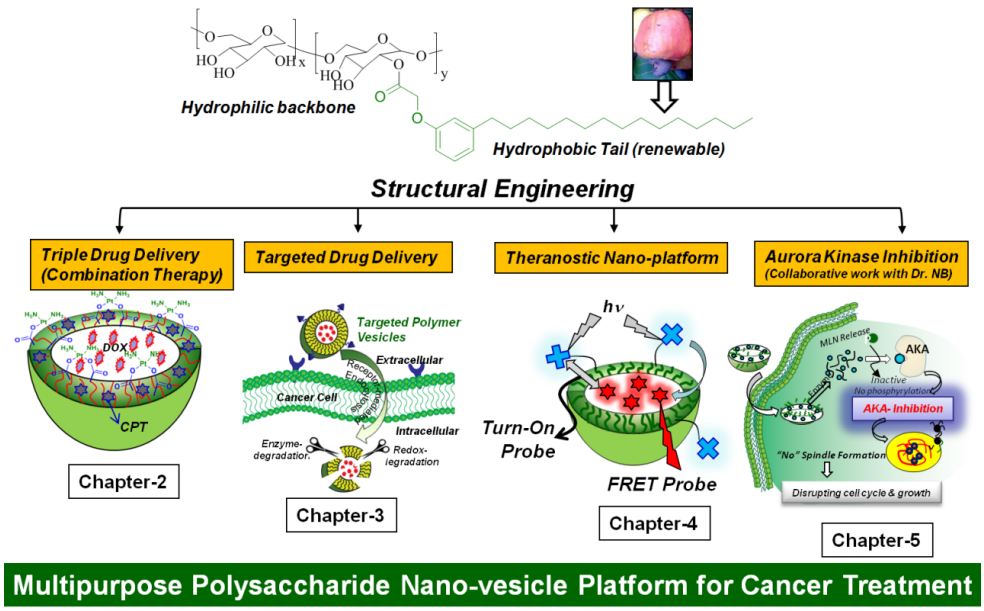

Figure 1.35: *New polysaccharide vesicular designs and problems reported in the thesis work.*

Combination therapy has become essential for the survival of breast and ovarian cancer patients and many clinical attempts are currently in progress to find suitable treatment protocols. Non-response to Pt-drug treatment by breast and ovarian cancer tisues has identified to be main cause and more than 45 % of the patients are vulnerable to metastasis in less than 10 years after the diagnosis of the disease. One of the main reason associate with the limitation in combination therapy is associated with the lack of appropriate self-assembled nano-carriers for chemical conjugation of Pt-drugs and also the encapsulation anticancer drugs of different solubility parameter in single system. Most of the Pt-drug nano-carriers are based on organic or inorganic nanoparticles and these nano-objects were inferior and not capable of encapsulating both water soluble and water insoluble anticancer drugs along with Pt-drug conjugation. In chapter 2, new "*cisplatin-stitched polysaccharide vesicle*" was created to deliver triple antagonistic drugs: cisplatin, doxorubicin (DOX) and camptothecin (CPT) together from single nano-scaffold to accomplish synergistic breast cancer treatment. Polymer nano-vesicles are excellent choice for this purpose since they are capable of loading both water insoluble (like DOX) and water soluble (like CPT) anticancer drugs in the hydrophobic layer and hydrophilic core, respectively. The custom designed new polysaccharide vesicle enabled the combination therapy of clinically important antagonistic drugs (cisplatin, DOX and CPT) together to accomplish synergistic breast cancer treatment. Receptor-mediated endocytosis of nano-carriers are emerging as one of the important approaches for targeted delivery of anticancer drugs or genes to cancer tissues. Biotin is one of the excellent targeting ligand for streptavidin (avidin class of proteins) at the cell membrane surface with high association constant in the range of 10^{13} to10^{15} M^{-1}. In chapter 3, one of the first examples of the receptor-mediated endocytosis concept based on biotin-tagged and multi-stimuli-responsive polysaccharide vesicles and the concept was successfully demonstrated in vitro by carefully designed time-dependent cellular uptake studies in cancer cells. The polysaccharide (dextran) vesicle was cleverly designed with three important components: (i) biotin-anchored at dextran backbone for receptor-mediated targeting, (ii) the high levels of glutathione (GSH) at the intracellular level (1 mM) act as redox-trigger (stimuli-1) for drug delivery, and (iii) the biodegradation of aliphatic ester linkages by the esterase enzyme in lysosomal compartments releases to release drug at

the intracellular level (stimuli-2). Thus, the polysaccharide vesicles are in-built with multi-stimuli-responsiveness for intracellular biodegradation in combination with receptor-mediated endocytosis. In chapter 4, enzyme responsive fluorescent polysaccharide vesicle were designed and developed as "Turn ON" probe and for bio-imaging purpose in cancer cells. Polysaccharide dextran backbone was decorated with a special aggregation induced emissive (AIE) fluorophore tetraphenylethene (TPE) along with vesicular director hydrophobic source pentadecyl phenol (PDP). These dextran-PDP-TPE derivatives are non-fluorescent in nature when dissolved in organic solvents where as gives blue color emission in aqueous medium. DOX loaded TPE-vesicles were constructed as intracellular turn-off to Turn-On probe for real-time monitoring of DOX release at the cellular level. FRET probe was constructed between TPE-vesicles and fluorophores such as Rhodamin-B, Nile red and Rose Bengal and their applications was demonstrated for bio-imaging in cancer cells. In chapter 5, the polymer nano-carrier concept was employed for the selective inhibition of Aurora kinase A in cancer cells. This research contribution and outcome of the investigation has shed more light on how the selective delivery of Aurora kinase inhibitors could contribute to breast cancer treatment. It also would provide a tool to differentially inhibit AKA vs AKB, helping evaluate their relative contribution to distinct cellular functional pathways. The present investigation provides first insights into the drug delivery approach based on polysaccharide vesicle platform, and the proof-of-concept is successfully demonstrated in cancer cells. The polysaccharide vesicles were made through tailor-made approaches process; thus, both the drug delivery concept and the targeted dextran vesicles are new entries for biomaterial applications. This research contribution and outcome of the investigation in the thesis is urgently required in the development of biodegradable polymer scaffold for cancer treatment.

1.7 References

1. Triggle, D. J. *Med. Princ. Pract.* **2007**, *16*, 1-14.
2. Knowles, J.; Gromo, G. *Nat. Rev. Drug Discov.* **2003**, *2*, 63-69.
3. Rosen, H.; Abribat, T. *Nat. Rev. Drug Discov.* **2005**, *4*, 381-385.
4. Hughes, J. P.; Rees, S.; Kalindjian, S. B.; Philpott, K. L. *Br. J. Pharmacol* . **2011**, *162*, 1239-1249.
5. Kola, I.; Landis, J. *Nat. Rev. Drug Discov.* **2004**, *3*, 711–715.
6. Mitagotri, S.; Burke, P. A.; Langer, R.; *Nat. Rev. Drug Discov.* **2014**, *13*, 655-672.
7. Mi, Z, H.; Burke, T. G. *Biochemistry*, **1994**, *33*, 10325-10326.
8. Taslim, A.; Hilal, A. L.; Alma, F.; Byun, Y. *Adv. Drug. Deliv. Rev.* **2013**, *65*, 845-864.
9. Yamashita, F.; Hashida, M. *Adv. Drug. Deliv. Rev.* **2013**, *65*, 139-147.
10. Ringsdorf, H. *J. POLYMER SCI.* **1975**, *51*, 135-153
11. Duncan, R. *Nat. Rev.* **2006**, *6*, 688-701
12. Zhong, Y.; Meng, F.; Deng, C.; Zhong, Z. *Biomacromoleculs* **2014**, *15*, 1955-1969.
13. Mura, S.; Nicolas, J.; Couvreur, P. *Nat. Mater.* **2013**, *12*, 991-1003
14. Matsumura, Y.; Maeda, H. *Cancer Res.* **1986,** *46*, 6387−6392.
15. Maeda, H. *Bioconjugate Chem.* **2010,** *21*, 797−802.
16. Abdalla, A. M. E.; Xiao, L. Ullah, M. W.; Yu, M.; Ouyang, C.; Yang, G. *Theranostics* **2018**, *8*, 533-549
17. Doncom, K.E.B.; Blackman, L.D.; Wright, D.B.; Gibson, M.I.; O'Reilly, R.K. *Chem. Soc. Rev*. **2017**,*46*, 4119-4134.
18. Lee, S. W.; Yun, M. H.; Geonj, S. W.; In, C. H.; Kim, J. Y.; Seo, M. H.; Pai, C. M.; Kim, S. O. *J. Controlled Release* **2011,** *155***,** 262-271**.**
19. Elsabahy, M.; Samarajeewa, S. Raymond, J. E.; Clark, C.; Wooley, K. L.; *J. Mater. Chem. B* **2013,** *1***,** 5241-5255**.**
20. Bharadwaj.,V.; Kumar Ravi, M.N.V.; Advances in Delivery Sciences and Technology, Springer, Heidelberg, 2012, 8, 493-516.
21. Gianeti, M.D.; Wagemaker, T.A.L.;Seixas, V.C.;Maiacapmos *Curr. Nanosci.* **2012**, *8*, 526-534.
22. Sinn Aw, M.; Kurian, M.; Losic, D. *Chem. Eur. J.* **2013,***19*, 12586-12601.
23. Emoto, K.; Nagasaki, Y.; Kataoka, K. *Langmuir* **1999,** *15*, 5212-5218.
24. Hsieh, Y.;Hsiao, Y.; Jan, J. *Soft Matter* **2014,** *10*, 9568-9576
25. Liu, S.;Tuan-Mu, H.; Hu, J.; Jan. J. *RSC Adv.* **2015,** *5*, 87098-87107.
26. Yu, H.; Li, J.; shi, K.; Huang, Q. *Food Funct.* **2011,** *2*, 373-380.
27. Mirsharghi, S.; Knudsen, K. D.; Bagherifam, S.; Nystrom, B.; Boas, U. *New J. Chem.* **2016,** *40*, 3597-3611.

28. Samad, A. A.; Bakkour, Y.; Fanny, C.; Omar, F. E.; Coudane, J.; Nottelet, B. *Polym. Chem.* **2015,** *6,* 5093-5102.
29. Manjili, H. K.; Sharafi, A.; Danafar, H.; Hosseini, M.; Ramazani, A.; Ghasemi, M. H. *RSC Adv.* **2016,** *6,* 14403-14415.
30. Lin, T. C.; Chen, J.; Chen, Y.; Teng, T.; Su, C.; Hsu, S. *J. Mater. Chem. B* **2013,** *1*,5977-5987.
31. Soo, P. L.; Lovric, J.; Davidson, P.; Maysinger, D.; Eisenberg, A. *Molecular Pharmaceutics* **2005,** *2,* 519-527.
32. Hu, Y.; Jiang, Z.; Chen, R.; Wu, W.;Jiang, X. *Biomacromolecules* **2010,** *11,* 481-488.
33. Talingting, M. R.; Munk, P.; Webber, S. E. *Macromolecules* **1999,** *32,* 1593-1601.
34. Qin, A.; Tian, M.;Ramireddy, C.; Webber, S. E.; Munk, P. *Macromolecules* **1994,** *27,* 120-126.
35. Khougaz, K.; Zhong, X. F.; Eisenberg, A. *Macromolecules* **1996,** *29,* 3937-3949.
36. Li, Z.; Liu, R.; Mai, B.; Feng, S.; Wu, Q.; Liang, G.; Gao, H.;Zhu, F.*Polym. Chem.***2013**, *4,* 954-960.
37. Su, M.; Wang, L.; Zhang, G.; Huang,Y.; Su, Z. *RSC Adv.* **2015,** *5,* 4350-4354.
38. Lee, E. S.; Kim, J.; Sim, T.; Youn, Y.; Lee, B.; Oh, Y. T.; Oh, K. T. *J. Mater. Chem. B* **2014,** *2,*1152-1159.
39. Liu, D.; Han, H.;Lu, H.;Wu, G.;Wang, Y.; Ma, J.; Gao, H. *RSC Adv.* **2014,** *4,* 37130-37137.
40. Liu, G.; Ma, R.; Ren, J.;Li, Z.; Zhang, H.; Zhang, Z. *Soft Matter* **2013,** *9,* 1636-1644.
41. Arimura, H.; Ohya, Y.; Ouchi, T. *Biomacromolecules* **2005,** *6,* 520-525.
42. Sill, K. N.; Sullivan, B.; Carie, A.; Semple, J. E. *Biomacromolecules* **2017,** *18,* 1874-1884.
43. Hans, M.; Shimoni, K.; Danino, D.; Siegel, S. J.; Lowman, A. *Biomacromolecules* **2005,** *6,* 2708-2717.
44. Tam, Y. T.; Gao, J,; Kwon, G. S. *J. Am. Chem. Soc.* **2016,** *138,* 8674-8677.
45. Ma. C.; Pan, P.; shan, G.; Bao, Y.; Fujita, M.; Maeda, M. *Langmuir* **2015,** *31,* 1527-1536.
46. Li, J.;Guo, S.; Wang, M.; Ye, L.; Yao, F. *RSC Adv.* **2015,** *5,* 19484-19492.
47. Mao, H.; Shan, G.;Bao, Y.; Wu, Z.; Pan, P. *Soft Matter* **2016,** *12,* 4628-4637.
48. Repollet-Pedrosa, M. H.; Mahanthappa, M. K. *Soft Matter* **2013,** *9,* 7684-7687.
49. Deng, W.; Chen, J.; Kulkarni, A.; Thompson, D. H. *Soft Matter* **2012,** *8,* 5843-5846.
50. Zhang, Y.; Song, M.;Diao, Y.; Li, B.; Shi, L.; Ran, R. *RSC Adv.* **2016,** *6,* 112468-112476.

51. Kozlov, M.; Quarmyne, M.; Chen, W.; McCarthy, T. J. *Macromolecules* **2003,** *36,* 6054-6059.
52.
53. Knop, K.; Hoogenboom, R.; Fischer, D.; Schubert, U. S. *Angew. Chem. Int. Ed.* **2010,** *49,* 6288-6308.
54. Larson, N.; Ghandehari, H. *Chem. Mater.* **2012,** *24,* 840-453.
55. Surnar, B.; Jayakannan, M. *ACS Biomater. Sci. Eng.* **2016,** *2,* 1926-1941.
56. Zhang, C.; Jin, S.; Li, S.; Xue, X.; Liu, J.; Huang, Y.; Jiang, Y.; Chen, W.; Zou, G.; Liang, X. *ACS Appl. Mater. Interfaces* **2014,** *6,* 5212-5220.
57. Yuan, Y.;Kwok, R. T. K.; Tang, B. Z.; Liu, B. *J. Am. Chem. Soc.* **2014,** *136,* 2546-2554.
58. Gunkel-Grabole, G.; Sigg, S.; Lomora, M.;Lorcher, S.; Palivan, C. G.; Meier, W.P. *Biomater. Sci.***2015,** *3,* 25-40.
59. Thambi, T.; Park, J. H.; Lee, D. S. *Biomater. Sci.***2016,** *4,* 55-69.
60. *Science* **2002,** *297,* 967-673.
61. Discher, D. E. Ahmed, F. *Annu. Rev. Biomed. Eng.* **2006,** *8,* 323-341.
62. Israelachvili, J. N.; Mitchell, D. J.; Ninham, B. W. *Biochemica et Biophysica Acta* **1977,** *470,* 185-201.
63. *Kashyap, S.; Jayakannan, M. J. Phys. Chem. B* **2012,***116,* 9820-9831.
64. Hu, X.; Zhang, Y.; Xie, Z.; Jing, X.; Bellotti, A.; Gu, Z. *Biomacrolomecules,* **2017,** *18,* 649-673.
65. Ahmed, F.; Pakunlu, R. I.; Brannan, A.; Bates, F.; Minko, T.; Discher, T. E. *J. Controlled Release* **2006,** *116,* 150-158.
66. Pattni, B. S.; Chupin, V. V.; Torchilin, V. P. *Chem. Rev.* **2015,** *115,* 10938-10966.
67. Barenholz, Y. *J. Controlled Release* **2012,** *160,* 117-134.
68. Gao, W.; Hu, C. M. J.; Fang, R. H.; Zhang, L. *J. Mater. Chem. B* **2013,** *1,*6569-6585.
69. Lee, S. M.; Nguyen, S. T.; *Macromolecules,* **2013,** *46,* 9169-9180.
70. Curcio, M.; Fernandez, B. B.; Gomez, L. D.; Concheiro, A.; Alvarez-Lorenzo, C. *Bioconjugate. Chem.* **2015**, *26,* 1900-1907.
71. Rosenblum., D.; Joshi., N.; Tao., W.; Karp., J. M.; Peer., D. Nat. Commun. 2018, 9, 1-12.
72. Pawar. P. V.; Gohil., S., V.; Jain. J.P.; Kumar., N. Polym. Chem. 2013, 4, 3160-3176.
73. Zhu, L.; Zhao, L.; Qu, X.; Yang, Z. Langmuir 2012, 28, 11988−11996.
74. Lu, L.; Zou, Y.; Yang, W.; Meng, f.; Deng, C.; Cheng, R.; Zhong, Z. *Biomacromolecules* 2015, 16, 1726−1735.
75. Du, Y.; Chen, W.; Zheng, M.; Meng, F.; Zhong, Z. *Biomaterials* 2012, 33, 7291-7299.
76. Herna´ndez, J. R.; Lecommandoux, X. *J. Am Chem. Sco* 2005, 127, 2027.

77. Yassin,M. A.; Appelhans, D.; Mendes, R.G.; Rmmeli, M. H.; Voit, B. *Chem. Eur. J*. 2012, 18, 12227 – 12231.
78. Liu, G.; Ma, S.; Li, S.; Cheng, R.; Meng, F.; Liu, H.; Zhong, Z. *Biomaterials* 2010, 31, 7575-7585.
79. Lee, J. S.; Groothuis, T.; Cusan, C.; Mink, D.; Feijen, J. *Biomaterials* 2011, 32, 9144-9153.
80. Li, Y.; Liu, G.; Wang, X.; Hu, J.; Liu, S. *Angew. Chem* 2016, 55, 1760 –1764.
81. Jia, L.; Cui, D.; Bignon, J.; Cicco, A. D.; Bakala, K. W.; Liu, J.; Li, M. H. *Biomacromolecule*s 2014, *15*, 2206-2217.
82. Zhang, W.; Zhou, X.; Li, H.; Fang, Y.; Zhanng, G. *Macromolecules* 2005, *38*, 909-914.
83. Thambi, T.; Deepagan, V. G.; Ko, H.; Lee, D.S.; Park, J. S.; J. Mater. Chem. 2012, 22, 22028-22036.
84. Deng, Z.; Qian, Y.; Yu, Y.; Liu, G.; Hu, J.; Zhang, G.; Liu, S. *J. Am Chem. Sco.* 2016, 138, 10452−10466.
85. Liu, H.; Wang, R.; Wei, J.; Cheng, C.; Zheng, Y.; Pan, Y.; He, X.; Ding, M.; Tan, H.; Fu, Q. *J. Am Chem. Sco* 2018, 140, 6604−6610.
86. Mizrahy, S.; Peer, D. *Chem. Soc. Rev.* **2011**, *41*, 2623-2640.
87. Sinha, V. R.; Kumaria, R.; *Int. J. Pharm.* **2001**, *224*, 19-38.
88. Liu, Z.; Jiao, Y.; Wang, Y.; Zhou, C.; Zhang, Z. *Adv. Drug. Deliv. Rev.* **2008**, *60*, 1650-1662.
89. Rempel, B.P.; Withers, S.G. *Glycobiology* **2008**, *18*, 570–586.
90. Mehvar, R. *Curr. Pharm. Biotechnol.* **2003**, *4*, 283–302.
91. Jian, F.; Zhang, Y.; Wang, J.; Ba, K.; Mao, R.Y.; Lai, W.L.; Lin, Y.F. *Curr. Drug Metabol.* **2012**, *13*, 440–446.
92. Kumar, M.N.; Muzzarelli, R.A.; Muzzarelli, C.; Sashiwa, H.; Domb, A.J. *Chem. Rev.* **2004**, *104*, 6017–6084.
93. Mourya, V.K.; Inamdar, N.N. Trimethyl *J. Mater. Sci. Mater. Med.* **2009**, *20*, 1057–1079.
94. Wen., Y.; Oh., J.K. *Macromol Rapid Commun*. **2014**, *35*, 1819-1832.
95. Basu., A.; Kunduru, K.R.; Abtew., E.; Domb., A.J. *Bioconjugate Chem*. **2015**, *26*, 1396-1412.
96. Mahanta., A. K.,; Mittal., V.; Singh., N.; Dash., D.; Malik., S.; Kumar., M.; Maiti, P. *Macromolecules* **2015**, *48*, 2654-2666.
97. Meng., L.; Haung., W.; Wang., D.; Haung., X.; Zhu., X.; Yan., D. *Biomacromolecules* **2013**, *14*, 2601-2610.
98. Ho. D. K.; Frisch., S.; Biehl., A.; Terriac., E.; Rossi., C., D.; Scharzkopf., K.; Lautenschlager, F.; Loretz., B.; Murgia., X.; Lehr., C.M. *Biomacromolecules* **2018**, *19*, 3489-3501.
99. Ahmad., S.; Ikram., S. *Achievements in the life Sciences* **2016,** *10*, 27-37.

100. Nakeeb., A.L.; Willersin., J.; Schmidt., B.V.K *Biomacrolecules* **2017**, *18*, 3695-3705.
101. Liu. Y.; Wang., Y.; Zhang., C.; Zhou., P.; Liu., Y.; An., T.; Sun., D.; Zhang., N.; Wang., Y. *ACS Appl. Mater. Interfaces* **2014**, *6*, 18712-18720.
102. Li., H.; Cui., Y.; Sui., J.; Bian., S.; Sun., Y.; Fan., Y.; Zhang., X. *ACS Appl. Mater. Interfaces* **2015**, *7*, 15855-15865.
103. Zhou., J.; Wali., A.R.M.; Ma., S.; He., Y.; Yue., D.; Tang., J. Z.; Gu., Z. *Biomacromolecules* **2018**, *19*, 2214-2226.
104. Mehvar, R. *J. Control. Rel.* **2000,** *69*, 1-25.
105. Raemdonck, K.; Naeye, B.; Buyens, K.; Vandenbroucke, R.E.; Hogset, A.; Demeester, J.; De Smedt, S. C. *Adv. Funct. Mater.* **2009**, *19*, 1406-1415.
106. Morais, M.; Subramanian, S.; Pandey, U.; Samuel, G.; Venkatesh, M.; Martins, M.; Pereira,S.; Correia, J. D. G.; Santos, I. *Mol. Pharm.* **2011,** *8*, 609-620.
107. Raemdonck, K.; Thienen, T.G.V.; Vandenbroucke, R.E.; Sanders, N.K.; Demeester, J.; De Smedt, S. C. *Adv. Funct. Mater.* **2008**, *18*, 993-1001.
108. Heinze, T.; Liebert, T.; Heublein, B.; Hornig, S. *Adv.Polym..Sci.* **2006**, *205*, 199-291.
109. Li., Y. L.; Zhu., L.; Liu., Z.Z.; Cheng., R.; Meng., F.; Cui., J.H.; Ji., S. J.; Zhong., Z. *Angew. Chem. Int. Ed.* **2009**, *48*, 9914-9918.
110. Wang., W.; Liu., S.; Huang., Y.; Jing., X.; Xie., Z. *J. Mater. Chem. B* **2015**, *3*, 5753-5759.
111. Li. M.,; Tang., Z.; Zhang., D.; Sun., H.; Liu., H.; Zhang., Y.; Zhnag., Y.; Chen., X. *Biomaterials* **2015**, *51*, 161-172.
112. Houga., C.; Giermanska., J.; Leccomandoux., S.; Borsali., R.; Taton., D.; Gnanou., Y.; Le Meins., J. F. *Biomacromolecules* **2009**, *10*, 32-40.
113. Pramod, P. S.; Takamura, K.; Chaphekar, S.; Balasubramanian, N.; Jayakannan, M. *Biomacromolecules* **2012**, *13*, 3627−3640.
114. Pramod, P. S.; Shah R.; Chaphekar, S.; Balasubramanian, N.; Jayakannan, M. *Nanoscale* **2014**, *6*, 11841-11855.
115. Pramod, P. S.; Shah R.; Jayakannan, M. *Nanoscale*, **2015**, *7*, 6636-6652.
116. Pramod, P. S.; Deshpande, N. U.; Jayakannan, M. *J. Phys. Chem. B* **2015**, *119*, 10511-10523

Chapter-2

Cisplatin-Stitched Polysaccharide Vesicles for Synergistic Cancer Therapy of Triple Antagonistic Drugs

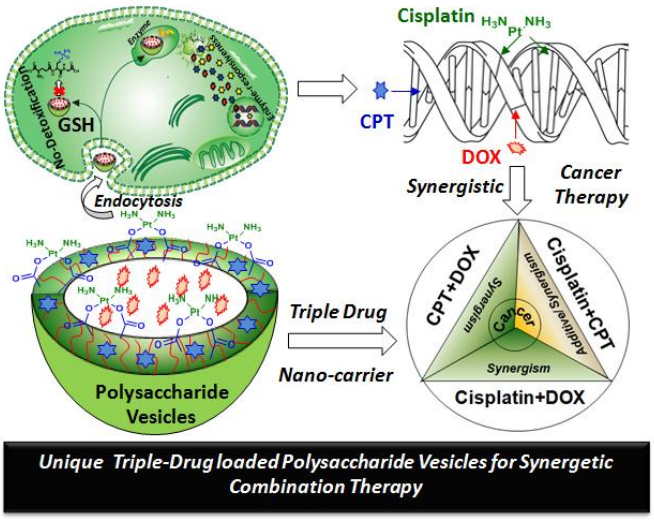

Abstract

New cisplatin-stitched polysaccharide vesicular nano-carrier is developed for combination therapy of three clinical important antagonistic drugs together to accomplish synergistic cancer therapy in breast cancer treatment. Carboxylic functionalized dextran was tailor-made for the chemical conjugation of cisplatin and renewable hydrophobic unit was anchored in the backbone to inter-digitize the chains to self-assemble as cisplatin-stitched polysaccharide nanovesicles. Water soluble DNA-intercalating drug doxorubicin.HCl (DOX) and water insoluble topoisomerase type I inhibitor drug camptothecin (CPT) were encapsulated in these vesicles to produce dual or triple drug loaded vesicular nano-carrier. This unique cisplatin, DOX and CPT triple drugs loaded dextran vesicles were stable in aqueous medium and the vesicular geometry acted as a shield for Pt-polymer drug conjugate against glutathione (GSH) detoxification under physiological conditions. Lysosomal enzymes ruptured the nano-vesicle exclusively at the intracellular compartments to deliver the combination of all three drugs simultaneously to maximize the therapeutic efficacies. In vitro cytotoxicity studies revealed that free cisplatin was highly detoxified by the GSH in breast cancer cells whereas the enhanced stability of Pt-stitched dextran vesicle against GSH facilitated ~ 99 % cell killing in breast cancer cells. Combination therapy studies revealed that the free cisplatin, DOX, and CPT were found to be antagonistic to each others. Dual drug loaded vesicles exhibited synergistic cancer cell killing while delivering these antagonistic drugs from dextran vesicular platform. Remarkable synergistic cell killing was accomplished in cisplatin, DOX and CPT triple drug loaded vesicles at nanogram concentrations in breast cancer cells. The internalization of drugs and cellular uptake were confirmed by confocal microscope and flow cytometry analysis. The drugs were taken by the cancer cells in large amounts while delivering them from dextran vesicles compared to their free form. This spectacular results opened new opportunity for synergistic cancer therapy for GSH-over expressed breast cancer using triple drug loaded polysaccharide vesicular nano-carriers.

2.1 Introduction

Combination therapies are emerging as important treatment protocol to overcome the Pt-drug resistance in breast and ovarian cancers at the second and third levels of chemotherapy to improve the patient compliance and survival against metastasis.[1,2] The inherent ability of breast cancer tissues to develop resistance against Pt-drugs directly associated with various biochemical processes including glutathione (GSH) over expression, poor uptake of the anticancer drugs, and DNA auto-repair mechanism and so on so forth.[3] Breast (also ovarian) cancer tissues are estimated to be over expressed with glutathione (GSH, 20 mM) compared to normal tissues (1.0 mM);[4-5] as a result, the highly reactive Pt-drugs were readily detoxified by the GSH through the formation of stable Pt-S bond and excreted from the cytoplasm prior to their action at the nucleus.[6-8] The absence or low expression of CTR1 protein in the cell membrane was also responsible for the poor transportation of Pt-drug. DNA auto-repairing process at the Pt-Guanine-N_7 position by NER proteins was also accounted for the cell proliferation and increasing the chances of metastasis.[9] To overcome some of these limitations, combination therapy were developed for cisplatin (CP) along with DNA specific drugs such as doxorubicin (DOX) [10-12] and paclitaxel,[13-15] etc. In one such attempt a multidrug carrier was made using the crosslink polymeric network[12]. This design includes Pt (IV) prodrug and other two drugs which are released in controlled manner from polymeric nanoparticles. The polymer structure and their drug loading schematics are shown in figure 2.1.

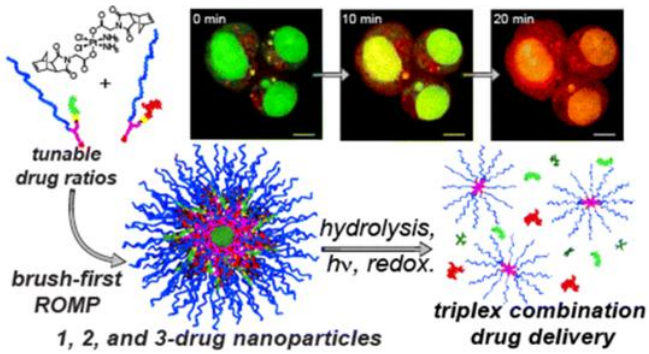

Figure 2.1: *A multidrug polymeric nanocarriers for triplex combination drug delivery to cancer cells. Adopted from Liao et al. J. Am. Chem. Soc. 2014, 136, 5896-5899.*

The cellular uptakes of the Pt-drugs were improved using small molecular nano-vectors[16-21] and polymeric nano-carriers[11-13,22-35] to accumulate them at the cancer tissues via enhanced permeability and retention (EPR) effect.[36-38] Polymer nanovesicles[39-44] (or polymersomes) and liposomes[45] are excellent choice for this purpose since they are capable of loading both water insoluble and water soluble anticancer drugs simultaneously in the hydrophobic layer and hydrophilic core, respectively. Cisplatin loaded liposomes were developed to enhance the membrane protein trafficking,[46] efficacy in triple negative breast cancer tumors,[47] and in glioma cells.[48] It was found that cisplatin encapsulation induced usual rigidity in the liposome layers; however, they were successfully taken up by the cancer cells compared to free drug.[49] Cell penetrating peptide anchored liposomes were also developed for loading and delivering of DOX in brain glioma in animals.[50-51] Zong et al prepared liposomes conjugated with cell penetrating peptide (TAT) and transferrin (T7) for transportation of the drug across the blood brain barrier and subsequent targeting of glioma. This targeting effects were evaluated both *invitro* and *invivo* and showed enhanced efficacy. The schematics of the design are showed in figure 2.2.

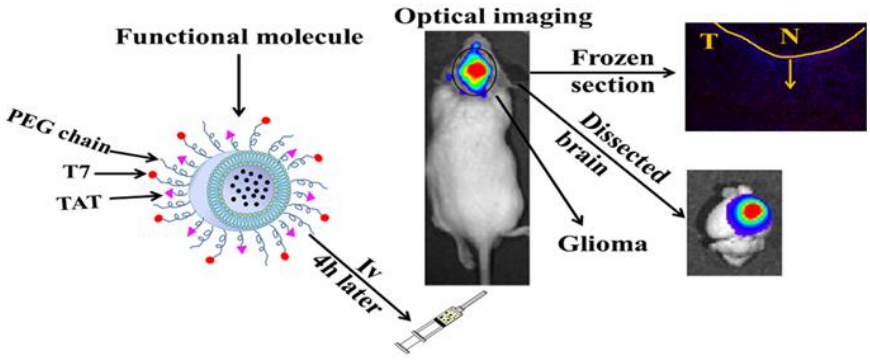

Figure 2.2: *Schematics of cell penetrating peptide (TAT) and transferrin (T7) conjugated liposomes and their invivo distribution. Adopted from Zong et al. Mol. Pharmaceutics 2014, 11, 2346-2357.*

Few attempts were also made on the co-delivery of cisplatin with other anticancer drugs to accomplish combination therapy.[52-53] Synthetic polymer vesicles are excellent nano-carriers with enhanced stability in the blood plasma and also has structural feasibility for chemical conjugation of drugs such as cisplatin in cancer treatment.[43]

However, there is no effort has been taken to deliver cisplatin along with other anticancer drugs in synthetic polymer vesicles. Thus, by designing polymer vesicular nano-scaffold with appropriate provision for cisplatin conjugation would facilitate the co-delivery of clinical important multiple anticancer drugs together from single polymer dose. Further, the combination therapy of anticancer drugs encounter several challenges prior to their application in clinical studies and few of these important problems are: (i) Pt-drug detoxification by GSH in the cytoplasm,[6,35] (ii) antagonism of cisplatin drug towards DNA intercalating drugs like DOX,[11] (iii) lack of appropriate nano-carrier design for chemical conjugation of Pt-drug along with the encapsulation of water soluble and insoluble drugs, etc. To solve this multi-task problem; it is necessary to design and develop new biodegradable and biocompatible polymer nano-carriers having competence to overcome GSH detoxification, provision for cisplatin conjugation and ability to load multiple anticancer drugs of different solubility parameters. Among the polymer structures, polysaccharides are excellent candidates due to their biocompatibility, ability to interact with the cell membrane receptors, and also provide opportunity for chemical modification and so on so forth. [44] Thus, in the present investigation polysaccharide-dextran is chosen and the new triple drug delivering polysaccharide nano-vesicle concept is shown in figure 2.3.

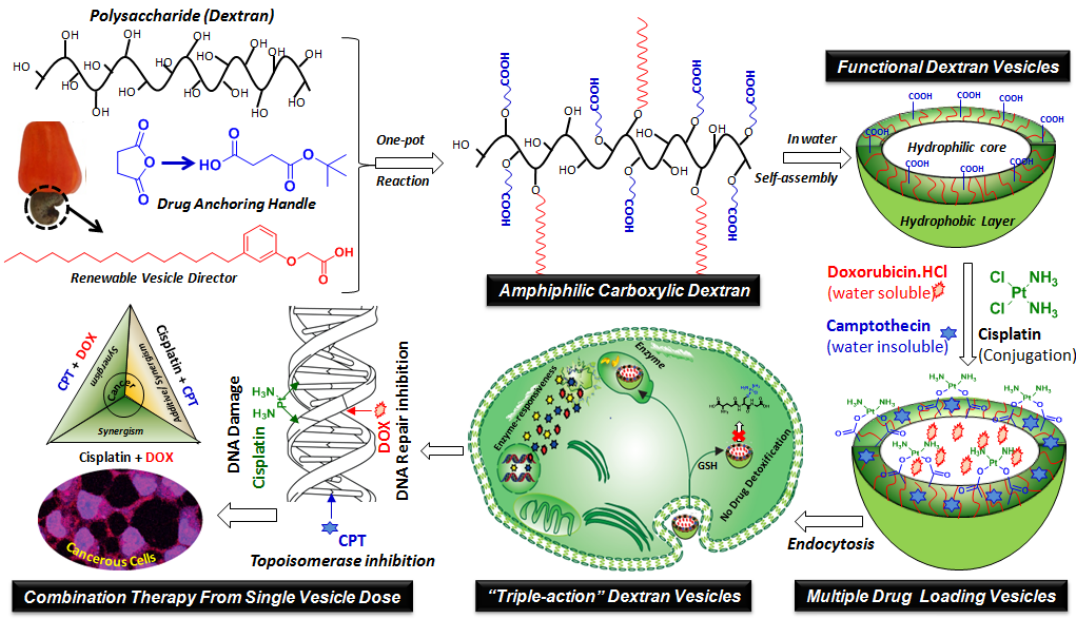

Figure 2.3: *A novel cisplatin-stitched polysaccharide vesicular nano-carrier design for the synergistic combination therapy of antagonistic drugs: cisplatin, doxorubicin.HCl and camptothecin against GSH detoxification in breast cancer treatment.*

To accomplish synergetic combination therapy of antagonistic drugs, here we have created new "*cisplatin-stitched polysaccharide vesicle*" nano-carrier and demonstrated the combination therapy of triple antagonistic drugs together from single nano-scaffold to accomplish synergistic breast cancer treatment. The new carboxylic polysaccharide vesicular design was conceived based on our previous experience in designing pH[54] and enzyme-responsive[55-58] dextran vesicles in drug delivery applications. Earlier studies from our laboratory using caveolae knock out (-) and caveolae (+) cell models revealed that these dextran vesicles are unique in transporting anticancer drugs in caveolae (-) cells similar to that of breast cancer cells.[55] Thus, the selection of dextran vesicular design is appropriate choice for exploring the triple drug delivery concept to improve the efficacies of drug-resistance breast cancer cells. Polysaccharide nanoparticles (not vesicles) based on hyaluronic acid;[59-60] heparin,[61] alginate[62] and modified dextran[63-65] were explored for cisplatin conjugation; however, up to our knowledge, no effort has been made to explore polysaccharide vesicles for the triple drug combination therapy of anticancer drugs. In the present investigation, a new class of carboxylic dextran vesicle was tailor made using renewable resource 3-pentadecyl phenol (produced from cashew nut shell liquid)[66] as vesicle director[67] and succinic acid unit was

introduced for cisplatin chemical conjugation. These cisplatin-stitched vesicles were capable of encapsulating water soluble DOX.HCl and water insoluble CPT to obtains cisplatin, DOX and CPT triple drug loaded polymer nano-vesicle. *In vitro* drug release kinetics confirmed that the cisplatin drug is preserved in the active form in the dextran vesicular scaffold against the GSH detoxification. These drug loaded vesicles were stable at extracellular conditions and they exclusively biodegraded by lysosomal enzymes at the intracellular compartments to release all three drugs. In breast cancer cells, the free cisplatin drug became ineffective due to GSH detoxification whereas the cisplatin loaded vesicle V_{CP} exhibited very good cell killing. Combination therapies were designed for the cocktail of free drugs, cocktail of individual drug loaded vesicles and dual or triple drug loaded vesicles. It was found that the free drugs were antagonistic to each other whereas the dual or triple drug loaded vesicles exhibited excellent synergistic combination therapy in breast cancer cells. Confocal microscopic imaging and flow cytometry analysis were employed to study the drug internalization and accumulation at the perinuclear environment. The present investigation opens new polysaccharide vesicular concept for the combination therapy of antagonistic drugs together to accomplish synergistic breast cancer treatment.

2.2 Experimental Section

2.2.1 Meterials: Dextran (M_w = 6,000), succinic anhydride, dicyclohexylcarbodiimide (DCC), 4-dimethylamino pyridine, 3-pentadecylphenol (PDP), triethylamine, 20-(S)-camptothecin (CPT), doxorubicin hydrochloride (DOX), Rhodamin-B, cisdiaminedichloroplatinum (II) (cisplatin, CP), silver nitrate, glutathione (GSH) and horse liver esterase enzyme were purchased from Aldrich chemicals. Wild-type mouse embryonic fibroblasts (Wt-MEFs), and human breast cancer cells (MCF-7) were maintained at 37 °C under a 5% CO_2 atmosphere as described earlier.[56] All other instrumentation details, cell viability assay, confocal microscope imaging, flow cytometry analysis procedures are given in the supporting information. Compound (**1**) in the synthetic scheme was synthesized using the procedure from our earlier report.[56]

2.2.2 General Methods: ^{1}H and ^{13}C was recorded using both 400-MHz JEOL and Bruker NMR Spectrophotometer using $CDCl_3$ or DMSOd6 containing TMS as internal

standard. FT-IR, absorption and emission spectra were recorded using Bruker alphaT Fourier transform IR spectrometer, Perkin-Elmer Lambda 45 UV-Visible spectrophotometer and SPEX Flurolog HORIBA JOBIN VYON fluorescence spectrophotometer. The size determination of the dextran derivatives were carried out by dynamic light scattering (DLS), using a Nano ZS-90 apparatus utilizing 633 nm red laser (at 90 ° angle) from Malvern instruments. The data represents the mean value from at least three independent measurements. Atomic force microscope images were recorded by drop-casting the samples on mica surface using Agilent instruments. The samples were drop casted on freshly cleaved mica surface. The imaging was carried out in tapping mode using TAP-190AL-G50 probe from Budget sensors with a nominal spring constant of 48 N/m and resonance frequency of 190Hz. FE-SEM images were recorded using Zeiss Ultra Plus scanning electron microscope. The samples for FE-SEM analysis were prepared by drop casting on silicon wafers. For TEM Analysis, the samples were prepared by drop casting on copper grid. Samples were dried for 24 hours and then imaged. For imaging the cells, LSM10 Confocal Microscope was used.

2.2.3 Synthesis of 4-(tert-butoxy)-4-oxobutanoic acid (2) : Succinic anhydride (5.0 g, 50 mmol), N-hydroxy succinimide (1.72 g, 15 mmol), triethylamine (2.0 mL, 15 mmol), tertiary butanol (8.0 mL,80 mmol) and DMAP (0.62 g, 6 mmol) were dissolved in 50 mL of dry toulene and refluxed for 24 h. Then solution was cooled and diluted with ethyl acetate (50.0 mL), washed with 10 % citric acid (2X50 ml), brine and finally dried over anhydrous Na_2SO_4 and concentrate to give brown oil. The product was purified passing over silica (100-200 mesh) column using 10% ethyl acetate:pet ether as a eluent. Yield = 2.80 g (30 %). ^{1}H-NMR (400 MHz, d_6-DMSO) δ (ppm) : 2.56 (m, **4H**), 1.36 (s, 9**H**). ^{13}C-NMR (100 MHz, $CDCl_3$) δ 178.80 (C=O acid), 171.44 (C=O ester), 81.52 (tert. carbon), 30.20, 28.90, 27.56 (primary carbons). FT-IR (KBr, cm−1), 3380 (carboxyl –OH Stretch), 2990, 2854 (aliphatic C−H stretch), 1762 (ester C=O stretch), 1208 (C(=O)-O stretch). MALDI TOF-TOF, (MW: 174.09), m/z = 213 (M + K+). HR-MS (ESI+): m/z [M + H+], calculated for $C_8H_{14}O_4$ [M+]: 175.09; found: 175.09

2.2.4 Synthesis of DEX-PDP-C5 teriary butyl ester : Dextran (M_w= 6,000, 1.0 g, 6.2 mmol of anhydroglucose unit), PDP acid (0.54 g, 1.50 mmol) and tert. butyl succinate (0.22 gm 1.26 mmol), were dissolved in anhydrous DMSO (25.0 mL) and the solution was purged with dry nitrogen. To the above content, DMAP (0.10 g, 0.84 mmol) in anhydrous DMSO (3.0 mL) and DCC (0.86 g, 4.16 mmol) in anhydrous DMSO (3.0 mL) were added. The reaction mixture was stirred for 24 hour at room temperature. The solution was filtered to remove dicyclohexyl urea and the solvent was removed under reduced pressure. The thick viscous liquid was precipitated by adding into acetone (100 mL). The solid was filtered and washed several times with acetone. It was dissolved again in DMSO and the purification via the precipitation technique was done at least twice. The product filtered out and dried under vacuum at 60 ^oC to get yellowish white solid as product. Yield = 0.77g (66 %). ^1H NMR (400 MHz, DMSOd6): δ: 7.10 ppm (s, 1H, Ar-**H**), 6.70 ppm (m, Ar-**3H**), 4.49, 4.72, 4.78 ppm (s, hydroxyl of dextran) 4.61 ppm (s, dextran anomeric proton), 3.14-3.69 ppm (dextran glucosidic protons),2.6 ppm (m,4H) methylene protons of SA, 2.49 ppm (2H, Ar-C**H**$_2$), 1.48 ppm (2H, Ar-CH_2-C**H**$_2$),1.34 ppm (s, 9H) tert. Butyl, 1.18-0.80 ppm (Aliphatic protons).^{13}C NMR(400MHz, d6-DMSO):177.2 (ester C=O), 172.41 (tert. butylester C=O),171.92 (ester C=O), 156.60, 145.97, 127.00, 120.19, 113.3, 110.2 (Ar-C), 98.40 (dextran anomeric carbon), 79.36 (tertiary carbon of tertiary butyl group), 74.41, 72.23, 70.45, 69.39, 65.6 (dextran glucosidic carbons), 65.76 (-O=C-CH_2), 35.33, 31.29, 30.67, 22.00, 13.97 (PDP Aliphatic Carbons), 28.84, 28.59, 27.61 (Aliphatic carbons of tertiary butyl succinate).

2.2.5 Synthesis of DEX-PDP-C10 tertiary butyl ester: Dextran (M_w= 6,000, 1.0 g, 6.2 mmol of anhydroglucose unit), PDP acid (0.54 g, 1.50 mmol) and tert. butyl succinate (0.32 g 1.84 mmol), were dissolved in anhydrous DMSO (25.0 mL) and the solution was purged with dry nitrogen. To the above content DMAP (0.106 g, 0.86 mmol) in anhydrous DMSO (3.0 mL) and DCC (1.08 g, 5.24 mmol) in anhydrous DMSO (3.0 mL) were added. The reaction mixture was stirred for 24 hour at room temperature. The solution was filtered to remove dicyclohexyl urea and the solvent was removed under reduced pressure. The thick viscous liquid was precipitated by adding into acetone (100 mL). The solid was filtered and washed several times with acetone. It was dissolved

again in DMSO and the purification via the precipitation technique was done at least twice. The product filtered out and dried under vacuum at 60 ^{o}C to get yellowish white solid as product. Yield = 0.80 (63 %). ^{1}H NMR (400 MHz, d_6 DMSO): δ: 7.12 ppm (s, 1**H**, Ar-**H**), 6.72 ppm (m, 3**H**, Ar-**H)**, 4.47, 4.82, 4.88 ppm (s, hydroxyl of dextran) 4.63 ppm (s, dextran anomeric proton), 3.14-3.69 ppm (dextran glucosidic protons),2.6 ppm (m,4H) methylene protons of SA, 2.49 ppm (2H, Ar-C**H**$_2$), 1.48ppm (2H, Ar-CH_2-C**H$_2$**),1.34 ppm (s, 9H) tert. butyl, 1.18-0.80 ppm (Aliphatic protons). ^{13}C NMR (400 MHz, d6 DMSO): 178.2 (ester C=O), 171.41 (tert.butyl ester C=O), 170.92 (ester C=O),157.60 143.97 ,129.00, 121.19 (Ar-5C), 98.10 (dextran anomeric carbon), 79.86 (tertiary Carbon of tertiary butyl group),73.21, 71.13, 70.25, 69.99, 65.95 (dextran glucosidic carbons), 65.46 (-O=C-CH_2), 35.03, 31.19, 30.77, 22.00, 13.97 (PDP Aliphatic Carbons), 28.94, 28.61, 27.65 (Aliphatic carbons of tertiary butyl succinate).

2.2.6 Synthesis of DEX-PDP-C20 tertiary butyl ester: Dextran (M_w= 6,000, 1.0 g, 6.2 mmol of anhydroglucose unit), PDP acid (0.54 g, 1.50 mmol) and tert. butyl succinate (0.56 g, 3.22 mmol) were dissolved in anhydrous DMSO (25.0 mL) and the solution was purged with dry nitrogen. To the above content DMAP (0.106 g, 0.87 mmol) in anhydrous DMSO (3.0 mL) and DCC (1.20 g, 5.81 mmol) in anhydrous DMSO (3.0 mL) were added. The reaction mixture was stirred for 24 hour at room temperature. The solution was filtered to remove dicyclohexyl urea and the solvent was removed under reduced pressure. The thick viscous liquid was precipitated by adding into acetone (100 mL). The solid was filtered and washed several times with acetone. It was dissolved again in DMSO and the purification via the precipitation technique was done at least twice. The product filtered out and dried under vacuum at 60 ^{o}C to get yellowish white solid as product. Yield = 0.62 g (45 %). ^{1}H-NMR (400 MHz, d_6-DMSO) δ ppm: 7.12 ppm (s, 1H, Ar-H), 6.72 ppm (m, 3H, Ar-H), 4.47, 4.82, 4.88 ppm (s, hydroxyl of dextran) 4.63 ppm (s, dextran anomeric proton), 3.14-3.69 ppm (dextran glucosidic protons), 2.6 ppm (m,4H) methylene protons of SA, 2.49 ppm (2H, Ar-C**H**$_2$), 1.48 ppm (2H, Ar-CH_2-C**H$_2$**),1.34 ppm (s, 9H) tert. butyl, 1.18-0.80 ppm (aliphatic protons). ^{13}C-NMR (100 MHz, d6-DMSO) δ (ppm) : 178.2 (ester C=O), 171.41 (tert butylester C=O),170.92 (ester C=O), 157.60, 143.97, 129.00, 121.19 (Ar-5C), 98.10 (dextran

anomeric Carbon), 79.86 (tertiary carbon of tertiary butyl group),73.21,71.13,70.25,69.99,65.95 (dextran glucosidic carbons),65.46 (-O=C-CH_2), 35.09, 31.23, 30.99, 22.58, 13.27 (PDP aliphatic carbons), 28.90, 28.66, 27.60 (aliphatic carbons of tertiary butyl succinate).

2.2.7 Synthesis of DEX-C20: Dextran (M_w= 6,000, 1.0 g, 6.2 mmol of anhydroglucose unit), tert. butyl succinate (0.56 g 3.22 mmol), were dissolved in anhydrous DMSO (25.0 mL) and the solution was purged with dry nitrogen. 4-(dimethylamino) pyridine (0.1 g, 0.82 mmol) in anhydrous DMSO (3.0 mL) and dicyclohexylcarbodiimide (0.92 g, 4.46 mmol) in anhydrous DMSO (3.0 mL) were added. The reaction mixture was stirred for 24 hour at room temperature. The solution was filtered to remove dicyclohexyl urea and the solvent was removed under reduced pressure. The thick viscous liquid was precipitated by adding into acetone (100 mL). The solid was filtered and washed several times with acetone. It was dissolved again in DMSO and the purification via the precipitation technique was done at least twice. The product filtered out and dried under vacuum at 60 ^oC to get yellowish white solid as product. Yield = 0.70 g (56 %). ^1H NMR (400 MHz, d_6 DMSO): δ: 4.47, 4.82, 4.88 ppm (s, hydroxyl of dextran) 4.63 ppm (s, dextran anomeric proton), 3.14-3.69 ppm (dextran glucosidic protons), 2.6 ppm (m, 4H) methylene protons of SA, 1.34 ppm (s, 9H) tert. Butyl. ^{13}C NMR (400MHz, d6 DMSO): 178.2 (ester C=O), 171.41 (tert.butylester C=O), 98.10 (dextran anomeric Carbon), 79.86 (tertiary Carbon of tertiary butyl group), 73.21, 71.13, 70.25, 69.99, 65.95 (dextran glucosidic carbons), 28.94, 28.61, 27.65 (Aliphatic carbons of tertiary butyl succinate)..

2.2.8 Deprotection of DEX-PDP-5 tertiary butyl ester: 0.5 gm (1.57 mmol) of DEX-PDP-5 was dissolve in 4.0 mL of dried DMSO to which 0.12 mL (1.49 mmol) of TFA was added and stirred for 4 hours. After evaporating TFA on rotary evaporator, the polymer was further purified by dialyzing against distilled water using dialysis membrane (MWCO 3500) for 24 hours, and then sample was lyophilized to get brownish colored powder. Yield = 0.31 g (65 %). ^1H NMR (400 MHz, d_6 DMSO): δ: 7.12 ppm (s, 1H, Ar-H), 6.72 ppm (m, 3H, Ar-H), 4.47, 4.82, 4.88 ppm (s, hydroxyl of dextran) 4.63 ppm (s, dextran anomeric proton), 3.14-3.69 ppm (dextran glucosidic protons), 2.6 ppm (m,4H)

methylene protons of SA, 2.49 ppm (2H, Ar-C**H**$_2$), 1.48 ppm (2H, Ar-CH$_2$-C**H$_2$**), 1.18-0.80 ppm (Aliphatic protons). ^{13}C NMR (400MHz,d6 DMSO): 176.2 (ester C=O), 170.41 (tert.butylester C=O),1690.92 (ester C=O), 158.60, 145.97, 129.00, 122.29 (Ar-5C), 98.20 (dextran anomeric Carbon), 73.29, 72.23, 70.45, 69.29, 65.75 (dextran glucosidic carbons), 64.46 (-O=C-CH$_2$), 34.03, 32.19, 31.77, 22.50, 13.47 (PDP Aliphatic Carbons), 28.44, 28.31, (Aliphatic carbons of tertiary butyl succinate

2.2.9 Deprotection of DEX-PDP-C10 tertiary butyl ester: 0.5 g (1.57 mmol) of DEX-PDP-C5 was dissolve in 4.0 mL of dried DMSO to which 0.22 mL (2.84 mmol) of TFA was added and stirred for 4 hours. After evaporating TFA on rotary evaporator, the polymer was further purified by dialyzing against distilled water using dialysis membrane (MWCO 3500) for 24 hours, then sample was lyophilized to get brownish colored powder. Yield = 0.46 g (58 %). ^{1}H NMR (400 MHz, d$_6$ DMSO): δ: 7.12 ppm (s, 1H, Ar-H), 6.72 ppm (m, 3H, Ar-H), 4.47, 4.82, 4.88 ppm (s, hydroxyl of dextran) 4.63 ppm (s, dextran anomeric proton), 3.14-3.69 ppm (dextran glucosidic protons),2.6 ppm (m,4H) methylene protons of SA, 2.49 ppm (2H, Ar-C**H**$_2$), 1.48 ppm (2H, Ar-CH$_2$-C**H$_2$**), 1.18-0.80 ppm (Aliphatic protons). ^{13}C NMR (400MHz,d6 DMSO): 178.2 (ester C=O), 171.41 (tert.butylester C=O), 170.92 (ester C=O), 157.60, 143.97, 129.00, 121.19 (Ar-5C), 98.10 (dextran anomeric Carbon), 73.21, 71.13, 70.25, 69.99, 65.95 (dextran glucosidic carbons), 65.46 (-O=C-CH$_2$), 35.31, 31.22, 30.57, 22.58, 13.77 (PDP Aliphatic Carbons), 28.84, 28.11, (Aliphatic carbons of tertiary butyl succinate).

2.2.10 Deprotection of DEX-PDP-C20 tertiary butyl ester: 0.5 g (1.57 mmol) of DEX-PDP-C20 was dissolve in 4.0 mL of dried DMSO to which 0.39 mL (5.04 mmol) of TFA was added and stirred for 4 hours. After removing TFA on rotary evaporator, the polymer was further purified by dialyzing against distilled water using dialysis membrane (MWCO 3500) for 24 hours, and then sample was lyophilized to get brownish colored powder. Yield = 0.32 g (72 %) ^{1}H-NMR (400 MHz, d$_6$ DMSO) δ: 7.12 ppm (s, 1H, Ar-H), 6.72 ppm (m, 3H, Ar-H), 4.47, 4.82, 4.88 ppm (s, hydroxyl of dextran) 4.63 ppm (s, dextran anomeric proton), 3.14-3.69 ppm (dextran glucosidic protons), 2.6 ppm (m, 4H) methylene protons of SA, 2.49 ppm (2H, Ar-C**H**$_2$), 1.48 ppm (2H, Ar-CH$_2$-C**H$_2$**), 1.18-

0.80 ppm (Aliphatic protons). ^{13}C-NMR (100 MHz, d_6-DMSO) δ (ppm): 176.2 (ester C=O),169.41 (tert.butylester C=O),170.92 (ester C=O), 155.60, 145.97, 130.00, 121.32 (Ar-5C), 98.20 (dextran anomeric Carbon), 73.26, 71.58, 70.85, 69.29, 65.66 (dextran glucosidic carbons), 65.48 (-O=C-CH_2), 35.23, 31.58, 30.70, 22.58, 13.80 (PDP aliphatic carbons), 28.74 and 28.31 (aliphatic carbons of tertiary butyl succinate

2.2.11 Deprotection of DEX-C20 tertiary butyl ester: 0.5 g (1.57 mmol) of DEX-PDP-C20 was dissolve in 4.0 mL of dried DMSO to which 0.39 mL (5.04 mmol) of TFA was added and stirred for 4 hours. After evaporating of TFA on rota vap, the polymer was further purified by dialyzing against distilled water using dialysis membrane (MWCO 3500) for 24 hours, and then sample was lyophilized to get brownish colored powder. Yield = 0.31 g (70 %). ^{1}H NMR (400 MHz, DMSOd6): δ: 4.47, 4.82, 4.88 ppm (s, hydroxyl of dextran) 4.63 ppm (s, dextran anomeric proton), 3.14-3.69 ppm (dextran glucosidic protons), 2.6 ppm (m, 4H) methylene protons of SA. ^{13}C NMR (400MHz, DMSOd6): 178.2 (ester C=O), 171.41 (tert. butyl ester C=O), 170.92 (ester C=O), 98.52 (dextran anomeric Carbon), 73.81, 71.83, 70.85, 69.69, 65.85 (dextran glucosidic carbons), 28.64, 28.61, (Aliphatic carbons of tertiary butyl succinate).

2.2.12 Preparation of aquated cisplatin [Pt $(NH_3)_2(OH_2)_2]^{2+}$: The aquated cisplatin was synthesized following the reported procedure.[35] For the synthesis of aquated cisplatin, 20 mg (0.066 mmol, 1 equiv) of cisplatin was dissolved in 20.0 mL of H_2O. To this solution, 22.5 mg (0.132 mmol, 2 equiv) of silver nitrate was added with continuous stirring at 37 °C for 24 hours. The resulting milky white silver chloride precipitate confirmed the aquated cisplatin formation. The precipitate was removed by centrifuging at 10,000 rpm for an hour followed by filtration using a 0.45 μm filter. The obtained solution was then lyophilized to get light green colored powder which was stored at 4 °C.

2.2.13 Synthesis of polymer-cisplatin Conjugate: The procedure for cisplatin conjugation to DEX-PDP-C20 is explained in detail. DEX-PDP-C20 (20 mg) polymer was dissolved in 4 mL NaOH (1 mg / mL) solution and left for stirring at 37 ^{o}C for 30 minutes. This was followed by addition of the aquated cisplatin (3.4 mg, 0.012 mmol) to the prepared activated polymer solution and stirred it for another 48 hours at 37 ^{o}C in the

dark. The solution was dialyzed (MWCO=3500) against distilled water for 2 days with periodically changing water to remove the un-encapsulated molecules. The solution from the dialysis bag was filtered through 0.4 µm filter, lyophilized and stored at 4 °C. FT-IR (KBr, cm−1): 3300, 2920, 2880, 1660, 1560, 1395, 1360, 1090, 1050, 930, 830 and 548. (Please see figure 2.9 for FT-IR)

A similar procedure was followed to make cisplatin stitched DEX-PDP-C5 and DEX-PDP-C10 derivatives. The drug loading efficiency (DLE) and drug loading content (DLC) were determined by using OPD colorimetric assay from the equations as reported earlier[35].

2.2.14 Preparation of Drug encapsulated Dextran nanovesicles: Typically 0.2 mg of the drug and 10 mg of DEX-PDP-C20 polymer were dissolved in 1ml of DMSO and 1ml of milli-q water was added slowly for 30min. The resulting solution was stirred for 12 hours and then extensively dialysed (MWCO:3500) against milli-Q water to remove any unencapsulated drug molecule. Dialysed solution was then filtered through 0.4 µm filter,lyophilised and used for the further experiments. To determine drug loading content and encapsulation efficiency, 1 mg of freeze-dried drug loaded polymer was dissolved in 1.0 mL of DMSO. A total of 100 µL of this solution was diluted to 3.0 mL with DMSO and the absorbance at 480 nm was measured on UV−visible spectrophotometer. The amount of drug encapsulated in the vesicles was determined using the respective molar extinction coefficients of the drugs. Molar Extinction coefficient for doxorubicin and camptothecin in water are 11500 and 11250 L mol^{-1} cm^{-1} respectively[47] for the determination of DLC and DLE. For making double and triple loaded samples a similar procedure was followed.

2.2.15 *In Vitro* Drug release studies for Cisplatin: Cisplatin loaded vesicles were taken in a dialysis bag (in 3 mL) and they were immersed in 100 mL beaker and dialyzed at 37 °C with constant stirring. At specific time intervals, 1.0 mL of the dialysate was withdrawn and replaced with an equal volume of fresh buffer (or) saline. The amount of molecule (or drug) released in each aliquot was measured using OPD colorimetric assay by using absorption spectroscopy[35] to quantify their percentage of cumulative release.

Cumulative release (%) = C_n x V_o / m x 100, where C_n is amount of loaded cargo in n^{th} sample, V_o is total volume and m is total amount loaded in vesicles. For esterase assisted release studies 10 units of enzyme was used, above mentioned procedure was followed for calculation of cumulative release.

2.2.16 *In Vitro* Drug Release Studies for DOX.HCL and CPT: Dialysis method was adopted to monitor the in vitro release profile of DOX and CPT from DEX-PDP-20 nano-vesicles. Briefly, 3.0 mg DEX-PDP-20/ DEX-PDP-C20-CP vesicles encapsulated with DOX.HCL or CPT was dispersed in 3.0 mL of PBS and placed in a dialysis tube. The tube was dipped in 100 mL of phosphate buffer saline maintained at pH 7.4 were taken in a beaker and incubated at 37 °C. At predetermined time intervals, 3.0 mL of solution was taken out and replaced with equal volume of fresh PBS. Absorbance of the each of the solution taken out has been measured and amount of the DOX.HCl and CPT released were calculated using Beer's law. For esterase assisted drug release studies, the same protocol was followed with the addition of 10 U esterase enzymes into the dialysis bag.

2.2.17 Cell Viability Assay and Cellular imaging: To recognize the internalization of drugs and their consequent toxicities, drug-loaded vesicles and polymers alone were exposed to human cells. While the cell viability experiment was carried out using wild type mouse embryonic fibroblast (WT-MEF) cells and human breast cancer (MCF 7) cell line (using MTT Assay), the MCF-7 cells were employed to understand drug localization in cells. For MTT assay (tetrazolium salt, 3,4,5-dimethylthiazol-2,5-diphenyltetrazolium bromide assay) 96-well plate were seeded with 1000 cells per well in 100 µL of complete DMEM and allowed to grow for 16 hours. Cells were treated with six different concentrations of the drug and respective drug loaded vesicles. A blank control in the absence of compound was used in each experiment. After 72 hours of incubation, the media from the cells were removed and they were treated with 100 µL freshly prepared MTT solution (0.5 mg/ mL in complete media) and incubated for another 4hours at 37 °C. MTT solution was removed from the wells and the formed formazan crystals were dissolved by adding 100 µL DMSO to each well and the absorbance was immediately measured using micro plate reader at 570 nm. The data represents the mean value from at

least three independent measurements. The relative percentage values, with respect to control, were calculated for drug, the vesicle alone and drug-loaded vesicles. On the other hand to examine the cellular internalisation of the free drugs and drug loaded vesicles, MCF 7 cells were seeded at a density of 1×10^5 cells on cover slips placed in 6 well-plates containing complete DMEM medium and incubated at 37 °C for 16 h. After 16 hours the cells were treated with the optimum concentration of drug alone and drug loaded vesicles and then incubated for next 4 hours in CO_2 atmosphere. After 4 hours incubation, the drug-containing medium was removed from each well, and cells were washed two times with 1X PBS (2 ×1 mL) and then fixed with 4% paraformaldehyde solution in PBS for 10 min at room temperature. The cells were again washed twice with 1X PBS (2 × 1 mL) and stained with DAPI solution in PBS. After incubation for 2 min, at room temperature in the dark, the excess dye was removed by washing the cells with 1X PBS for 1 min. The cover slips were then mounted on slides using Fluoromount™ mounting medium (Southern Biotech) and dried overnight at room temperature in the dark. The cells were imaged using a confocal microscope using the λ = 420 nm (blue channel) and λ = 560 nm (red channel) lasers. Image J software was used for processing and analyzing the images.

2.2.18 Flow Cytometry Measurements: To further confirm the cellular uptake of the nano-vesicles in the human breast cancer cells (MCF 7) flow cytometry experiment was done as follows: cells were seeded in 6-well plate at a density of $1*10^5$ cells in each well containing complete DMEM media and then incubated for 16 hour at 37°C. After 16 hour, the cells are treated free DOX and DOX loaded vesicles and incubated for 9 hour. After 9 hour, the media was removed from the each well and then each well was washed with 1X PBS (2 mL) to remove any unwanted impurity. The cells were detached using 0.5 mL of trypsin enzyme with 1 min of incubation. The cell suspension in the media was centrifuged at 10,000 rpm for 5 min and then the pellet was resuspended in 1 mL of 1X PBS and taken for Flow cytometry studies. The studies were carried out by using the BD LSRFortessa SORP cell analyzer which is equipped with five lasers and can detect 18 colours simultaneously. The 561 nm laser was used for the excitation of DOX

and the band pass filter was chosen as 610 ± 10 nm. The fluorescence histograms were recorded from a population of 10000 cells.

2.3 Results and Discussion

2.3.1 Dextran-Cisplatin Vesicular Conjugates

Amphiphilic dextran was synthesized using renewable hydrophobic carboxylic functionalized 3-pentadecyl phenol (PDP) derivative (**1**) and mono t-butyl ester of succinic acid (SA) (**2**) as shown in Figure 2.4. The compounds **1** and **2** were substituted in the dextran backbone via aliphatic ester linkage so that these chemical linkages could be readily cleaved at the intracellular level by lysosomal enzymes to deliver the drugs.[35,56] The de-protection of succinic t-butyl ester yielded amphiphilic dextran having hydrophobic PDP unit along with carboxylic functional groups, DEX-PDP-Cx, where Cx represents the amount of carboxylic units.

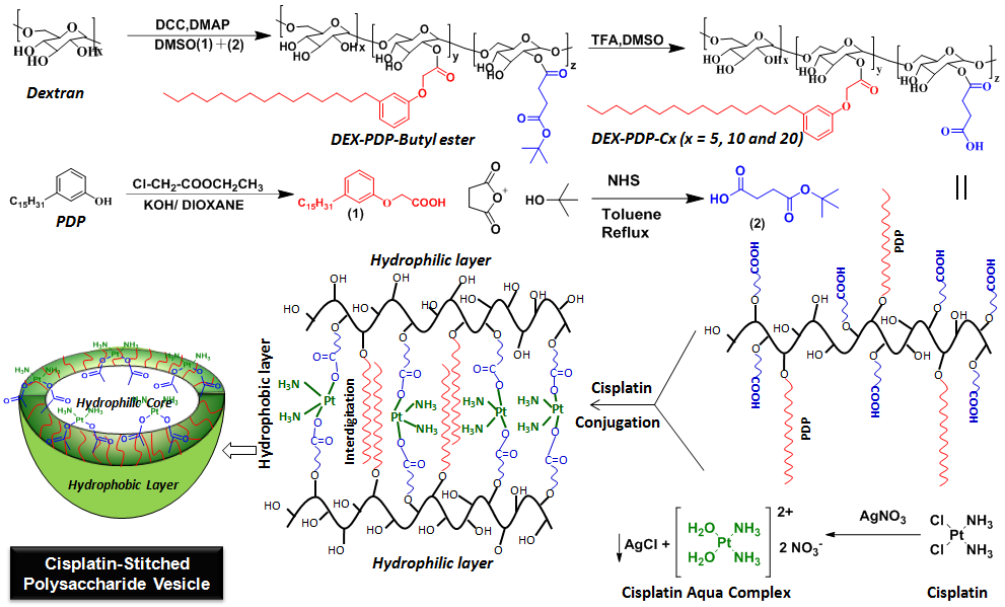

Figure 2.4: *Synthesis of PDP and carboxylic substituted amphiphilic dextran derivatives and cisplatin conjugation to produce Pt-stitched polysaccharide vesicles.*

The substitution of the PDP and SA units on the dextran backbone was confirmed by ^{1}H-NMR, ^{13}C-NMR and 2D NMR HSQC experiments. As shown in figure 2.5 and 2.6, the structure of newly designed dextran derivatives and respective peaks are assigned alphabetically in their ^{1}H NMR and ^{13}C NMR respectively. The degree of substitution of hydrophobic unit (PDP) on dextran back bone was calculated by comparing the peak intensities of the anomeric protons in dextran at 4.62 ppm and PDP aromatic protons at

7.2 ppm. The degree of substitution for tertiary butyl succinate unit on dextran back bone was calculated by comparing the peak intensities of the anomeric protons in dextran at 4.62 ppm and tertiary butyl protons at 1.34 ppm. Disappearance of tertiary butyl group (shown by green arrow) confirms the deprotection of the polymer. Similarly in ^{13}C NMR, peak at 27.68 ppm and 79.52 ppm corresponding to tertiary

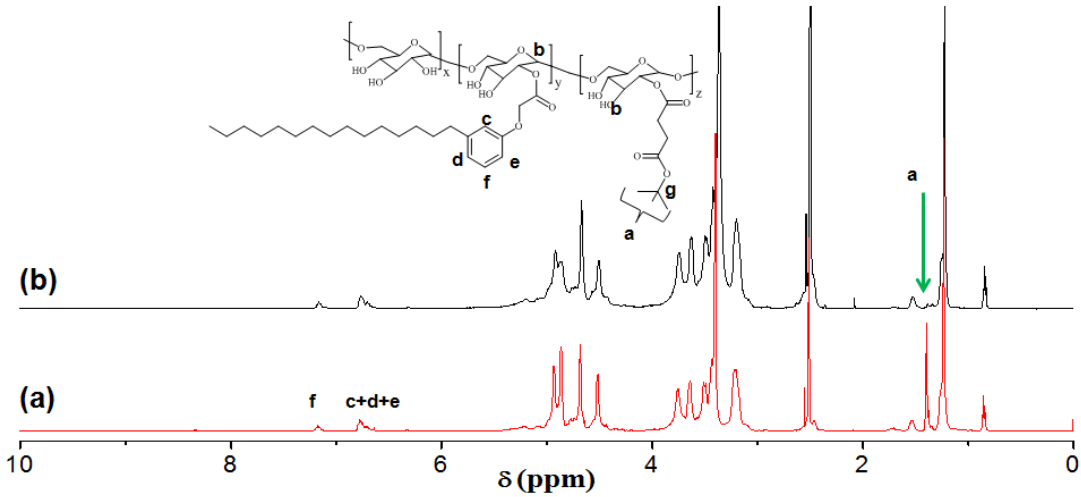

***Figure 2.5**: ^{1}H NMR of DEX-PDP-20 tertiary butyl ester (a) DEX-PDP-C20 and (b). ^{1}H NMR were recorded in DMSOd6.*

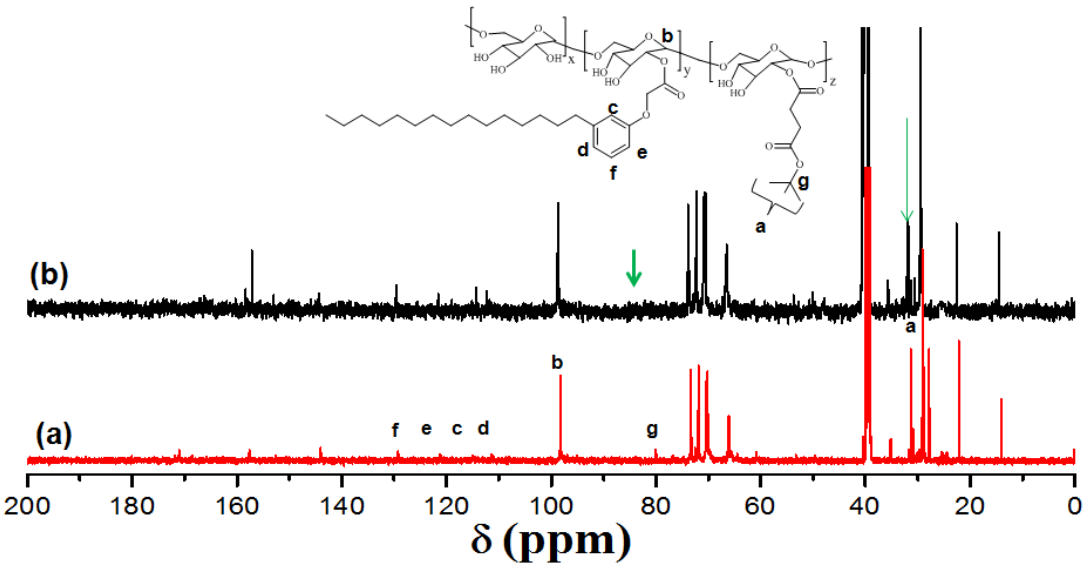

***Figure 2.6:** ^{13}C NMR for DEX-PDP-20 tertiary butyl ester (a), DEX-PDP-C20 (b). 13C NME was recorded in DMSOd6.*

butyl group and the tertiary carbon of tertiary butyl group are vanished up on TFA deprotection confirmed the deprotection of the polymers. The disappeared peaks are shown by green arrows. Further to assess the correlation between the tertiary butyl group protons and carbons, a 2D HSQC NMR experiment was carried out and spectrum is showed in figure 2.7. The counter marked as "a" in the spectrum corresponds to methyl groups of the -C-$(CH_3)_3$ which comes in ^{13} C NMR at 27.62ppm has correlation with protons at 1.38 ppm in ^{1}H NMR Spectrum. This correlation between the carbon and proton of tertiary butyl groups in the newly designed dextran derivatives validates the substitution of this group on dextran backbone. The PDP-acid (**1**) was fixed and the amount of SA-derivative (**2**) was varied to produce different amount of carboxylic units in the dextran backbone. From the ^{1}H-NMR spectra, the degree of substitution in dextran was estimated as 5 % of PDP (fixed in all samples) and the SA contents were varied as 5, 10 and 20 %.

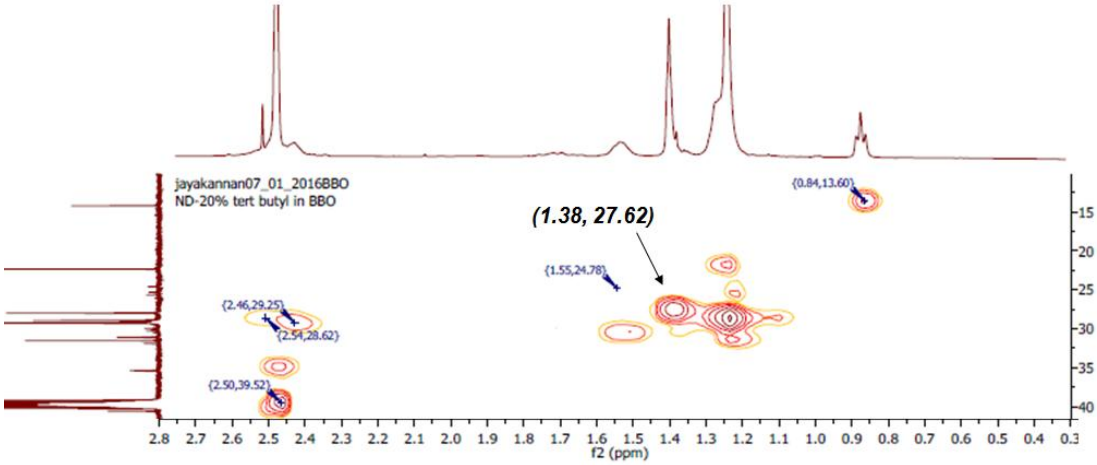

Figure 2.7: *2D HSQC NMR of DEX-PDP-C20 tertiary butyl ester showing the correlation between protons and carbons of tertiary butyl group.*

These samples were named as DEX-PDP-C5, DEX-PDP-C10 and DEX-PDP-C20. At higher PDP (> 5 %) and SA contents (> 20 %); the dextran samples were found to be insoluble or partially soluble in water and not useful for drug delivery. Additionally two dextran derivatives were also prepared having 5 % PDP alone (named DEX-PDP) or 20 % SA alone (named as DEX-C20) to study the role of the substitution on the self-assembly of dextran derivatives. Synthetic scheme and their NMR spectrum are shown in figure 2.8 and 2.9.

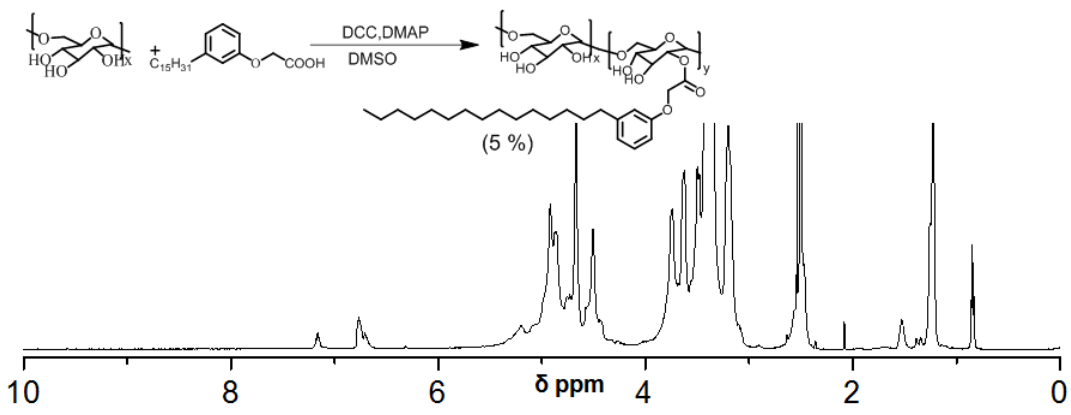

Figure 2.8: *Synthetic scheme and ^{1}H NMR for DEX-PDP.*

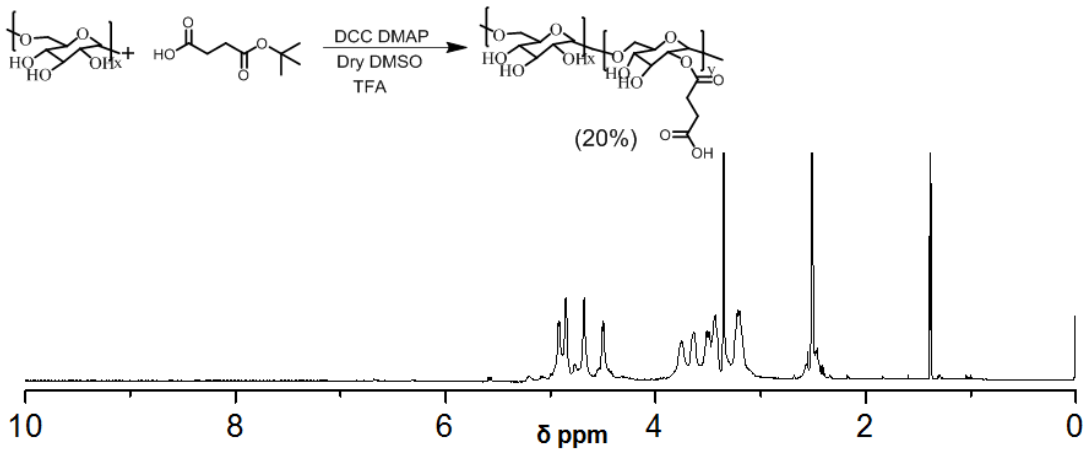

Figure 2.9: *Synthetic scheme and ^{1}H NMR for DEX-C20tertiary butyl ester.*

To assess the thermal stability dextran derivatives and study the effect of PDP substitution of amorphous nature of dextran, thermo gravimetric (TGA) and differential scanning calorimetry (DSC) analysis was carried out and the thermograms are showed in figure 2.10. From the TGA plot it was observed that these formed dextran derivatives are thermally stable up to 250 °C and they were also found to be amorphous as can be seen from DSC plot. The cis-diamine-diaquo-platinum (II) complex was produced by treating cisplatin with $AgNO_3$ in Milli-Q water and removed the resultant AgCl precipitate by filtration (see Figure 2.4).[35] The cisplatin aqua complex was reacted with sodium salt of DEX-PDP-C-X (X= 5, 10 and 20) in deionised water for 48 hours in dark. The ratio of cisplatin aqua complex to carboxylic acid groups in DEX-PDP-Cx was kept as 1.0: 1.1

(in mole %) to ensure the complete Pt-drug conjugation in the dextran derivative. The resultant dextran-cisplatin conjugate was filtered through 0.45 µm filter and lyophilized and stored at 4 ^{o}C under dark.

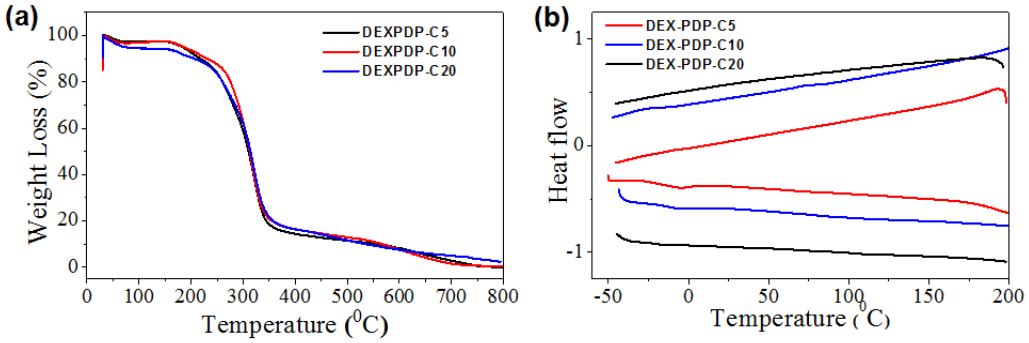

Figure 2.10: *A theromograms showing TGA for DEX-PDP-C5,10 and 20 (a), thermogram showing DSC for DEX-PDP-C5,10 and 20 (b).*

FT-IR is the most widely used technique to confirm the cisplatin conjugation, hence FT-IR analysis was carried out for both cisplatin conjugated dextran derivatives and acid functionalised dextran derivatives and the spectra are showed in figure 2.11. In spectrum of DEX-PDP-C20, where dextran has carboxyl functional group as well as ester functional group showed a distinct peak at 1740 cm-1 corresponding to ester –C=O peak. But upon complexation with cisplatin aquo complex DEX-PDP-C20-CP (V_{CP}) displayed a discrete stretching band at 1650 cm^{-1} with respect to Pt-O-C=O stretching frequency of carboxylic acid functional group. Additionally, a distinct peak at around 480 cm^{-1} corresponding to the Pt–O (metal alkoxide) bond stretching was clearly visible in the drug–polymer conjugate. This experiment confirmed the cisplatin conjugation on the dextran backbone. The drug loading content (DLC) and the drug loading efficiencies (DLE) of the polymer-cisplatin conjugates were determined using orthophenylenediamine colorimetric assay and given in figure 2.10 . The DLC for dextran-cisplatin conjugates were obtained as 3.5 %, 5.2 % and 9.3 % for DEX-PDP-C5, DEX-PDP-C10, DEX-PDP-C20, respectively (DLEs are obtained as 46 %, 61 % and 55 % for DEX-PDP-C5, DEX-PDP-C10, DEX-PDP-C20, respectively). Statically, two carboxylic acid units can be coordinated at each Pt-centre; thus, the DLC values indicate that almost all the carboxylic acids are coordinated to the cisplatin residues.

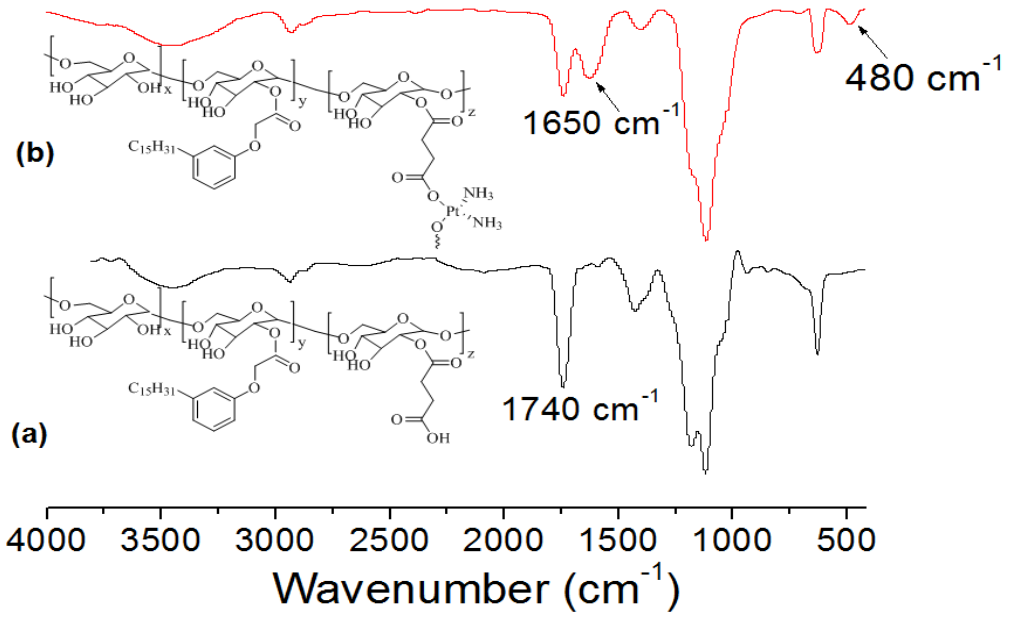

Figure 2.11: FT-IR spectra of the DEX-PDP-C20 and DEX-PDP-C20-CP.

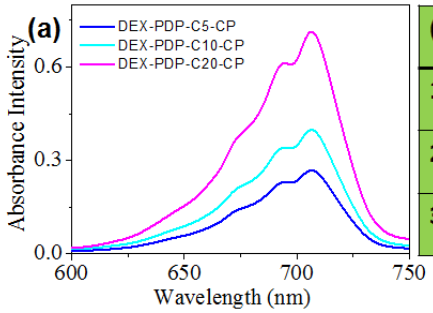

(b) S.No	Polymers	DLC (%)
1	DEX-PDP-C5-CP	3.5
2	DEX-PDP-C10-CP	5.2
3	DEX-PDP-C20-CP	9.3

Figure 2.12: *Absorbance plot of OPD colorimetric assay for determining the cisplatin content (a) and drug loading content (DLC) table for different cisplatin stitched dextran vesicles (b).*

2.3.2 Aqueous Self Assembly

To study the self-assembly of the dextran derivatives, the polymer samples were dissolved in DMSO + water and subjected to dialysis using semi-permeable membrane with MWCO = 3000 g/mol. The dextran samples DEX-PDP-C5 and DEX-PDP-C20 were found to produce stable aqueous clear polymer solution (see the figures 2.11 a and b). Dynamic light scattering (DLS) analysis of these aqueous polymer solution exhibited mono-model distribution with good autocorrelation with respect to the formation of

uniform size distribution of nano-aggregates of diameter < 200 nm (see Figures 2.11 a and b). The cisplatin stitched DEX-PDP-C20 sample also showed mono-modal distribution with 180 nm size nano-objects indicating that the cisplatin conjugation did not alter the size of the nano-assemblies in water (see Figure 2.11 c). AFM is a very powerful tool to differentiate the polymers vesicles from other nano-objects.[57] AFM images of DEX-PDP-C5 and DEX-PDP-C20 are shown in figures 2.11 d and 2.11 e , the AFM image for DEX-PDP-C10 is showed in figure 2.12 a

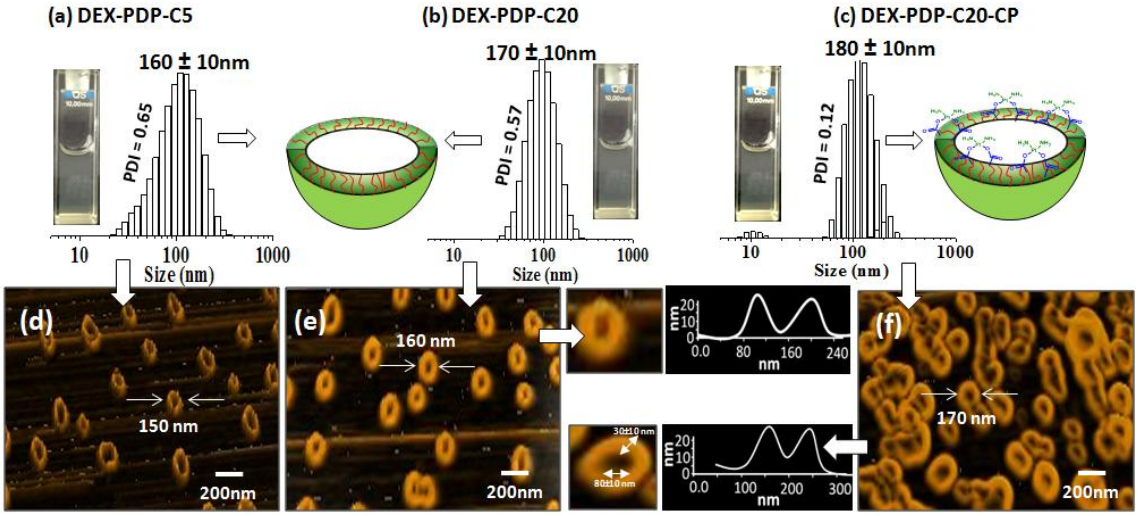

Figure 2.11: *DLS histograms of DEX-PDP-C5 (a), DEX-PDP-C20 (b), and cisplatin conjugated DEX-PDP-C20 (c). AFM images of DEX-PDP-C5 (d), DEX-PDP-C20 (e), and cisplatin conjugated DEX-PDP-C20 (f).. The photographs of vials showed the dextran vesicles. Concentration of the samples was maintained as 0.1mg/mL for DLS and 0.05mg/ml for AFM imaging.*

The PDP and carboxylic substituted dextran samples showed donut-shaped images with respect to the formation of vesicles. The tendency for the vesicular scaffold formation was not disturbed by the various amounts of SA units from 5 to 20 %. The dextran-cisplatin conjugate DEX-PDP-C20 also exhibited the formation of vesicles confirming that the new dextran design is very unique in preserving the vesicular geometry even after the chemical conjugation of drugs (see figure 2.11 f). The height profiles of the images showed typical two hump profiles with respect to the vesicles (see figures 2.11 d to 2.11 f). The average sizes of the vesicles were calculated from AFM images and they were determined to be 160 ± 10 nm; 170 ± 10 nm and 180 ± 10 nm for DEX-PDP-C5; DEX-PDP-C20 and cisplatin conjugated DEX-PDP-C20, respectively.

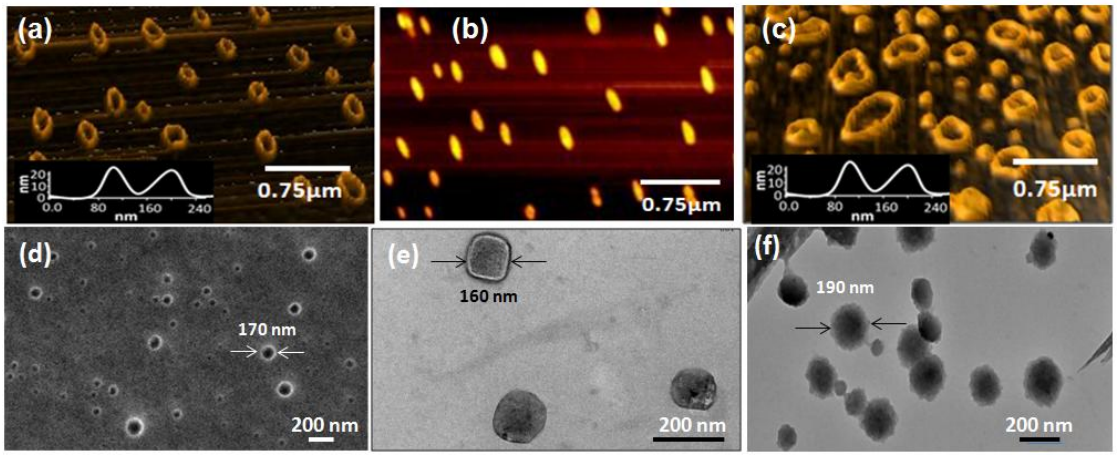

Figure 2.12: *AFM images of DEX-PDP-C10 (a), DEX-C20 (b) and DEX-PDP (c), FESEM image of DEX-PDP-C20 (d), HR-TEM image of DEX-PDP-C20 (e), and HR-TEM image of cisplatin conjugated DEX-PDP-C20 (f) The concentration used for imaging is 0.1 mg/mL.*

AFM image of SA alone substituted dextran derivative DEX-C20 (without PDP) was found to be nanoparticle rather than vesicles is showed in figure 2.12 b and PDP alone substituted dextran sample DEX-PDP (without SA unit) exhibited vesicular geometry is showed in figure 2.12 c. This trend clearly supports that the introduction of the PDP units is very much crucial for the formation of carboxylic dextran vesicles as shown in figure 2.4. This PDP hydrophobic tail forms a bilayer in the aqeous solution and this bilayer folds to form the vesicular geomerty. During the cisplatin conjugation, the smaller succinic acid units present in the hydrophobic layer behave as anionic ligands to stitch the cisplatin aquo-complex without disturbing the vesicular geometry (see Figure 2.11 c). The FESEM image for DEX-PDP-C20 showed the formation of spherical nano objects of 170 ± 20 nm (see figure 2.12 d). HR-TEM image of DEX-PDP-C20 sample showed formation of spherical nano-vesicles with distinct layer and core and directly evident for the formation of vesicular assemblies[55] (see figure 2.12 e). HR-TEM image of cisplatin conjugated of DEX-PDP-C20 sample also showed spherical shapes and dark contrast for the presence of cisplatin metal-particles (see figure 2.12 f). Based on the DLS studies and morphological characterization by AFM, FESEM and HRTEM; it can be conformed that the newly designed carboxylic dextran vesicles are very unique in producing vesicular geometry and retaining its shape and size even after the cisplatin conjugation. The DEX-PDP-C20 has highest amount of carboxylic acid substitution and

it also showed higher DLC values for cisplatin content compare to all other samples. Thus for all further discussion, the cisplatin conjugated dextran vesicle DEX-PDP-C20 is used and it is referred as V_{CP} (V- vesicle and CP- cisplatin). The polymer vesicular assemblies are very unique nano-structures that they can encapsulate water soluble dye like Rhodamin-B in the inner hydrophilic cavity unlike other nano-objects such as nanoparticles or micelles.[48] The photographs of vials in figure 2.13 clearly indicate that the dextran vesicles DEX-PDP-Cx could able to load both Rh-B whereas the DEX-SA (without PDA substitution) nanoparticles did not load Rh-B. Further, the vesicles DEX-PDP-Cx were also found to load water insoluble dye Nile red in the hydrophobic layer (see figure 2.13). The size of the Rh-B loaded DEX-PDP-C20 showed mono-model distribution with diameters < 200 nm and its AFM images confirmed the retaining of the vesicular geometries (see figure 2.13).

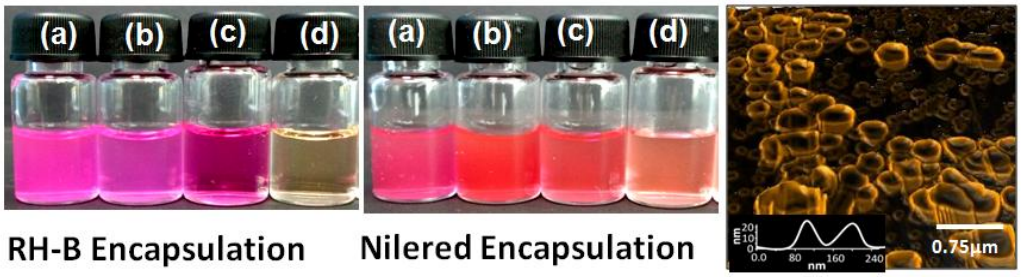

Figure 2.13: *Photographs of vials showing the Rhodamin-B and Nile red encapsulation for (a) DEX-PDP-C5 (b) DEX-PDP-C10 (c) DEX-PDP-C20 (d) DEX-C20. AFM morphology of Rh-B loaded DEX-PDP-C20 Vesicles.*

Among all the samples the DEX-PDP-C20 seems to be excellent candidates for loading both water soluble and insoluble dyes; thus, it was chosen for further studies. As evident from the loading capabilities of dextran vesicular structures for both water soluble and water insoluble molecules; two anticancer drugs with different solubility are chosen for encapsulation. Water insoluble drug camptothecin (CPT, type-I topoisomerase inhibitor) and water soluble drug doxorubicin.HCl (DOX.HCl, type-II topoisomerase inhibitor and DNA intercalating agent) were chosen to load in DEX-PDP-C20 vesicle. These vesicles are referred as V_{DOX} and V_{CPT} for DOX and CPT loading, respectively. Dual drug loaded vesicles $V_{CP\text{-}DOX}$ and $V_{CP\text{-}CPT}$ were prepared by encapsulating DOX and CPT in $V_{CP.}$ Dual drug loaded $V_{DOX\text{-}CPT}$ was prepared by loading DOX and CPT together in DEX-PDP-C20. The DLCs of individual drug loaded vesicles V_{DOX} and V_{CPT} were

obtained as 1.2 % and 0.8 %, respectively (DLEs = 68 % and 43 % for DOX and CPT). DLCs of dual drug loaded vesicles $V_{CP\text{-}DOX}$ were obtained as 9.0 % and 1.3 % for CP and DOX, respectively (DLE = 54 % and 73 % for CP and DOX); $V_{CP\text{-}CPT}$ were obtained as 9.5 % and 0.6 % for CP and CPT, respectively (DLE = 56 % and 43 % for CP and CPT); and $V_{DOX\text{-}CPT}$ were obtained as 1.8 % and 0.5 % for DOX and CPT, respectively (DLE = 65 % and 43 % for DOX and CPT). From the DLC values, cisplatin to DOX ratio was obtained as 7.0 : 1.0; cisplatin to CPT ratio as 16 : 1.0; and DOX to CPT as 3.6 : 1.0 in dual loaded dextran vesicles. Since DOX and CPT are luminescent drugs, the drug loaded vesicles were subjected to photophyical studies (see figure 2.14 a and c). Absorbance and emission spectra of V_{DOX} and $V_{CP\text{-}DOX}$ were almost identical whereas $V_{DOX\text{-}CPT}$ exhibited features of both CPT and DOX chromophores. Similarly the vesicular samples V_{CPT} and $V_{CP\text{-}CPT}$ were also exhibited CPT absorption and emission spectra showed in figure 2.14 a and b

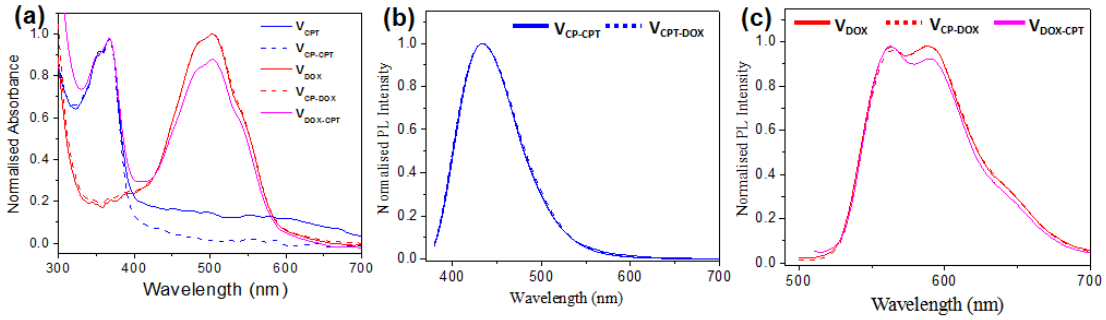

Figure 2.14: *Absorbance spectrum of V_{CPT}, $V_{CP\text{-}CPT}$, V_{DOX}, $V_{CP\text{-}DOX}$ and $V_{DOX\text{-}CPT}$ (a), emission spectrum of CPT loaded vesicles i.e., $V_{CP\text{-}CPT}$ and $V_{DOX\text{-}CPT}$ (b) and emission spectrum of V_{DOX}, $V_{CP\text{-}DOX}$ and $V_{DOX\text{-}CPT}$ (c).*

The photographs of vials containing V_{DOX} and $V_{CP\text{-}DOX}$ exhibited red-color and $V_{DOX\text{-}CPT}$ showed magenta color with respective to their photophyical characteristics (see figure 2.15). The dual drug loaded $V_{DOX\text{-}CPT}$ did not exhibit any energy transfer process from CPT to DOX upon excitation at the CPT confirming that the optical purity of drugs were retained in the vesicular scaffold as showed in figure 2.14. DLS histograms of these drug loaded samples showed the formation of vesicles of < 150 nm (see figure 2.15). AFM images confirmed their vesicular geometry with respect to the donut shaped spherical objects as showed in figure 2.15.

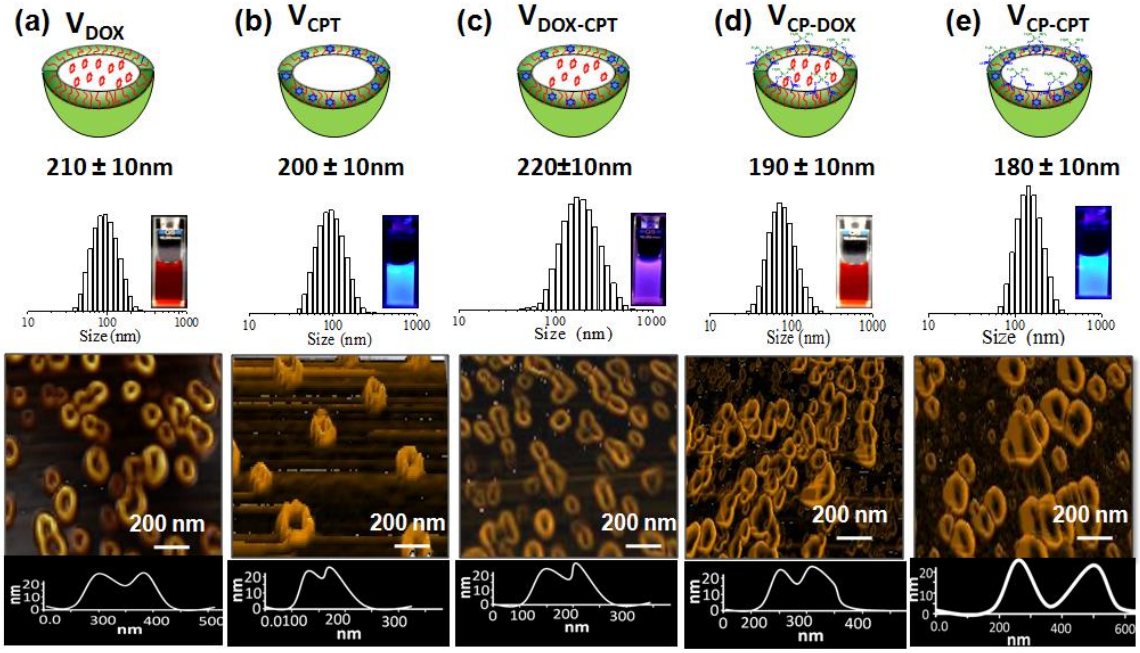

Figure 2.15: *Schematics of vesicles, DLS histograms, AFM morphology and photographs of the vials of drug loaded vesicles V_{DOX} (a), V_{CPT} (b), $V_{DOX\text{-}CPT}$ (c), $V_{CP\text{-}DOX}$ (d), and $V_{CP\text{-}CPT}$ (e). Concentration of the samples was maintained as 0.1mg/mL for DLS and 0.05mg/ml for AFM imaging.*

This revealed that the custom designed carboxylic dextran vesicles are unique classes nano-carriers: (i) it has ability to conjugate cisplatin drug, (ii) capable of loading water soluble drug DOX.HCl, (iii) able to encapsulate water insoluble drug CPT, and (iv) it also exhibited excellent capability of dual drug loading of these three drugs in a single vesicular-carrier.

2.3.3 GSH Detoxification and Enzyme Responsiveness

Pt-based pro-drugs encounter three important challenges under the physiological conditions as shown in figure 2.16 a: (i) undesirable cleavage of Pt-OOC bond by the chloride and other ions present in the plasma or saline, (ii) Pt-drug detoxification by GSH, and (iii) lysosomal enzyme-responsiveness to release the Pt-drugs. The in vitro stability of the cisplatin-polymer drug conjugates were tested in phosphate buffer saline (PBS) and water at 37 °C by dialysis method. The cisplatin is conjugated at the polymer backbone through Pt-OOC-polymer bond which is susceptible to cleave by ions such as Cl^- in saline (or PO_4^{2-} in PBS) to produce free cisplatin drug

(destabilization of drug).[68] The extracellular conditions estimated to have [Cl^-] = 100 mM which is much higher compared to the intracellular environment, [Cl^-] = 3 - 20 mM.[6] Hence, it is important to test the stability of V_{CP} in saline [Cl^-] = 154 mM) which is the regular carrier medium for the intracellular administration of drugs in chemotherapy. To test this process, the polymer-drug conjugate was dispersed in saline (also in PBS) and it was subjected to incubation in semi-permeable membrane of MWCO= 3500 g/mol. Cisplatin aliquots were collected in the reservoir and subjected to *o*-phenylenediamine (OPD) colorimetric assay to estimate the cumulative drug release. The cisplatin stitched dextran vesicles V_{CP} showed > 90 % stability both in saline and water at 37 °C (see figure 2.17 b). In PBS, the dextran-cisplatin conjugates were found to break < 20 % of the cisplatin due to decHeLation by phosphate ions (PO_4^-) in the PBS.[60] This study confirmed that the V_{CP} preserved the Pt-polymer conjugation in saline for intravenous administration against the attack of the ions. Reaction of GSH with cisplatin is known to produce the S–Pt (see Figure 2.16 a) bond that could be monitored by absorption spectroscopy.[6,35] Both free cisplatin and oxaliplatin were employed as references to study the GSH reaction with pt-residues. Oxaliplatin is represents the small molecular prodrug counter part for polymer-cisplatin conjugates. The GSH reaction with dextran-cisplatin conjugate (or with cisplatin and oxaliplatin) was carried out in 0.1 mM Tris-HCl buffer by incubating at 37 °C for 12 h under dark.[35] The UV–Vis absorbance spectra of the reaction product of free cisplatin with GSH are shown in figure 2.16 b. Similar experiment was carried out with cisplatin analogue, oxaliplatin which mimics the polymer drug conjugate design and the data is shown in figure 2.16 c. Both cisplatin and oxaliplatin reacted with GSH and produced a new absorbance peak at 260 nm with respect to the formation of the Pt–S bond. Interestingly, the reaction product of GSH with V_{CP} vesicles showed negligible absorption at 260 nm for Pt-S bond as showed in figure 2.16 d. The extent of the reaction of GSH with cisplatin, oxaliplatin and V_{CP} were determined form absorbance spectra and plotted in figure 2.16 e. These plots showed that both free cisplatin and oxliplatin readily detoxified by GSH and more than 95 % of the drugs became inactive. On the other hand, the dextran-cisplatin conjugate V_{CP} was protected from detoxification against GSH and only < 20 % drug was detoxified. This

experiment is clearly evident for the unique capability of dextran vesicular structure for shielding the cisplatin-polymer conjugate from the GSH detoxification under physiological conditions.

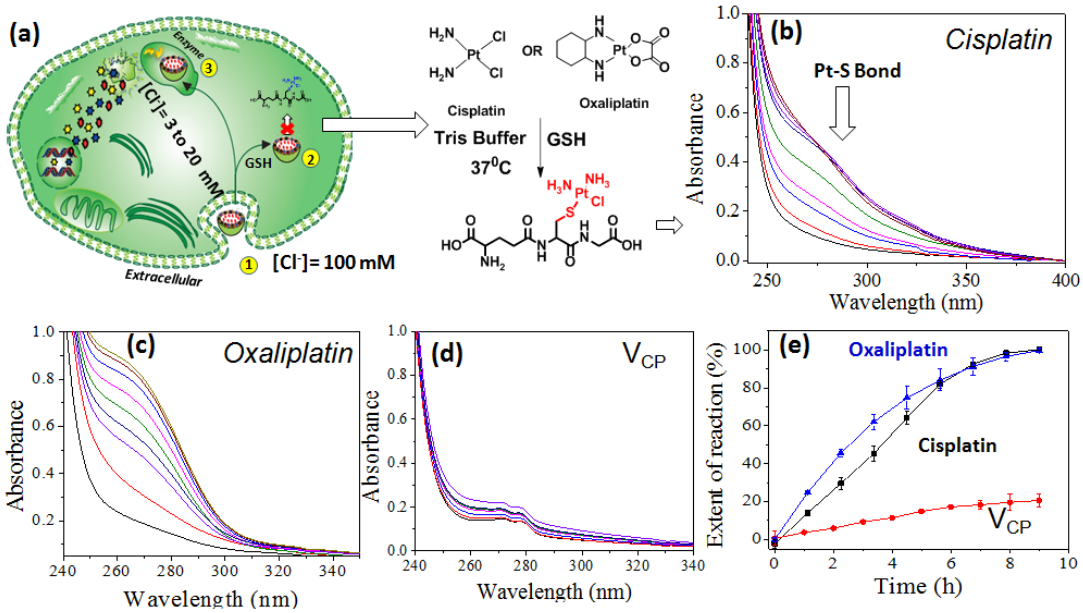

Figure 2.16 *Schematic representation of fate of dextran vesicle in the extracellular and intercellular level (a), Absorbance spectra of reaction with 10 mM GSH in tris-buffer (pH = 7.4) at 37 ℃ for cisplatin (b), fro oxaliplatin (c) and for V_{CP} (d). The plot of extent of reaction of free cisplatin and oxaliplatin and V_{CP} over time. Concentration of the free cisplatin and V_{CP} used for GSH detoxification is 30 µg.*

The PDP and SA units in the dextran vesicle were connected via aliphatic ester linkages in the dextran backbone. Aliphatic ester linkages are biodegradable in enzyme rich lysosomal compartment;[57,35] thus, the enzyme-responsiveness of dextran vesicles in releasing drugs was investigated in pH = 7.4 at 37 °C. The *in vitro* kinetics were performed both in the presence of 10 U of esterase enzyme and in the absence of enzyme and their release profiles are shown in figures 2.17 b, c and d. The amount of the cisplatin released was monitored by OPD colorimetric assay and the release of DOX and CPT were estimated directly by measuring their absorption. In figure 2.17 b, the dextran-cisplatin conjugate exhibited good stability and exhibited ~ 20 % leaching in PBS. Up on exposure to esterase enzyme, the vesicles were ruptured to release the cisplatin drug more than 70 % (see Figure 2.17 b). A similar trend was observed for DOX and CPT release

from V_{DOX} and V_{CPT} in PBS (~ 30 %) and more than 85 % release in the presence of enzyme (see figure 2.17 c).

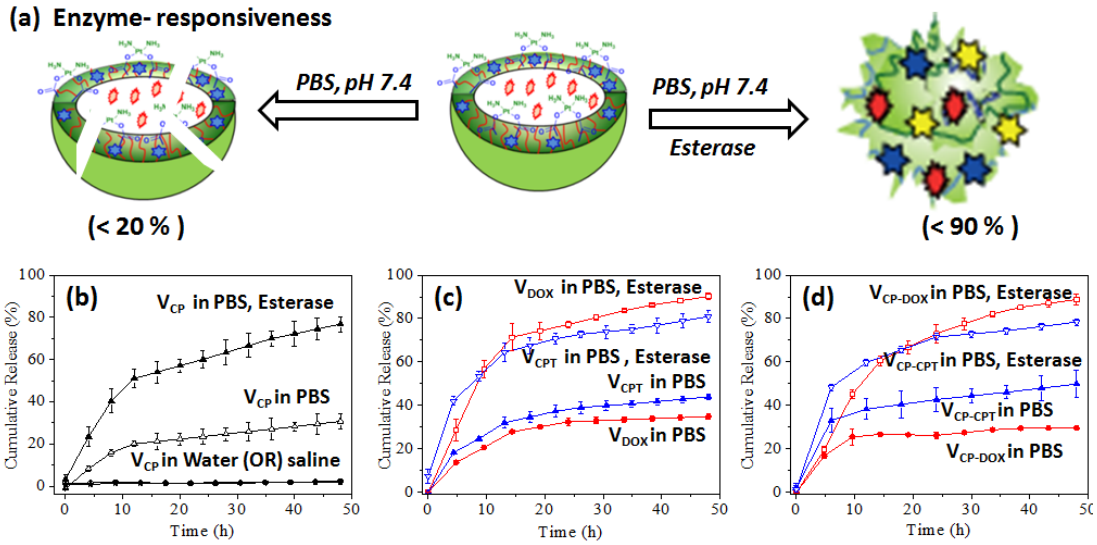

Figure 2.17: *Schematics of vesicles cleavage in PBS at pH7.4 and in the presence of esterase enzyme at pH 7.4 (a), Cumulative release of cisplatin from V_{CP} in PBS (pH= 7.4), saline (pH= 6.9), distilled water (pH = 7.0) at 37 ℃ and in the presence of esterase 10 U in PBS PBS (pH= 7.4) at 37 ℃ (b), Cumulative drug release of V_{DOX} and V_{CPT} in PBS (pH= 7.4) at 37 ℃ in the absence and in the presence of esterase enzyme 10 U (c), Cumulative drug release of dual loaded $V_{CP\text{-}DOX}$ and $V_{CP\text{-}CPT}$ in PBS (pH= 7.4) at 37 ℃ in the absence and in the presence of esterase enzyme 10 U(d). Concentration of the doxorubicin and Camptothecin used for enzyme responsive release experiments 42 ± 10 µg and 24 ± 10 µg, respectively.*

The DOX release from the dual loaded vesicle $V_{CP\text{-}DOX}$ (see figure 2.17 d) seems to be same as that of the V_{DOX} indicating that the reputing of dextran vesicles by the enzyme followed almost identical kinetics in both dextran vesicles and well as dextran-cisplatin vesicles. The release for the CPT trend from V_{CPT} and $V_{CP\text{-}CPT}$ (see figures 2.17 d) was also appeared to be almost identical to that of the DOX release in the presence of esterase enzyme. Based on the above *in vitro* release studies; it may be concluded that the enzymatic release of the physically loaded drugs like CPT and DOX as well as the chemically conjugated cisplatin followed identical release kinetics for single and dual drug loaded forms. This observation proves that these dextran vesicles can be cleaved exclusively in the presence of enzyme to release the drugs at the intracellular compartments.

2.3.4 Combination Therapy and Synergistic Effect

Two cell lines having large difference in the GSH content were chosen to test ability of the cisplatin conjugated dextran vesicles against GSH detoxification. Breast cancer cells (MCF 7) have 20 times over-expression of GSH (in 20 mM) compared to wild-type mouse embryonic fibroblasts (WT-MEFs, normal cells, [GSH] = 0.5 to 1.0 mM).[4-5] The cytotoxicity of the nascent dextran vesicles were checked in WT-MEF and MCF 7 cell lines and the data exhibits > 95 % cell viability up to 80 µg/ mL as can be seen from 2.18. Cytotoxicity of free cisplatin, DOX and CPT drugs and their drug loaded vesicles V_{CP}, V_{DOX} *and* V_{CPT} were tested and the data is shown in Figures 2.19 a to f. In WT-MEF (normal cell) cell line, the V_{CP} was found to be less toxic (< 50 %) compared to the free cisplatin that exhibited > 90 % cell killing (see Figure 2.19 a). Similarly V_{DOX} and V_{CPT} were also found to be relatively less toxic (< 60 %) to normal cells compared to their free drugs (see Figures 2.19 b and c). This is an important observation since vesicle loaded drugs are less toxic to normal cells which is more desirable for cancer therapy. In breast cancer cell line (MCF 7), free cisplatin drug was highly detoxified by GSH content in the cytoplasm and only < 50 % killing was achieved. On the other hand, V_{CP} was very stable against GSH attack and this property facilitated > 95 % cell growth inhibition killing by V_{CP} with IC_{50} at 1.0 µg/ mL. Similarly, the V_{DOX} and V_{CPT} also exhibited better cell killing in MCF-7 while delivering them from dextran vesicles compared to their free form.

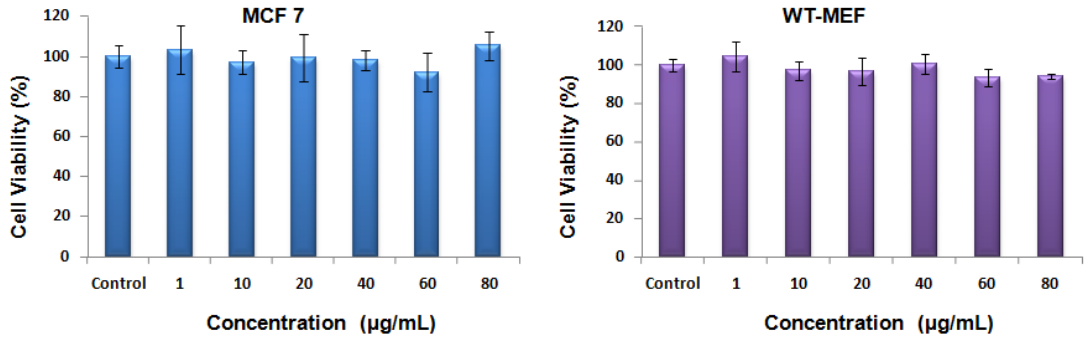

Figure 2.18: *Plots showing cytotoxicity of DEX-PDP-C20 in MCF 7(a) and in WT-MEF cell lines (b)*

These studies emphasized the need for the encapsulation of DOX and CPT and also the chemical conjugation of cisplatin in the dextran vesicles for higher cell growth

inhibition in breast cancer cells. Cytotoxicity of free cisplatin, DOX and CPT drugs and their drug loaded vesicles V_{CP}, V_{DOX} *and* V_{CPT} were tested and the data is shown in Figures 2.19 a to f. In WT-MEF (normal cell) cell line, the V_{CP} was found to be less toxic (< 50 %) compared to the free cisplatin that exhibited > 90 % cell killing (see Figure 2.19 a). Similarly V_{DOX} and V_{CPT} were also found to be relatively less toxic (< 60 %) to normal cells compared to their free drugs (see Figures 2.19 b and c). This is an important observation since vesicle loaded drugs are less toxic to normal cells which is more desirable for cancer therapy. In breast cancer cell line (MCF 7), free cisplatin drug was highly detoxified by GSH content in the cytoplasm and only < 50 % killing was achieved. On the other hand, V_{CP} was very stable against GSH attack and this property facilitated > 95 % cell growth inhibition killing by V_{CP} with IC_{50} at 1.0 µg/ mL. Similarly, the V_{DOX} and V_{CPT} also exhibited better cell killing in MCF-7 while delivering them from dextran vesicles compared to their free form.

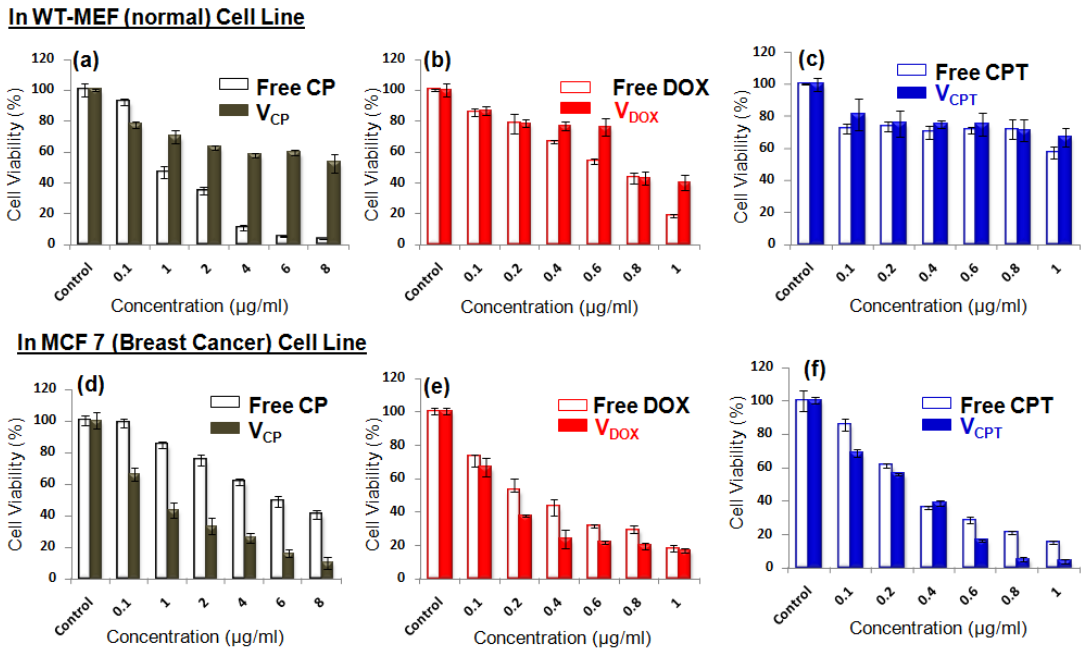

Figure 2.19: *Histograms depicting the cytotoxicity of free drugs along with* V_{CP} *(a),* V_{DOX} *(b) ,* V_{CPT} *(c) in Wt-MEF cells and cytotoxicity of* V_{CP} *(d),* V_{DOX} *(e),* V_{CPT} *(f) in MCF 7 cells.*

To study the dextran vesicles in cisplatin combination therapy; the dual drug loaded samples $V_{CP\text{-}DOX}$, $V_{CP\text{-}CPT}$ and $V_{DOX\text{-}CPT}$ were employed. The cytotoxicity experiments

were tested in cisplatin resistant human breast cancer MCF-7 cells. Cytotoxicity studies for the dual loaded vesicles i.e. $V_{CP\text{-}DOX}$, $V_{CP\text{-}CPT}$ and $V_{DOX\text{-}CPT}$ were carried out at various concentrations and the data is summarized in Figures 2.20 a to f. Since, the weight ratios of the drugs in the dual drug loaded vesicles have inherent compositions of 7.0 : 1.0 for CP vs DOX; 16 : 1.0 for CP vs CPT ; as 3.6 : 1.0 for and DOX vs CPT; a similar drug ratios were retained for the cocktails of individual drug loaded vesicles and for free drugs. The combination drug treatment was tested for the dual loaded vesicles along with cocktail of individual drug loaded vesicles and free drugs and the data is shown in figures 2.20 a to f. The comparison of data in figures 2.20 a and d revealed that IC_{50} was accomplished by dual loaded $V_{CP\text{-}DOX}$ much better compared to their cocktails V_{DOX} + V_{CP} and also that of free CP+DOX. Similar results were obtained for the $V_{CP\text{-}CPT}$ versus V_{CPT} + V_{CP} (see Figures 2.20 b and e) and $V_{DOX\text{-}CPT}$ versus V_{DOX}+V_{CPT} (see Figures 2.18 c and f). The results obtained from the cytotoxicity data clearly revealed that the dual loaded vesicles better in exhibiting cell killing compared to their cocktails.

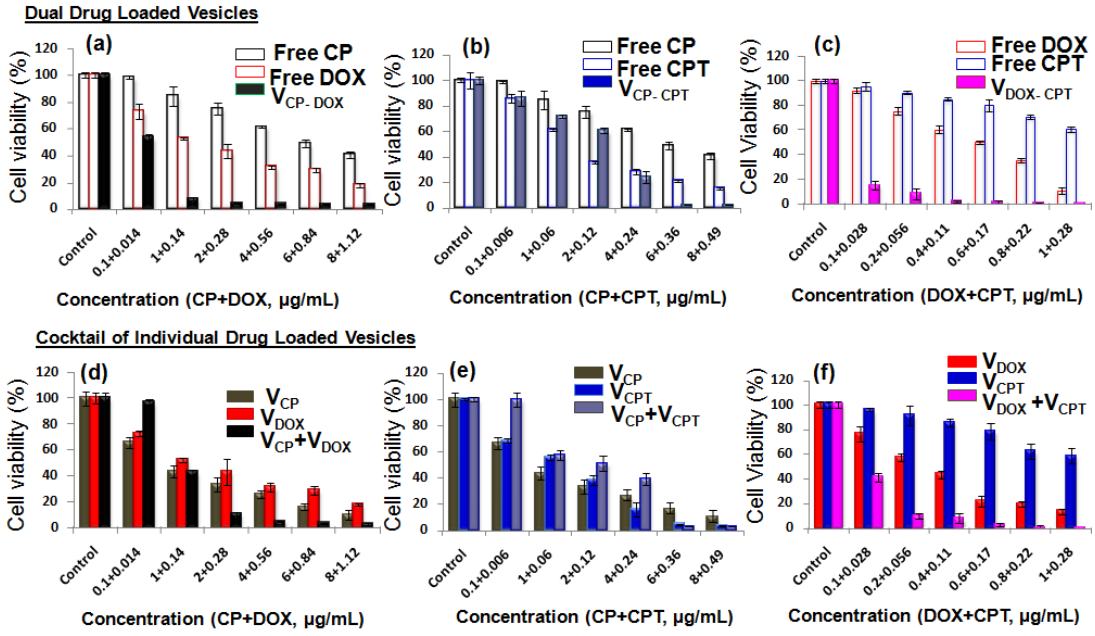

Figure 2.20: *Histograms depicting the cytotoxicity of cocktails of free drugs and dual drug loaded vesicles for CP and DOX (a), CP and CPT (b) and DOX and CPT (c) in MCF 7 cell line. Histograms depicting the cytotoxicity of cocktails of individual drug loaded vesicles for CP and DOX (d), CP and CPT (e) and DOX and CPT (f) in MCF 7 cell line.*

Hence from the cytotoxicity data, the IC_{50} values were calculated for drug encapsulated nanovesicles and are tabulated in table 2.1.

Table 2.1: *Table showing IC_{50} values for drug loaded nanovesicles in MCF 7 cells. IC_{50} values are given in µg/mL.*

V_X	V_{CP}	V_{DOX}	V_{CPT}	V_{CP-DOX}	V_{CP-CPT}	$V_{DOX-CPT}$	$V_{CP-DOX-CPT}$
Cisplatin	**1**	**-**	**-**	**0.1**	**3**	**-**	**0.1**
Doxorubicin	**-**	**0.15**	**-**	**0.014**	**-**	**0.03**	**0.023**
Camptothecin	**-**	**-**	**0.30**	**-**	**0.16**	**0.010**	**0.016**

To analyse the synergism of the drug action in the combination delivery of two drugs, the following formula was employed:[69] $CI = D_1/D_{m1} + D_2/D_{m2}$, where, D_1 and D_2 are the concentrations of drug 1 and drug 2 that in combination produce a certain level of cytotoxicity, while Dm_1 and Dm_2 are the concentrations of the single drugs, administered separately, which produce the same effect. $CI < 1.0$ indicate synergism, $CI = 1.0$ indicate an additive effect, and CI values > 1.0 indicate antagonism.[70] In Figures 2.21 a to c, the plots provide quantitative information about the extent of drug interactions. From the plot, it is very clear that the dual loaded V_{CP-DOX} exhibited values well below 1.0 suggesting the synergistic effect in MCF-7 cell line (see Figure 2.21 a). On the other hand, the cocktails of free drugs and cocktails of individual drug loaded vesicles $V_{DOX}+V_{CP}$ showed antagonism (see Figure 2.21 b). In case of V_{CP-CPT}, the dual loaded system showed additive effect whereas its cocktails exhibited antagonism. In the combination of DOX and CPT, the dual loaded $V_{DOX-CPT}$ and individual drug loaded vesicles ($V_{DOX} + V_{CPT}$) exhibited synergistic effect compared the antagonistic effect of cocktail of the free drugs (see Figure 2.21 c). For better clarity and easy understanding; a triangle diagram is drawn to summarize the synergistic, additive and antagonise effect of three important clinical drugs in combination therapy. The following conclusion may be drawn from the diagrams. All three drugs cisplatin, DOX and CPT were antagonistic to each other while administrating them in free forms (see Figure 2.21 d).

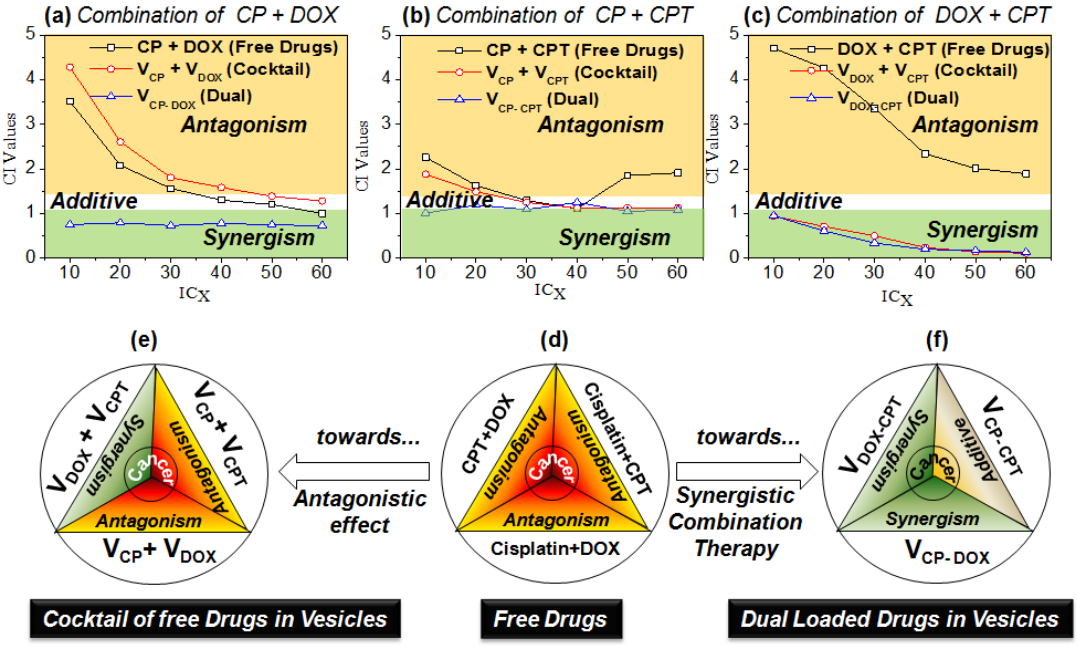

Figure 2.21: *Combination index (CI) plotted against the IC_X values for free drugs, cocktails of the individually loaded vesicles and dual loaded vesicles for cisplatin and DOX system (a), cisplatin and CPT system (b) and DOX and CPT system (c). Triangle models are showing the synergistic, antagonistic and additive effects in the combination therapy of free drugs (d), individual drug loaded vesicles (e) and dual drug loaded vesicles (f).*

The cocktails of individual drug loaded vesicles exhibited diverse results: for example, antagonistic effect for V_{CP} + V_{DOX}; additive effect for V_{CP} +V_{CPT}; and synergistic for V_{DOX} + V_{CPT} (see figure 2.21 e). Exceptionally, both DOX loaded dual vesicles $V_{CP\text{-}DOX}$ and $V_{DOX\text{-}CPT}$ showed synergist effect in combination therapy (see Figure 2.21 f). The dual drug loaded vesicle of $V_{CP\text{-}CPT}$ still showed additive effect and need additional improvement. Hence, the custom dextran vesicles are unique classes of nano-carriers for accomplishing synergistic cancer therapy of clinical antagonistic drugs cisplatin plus DOX and DOX plus CPT for breast cancer treatment.

2.3.5 Cellular uptake and Flow Cytometry

The cellular uptake studies were done by confocal microscopic imaging and flow cytometry. Since the cisplatin is a non-fluorescent drug, cellular uptake studies were done for V_{DOX}, $V_{CP\text{-}DOX}$, V_{CPT}, $V_{CP\text{-}CPT}$ and $V_{DOX\text{-}CPT}$ in MCF 7 cells. The red fluorescence

from doxorubicin at 520 nm was monitored through the red channel (λ = 568 nm) and the blue fluorescence produced by the cell nuclei by CPT or by DAPI staining (λ = 461 nm) depending upon the requirement. The images corresponding to free DOX and V_{DOX} and $V_{CP\text{-}DOX\ and}$ $V_{DOX\text{-}CPT}$ are shown in figure 2.22 a. The merged image corresponding to the free DOX in the first panel clearly indicates that the free DOX accumulation in the nucleus is relatively less. On the other hand, the V_{DOX} taken up cells at much higher drug concentration and the DOX was accumulated both in the cytoplasm and at the nucleus. The imaged images appeared as magenta colour corresponding to perfect accumulation of DOX at the nucleus long with DAPI. Further, the CLSM images of $V_{DOX\text{-}CPT}$ in figure 2.22 clearly showed the CPT and DOX emission in the blue and red channels and the merged image showed magenta colour corresponding mixed emission. The cellular uptake of V_{DOX}, $V_{CP\text{-}DOX}$ and $V_{DOX\text{-}CPT}$ were found to be almost identical which suggesting that the DOX release was not disturbed by the cisplatin-stitching.

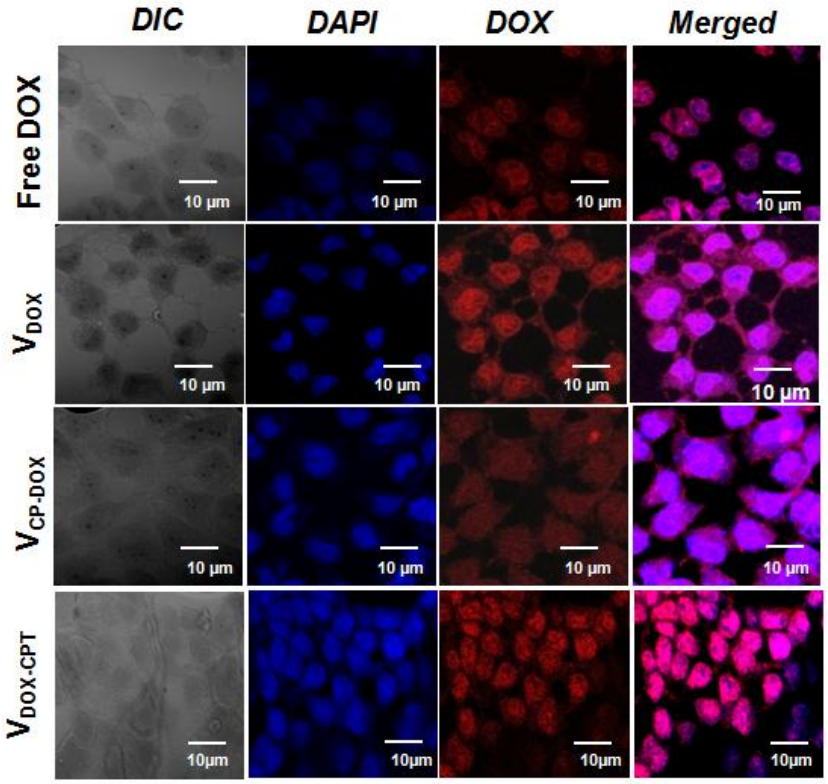

Figure 2.22: *CLSM images of MCF 7 cells incubated with free DOX, V_{DOX} and $V_{CP\text{-}DOX}$ and $V_{DOX\text{-}CPT}$ at 37°C. For each panel, the images from the left to right show differential interference contrast (DIC), staining of cell nuclei by DAPI, DOX fluorescence in the cells, and an overlay of the three images.*

The cellular internalisations for free CPT and V_{CPT} were done (nucleus was not stained with DAPI). CPT is blue luminescent drug and the images in Figure 2.23 a and b showed that the CPT accumulation at the nucleus better while delivering it from dextran vesicles. Similarly, imaging was done for $V_{CP\text{-}CPT}$ and obtained results are showed in figure 2.23 c. In order to rule out the background signal from the cells in red and blue channels; controls cells were exposed to the red and blue channels using parameters employed for drug loaded samples. These control did not show any significant background emission as can be seen from figure 2.23 d; thus, confirming that the red and blue images were observed as the result of drugs accumulated in the cytoplasm and nuclei.

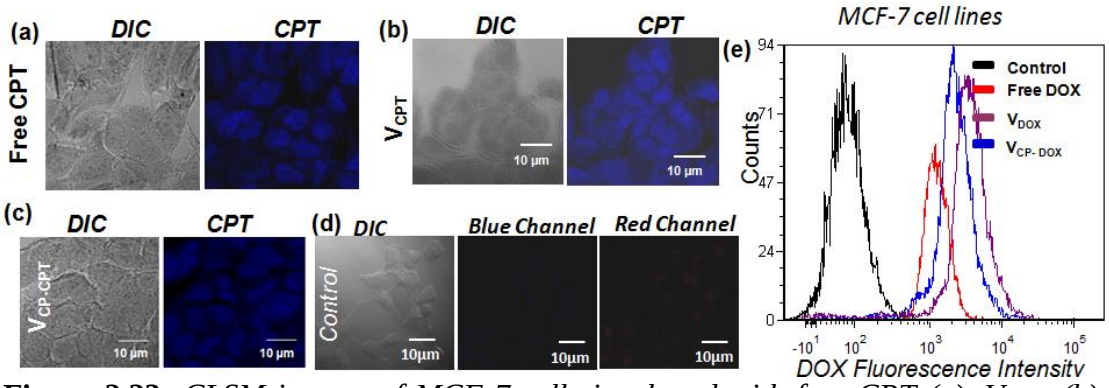

Figure 2.23: *CLSM images of MCF 7 cells incubated with free CPT (a), V_{CPT} (b) and $V_{CP\text{-}CPT}$ (c) and a control cells (d). In case of CPT nuclei is not stained with DAPI. Flow cytometry plots for control, free DOX , V_{DOX} and V_{CP0DOX} (e) in MCF 7 cell line after 9 h incubation (DOX concentration = 2 µg/ mL and 10000 cells used for measurements).*

To further confirm the cellular uptake of the vesicles, flow cytometry analysis was carried out for free DOX and DOX loaded vesicles V_{DOX} and $V_{CP\text{-}DOX}$ (see figure 2.23 e). The histograms clearly indicate that the DOX internalization by V_{DOX} and $V_{CP\text{-}DOX}$ is twice and 1.5 times better than the free DOX in MCF-7 cells. The higher uptake of V_{DOX} and $V_{CP\text{-}DOX}$ suggested that the drugs were taken up by the cells while delivering from vesicular nano-scaffold much better compared to their free forms. The comparisons of the cytotoxicity data in figures 2.19 d-e (also 2.20 a-b) with the CLSM images 2.22 and flow cytometry (2.23 e) confirmed that the higher amount of DOX uptake by the cells exhibited better cell killing. From the

above observations, it can be concluded that dextran vesicles has ability to internalise both water soluble (DOX) and water insoluble (CPT) anticancer drugs to exhibit its antitumor efficacy.

2.3.6 Cisplatin, DOX and CPT Triple Drug Loaded Vesicles

A unique triple drug loaded dextran vesicle $V_{CP\text{-}CPT\text{-}DOX}$ was produced by conjugating cisplatin and loading both water soluble DOX.HCl and water insoluble CPT in single dose as shown in figure 2.24 a. The DLCs in $V_{CP\text{-}DOX\text{-}CPT}$ were obtained as 9.3 % , 2.2 % and 1.5 % for cisplatin, DOX and CPT, respectively (DLE= 52 %, 50 % and 40 % for cisplatin, DOX and CPT, respectively). The average size and the morphology of these triple loaded vesicles were determined by DLS and AFM as 200 ± 10 nm (see figures 2.24 a). The enzyme-responsiveness of this triple loaded dextran vesicles in releasing drugs was investigated in PBS pH = 7.4 at 37 °C.

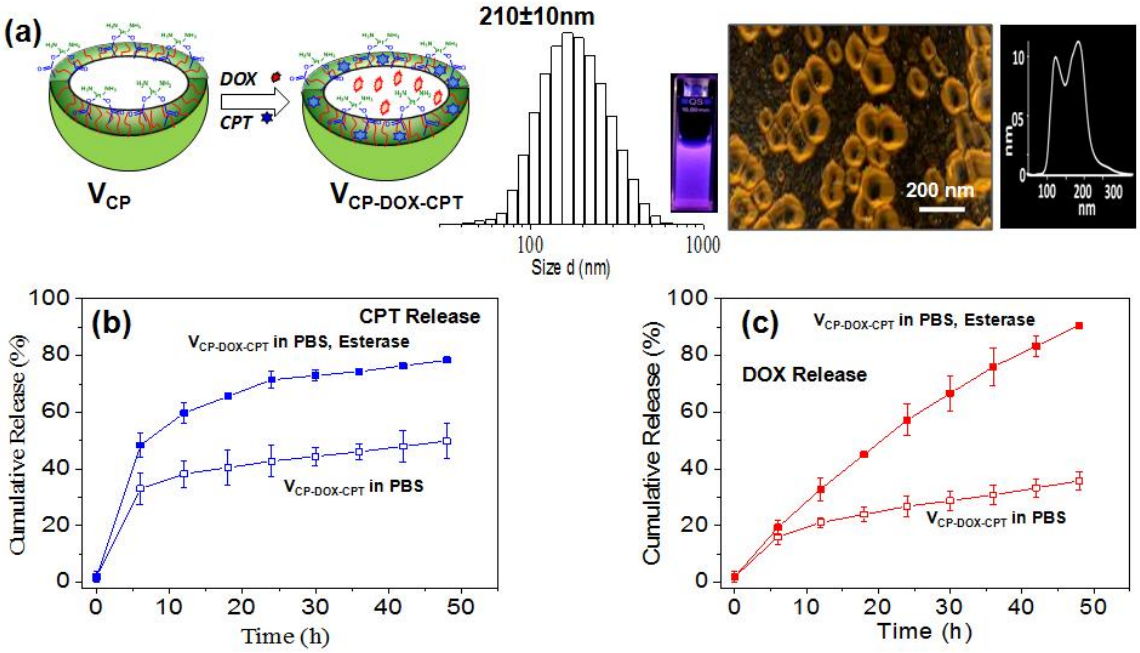

Figure 2.24: *(a) Schematic representation of triple drug loading, DLS histograms and AFM images of triple drug loaded vesicles $V_{CP\text{-}DOX\text{-}CPT}$ (a), Cumulative drug release of triple loaded $V_{CP\text{-}DOX\text{-}CPT}$ in PBS (pH= 7.4) at 37 ℃ in the absence and in the presence of esterase enzyme 10 U(b and c).*

In vitro kinetics revealed that the vesicles ruptured exclusively in the presence of esterase enzyme to release the drugs and showed in figure 2.24 b and c. Confocal microscope

images confirmed the cellular internalisation of both DOX and CPT from the dextran vesicles. This cellular uptake data is showed in figure 2.25. The cytotoxicity profiles of the triple loaded dextran vesicle in MCF 7 cell line is shown in figure 2.26. The triple loaded vesicles could able accomplish 100 % cell death at very low concentrations of drugs with the IC_{50} values of 0.1µg/mL of cisplatin, 0.02 µg/mL of DOX and 0.02 µg/mL of CPT. These IC_{50} values are much lesser compared to their dual and individual loaded vesicles as showed earlier in table 2.1. The cytotoxicity profiles for the individually loaded vesicles and their cocktail form were shown in figure 2.26. The cocktail of individual drug loaded vesicles showed better cell killing compared to their individual components.

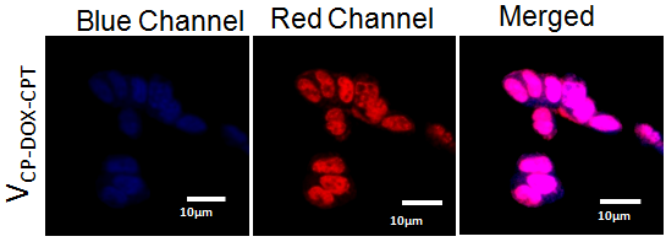

Figure 2.25: *CLSM images of MCF 7 cells incubated with $V_{CP\text{-}DOX\text{-}CPT}$ at 37°C. For a panel, the images from the left to right show differential interference contrast (DIC), CPT fluorescence in the cells, DOX fluorescence in the cells, and an overlay of the three images. For this imaging the nuclei is not stained with DAPI*

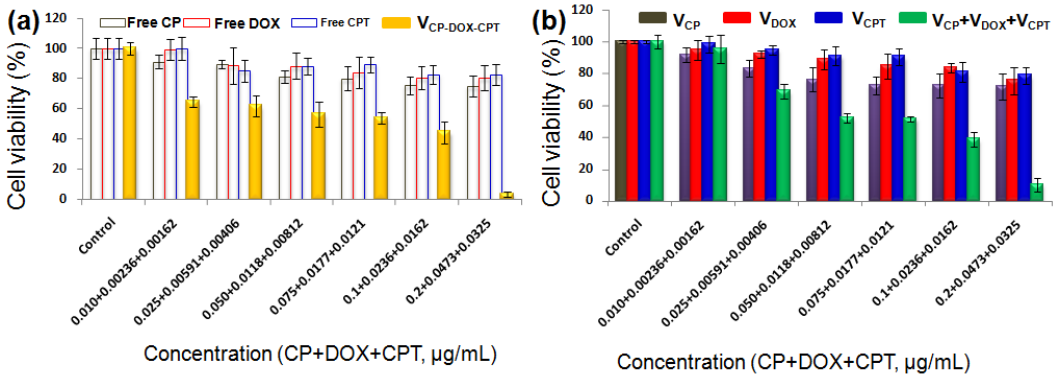

Figure 2.26: *Histograms depicting the cytotoxicity of the free drugs and triple drug loaded vesicles (a) Histograms depicting the cytotoxicity of individually loaded vesicles and cocktails of individual drug loaded vesicles in MCF 7 cell line (b).*

To evaluate its combination therapy effect, the combination index values were calculated using the equation $CI = D_1/D_{m1} + D_2/D_{m2} + D_3/D_{m3}$ and the values are plotted

against IC_x in figure 2.27. The results obtained for the triple loaded vesicles, their cocktail form were depicted using a triangle model as shown in figure 2.24 f. These data emphasized the synergistic effect for triple drug loaded vesicles and cocktails of individual loaded vesicles.

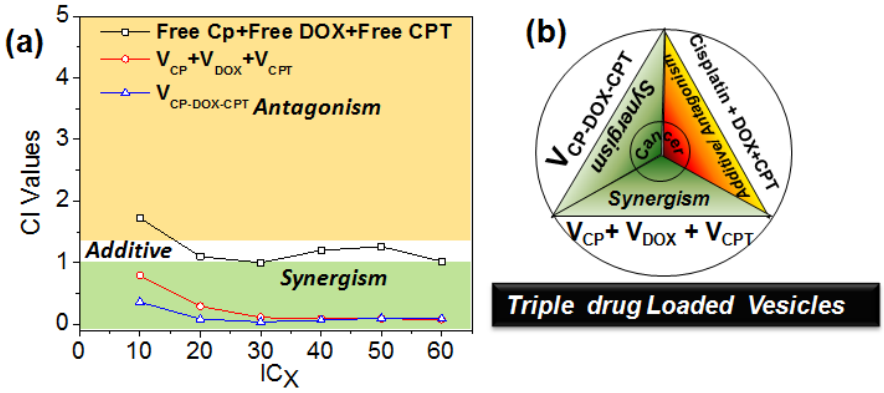

Figure 2.27: *Combination index (CI) plotted against the IC_X values for free drugs, cocktails of the individually loaded vesicles and triple loaded vesicles (a), Triangle models are showing the synergistic, antagonistic and additive effects in the combination therapy of triple antagonistic drug (b).*

On the other hand, the physical mixture of the free drugs showed the antagonistic or additive effect. Thus, it may summarized that the cisplatin stitched dextran vesicles could able to load and deliver both the hydrophilic and hydrophobic drugs together to achieve the synergistic cell killing in human breast cancer cell lines (MCF 7) at very low drug concentration. In the present investigation, the carboxyl dextran vesicle was successfully demonstrated as efficient multiple drug nano-carrier for the intracellular internalisation of cisplatin, DOX and CPT to boost the synergistic breast cancer therapy.

2.4 Conclusion

In conclusion, the present investigation demonstrates one of the first examples of cisplatin-stitched polysaccharide vesicles for combination therapy of three antagonistic anticancer drugs together to accomplish synergistic cancer therapy. Dextran was anchored with self-assembly directing renewable hydrophobic unit 3-pentadecylphenol (PDP) along with carboxyl functionality which enables the vesicle formation as well as cisplatin conjugation. The vesicles were found to retain their size and shape in the cisplatin-stitched form and also exhibited excellent encapsulation capability for water soluble DOX and water insoluble CPT in the core and layer, respectively. The cisplatin-polymer conjugate was stabilized by the dextran vesicular geometry against the GSH drug detoxification which was very crucial for the delivery of the drugs in the active form in the cytoplasm. *In vitro* drug release kinetics confirmed that the dextran vesicles were readily cleaved by lysosomal esterase enzymes at the intracellular conditions to deliver the drugs to the nucleus. Cytotoxicity studies in breast cancer cells (MCF 7) revealed that of the cisplatin stitched vesicles accomplished > 90 % cell killing whereas the free cisplatin was ineffective. Both CPT and DOX was also exhibited better cell killing breast cancer cell lines while administrating them from the vesicle compare to free form. Combination therapy of the drug loaded vesicles and free drugs were studied in cisplatin resistant breast cancer cells MCF 7 cells. The results from the combination index values showed that the physical mixture of the free drugs cisplatin, DOX and CPT were turned out to be antagonistic in all the three combination. Exceptionally, the dual loaded vesicles showed synergistic cell killing at lower concentration than that of their free drugs or cocktails of individual drug loaded vesicle counterparts. The vesicles are very unique to load all three drugs together in single platform to produce triple drug loaded nano-carriers. This triple drug loaded vesicle exhibited excellent synergistic killing in breast cancer cells at nanogram concentration level which is very remarkable for future therapeutic applications. Thus, the dextran vesicle nano-carrier overcome the antagonistic effect of three important anticancer drugs like cisplatin, doxorubicin and camptothecin in combination therapy to accomplish synergistic cell killing in breast cancer cells. Confocal microscopic and Flow cytometry analysis revealed that these vesicles were taken up by the cells and they are accumulated in nucleus and peri-nucleuar region. The

polysaccharide vesicles are proven as excellent biocompatible nano-carrier for multiple drug delivery irrespective of physical loading or chemical conjugation of drugs, their water solubility or insolubility and antagonistic effect. Thus, the dextran vesicular scaffold is not restricted only to these anticancer drugs, and in principle, it can be expanded to wide ranges of other water soluble and water insoluble anticancer drugs to achieve synergistic effect in other cancer diseases.

2.5 References

1. Holmes, D. *Nature* **2015**, *527*, S218-S219.
2. Al-Liziakani, B.; Banerji, U.; Workman, P. *Nature Biotechnology* **2012**, *7*, 1-13
3. Kelland, L. *Nat. Rev. Cancer* **2007**, *7*, 573-584.
4. Kasherrman, Y.; Sturup, S.; Gibson, D. J. Med. Chem. **2009**, *52*, 4319–4328
5. Rosi, N.; Grande, S.; Luciani, A. M.; Palma, A.; Giovannini, C.; Guidoni, L.; Sapora, O.; Viti. V. *Radiat. Res.* **2007**, *167*, 268–282.
6. Min, Y.; Mao, C-Q.; Chen, S.; Ma, G.; Wang, J.; Liu, Y. *Angew. Chem. Int. Ed.* **2012**, *51*, 6742-6747.
7. Fuertes, M.; Alsono, C.; Jose, P. *Chemical reviews* **2003**, *103*, 645-662.
8. Siddik, H. Cisplatin: *Oncogene* **2003**, *22*, 7265–7279.
9. Holzer, A.; Manorek, G.; Howell, S. *Mol. Pharmacol*. **2006**, *70*, 1390-1394.
10. Kang, H-C.; Cho, H.; Bae, Y-H. *Mol. Pharmaceutics* **2015**, *12*, 2845−2857.
11. Lee, S-M.; O'Halloran, T. V.; Nguyen, S. B. T. *J. Am. Chem. Soc.* **2010**, *132*, 17130-17138.
12. Liao, L.; Liu, J.; Dreaden, E. C.; Morton, S.W.; Shopsowitz, K. E.; Hammond, P. T.; Johnson, J. A. *J. Am. Chem. Soc*. **2014,** *136*, 5896−5899.
13. Kolishetti, N.; Dhar, S.; Valencia, P.; Lin, L.; karnik, R.; Lippard, S.; Langer, R.; Farohkzad, O. *Proc. Natl. Acad. Sci. USA* **2010, 1***07*, 17939-17944.
14. Fleming, G.; Brunetto, V.; Cella, D.; Look, K.; Reid, G.; Munkurah, A.; Kline, R.; Burger, R.; Goodman, A.; Burks,R. *J. Clin. Oncol*. **2004**, *22*, 2159-2166.
15. Xiao, H.; Song, H.; Yanhg, Q.; Cai, H.; Qi, R.; Yan, L.; Liu, S.; Zheng, Y.; Haung, Y.; Liu, T.; Jing,X. *Biomaterials* **2012**, *33*, 6507-6519.
16. Yuan, Y.; Kwok, R. T. K.; Tang, B. Z.; Liu, B. *J. Am. Chem. Soc.* **2014**, *136*, 2546-2254.
17. Khiati, S.; Luvino, D.; Oumzil, K.; Chauffert, B. Campio, M.; Barthelemy, P. *ACS Nano* **2011**, *5*, 8649-8655.
18. Zheng, Y-R.; Suntharalingam, K.; Jhonstone, T.C.; Yoo, H.; Lin, W.; Brooks, J. G.; Lippard, S. J. *J. Am. Chem. Soc.* **2014**, *136*, 8790-8798.
19. Dhar, S.; Lippard, S. J. *Proc. Natl. Acad. Sci. USA* **2009**, *106*, 22199-22204.
20. Pathak, R. K.; Marrache, S.; Choi J.H.; Berding, T.B.; Dhar, S. *Angew. Chem. Int. Ed.* **2014**, *53*, 1963-1967.
21. Guo, S.; Wang, Y.; Miao, L.; Xu, Z.; Lin, C.M.; Zhang, Y.; Huang, L. *ACS Nano* **2013**, *7*, 9896-9904
22. Aryal, S.; Hu, C-J. J.; Zhang. L. *ACS Nano* **2010**, *4*, 251–258.
23. Ohya, Y.; Oue, S.; Nagatomi, K.; Ouchi, T. *Biomacromolecules* **2001,** *2*, 927-933.
24. Shen, W.; Luan, J.; Cao, L.; Sun, J.; Yu, L.; Ding, J. *Biomacromolecules* **2015**, *16*, 105−115.
25. Huynh, V. T.; Chen, G.; De souza, P.; Stenzel, M. H. *Biomacromolecules* **2011,** *12*, 1738-1751.

26. Nishiyama, N.; Okazaki S.; Cabral, H.; Miyamato, M.; Sugiayama, Y.; Nishio, K.; Mastumura, Y.; Kataoka, K. *Cancer Res.* **2003,** *63*, 8977-8983.
27. Johnstone, T. C.; Kulak, N.; Pridgen, E. C.; Farokhzad, O. C.; Langer R.; Lippard, S. J. *ACS Nano* **2013**, *7*, 5675–5683.
28. Yao, X.; Xie, C.; Chen, W.; Yang, C.; Wu, W.; Jiang, W. *Biomacromolecules* **2015,** *16*, 2059−2071.
29. Casolaro, M.; Cini, R.; Bello, B.D.; Ferrali, M.; Maellaro, E. *Biomacromolecules* **2009**, *10*, 944–949.
30. Huang, C.; Neoh, K. G.; Liqun, X.; Kang, E. T.; Chiong, E. *Biomacromolecules* **2012**, *13*, 2513−2520.
31. He, S.; Qi, Y.; Kuang, G.; Zhou, D.; Li, J.; Xie, Z.; Chen, X.; Jing, X.; Huang, Y. *Biomacromolecules* **2016**, *17*, 2120−2127.
32. Shirbin, S. J.; Ladewig, K.; Fu, Q.; Klimak, M.; Zhang, X.; Duan, W.; Qiao, G. G. *Biomacromolecules* **2015**, *16*, 2463−2474.
33. Osada, K.; Cabral, H.; Mochida, Y.; Lee, S.; Nagata, K.; Matsuura, T.; Yamamoto, M.; Anraku, Y.; Kataoka, K. *J. Am. Chem. Soc.* **2012**, *134*, 13172-13175.
34. Surnar, B.; Pramod, P. S.; Jayakannan, M. *Z. Anorg. Allg. Chem.* **2014**, *640*, 1119–1126.
35. Surnar, B.; Sharma, K.; Jayakannan, M. *Nanoscale* **2015**, *7*, 17964–17979.
36. Matsumura, Y.; Maeda, H. *Cancer Res.* **1986,** *46*, 6387−6392.
37. Maeda, H. *Bioconjugate Chem.* **2010,** *21*, 797−802.
38. Paraskara, A. S.; Soni, S.; Chinc, K. T.; Chaudhuria, P.; Mutoc, K. W.; Berkowitzc, J.; Handlogtend, M. W.; Alvesd, N. J; Bilgicerd, B.; Dinulescub, D. M.; Mashelkar, R. A.; Sengupta, S. *Proc. Natl. Acad. Sci. USA* **2010**, *107*, 12435-12440.
39. Meng, F.; Zhong, Z.; Feijen, J. *Biomacromolecules* **2009**, *10*, 197-209.
40. Feng, A.; Yuan,J. *Macromol. Rapid. Commun*. **2014**, *35*, 767-779.
41. Schatz, C.; Louguet, S.; Meins, J.; Leccomoandoux, S. *Angew. Chem Int. Ed.* **2009**, *48*, 2572-2575.
42. Thambi, T.; Park, J.; Sung Lee, D. *Biomater. Sci*. **2016**, *4*, 55-69.
43. G. Palivan, C.; Goers, R.; Najer, A.; Zhang, X.; Car, A.; Meier, W. *Chem. Soc. Rev*. **2016**, *45*, 377-411.
44. Mizarphy, S.; Peer, D. *Chem. Soc. Rev*. **2012**, *41*, 2623-2640.
45. Li, Y.; Liu, G.; Wang, X.; Hu, J.; Liu, S. *Angew. Chem. Int. Ed*. **2016**, *55*, 1760-1764.
46. Xue,X.; Hall, M. D; Zhang, Q. ; Wang, P, C.; Gottesman,M. M ;Liang, X. J. ; *Nanoscale*, **2013**, *7*, 10452-10464.
47. Stras, S.; Holleran, T. ; Howe, A.; Sofou, S. *Mol. Pharmaceutics* **2016**, 13, 3224-3233.

48. Shein, S.,A. ; Kuznestov,I.,I.; Abkumova, T., O. ; Chelishkin, P.,S. ; Melnikov, P. A. ; Korchagina, A.,A. ; Bychkov, D., A. ; Seregina,I., F. ; Bolshov, M., A. ; Kabanov, A., V. ; Chekhonin, V.,P. ; Nukolova,N., V. *Mol. Pharmaceutics* **2016**, 13, 3712-3723.
49. Ramachandran, S.; Quist, A. P. ; Kumar, S. ; Lal, R. *Langmuir*, **2006,** 22, 8156-8162.
50. Du, H. ; Cui, C. ; Wang, L. ; Liu, H. ; Cui, G. *Mol. Pharmaceutics* **2011**, 8, 1224-1232.
51. Zong, T. ; Mei, L. ; Gao, H. ; Cai, W. ; Zhu, p., ; Shi, K. ; Chen, j. ; Wang, Y., ; GAo, F. ; He, Q. *Mol. Pharmaceutics* **2014**, 11 , 2345 - 2357.
52. Arrieta, O. ; Medina, LA. ; Lobato, E., E. ; Pedro, N. H. ; Rodriguez, G., V. ; Barrera, L., M. ; Macedo EO. ; Rodriguez, V., L. ; Kuba, D., M. ; Cruz, JF., C. *Br. J. cancer* **2012,** 106, 1027-1032.
53. Reddy, J. , A. ; Dorton, R. ; Bloomfield, A. ; Nelson, M. ; Vetzel, M. ; Guan, J. ; Leamon, C., P. *Clin. Cancer Res*, **2008**, 20, 2104-2114.
54. Pramod, P. S.; Shah R.; Jayakannan, M. *Nanoscale*, **2015**, *7*, 6636-6652.
55. Pramod, P. S.; Shah R.; Chaphekar, S.; Balasubramanian, N.; Jayakannan, M. *Nanoscale* **2014**, *6*, 11841-11855.
56. Pramod, P. S.; Takamura, K.; Chaphekar, S.; Balasubramanian, N.; Jayakannan, M. *Biomacromolecules* **2012**, *13*, 3627−3640.
57. Pramod, P. S.; Deshpande, N. U.; Jayakannan, M. *J. Phys. Chem. B* **2015**, *119*, 10511-10523.
58. Sridhar, U.; Pramod, P. S.; Jayakannan, M. *RSC Adv.* **2013**, *3*, 21237-21241.
59. Li, S.; B. howell, S. *Mol. Pharmaceutics*. **2010**, *7*, 280-290.
60. Ling, X.; Shen, Y.; Sun, R.; Zhang, M.; Li, C.; Mao, J.; Xing, J.; Sun, C.; Tu, J. *Polym. Chem*. **2015**, *6*, 1541-1552.
61. Peng, X.; Wang, Y.; Huang, D.; Wang, Y.; JucShin, H.; Chen, Z.; B.Spewak, M.; Mao, X.; Wang, Y.; (Gergia) Chen, Z. *ACS Nano* **2011**, *12*, 9480-9493.
62. Wang, Y.; Zhou, J.; Qiu,L.; Wang, X.; Chen, L.; Liu, T.; Di, W. *Biomaterials* **2014**, *34*, 4297-4309.
63. Li, M.; Tang, Z.; Zhang, D.; Sun, H.; Liu, H.; Zhang, Y.; Zhang, Y.; Chen, X. *Biomaterials*, **2015**, *51*, 161-172.
64. Li, M.; Tang, Z.; Lv, S.; Song, W.; Hong, H.; Jing, X.; Zhang, Y.; Chen, X. *Biomaterials* **2014**, *35*, 3851-3864.
65. Li, M.; Tang, Z.; Zhang, Y.; Lv, S.; Yu, H.; Zhang, D.; Hong, H.; Chen, X. *J. Mater. Chem. B.* **2104**, *2*, 3490-3499.
66. Balchandran, S. V.; Jadhav, S.R.; Vemula, K.V.; John, G. *Chem. Soc. Rev.* **2013**, *42*, 427-438.
67. Kashyap, S.; Jayakannan, M. *J. Phys. Chem. B.* **2012**, *116*, 9820-9831.

68. Todd, R. C.; Lovejoy, K. S.; Lippard, S. J. *J. Am. Chem. Soc.* **2007**, *129*, 6370-6371.
69. Chou, T.-C.; Talalay, P. *Trends Pharmacol. Sci.* **1983**, *4*, 450–454.
70. Chen, F.; Zhao, Y.; Pan, Y.; Xue, X.; Zhang, X.; Kumar, A.; Liang, X. *Mol. Pharmaceutics*. **2015**, *12*, 2237-2244.

Chapter-3

Biotin-Tagged Polysaccharide Vesicular Nanocarriers for Receptor-Mediated Anticancer Drug Delivery in Cancer Cells

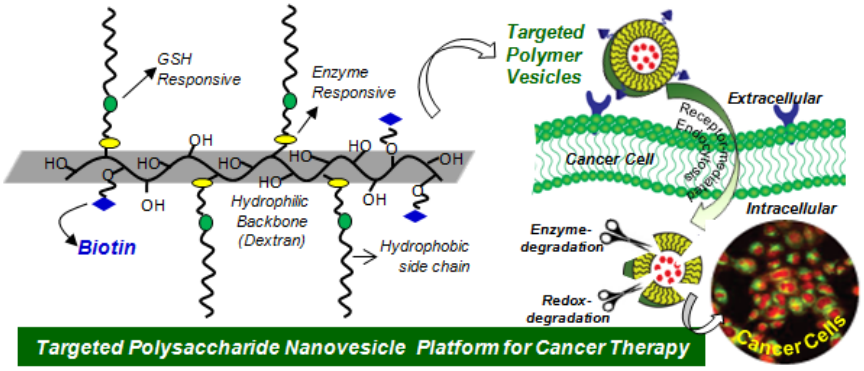

Abstract

Biotin-conjugated multi-stimuli-responsive polysaccharide vesicular nanocarriers are designed and developed, for the first time, to accomplish receptor-mediated endocytosis in cancer cells and to deliver anticancer drugs at the intracellular compartments. For this purpose, a new renewable hydrophobic unit was custom designed with redox-degradable disulphide and enzyme-biodegradable aliphatic ester chemical linkages and it was conjugated along with biotin on the dextran backbone. The dextran derivative self-assembled into nanovesicles of < 200 nm in size which were characterized by dynamic and static light scattering, electron and atomic force microscopes. Avidin-HABA assay established the high affinity of biotin-tagged dextran vesicles towards membrane-receptors up to 25 nM concentration. Doxorubicin-hydrochloride (DOX.HCl) loaded dextran vesicles exhibited stable formulation in PBS and FBS. Redox-degradation by glutathione (GSH) showed 60 % drug release whereas lysosomal esterase enzyme enabled > 98 % drug release in 12 h. Confocal microscope and flow cytometry assisted time-dependent cellular uptake studies revealed that the biotin-receptor over expressed cervical cancer cells (HeLa) exhibited larger drug accumulation through receptor-assisted endocytosis process. This process enabled the delivery of higher amount of DOX and significantly enhanced the killing in cancer cells (HeLa) compared to wild-type mouse embryonic fibroblast cells (WT-MEF, normal cells). Control experiments such as biotin pre-treatment in cancer cells and energy-suppressed cellular uptake at 4 ℃ further supported the occurrence of receptor-mediated endocytosis by the biotin-tagged polymer vesicles. This report provides first insights into the targeted polysaccharide vesicle platform, and the proof-of-concept is successfully demonstrated in biotin receptors over expressed cervical cancer cells.

3.1 Introduction

Receptor-mediated endocytosis of nano-carriers is emerging as one of the important approaches for targeted delivery of anticancer drugs or genes to cancer tissues under physiological conditions.[1-4] Cancer cells are over expressed by large number of signalling receptors for metastasis and also enriching the nutrient supply to the fast and uncontrolled cell growth. [5-7] These receptors exhibit high binding affinity towards targeting ligands such as biotin (vitamin B7),[8-9] folic acid[10-13] and RGD peptide,[14] tranSerrin[15] etc. Nano-assemblies tagged with these targeting ligands enhance the delivery of payload at the cancer tissue site through receptor-ligand interaction.[3] Biotin is one of the excellent targeting ligands for streptavidin-type membrane proteins (avidin class of proteins) at the cell surface with high association constant[16] in the range of 10^{13} to10^{15} M^{-1}. Various cancer cells such as cervical, breast, lung, and ovarian are over expressed with biotin receptors.[17] Biotin-conjugated nano-assemblies from small molecules,[18] block copolymers,[19-21] dendrimers,[12] gold nanoparticles,[22] and carbon nano-tubes,[23] etc were explored for delivering chemotherapeutic agents. In one such attempt Tau et al reported the synthesis biotin conjugated diblock copolymer of polyethylene glycol and methacrylate monomer. Polymer self assemblies were fabricated by biotin-streptavidin interaction which showed temperature responsive phase transitions behaviour from vesicles to spherical micelles. This polymer was used for protein conjugation. The polymer structure and schematics of self assembly are showed in figure 3.1

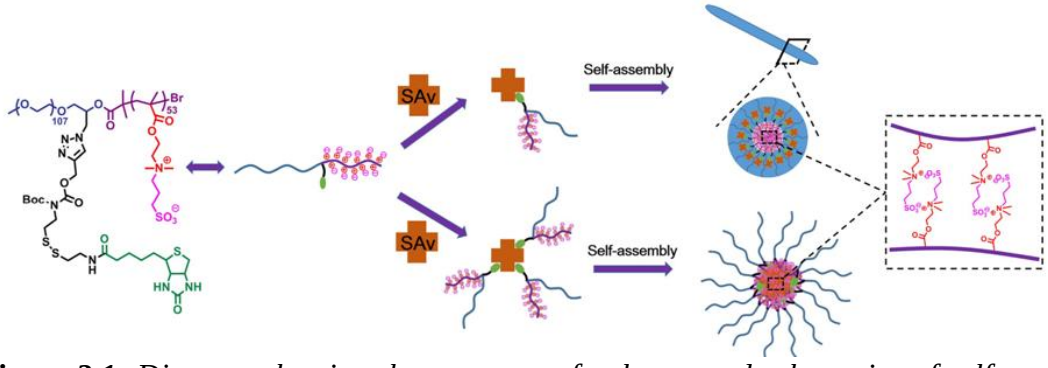

Figure 3.1: *Diagram showing the structure of polymer and schematics of self assembly. Adopted from Tau et al. Macromolecules 2017, 50, 2284-2295.*

The polymer nano-carriers are particularly important since they have unique capability to passive selectively target the cancer tissue via enhanced permeability and

retention effect (EPR).[24-25] Thus, the receptor-mediated endocytosis in macromolecular nano-carriers is an appropriate choice for both active and passive selectively targeting the cancer tissues. Bio-resource based polymer nano-carriers have recently gained significant importance in bio-medical field.[26-27] Polysaccharide nano-carriers are unique bio-resource systems due to their excellent biocompatibility associated with structural diversity,[28-31] and also possess sugar-type macromolecular backbone for enhanced internalisation via like-like interaction with lectins (carbohydrate-binding proteins) at the cell membrane.[32-34] Polysaccharide micelles,[35] nanoparticles,[36]capsules,[37] hydrogels,[38-40] and polymersomes (or vesicles)[28-31] were reported for drug and gene delivery. Among these nano-carriers; polysaccharide nanovesicles are very unique for delivering both water soluble and water insoluble anticancer drugs from single nano-carrier.[41] Zhang et al prepared redox responsive polysaccharide micelles from dextran-b-PBLG. These micelles are used for doxorubicin encapsulation. The GSH responsive behaviour of DOX encapsulated micelles was investigated and studies in HepG2 cells. These DOX loaded micelles showed better cell killing as compared to free drug. The schematics of self assembly and drug release are showed in figure 3.2

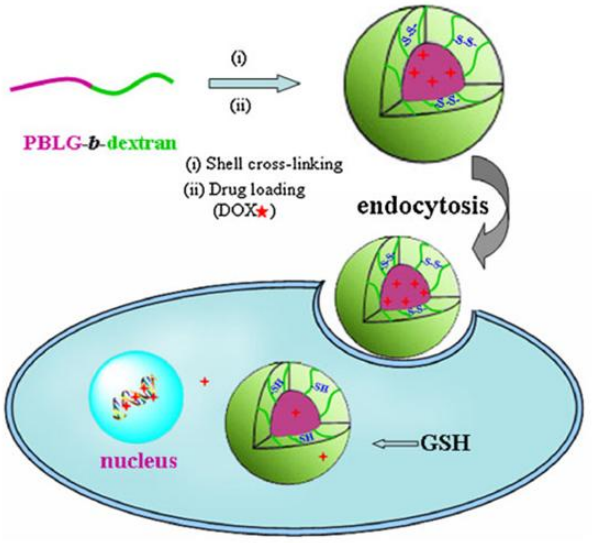

Figure 3.2: *Schematics of self assembly of PBLG-b-dextran polymer and their cellular internalisation. Adopted from Zhang et al. Macromol. Biosci. 2013, 13, 1249-1258.*

Earlier, dextran vesicles using stearyl chains as hydrophobic unit and folate as targeting ligand were reported for delivering doxorubicin.[42-43] From our group, new

classes of enzyme and pH responsive polysaccharide vesicles were reported based on dextran and renewable resource hydrophobic units from cashew nut shell liquid.[41, 44-45] Uptake studies using caveolae (+) plus and caveolae (-) nul cells revealed that the dextran vesicles were significantly taken up by the caveolae (-) nul type cells that resembled the membrane architectures of breast cancer cells.[46] Carboxylic functional dextran vesicles were designed to administrate three different antagonistic drugs like doxorubicin (DOX), camptothecin, and cisplatin together for synergistic combination therapy.[47] Polymersomes or polymer vesicles are one of the most important multipurpose nano-carriers for drug delivery; however, the concept of targeted polysaccharide vesicle is not fully explored for better treatment efficiencies in cancer. Despite biotin being known as excellent targeting ligand to cancer cells; there is no report on biotin-tagged polysaccharide vesicles in the literature. The lack of the non-availability of structural motifs for maintaining appropriate hydrophobic-hydrophilic balance is one of the reasons with respect to the difficulty in producing biotin-tagged polysaccharide vesicular assemblies. The present work is the first example to address this important idea and the proof-of-concept is successfully demonstrated in cancer cell lines. Here, we report biotin-tagged and multi-stimuli-responsive polysaccharide vesicles based on dextran backbone and renewable resource hydrophobic unit. The receptor-mediated endocytosis concept was successfully demonstrated *in vitro* by carefully designed time-dependent cellular uptake studies in cancer cells. This new concept is shown in figure 3.3.The present investigation is emphasised to make new biotin-conjugated and multi-stimuli-responsive polysaccharide vesicles and demonstrate the proof-of-concept for water soluble anticancer drug DOX.HCl in cancer cells. The polymer vesicles were tailor made using redox and enzyme degradable chemical linkages containing renewable resource 3-pentadecylphenol hydrophobic unit. The present polysaccharide (dextran) vesicle has following features: (i) biotin-anchored at dextran backbone for receptor-mediated binding at cancer cell membranes, (ii) the PDP hydrophobic units was connected on the hydrophilic dextran backbone via disulphide (S-S) and aliphatic ester chemical linkages (see Figure 3.3), (iii) the high levels of glutathione (GSH) at the intracellular level (1 mM) compared to extracellular level (1 μM) act as redox-trigger[48] (*stimuli-1*) for the -S-S- bond cleavage (marked green in Figure-3.3) and disrupt the vesicular assembly for

drug delivery, and (iv) the biodegradation of aliphatic ester linkages (marked yellow in Figure-3.3) by the esterase enzyme in lysosomal compartments[49-50] facilitated the drug release at the intracellular level (*stimuli-2*).

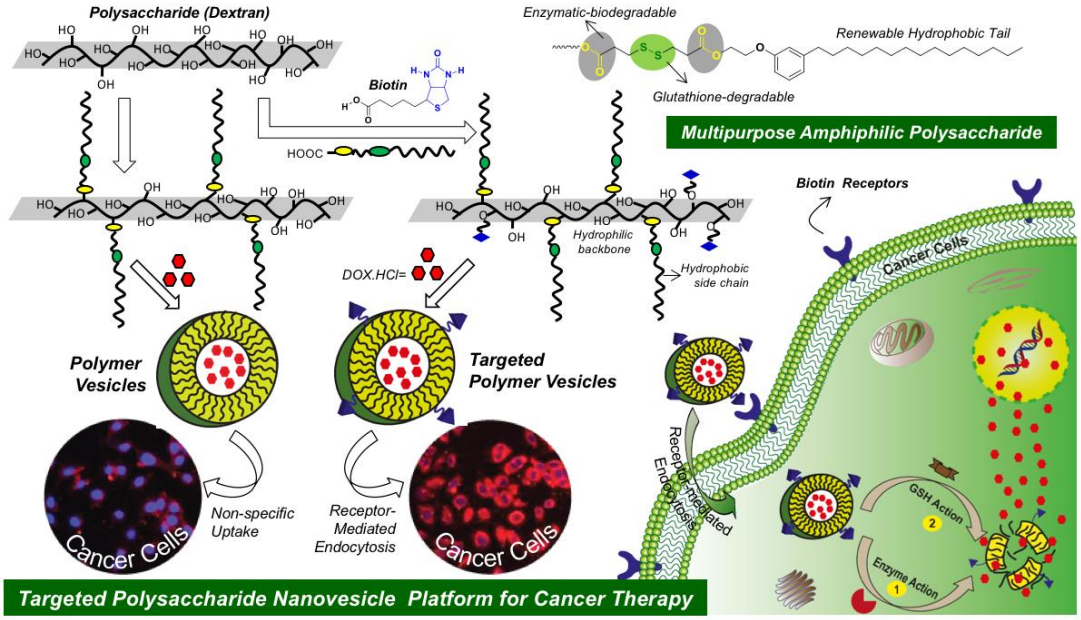

Figure 3.3: *Biotin-tagged polysaccharide nano-vesicular assemblies for receptor-mediated endocytosis in cancer cells and delivery of drugs at intracellular levels by GSH and enzyme multi-stimuli-responsiveness.*

The polymer vesicles provided unique opportunity to encapsulate water soluble anticancer drug doxorubicin-hydrochloride (DOX.HCl) and deliver them to cancer cells using receptor-mediated endocytosis. The nanovesicles produced were < 180 ± 30 nm in size and Avidin-HABA assay established the biotin-receptor affinity up to 25 nM concentration. *In vitro* studies revealed that the nanovesicles are stable under extracellular conditions and released drugs in response to intracellular stimuli such as GSH and esterase enzyme. The receptor-mediated endocytosis studies were performed in cervical cancer (HeLa) and WT-MEF (normal) cell lines. Time-dependent uptake studies by confocal microscope and FACS technique confirmed the occurrence of receptor-mediated endocytosis by biotin-tagged dextran vesicles. This was further corroborated by the time-dependent cytotoxicity studies wherein the cancer cells were found to be killed much better while delivering DOX.HCl from biotin-tagged vesicular platform compared to biotin free nano-vesicles. In a nut shell, the present investigation provides first insights

into the administration of water soluble anticancer drugs through receptor-mediated endocytosis based on biotin-tagged dextran vesicles and it opens up new opportunities for the development of targeted polymer vesicular nano-carrier platform for long term application in cancer treatment.

3.2 Experimental Section

3.2.1 Materials and Methods: 3-Pentadecylphenol (PDP), 2-bromoethanol, triethylamine, dextran (Mol. wt 6000), N-(3-dimethylaminopropyl)-N-ethylcarbodiimide hydrochloride (EDC.HCl), 4-dimethylamino pyridine, dithiothreitol (DTT), glutathione (GSH), doxorubicin hydrochloride (DOX.HCl), dicyclohexylcarbodidimide (DCC), 4-dimethyl amino pyridine (DMAP), biotin and horse liver esterase enzyme were purchased from Aldrich chemicals. Avidin was purchased from Alfa aesar and used as such. 4'-hydroxyazobenzene-2-carboxylic acid (HABA) was purchased from Loba Chemie and used as received. NaOH and all other necessary reagents and solvents like dimethylsulfoxide (DMSO), N,N-dimethylformamide (DMF) and dichloromethane (DCM) were purchased locally and purified following the standard procedures. The instrumentation details, structural characterization, biological data collection for MTT assay, confocal imaging and Flow cytometry analysis, tissue culture conditions, and the synthesis of compound (**1**) are given in the supporting information.

3.2.2 General Procedures: ^{1}H NMR and ^{13}C NMR spectra were recorded using a 400 MHz Jeol and 500-MHz Bruker NMR spectrometer using $CDCl_3$ or DMSOd6 containing a small amount of TMS as an internal standard. The absorption and emission spectra were recorded using Perkin-Elmer Lambda 45 UV−visible, and a Fluorolog HORIBA JOBIN VYON fluorescence spectrophotometer. The size determination of the polymers was carried out by dynamic light scattering (DLS), using a Nano ZS-90 apparatus utilizing a 633 nm red laser from Malvern instruments. The reproducibility of the data was checked doing at least three independent measurements. Atomic force microscope images were recorded by drop casting the samples on freshly cleaved mica surface using Agilent instrument. The imaging was carried out in tapping mode using TAP-190AL-G50 probe from Budget sensors with a nominal spring constant of 48 N/m and resonance frequency of 190. TEM images were recorded using a Technai-300 instrument. Differential scanning calorimetry (DSC) measurements were performed on a TA Q20 differential scanning calorimeter (DSC) at heating and cooling rates of 10.0 °C/min. FE-SEM images were recorded using Zeiss Ultra Plus scanning electron microscope. The samples for FE-SEM analysis were prepared by drop casting on silicon wafers. For TEM

Analysis, the samples were prepared by drop casting on copper grid. Confocal microscopic images were recorded using LSM10 Confocal Microscope. The mass analysis of the compounds was carried out using high-resolution mass spectrometry (HRMS-ESI-Q-TOF LC-MS) and Applied Bio system 4800 PLUS matrix-assisted laser desorption/ionization (MALDI) TOF/TOF analyzer. Static Light scattering (SLS) measurements were done using 3D-DLS instrument from LS instruments, Switzerland. The He Ne laser was used having wavelength of 632.8 nm and toluene was used as reference. The measurements were performed using autocorrelation mode from 20^0 to 130^0 by difference of 5^0.

3.2.3 Synthesis of 2-(3-pentadecylphenoxy) ethan-1-ol (1): This compound was synthesized following our earlier procedure (*Smita et al. J. Phys. Chem. B. 2012, 116, 9820-9831).* PDP (10.0 g, 33.0 mmol) and NaOH (2.63 g, 66.0 mmol) were dissolved in 100 mL water + ethanol (1:1) mixture solvent and refluxed for 30 minutes under nitrogen atmosphere. The reaction mixture was cooled to room temperature and 2-bromoethanol (3.0 mL, 43.0 mmol) was added drop wise. Reaction mixture was then refluxed for 24 hours. After 24 hours, the reaction mixture was poured into water (100.0 mL), washed with 5 % aqueous NaOH solution and the product was extracted using ethyl acetate. The organic layer was dried over anhydrous Na_2SO_4 and evaporated to get yellow solid as product. It was further purified by passing through silica gel column 60-120 mesh using 4 % ethyl acetate: pet ether solvent system. Yield = 8.9 g (78.0 %) ^{1}H NMR ($CDCl_3$, 400 MHz) δ: 7.15 ppm (t, 1H, Ar−H), 6.71 ppm (m, 3H, Ar−H), 4.15 ppm (t, 2H, Ar−OCH2), 3.89 ppm (t, 2H, CH_2−OH), 2.51 ppm (t, 2H, Ar−CH_2), 1.7−0.85 ppm (m, 29H, aliphatic H). ^{13}C NMR ($CDCl_3$, 100 MHz) δ: 155.76, 141.27, 127.81, 120.12, 113.59, 110.21 (Ar−C), 65.07 (Ar−O*CH*$_2$), 62.34 (CH_2−OH), 35.21, 31.22, 30.40, 28.98, 28.12, 28.36, 21.60, 13.92. MALDI −TOF (MW: 348.57): m/z = 348.02 (M + H^+). HR-MS (ESI+): m/z [M + H+] Calculated for $C_{23}H_{40}O_2$ [M+], 349.3078; found, 349.3106.

3.2.4 Synthesis of 3-((3-oxo-3-(2-(3-pentadecylphenoxy) ethoxy) propyl) disulfanyl) propanoic acid (2): 3, 3'-Dithiopropionic acid (DTPA) (5.0 g 24 mmol) and compound (**1**) (4.14 g 12 mmol) were dissolved in 100 mL dry THF and purged with nitrogen for 10

minutes. To the above mixture, DCC (3.19 g, 16 mmol) and DMAP (0.43 g, 4 mmol) dissolved in dry THF was added and the reaction continued for 12 hours at room temperature. Dicyclohexyl urea from the reaction mixture was separated by filtration and the organic solvent was evaporated. The product was purified by passing through silica gel column 60-120 mesh using 5 % ethyl acetate: pet ether solvent system. Yield = 5.8 g (36.0 %) ^{1}H NMR (400 MHz, d_6-DMSO) δ = 12.36 (s, 1 H), 7.16 (t, *J* = 7.9 Hz, 1 H), 6.81 - 6.67 (m, 3 H), 4.36 (dd, *J* = 3.8, 5.5 Hz, 2 H), 4.21 - 4.08 (m, 2 H), 2.97 - 2.82 (m, 4 H), 2.78 - 2.71 (m, 2 H), 2.64 - 2.57 (m, 2 H), 1.60 - 1.48 (m, 2 H), 1.34 - 1.18 (m, 24 H), 0.89 - 0.80 (m, 3 H). ^{13}C NMR (100 MHz, d_6-DMSO) δ: 172.4, 170.9, 158.0, 143.8, 128.9, 120.6, 114.3, 111.3, 65.2, 62.7, 39.9, 39.7, 39.5, 39.1, 38.9, 38.7, 35.0, 33.3, 33.1, 32.8, 32.4, 31.1, 30.6, 28.8, 28.8, 28.8, 28.7, 28.5, 28.5, 21.9, 13.7. MALDI −TOF (MW: 540.27): m/z = 563.28 $(M + Na)^+$. HR-MS (ESI+): m/z $[M + H]^+$ Calcd for $C_{29}H_{48}O_5S_2$ $[M]^+$, 541.2978; found, 541.3019.

3.2.5 Synthesis of DEX-SS-PDP: Dextran (M_w = 6,000, 1.0 g, 6.2 mmol of anhydroglucose unit), compound (**2**) (1.0 g, 1.83 mmol) were dissolved in anhydrous DMSO + DMF + DCM solvent mixture (15.0 mL: 8.0 mL: 2.0 mL). The formed reaction mixture was purged with dry nitrogen. To the above content, DMAP (0.22 g, 1.86 mmol) in DMSO (3.0 mL) and EDC.HCl (0.52 g, 2.72 mmol) in DMSO (3.0 mL) were added. The reaction mixture was stirred for 24 hours at room temperature. DMSO was removed; the liquid was precipitated in acetone. The purification was repeated at least twice to get pure dextran derivative which was dried under vacuum at 60 ^{o}C and stored. Yield = 0.65 g (65 %). ^{1}H NMR (400 MHz, d_6 DMSO) δ: 7.17-7.01 ppm (s, 1H, Ar-H), 6.76 - 6.72 ppm (m, 3H, Ar-H), 4.93, 4.85, 4.51 ppm (s) 4.68 ppm (s), 4.35ppm (t, 2H, Ar-O-*CH_2*), 4.16 ppm (t, 2H, -*CH_2*-OH), 3.14-3.69 ppm, 2.96 - 2.92 ppm (m, 4H, -*CH_2*-CH_2-S-S-), 2.76 - 2.72 (m,4H, -S-S-CH_2-*CH_2*-), 2.49 ppm (2H, Ar-*CH_2*), 1.53 ppm (2H, Ar-CH_2-*CH_2*), 1.18-0.80 ppm.

3.2.6 Synthesis of DEX-SS-PDP-Biotin: Dextran (M_w= 6,000, 1.0 g, 6.2 mmol of anhydroglucose unit), compound (**2**) acid (1.0 g, 1.83 mmol) and biotin (60.0 mg, 0.25 mmol) were dissolved in anhydrous DMSO+DMF+DCM solvent mixture (15.0 mL: 8.0

mL: 2.0 mL). The formed reaction mixture was purged with dry nitrogen. To the above content, DMAP (0.25 g, 2.04 mmol) in anhydrous DMSO (3.0 mL) and EDC.HCl (0.59 g, 3.08 mmol) in anhydrous DMSO (3.0 mL) were added. The rest of the procedure is followed as described for **DEX-SS-PDP.** Yield = 0.76 g (70 %). ^{1}H NMR (400 MHz, d_6 DMSO) δ: 7.17-7.01 ppm (s, 1H, Ar-H), 6.76 - 6.72 ppm (m, 3H, Ar-H), 6.42-6.36 ppm (biotin –NH protons), 4.93, 4.85, 4.51 ppm (s) 4.68 ppm (s), 4.35 ppm (t, 2H, Ar-O-CH_2), 4.27- 4.15 ppm (biotin –CH protons) 4.16 ppm (t, 2H, -CH_2-OH), 3.14-3.69 ppm, 2.96 - 2.92 ppm (m, 4H, -CH_2-CH_2-S-S-), 2.76 - 2.72 (m, 4H, -S-S-CH_2-CH_2-), 2.49 ppm (2H, Ar-CH_2), 2.15 ppm (s, 2H, biotin –CH_2), 1.60-1.30 (broad, 6H, biotin –CH_2), 1.53 ppm (2H, Ar-CH_2-CH_2), 1.18-0.80 ppm.

3.2.7 Synthesis of DEX -Biotin: Dextran (M_w = 6,000, 0.5 g, 3.18 mmol of anhydroglucose unit), Biotin (0.075 g, 0.308 mmol) were dissolved in anhydrous DMSO + DMF + DCM (15.0 mL: 8.0 mL: 2.0 mL) (25.0 mL) and the solution was purged with dry nitrogen. To the above content, DMAP (0.012 g, 0.098 mmol) in anhydrous DMSO (1.0 mL) and EDC.HCl (0.088 g, 0.47 mmol) in anhydrous DMSO (1.0 mL) were added. The reaction mixture was stirred for 24 hours at room temperature. The purification was done through precipitation technique as described for **DEX-SS-PDP.** The product filtered out and dried under vacuum at 60 ^{o}C to get white solid as product. The obtained white solid was further dissolved in DMSO and dialyzed against milli-q water to remove any non-conjugated biotin molecules. Further it is lyophilized and kept at 4 °C. Yield = 0.35 g (67 %). ^{1}H NMR (400 MHz, d_6 DMSO) δ: 6.39-6.34 ppm (biotin –NH protons), 4.92, 4.82, 4.50 ppm (s, hydroxyl of dextran) 4.68 ppm (s, dextran anomeric proton), 4.27-4.10 ppm (biotin –CH protons), 3.14-3.69 ppm (dextran glucosidic protons), 2.33 ppm (s, 2H, biotin –CH_2), 1.60-1.30 (broad, 6H, biotin –CH_2).

3.2.8 Determination of Critical Vesicular Concentration (CVC): The critical vesicular concentration for dextran vesicles were determined using pyrene as probe. Pyrene was dissolved in acetone and then 0.6 uM of pyrene solution was pipette in to the glass vials and acetone was allowed to evaporate slowly. To the above vials dextran conjugates with concentration ranging from 2.42 × 10^{-7} to 4.84 × 10^{-5} moles per litre were added and

allowed to sonicate for 4 hours and further equilibrated at room temperature for 4 hours. The emissions of the solution were recorded by fixing the excitation wavelength at 334 nm and slit width 2 nm. The ratio I_{371}/I_{382} was plotted against the dextran conjugate concentration and critical vesicular concentration was calculated.

3.2.9 HABA-Avidin Assay: This assay was carried out by following the procedure mentioned in the earlier report[19]. HABA solution was made by dissolving 24.2 mg of HABA in 10 mL of water followed by the addition of aqueous NaOH solution (100 µL). The avidin solution was made by dissolving 5.0 mg of avidin in 9.7 mL of PBS. In a typical experiment, HABA-avidin complex in 4:1 ratio was made in PBS and the complex formation was monitored at 505 nm. To the above solution, the different concentration of biotinylated samples (V_{BIOTIN}) were added and observed the change in the absorbtion maxima at 505 nm. The amount of free biotin molecules present on the V_{BIOTIN} were calculated using the formula mentioned in the report[19]. The similar conditions were used and the experiment was carried out in fetal bovine serum (FBS).

3.2.10 Stability of the V_{BIOTIN} serum using DLS Technique: To understand the *invitro* stability of the biotin conjugated dextran vesicles, 0.1 mg/mL of V_{BIOTIN} were made in 5 % fetal bovine serum (FBS), incubated at 37 ^{0}C for 24 hours. The size of V_{BIOTIN} in these solutions was measured using DLS every hour for the initial 6 hours and then at 9, 12 and 24 hours respectively.

3.2.11 Encapsulation of DOX.HCl in dextran Nano-vesicles: Drug encapsulation was done following our earlier procedure. [44,47] In a typical experiment 10.0 mg of the polymer and 0.2 mg of the DOX.HCl were dissolved in 1 mL HPLC grade DMSO and stirred for 10 minutes. To the above solution, 1.0 mL of Milli-Q water was added drop wise and the mixture is stirred for 12 hours and then dialyzed extensively against the milli-Q water using semi-permeable membrane (MWCO = 3500 Da) to remove any unencapsulated drug. The dialyzed solution is then lyophilised and stored at 4 °C. The Drug loading content (DLC) and drug loading efficiencies (DLE) were calculated using absorbance measurement method[41] for which the molar extinction coefficient for DOX.HCl is taken as 11,500 L mol^{-1} cm^{-1}.

DLC = (weight of drug in vesicles/ weight of drug loaded vesicles) × 100

DLE = (weight of drug in vesicles/ weight of drug in feed) × 100

The DLC and DLE for DOX.HCl loaded vesicles were found to be 2.1 ± 0.5 % and 70 ± 5 %, respectively. DOX.HCl was loaded in biotin conjugated dextran nanovesicles using DEX-SS-PDP-Biotin as described above. The DLC and DLE for DOX.HCl loaded vesicles were found to be 1.5 ± 0.7 % and 60 ± 5 %, respectively.

3.2.12 *In Vitro* Drug Release Studies: Drug release study was done following our earlier procedure [44,45]. The release profile of DOX.HCl from dextran nanovesicles was studied using dialysis method under physiological conditions.[41] Dialysed DOX.HCl encapsulated dextran nanovesicles solution 1.0 mL were taken in a dialysis membrane (MWCO: 3500 Da) and immersed in 10.0 mL of PBS at pH 7.4 taken in a beaker. At different time intervals 2.0 mL of PBS were taken out and replenished with equal volume of fresh PBS. The absorbance of each aliquot was measured using absorption spectroscopy. The absorbance at 480 nm was used to determine the amount of DOX released from the nanovesicles. Esterase assisted drug release studies were carried out by adding 10U esterase enzyme following the above-mentioned procedure. The cumulative release of the drug was calculated by using following equation:

Cumulative Release = (amount of drug release at time t/ total amount of drug taken in dialysis tube) × 100

3.2.13 Tissue Culture Conditions: : HeLa, wild type mouse embryonic fibroblast (WT-MEF) and breast cancer cells (MCF 7) were cultured in DMEM media supplemented with 5% fetal bovine serum (FBS) and 1 % penicillin-streptomycin at 37 °C under a 5% CO_2 humidified atmosphere. Cells were treated regularly with anti-mycoplasma agent sparfloxacin from Sigma to keep them mycoplasma free. Cells were detached using trypsin and seeded in 60mm dishes for all the biological experiments.

3.2.14 Cell Viability Assay and Cellular Imaging: To observe the effect of free drug and drug encapsulated vesicles, a cell viability assay was performed in WTMEF and HeLa cells using the tetrazolium salt, 3-(4,5 dimethylthiazol-)2,5-diphenyl tetrazolium bromide (MTT). For MTT assay following our earlier report.[44,47] Accordingly, 96-well

plate were seeded with 10^3 cells per well in 100 μL of complete DMEM and allowed to grow for 16 hours. Cells were then treated with different concentrations of the free drug and drug encapsulated vesicles. After 72 hours of incubation, the media from the cells were aspirated and 100 μL of freshly prepared MTT solution (0.5 mg/ mL in complete media) was added and incubated for another 4 hours at 37 °C. The formed formazan crystals were dissolved in 100 μL of DMSO and the absorbance was immediately measured using micro plate reader at 570 nm. The data represents the mean value from three independent measurements. The relative percentage values, with respect to control, were calculated for drug, the vesicle alone and drug-loaded vesicles. To visualise the cellular internalisation of the free drugs and drug loaded vesicles, WTMEF and HeLa cells were seeded at a density of 1×10^5 cells on cover slips placed in 6 well-plates containing 2.0 mL of complete DMEM medium and incubated at 37 °C for 16 hours. After 16 hours the cells were treated with the required concentration of drug alone and drug loaded vesicles and then incubated for next 9 hours or required time in CO_2 atmosphere. After required time incubation, the drug-containing medium was aspirated from each well, and cells were washed two times with 1X PBS (2 ×1 mL) and then fixed with 4 % paraformaldehyde solution in PBS for 10 min. at room temperature. The cells were again washed twice with 1X PBS (2 × 1 mL) and stained with DAPI solution in PBS. After incubation for 2 min, at room temperature in the dark, the excess dye was removed by washing the cells with 1X PBS for 1 min. The cover slips were then mounted on slides using Fluoromount™ mounting medium (Southern Biotech) and dried overnight at room temperature in the dark. The red fluorescence coming from doxorubicin at 520 nm was monitored through the red channel (λ = 561 nm) and the blue fluorescence produced by the cell nuclei by DAPI staining was monitored through blue channel (λ = 405). All the confocal images are recorded keeping all the parameters same for every measurement. DOX fluorescence intensity from the confocal images were calculated in Image J analysis software using the following equation:

Corrected Total Cell Florescence (CTCF) = Integrated Density – [Area of selected cell x Mean fluorescence of background reading]

3.2.15 Flow Cytometry Measurements: The cellular internalisation of the dextran nanovesicles in the WTMEF, cervical cancer cells (HeLa) were studied using flow cytometry experiment. In a typical experiment cells were seeded in 6-well plate at a density of 1×10^5 in each well and incubated for 16 hours at 37 °C. After 16 hours, the existing media were aspirated and the cells are treated fresh media containing free DOX and DOX loaded vesicles and incubated for another 9 hours. After 9 hours, the media was aspirated, each well was washed with 1X PBS (2 mL) to remove any unwanted impurity. The cells were detached using 0.5 mL of trypsin enzyme with 1 min of incubation. The cell suspension in the media was centrifuged at 1000 rpm for 5 min and then the pellet was resuspended in 1.0 mL of 1X PBS and taken for Flow cytometry studies. The studies were carried out by using the BD LSR Fortessa SORP cell analyzer which is equipped with five lasers and can detect 18 colours simultaneously (Central instrumentation facility, NCL Innovation Park, Pune, India). The 561 nm laser was used for the excitation of DOX and the band pass filter was chosen as 610 ± 10 nm. The fluorescence histograms were recorded from a population of 10000 cells.

3.2.16 Lysosomal Tracking of the Nanovesicles: In a typical experiment, 25000 cells were seeded in each well in live cell chamber and allowed to adhere for 16-18 hours. Further these cells were treated with required concentration of Fluorophore and incubated for another 6 hours. Finally the media was aspirated and cells were washed two times with PBS (1X) and cells were treated with 1.0 mL of DMEM media having 25.0 nM of Lysotracker green DND-26 and cells were imaged immediately.

3.2.17 Cellular Uptake at 4 ºC: In a typical experiment, 50000 cells were seeded in each well of six well plates and allowed to adhere for 16 hours. Media from the cells was then aspirated and fresh media containing the DOX loaded nanovesicles was added and cells were incubated at 4 ºC (on Ice) for 0.5 hour and finally fixed using paraformaldehyde. These cells were imaged using the confocal microscopy.

3.2.18 Cellular Uptake using Biotin Pre-treatment: 100000 cells were seeded in each well of six well plates and allowed to adhere for 16 hours. After 16 hours, cells were

treated with fresh media having 2.0 mM biotin concentration and incubated for another 1 hour at 37 ºC. Finally the media containing biotin was aspirated and cells were treated with fresh media having required concentration of DOX loaded nanovesicles and incubated for another 4 hours at 37 ºC. Finally cells were then fixed using paraformaldehyde and imaged using confocal microscopy.

3.3 Results and Discussion

3.3.1 Synthesis of Biotin-Conjugated Dextran

Biotin conjugated and dual responsive dextran derivatives were synthesized as shown in the scheme 3.1. A renewable resource and vesicular structure directing hydrophobic molecule 3-pentadecyl phenol (PDP)[41] from cashew nut shell liquid was coupled with 2-bromoethanol to yield the compound (**1**). The compound (**1**) was coupled at one end of the dithiopropionic acid through aliphatic ester linkages to yield compound (**2**).

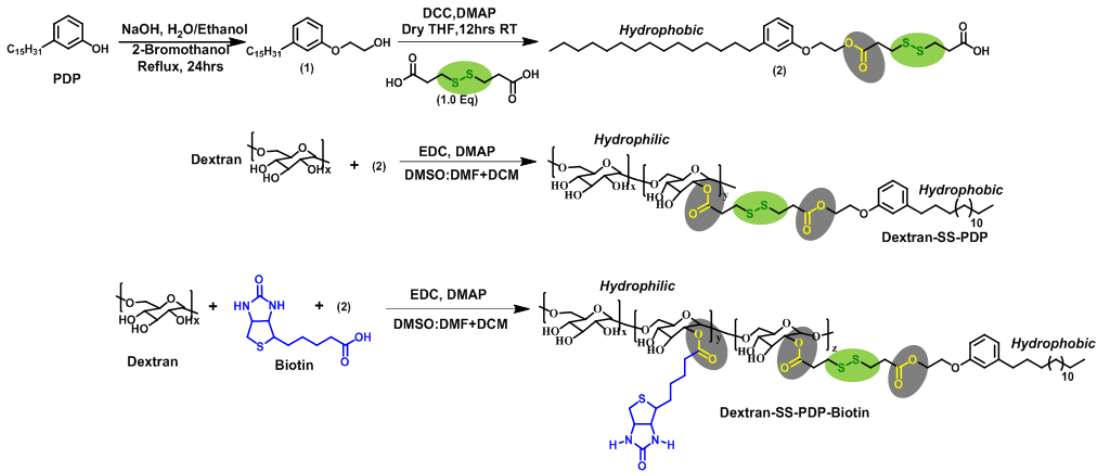

Scheme 3.1*: Synthesis of enzyme and GSH dual responsive and biotin-conjugated dextran derivatives.*

This hydrophobic unit (**2**) has the disulfide bond (-S-S) which is redox-degradable by glutothione (GSH) at intracellular compartmnets of cells (stimuli-1). The coupling of compound **2** in the dextran backbone produced DEX-SS-PDP. The conjugation of both compound **2** and biotin in the polysaccharide backbone in one-pot reaction yielded DEX-SS-PDP-Biotin. Both compound **2** and biotin were conjugated in the dextran backbone via aliphatic ester linkages that are enzymatically-biodegradable (stimuli-2) at the intracellular compartments. The structure of dextran derivatives were confirmed by ^{1}H-NMR. In figure 3.4 a, the PDP substituted unsymmetrical dithiopropionic acid molecule (**2**) showed expected number of protons and they are alphabetically assigned in the chemical structure. The carboxylic ester -$SCH_2C\mathbf{H}_2COOR$ (proton i) and carboxylic acid $SCH_2C\mathbf{H}_2COOH$ (proton L) appeared at 2.73 and 2.59 ppm, respectively. In figure 3.4, up on anchoring onto the dextran backbone, the carboxylic acid (proton L) vanished and the new ester peaks appeared together (proton i+L, double the intensity). Additionally,

the DEX-SS-PDP-Biotin dextran derivative showed peaks corresponding to PDP units at 6.8 to 7.3 ppm.

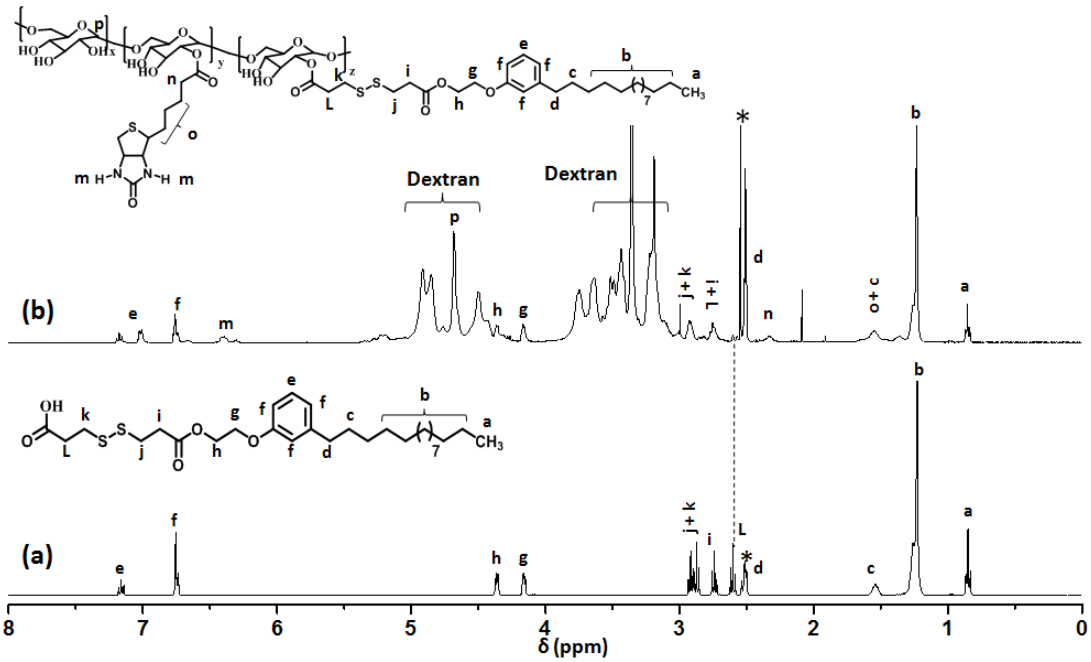

***Figure 3.4**: [1]H-NMR spectra of compound 2 (a) and DEX-SS-PDP-Biotin (b) in d_6-DMSO. The solvent peaks are assigned by asterisk.*

The broad peak at 6.5 ppm was assigned to N-H protons in biotin unit (proton m) and the new ester peak with respect to biotin conjugation in the dextran backbone appeared at 2.43 ppm (proton n). These peak assignments were further confirmed by comparing the [1]H-NMR spectra of DEX-SS-PDP (without biotin) and a control compound DEX-Biotin. To do so the control DEX-SS-PDP and DEX-Biotin were synthesised, their structures and NMR are given in figure 3.5 and 3.6.

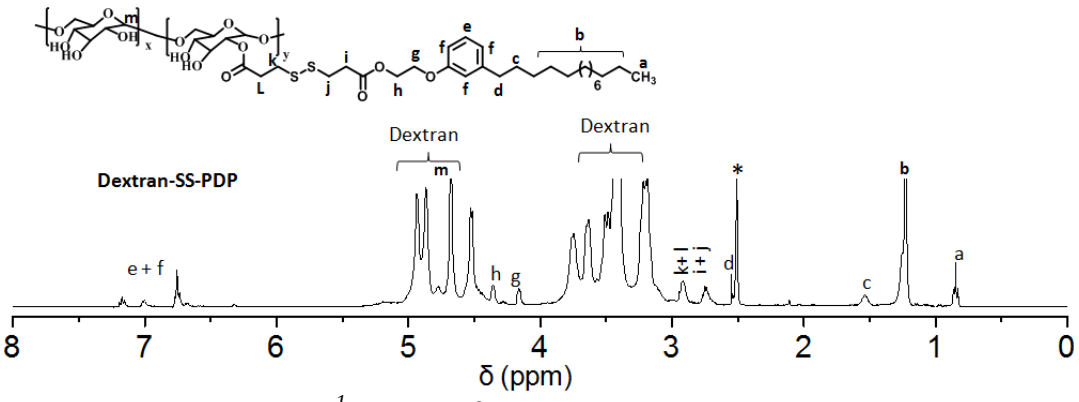

***Figure 3.5:** [1]H NMR of DEX-SS-PDP in DMSOd6.*

The peaks are assigned alphabetically as can be seen from figure 3.4 and 3.5. The degree of substitution of disulfide PDP on dextran backbone was determined by comparing the peak intensities of PDP aromatic protons at 6.8 ppm (proton e + f) or aliphatic protons of PDP (protons j + k) with dextran anomeric proton 4.6 ppm (proton p). The degree of substitution for biotin conjugation was determined by comparing the peak intensity of the biotin N-H peak at 6.4 ppm (proton-m) or ester peak at 2.43 ppm (proton n) with anomeric proton at 4.6 ppm (proton p).

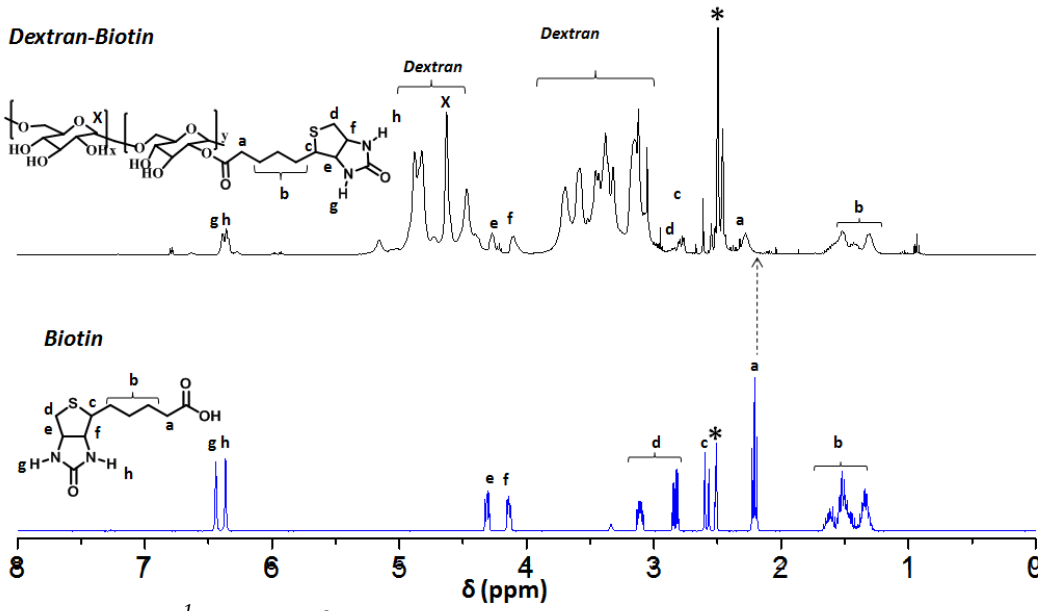

Figure 3.6: *^{1}H NMR of Biotin and DEX-biotin conjugate in DMSOd6.*

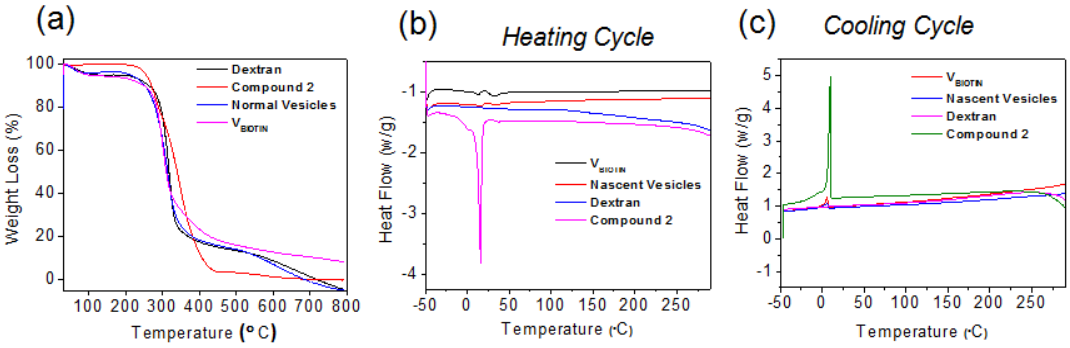

Figure 3.7: *Plots showing TGA of dextran,' compound 2, vesicle (V) and V_{BIOTIN} (a), Plot showing the heating cycles of DSC thermogram for $V_{BIOTIN.}$, nascent vesicles, dextran and compound 2 (b) and Plot showing the cooling cycles of DSC thermogram for $V_{BIOTIN.}$, vesicle (V), dextran and compound 2 (c).*

The degree of substitution of PDP and biotin were estimated to be 5.0 % and 2.0 %, respectively. The higher incorporation of PDP + biotin (more than 10 % in total) in the dextran backbone produced water insoluble polymers; thus the total degree of substitution was restricted to less than 10 %. To understand the thermally stability and effect of substitution on amorphous nature of dextran, TGA and DSC analysis of the polymer derivatives was carried out and showed in figure 3.7. The results obtained proved that they are thermally stable up to 250 °C and they were found to be largely amorphous in nature.

3.3.2: Dextran Nano-vesicles and DOX.HCl Encapsulation

In the present investigation, the hydrophilic polysaccharide backbone (dextran) was conjugated with hydrophobic amphiphilic unit based on PDP; thus in aqueous medium, the hydrophobic chain oriented away from the water to give amphiphilic sheet-like geometry. The inter-digitations of PDP chain from the apmphiphilic dextran resulted in bi-layer self-assemblies which folded into vesicular architectures through cooperative interactions. The evidence for the PDP chains inter-digitations in the vesicular geometry was proved by single crystal structure analysis of PDP units in our earlier work.[51-52]

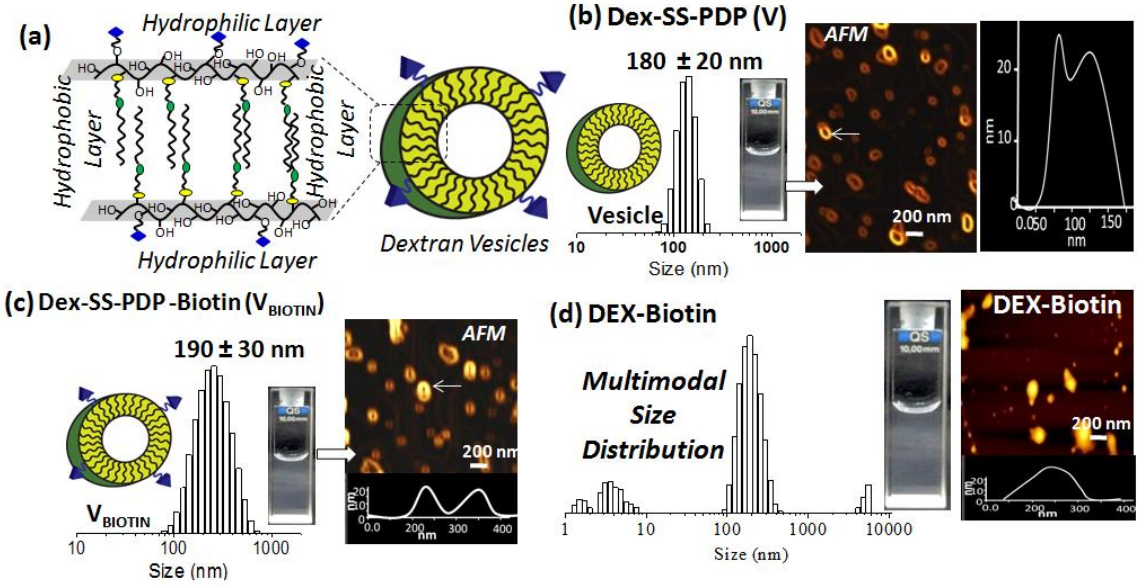

Figure 3.8: *Self-assembly of dextran derivative into vesicles (a), DLS histogram and AFM images of DEX-SS-PDP vesicles (V) (b), DLS histogram and AFM images of DEX-SS-PDP-Biotin vesicles (V_{BIOTIN}) (c), DLS histogram, AFM image of DEX-Biotin (d).*

Thus, it is anticipated that the PDP + dithiopropionic ester linkages in the present design is also expected to follow similar inter-digitation to produce well-defined dextran vesicles (see Figure 3.8 a). To study the self-assembly behaviours of newly designed dextran derivatives DEX-SS-PDP-Biotin, DEX-SS-PDP, and DEX-Biotin; they were subjected to dialysis in water. Typically, dextran derivatives were dispersed in water + DMSO and dialysed using semi-permeable membrane of MWCO = 3500 in milli-Q water. The dialysate was replenished with fresh water periodically to remove DMSO and at the end of 48 hours of dialysis, a transparent solution was produced (see Figure 3.9) which was lyophilized and stored at 4 °C. These dialysed dextran derivatives were subjected to dynamic light scattering (DLS) and atomic force microscope (AFM) analysis. In figure 3.8 b, DLS histograms of DEX-SS-PDP showed monomodal distribution with size 180 ± 20 nm. AFM is a very powerful tool to study the morphological features of soft-materials such as vesicles created from aqueous medium.[41] AFM images of DEX-SS-PDP in figure 3.8 b appeared as donut-shaped spherical objects with diameter 180 ± 30 nm with height of the nano vesicles around 20 ± 10 nm (see Figure 3.8 b). The sizes of the nano-vesicles in AFM image exactly matched with the DLS nano-aggregates in aqueous medium confirming that vesicular self-assembly was indeed created and preserved in the aqueous medium through the hydrophilic and hydrophobic interaction as represented in figure 3.8 a. DLS histograms and AFM images for DEX-SS-PDP-Biotin are shown in figure 3.8 c. The size of the assembly from DLS and AFM images were obtained as 190 ± 30 nm and 200 ± 20 nm, respectively, indicating that the vesicular nano-assembly was perfectly preserved in the biotin conjugated dextran derivative as well. Similarly DLS and AFM measurements for DEX-biotin (without SS-PDP unit) was carried out in showed in figure 3.8 d revealed that the polymer structure produced nanoparticles rather than vesicles. This emphasised the need of SS-PDP unit in the dextran backbone to produce vesicular geometry (see figure 3.8a) and the result was in accordance with our earlier observation[41,47] that the PDP unit was essential to self-assemble the dextran backbone into nano-vesicles in aqueous medium. Further static light scattering (SLS) studies were carried out to establish the nano-vesicle aggregates in solution state and histograms are showed in figure 3.9 a and b. SLS gives the radius of gyration (R_g) of the polymer assemblies and DLS provides the

hydrodynamic radius (R_h) of the polymer nano-assemblies. The ratio of the R_g/R_h =1 for polymer nano-vesicles as reported in the literature.[53-54,41] In the present investigation, the R_g = 70 nm was obtained as from SLS and R_h = 73 nm from DLS; thus the ratio R_g/R_h = 70 nm / 73 nm = 0.96 ≈ 1.0, which confirmed the formation of polymer nanovesicles in the solution state. The size of the nano-vesicles is matched very well with the DLS, AFM, FESEM images as shown in figure 3.8. To study the role of concentration of polymer on the nanovesicle formation, the self-assembly was carried out by dialysis method by varying the concentration from 0.001 to 1.0 mg/mL (1000 time dilution). DLS data of these dialyzed solutions showed in figure 3.9 c, revealed that the size of the nanovesicles were almost retained in the same range of 220 ± 20 nm irrespective of the variation in the concentration of polymer solution. Thus, we believe that the polymer vesicles formation was largely driven by the structure rather than concentration. Hence, the present design could produce vesicles of 200 ± 20 nm in size which is in the acceptable range for EPR effect.[55] The above dextran nano-vesicles DEX-SS-PDP and its biotin conjugated analogue DEX-SS-PDP-Biotin are hereafter referred as V and V_{BIOTIN}, respectively. The critical vesicular concentration of the dextran vesicles was determined using pyrene as probe.[41]

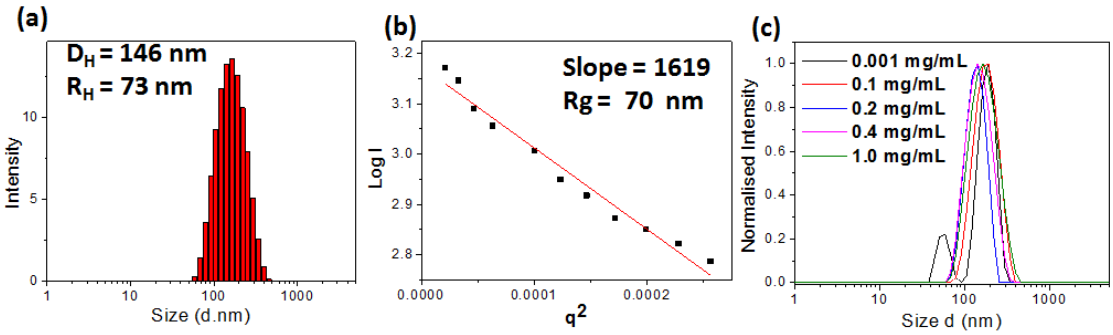

Figure 3.9: *DLS Histogram of V_{BIOTIN} (a), Guinier plot from SLS Experiment (b) and concentration dependent DLS histogram for V_{BIOTIN} (c).*

A fixed amount of pyrene (0.6μM) was used and the concentrations of the dextran conjugates were varied from 2.4 × 10^{-7} to 4.8 × 10^{-5} M. The obtained fluorescence spectrum and the plot of I_1/I_3 against concentration are showed in figure 3.10. From the ratio of the pyrene characteristic peaks (I_1/I_3), the critical vesicular concentration was determined as 2.4 × 10^{-6} M. One of the unique features of vesicles or polymersomes is

that they possess hydrophilic core for encapsulation of water soluble fluorophore dye like Rhodamine B (RhB) and water soluble anticancer drugs such as doxorubicin-hydrochloride DOX.HCl which are not possible in micelles or nanoparticles.[44] To study the encapsulation capability of newly designed dextran vesicles, V and V_{BIOTIN} were subjected for encapsulation of RhB and DOX.HCl by dialysis method using semi-permeable membrane MWCO = 3500 Da as described earlier. The DLS histogram of $V_{BIOTIN+DOX.HCl}$ showed the size of the nano-vesicles as 200 ± 20 nm (see Figure 3.11 a). AFM morphology confirmed the donut-shaped features with respect to vesicular morphology.

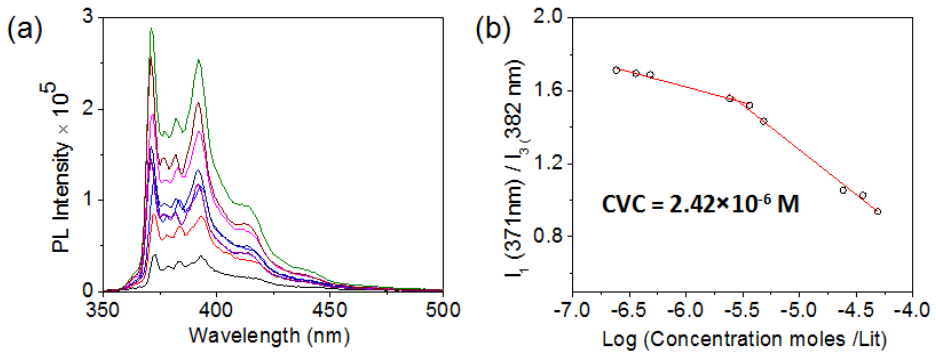

Figure 3.10: *Plot showing the emission spectrum of pyrene at varying concentration of* V_{BIOTIN} (a) *and Plot of* $I_1(371)/I_3(382)$*peal intensity versus the log of* V_{BIOTIN} *concentration (b).*

Field mission scanning electron microscope (FESEM) and transmission electron microscope (TEM) images further confirmed the spherical nature of the vesicular nano-assemblies with difference in contrast with respect to the layer and core (see Figure 3.11 a). DLS, AFM, FESEM and HR-TEM images showed the sizes < 200 nm and confirmed existence of the dextran nano-vesicles. $V_{DOX.HCl}$ (without biotin conjugation) and V_{RhB} and $V_{BIOTIN+RhB}$, they were also found to exist as nano-vesicles. The DLS spectrum for $V_{DOX.HCl,}$ V_{RhB} and $V_{BIOTIN+RhB}$ is showed in figure 3.11 b-d which confirmed the monomodal distribution of sizes. Using absorption spectroscopy, the drug (or dye) loading content (DLC) was obtained in the range of 1.5 to 2.0 %. The drug (or dye) loading efficiency (DLE) was typically obtained in the ranges of 50 to 60 % (see figure 3.12 a). The absorbance and fluorescence spectra for RhB and DOX.HCl encapsulated

nano-vesicles showed very good red-emission suitable for bio imaging process. The table showing the drug loading efficiencies and the absorbance and emission spectrum are given in figure 3.12. Other method like sonication was also explored for the encapsulation of DOX.HCl in the vesicles.

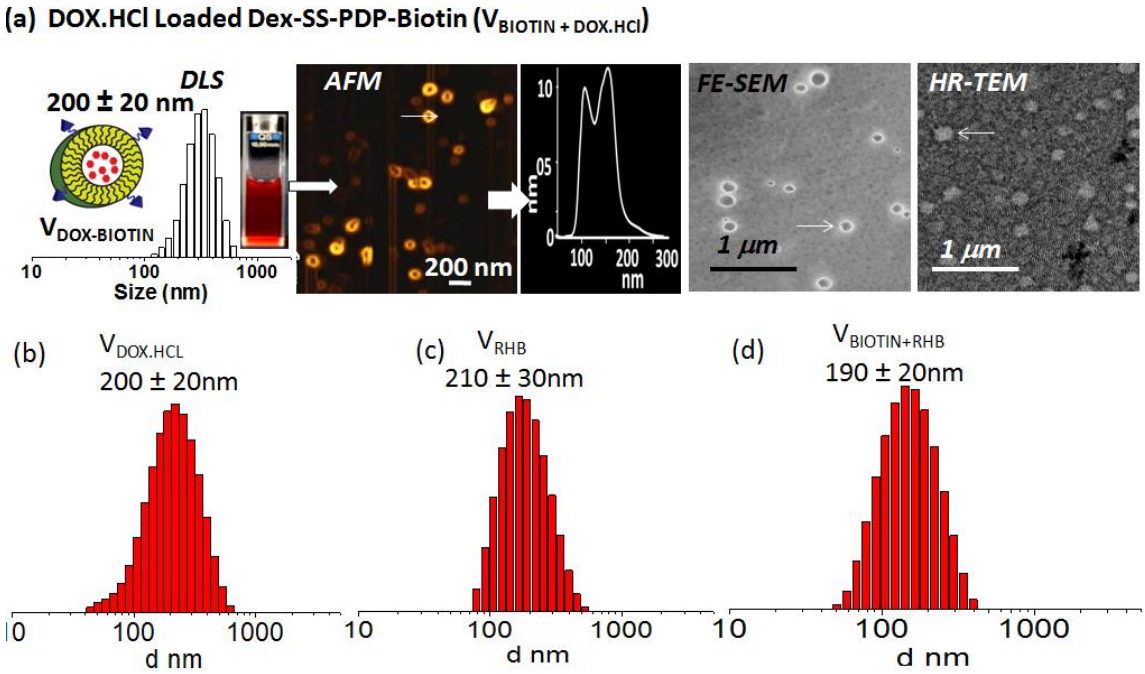

Figure 3.11: Schematics of DOX loaded vesicles, DLS histogram, AFM, FESEM and HRTEM images for $V_{BIOTIN+DOX.HCl}$, DLS histogram for $V_{DOX.HCl}$ (b), V_{RHB} (c) and $V_{BIOTIN+RHB}$ (d).

The sonication method gave much higher DLC = 37 %. However, further dialysis of the sonication-assisted sample exhibited premature leaching of the drug. At the end of the dialysis, the DLC was obtained as 1.8 % which is similar to that of direct dialysis process (without prior sonication). Hence, the dialysis procedure is the one of the best way to encapsulate water soluble drugs to produce stable DOX formulation in polysaccharide vesicles.

(a)

S.N.	Sample Name	DLC (%)	DLE (%)
1	$V_{DOX.HCl}$	2.1±0.5	58±5
2	$V_{BIOTIN+DOX.HCl}$	1.5±0.7	60±6
3	V_{RHB}	1.2±0.5	55±7
4	$V_{BIOTIN+ RHB}$	1.1±0.6	54±5

(b)

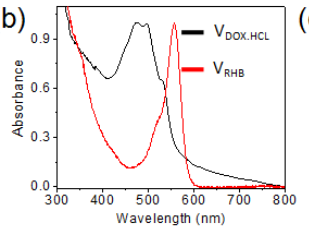

(c)

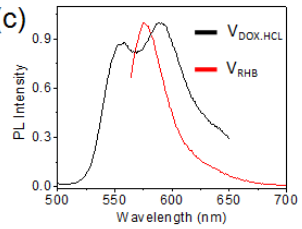

***Figure 3.12**: Table showing the drug loading content (DLC) and drug loading efficiencies for $V_{DOX.HCl}$, $V_{BIOTIN+ DOX.HCl}$, V_{RHB} and $V_{BIOTIN+RHB}$ (a), plot showing the absorbance spectrum for $V_{DOX.HCl}$ and V_{RHB} (b), plot showing the emission spectrum for $V_{DOX.HCl}$ and V_{RHB}(c).*

3.3.3 Avidin-Binding Assay and Stimuli-Responsive Delivery

The dextran vesicles are designed with three components which are responsive to cancer cells both at the extracellular and intracellular environments. These responsiveness are: (i) receptor-assisted endocytosis process at the periphery of the cell membranes (see Figure 3.13 a), (ii) redox-cleavable disulfide (S-S) chemical linkages to disassemble the vesicular assemblies by glutathione (GSH) residue in the cytosol, and (iii) lysosomal enzymatic-biodegradation of aliphatic ester linkage connecting the hydrophobic unit at the dextran backbone (see Figure 3.14 a. To study the receptor-mediated biological events, *in vitro* experiments were designed based on Avidin-HABA assay [19,56-57] and the data is summarized in Figures 3.13 b-d. Avidin has four binding sites for HABA (4'-hydroxyazobenzene-2-carboxylic acid); thus, 1:4 complex of Avidin-HABA was produced following the reported procedure.[19] Avidin-HABA complex showed unique absorption peak at 505 nm which is completely distinguished from either HABA or avidin and this information is showed in figure 3.13 b. This avidin-HABA complex was titrated with biotin conjugated vesicles (V_{BIOTIN}) and normal vesicles (V) and the data are shown in figure 3.13 c. As shown in figure 3.13 c, there is a gradual decrease in the absorption of Avidin-HABA complex at 505 nm with the increase in the concentration of V_{BIOTIN}. Interestingly, the non-biotin conjugated vesicles (V) did not show any changes in the absorption maxima of Avidin-HABA complex (see red line in Figure 3.13 c). This further confirmed that the biotin free vesicles (V) do not possess any binding towards Avidin. This trend clearly indicates that the HABA molecules are getting replaced by the V_{BIOTIN} in the Avidin-HABA complex. The reason for this replacement of HABA molecules by V_{BIOTIN} samples can be attributed to the higher association constant for

Avidin-Biotin compared to that of Avidin-HABA complex.[8] Thus, the decrease in the absorbance maxima followed by the additions of V_{BIOTIN} is arisen followed by the complexation of Avidin-biotin at the periphery of biotin conjugated (V_{BIOTIN}) nanovesicles. This decrease in the absorption was plotted as $[(A_0-A_C)/A_0]$ versus concentration of the biotin in the vesicles, where A_0 is the initial absorbance and A_C is the absorbance at concentration 'C'. As can be seen from the figure 3.13 d, the value of $[(A_0-A_C)/A_0]$ steadily increases and saturated at 25 nM. From the break point in the plot, it can be assured that the avidin-biotin interactions saturated at 25 nM of biotin at the periphery of vesicles.

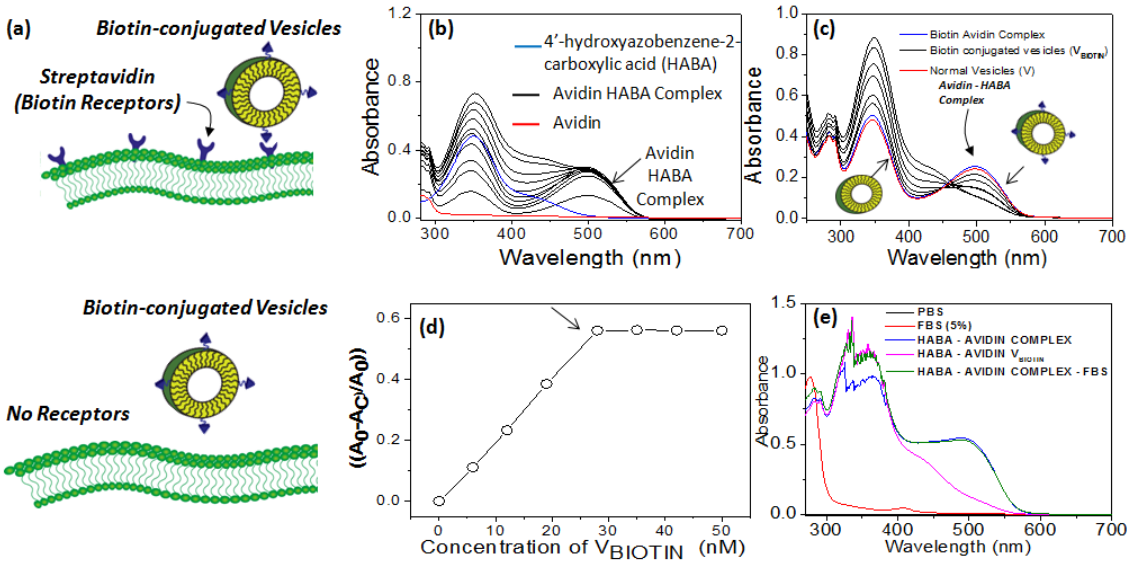

Figure 3.13: *Receptor mediated binding of biotin conjugated vesicles (V_{BIOTIN}) on the cell membrane(a), Absorbance spectra for HABA, avidin-HABA complex and avidin (b), Absorbance spectra of the Avidin-HABA complex upon additions of biotin conjugated dextran vesicles (V_{BIOTIN}) and biotin free vesicles (V) (c), Plot of* $[(A_0-A_C)/A_0]$ versus *the concentration of V_{BIOTIN} (d), HABA-Avidin complex in FBS and and HABA-Avidin complex in FBS with V_{BIOTIN} (e).*

The number of biotin molecules per polymer chains were determined by the method reported by Karen Wooley and co-workers.[19] It was found to be approximately one molecule of biotin present in each polymer chain which is calculated using the following equation,

1. *Calculations for no. of milimoles of biotinylated polymer sample (V_{Biotin})*
   = Amount of polymer used (mg) / Molecular weight of polymer

   = 0.16/6482

$= 2.46 \times 10^{-5}$ *mmol*

2. ΔA_{500} = *(0.9 × A500 HABA-Avidin) –* (A_{500}*HABA-AVIDIN-*V_{Biotin}*)*
   = (0.9 × 0.2492) - (0.09857)

   = 0.1257

3. *Milimoles of Biotin =* ΔA_{500}*/ 34000 × b* *(b = path length = 1)*
   = 0.1257/34000

   $= 3.69 \times 10^{-6}$

4. *Number of Biotin molecules per polymer chain = milimoles of* V_{Biotin} *× 10 / milimoles of Biotin*

   $= 3.698 \times 10^{-6} / 2.46 \times 10^{-5}$

   = 1.50 Biotin molecules per polymer chain.

The affinity of the biotin-nanovesicles towards Avidin is in accordance to the other polymer systems.[19,56-57] Thus, the current dextran vesicle possess significant amount of biotin to bind streptavidin like membrane protein on cancer cells surface for targeted delivery. To differentiate the circulating free biotin and biotin-conjugated vesicles towards their molecular interaction with avidin like receptors under physiological conditions, competitive binding assay was studied in fetal bovine serum (FBS) and showed in figure 3.13e. Interestingly, there was no replacement of HABA molecules from avidin-HABA complex by the residual biotin present if at all in FBS. The addition of biotin conjugated vesicles (V_{BIOTIN}) into this avidin-HABA complex in FBS immediately showed decrease in the spectroscopic signal at 505 nm with respect to the binding of biotin-conjugated vesicles (V_{BIOTIN} vesicles) in the avidin pocket. This control experiment provides direct evidence for the targeting ability of biotin-conjugated vesicles towards the membrane receptors under physiological conditions.

3.3.4 Enzyme and GSH Dual Responsiveness

The dextran vesicles are designed with two intracellular stimuli to break nano-carriers to release the drugs. Glutathione (GSH) is largely present in the cytosol of the

cells and its concentrations vary significantly from extracellular (1.0 μM) to intracellular level (1.0 mM)[48]. The polymer nano-carriers built with disulphide chemical linkages are susceptible to undergo redox-degradation by GSH[48] (see Figure 3.14 a). In the present case, the vesicles were constructed with –S-S- linkages in the hydrophobic units; thus, *in vitro* drug release kinetic studies were carried out for the DOX.HCl loaded nano-vesicles by exposing them to GSH in PBS. The GSH cleavage of the hydrophobic tail ruptured the nano-vesicular structure and the DOX.HCl gets released. The cumulative drug release was estimated by measuring the absorbance of DOX.HCl in the reservoirs and the release profile is shown in Figure 3.14 b and c. In the absence of GSH, about 20 % drug leaching was observed due to the presence of salts in PBS. The anions like PO_4^{2-} in PBS are well-known to influence on the stability of the polymer nano-assemblies through Hofmeister effect and salting-out of macromolecules in solution.[58] The PO_4^{2-} anion is typical salting-out type which induces the partial phase separation of the polymer nano-assemblies in PBS which accounts for 20 % leaching.[59] The stability of the dextran vesicles was further checked in FBS and since FBS are free of ions, DLS studies showed that the vesicles are stable for more than 24 hours and the results are showed in figure 3.14 d. The release was significantly influenced by the presence of GSH and about 60 % drug was released in a controlled manner. This suggested that once the nano-vesicles enter the cytosol, the GSH could partially disassemble the vesicles to release about 60 % of the drugs. Another important process in which the nano-vesicles are transported and digested across the cell membrane is mediated by endosome-lysosome compartments. Lysosomes typically have large abundance of digestive enzymes such as α-chymotrypsin, trypsin, esterase and phosphatase, etc[60]. Among this esterase enzyme could readily biodegrade aliphatic ester chemical linkages[49] to deliver the drugs. Aliphatic ester-linkages are readily susceptible to undergo lysosomal enzymatic biodegradation and this concept has been proven very well by us and few others in L-amino acids based polyesters,[49] poly(ester-amide)s,[60] substituted polycaprolctone block copolymers[61] and PEG-PLLA copolymers.[62] In the present design, the hydrophobic tail was conjugated with dextran using aliphatic ester chemical linkages (see Scheme-3.3). Thus, the *in vitro* drug release profile data shown in Figure 3.14 b in the presence of esterase enzyme in PBS is direct proof for the enzymatic biodegradation of the polysaccharide vesicles. Esterase enzyme docking studies from our

lab[45] had shown that the dextran-PDP ester linkage readily occupied the enzymatic pocket for biodegradation. Since the present vesicular structure has been built with aliphatic ester linkages that connect the hydrophobic unit in the dextran backbone, esterase enzyme was employed as stimuli to study the drug release kinetics. In figure 3.14 b, the drug release pattern was found much higher for esterase enzyme exposure and almost 90 % DOX.HCl was released in 12 hours. In order to study the combination effect of GSH and esterase-enzyme action together, the nano-vesicles were initially subjected to GSH incubation for 24 hours and subsequently esterase enzyme was added. In this process, the release kinetics data in figure 3.14 c showed GSH could release 60 % drugs and the remaining 40 % drug was essentially released by esterase. Hence, the combination of GSH and esterase enzyme stimuli are very good triggers to release water soluble DOX.HCl in controlled manner at the intracellular compartments of cells. Similarly, the non-biotin conjugated dextran vesicles were also subjected to drug release studies for GSH and enzyme responsiveness and results are showed in figure 3.16 b and c. The drug release patterns were found almost identical in both biotin-conjugated (see Figure 3.14 b and c) and biotin free dextran vesicles (see figure 3.14 e).

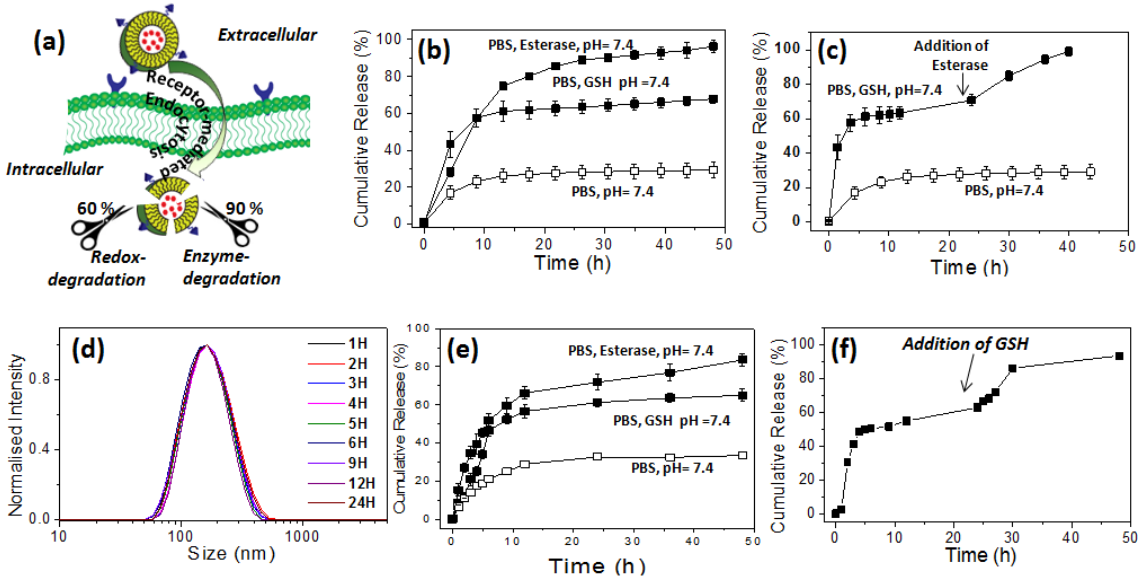

Figure 3.14: *Schematics of intracellular degradation of nanovesicles by GSH and Enzyme dual stimuli (a), Cumulative drug release plots showing the release of DOX. HCl from* $V_{BIOTIN+DOX.HCl}$ *vesicle in PBS at pH 7.4, 37°C, incubated in presence of 10 mM GSH, and incubated in presence of 10 U esterase enzyme (b), drug release plot showing the DOX release from* $V_{BIOTIN+DOX.HCl}$ *in PBS at pH 7.4 in presence of 10 mM GSH for 24 h and subsequent addition of 10 U of esterase enzyme(c), DLS histograms of* V_{BIOTIN} *in FBS at different time intervals (d), Plot showing doxorubicin hydrochloride release from*

$V_{DOX.HCl}$ in presence of 10 U of esterase enzyme and in presence of 10 mM glutathione (GSH) (e) and Plot showing doxorubicin hydrochloride release from $V_{BIOTIN+DOX.HCl}$ in presence of 10U of esterase enzyme upto 24hours and then followed by addition of GSH 10 mM (f).

To address the possibility of disassembly of nano-carriers in the cytosol by GSH and their further migration toward the endo-lysosomal compartment for biodegradation by enzymes; the drug release study was carried out by (i) initially incubating the DOX loaded polymer vesicles in the presence of esterase enzyme and then (ii) administrate glutathione (GSH, 10mM) in PBS. The drug release was done by dialysis method and monitored by absorption spectroscopy and showed in figure 3.16 d. From the results, it is clear that the esterase enzyme predominantly released the drug (65-70 %) and the remaining 30 % of the drugs released by GSH. This experiment along with the data in figure 3.14 f suggests that enzyme and GSH responsiveness work together in the intracellular compartment to maximize the digestion of nanovesicles for drug release rather than in sequential manner. The above studies confirmed that the newly designed dextran vesicles are efficient triple action nano-carriers to undergo receptor mediated interaction at the cell membrane, readily cleavable by GSH in the cytosol, and also completely digested by esterase enzyme at the lysosomal compartments.

3.3.4 Cytotoxicity and Lysosomal Degradation of Vesicles:

Cytotoxicity of the dextran vesicles was studied by MTT Assay. In cervical cancer cells (HeLa) and wild type mouse embryonic fibrolast (WT-MEF) cells (normal cell line), the dextran vesicles were found to be non-toxic to cells up to 80 µg/mL (see figure 3.15 a and c). DOX.HCl loaded dextran vesicles $V_{DOX.HCl}$ and $V_{BIOTIN+DOX.HCl}$ were treated in HeLa cells by varying the drug concentration ranging from 0.1 to 1.0 µg/mL. The vesicle assisted drug administration seems to be better in accomplishing cytotoxicity in HeLa cells compared to free drug (see figure 3.15 b). The effect of cell killing by the DOX loaded nanovesicle in MCF 7 is almost identical to that of HeLa (cervical) cancer cell line (see figure 3.15 e). This suggested that the approach is not restricted to one particular cancer cell lines. Further among the vesicles, the biotin-conjugated vesicles $V_{BIOTIN+DOX.HCl}$ were able to achieve much better IC_{50} at a concentration of 0.1 µg/mL which is almost 5 times better than the IC_{50} of 0.5 µg/mL by free drugs. When DOX.HCl

loaded dextran vesicles were tested in WT-MEF cell line (normal cells, see figure 3.15 d), they showed relatively less cytotoxicity compared to free drugs. This observation is particularly important since the free drug is more toxic to the WT-MEF cells compared to cancer cells. DOX-loaded vesicles largely kill the cancer cells (> 90 %); however, the effect was much lower in the normal cells (< 50 %). To compare the cytotoxicity effect induced by the GSH stimuli, two types of polymer vesicles were employed for MTT assay. For this purpose (i) vesicles without disulfide chemical linkages in the hydrophobic part reported in our earlier work[46] and (ii) vesicles with disulfide linkages (V_{BIOTIN}, reported here) were employed. It is important to mention that both types of vesicles have aliphatic ester linkages that connect the hydrophobic part in the dextran backbone; thus, these vesicles are readily biodegradable by lysosomal enzymes. These nanovesicles were encapsulated with DOX and their cytotoxicity data was carried out in breast cancer cells (MCF 7) and the details are summarized in figure 3.15 e and f.

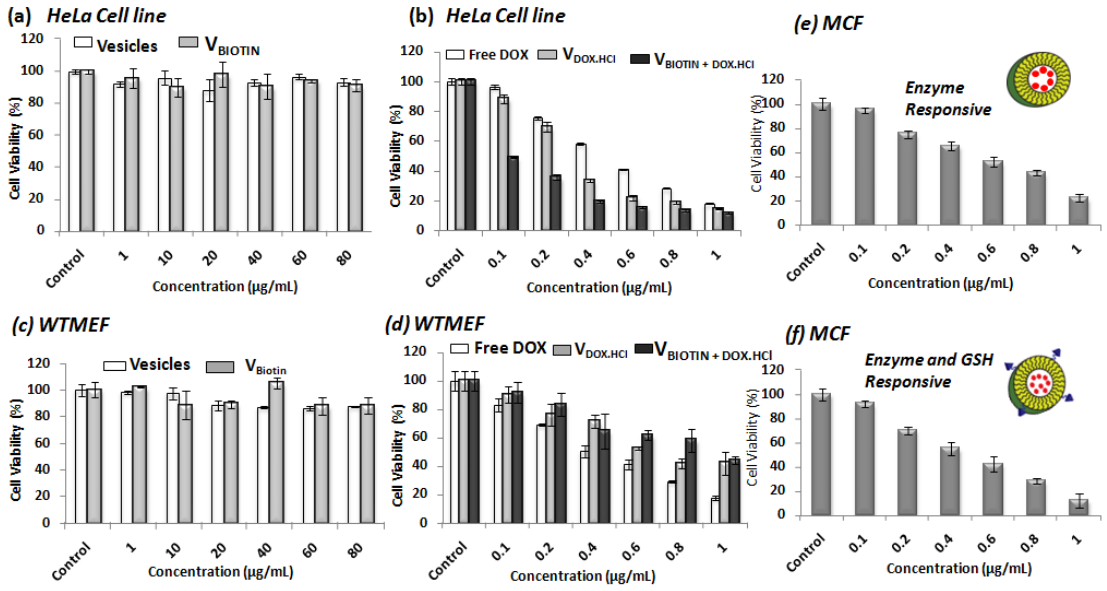

Figure 3.15: *Histogram showing the cytotoxicity profiles of dextran vesicles (V) and V_{BIOTIN} in HeLa cell line (a), Histogram showing the cytotoxicity profile for free DOX.HCl, $V_{DOX.HCl}$ and $V_{BIOTIN+DOX.HCl}$ in HeLa cell line (b), Histogram showing the cytotoxicity profiles of dextran vesicles (V) and V_{BIOTIN} in WTMEF cell line (c) Histogram showing the cytotoxicity profile for free DOX.HCl, $V_{DOX.HCl}$ and $V_{BIOTIN+DOX.HCl}$ in WT-MEF cell line (d), histogram showing cytotoxicity profile for $V_{BIOTIN+DOX.HCl}$ (enzyme and GSH dual responsive) (e) and $V_{DOX.HCl}$ (enzyme responsive) in MCF 7 cells(f).*

It is very clear from the data that the disulfide containing vesicles exhibited comparatively better killing at higher concentration compared to the non disulfide

vesicles. The data validated that GSH accelerated rupturing of the disulfide containing nanovesicles at the intracellular compartments. To study the cellular internalization and localization of the DOX.HCl loaded dextran vesicles and the digestion of dextran vesicles in the lysosomal compartments, live cell imaging was done using lyso-tracker in confocal scanning electron microscopy (see Figures 3.16 a and 3.16 b). The dextran vesicles $V_{DOX.HCl}$ and $V_{BIOTIN+DOX.HCl}$ showed significant amount of drugs at the nucleus and cytoplasm in red channels with respect to DOX emission. The lysosomes are stained in green colour and upon merging with the red channel, the merged images showed yellow colour in the cytosol and red in the nucleus. The yellow emission from the cytosol is an outcome of the co-localization of red emitting DOX and green lyso-tracker. This study confirmed that the dextran vesicles are indeed digested in the lysosomal compartments in cytosol.

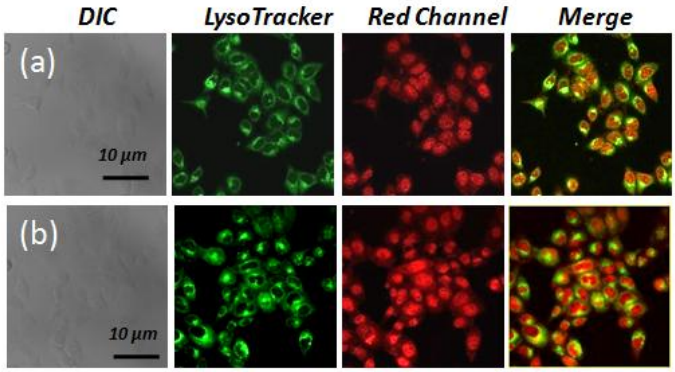

Figure 3.16: *Live cell confocal microscopic images in HeLa cells for the uptake of $V_{DOX.HCl}$ (a) and $V_{BIOTIN+DOX.HCl}$ (b). The concentration of the Lyso tracker green and drug used are 25 nM and 2 µM respectively. The cells were incubated for 4 h at 37 ° C.*

The DOX.HCl released from the vesicles accumulated in the nucleus to exhibit strong red-emission. From the above *in vitro* results, it can be concluded that the custom designed dextran vesicles can be used for targeting the biotin receptor that are over expressed in cancer cells as well as high cytotoxicity can also be achieved through GSH and lysosomal-enzyme stimuli.

3.3.5 Receptor-Mediated Endocytosis

The uptake of nano-carriers in cells is typically controlled by four independent pathways: (i) Macropincytosis[63], (ii) direct endocytosis through hydrophobic like-like

interactions between nano-carriers and membrane, (iii) endocytosis assisted by caveolae or clathrin proteins[64], and (iv) receptor-ligand interaction mediated endocytosis.[1-4] Among all these processes, the receptor-ligand mediated process seems to be very effective since many cancer cells are over expressed with multiple receptors for folic acid, biotin and RGD peptide, etc. To study the role of the receptor-mediated endocytosis process, two cell lines are chosen that are reported to have large difference in their membranes for biotin-receptors. Cervical cancer cells (HeLa) were found to be significantly over expressed with biotin-receptors compared to WT-MEF cells (normal cells).[17] Biotin receptor over expression is one of the well proven concept in HeLa cell line (cervical cancer) and HeLa cells were widely used by previous researchers to study the receptor-mediated uptake in biotin-tagged nano-assemblies and biotin-tagged polymer nanoparticles.[9,16-21,55,56] Hence, the HeLa cell line was chosen in the present investigation for studying the biotin receptor-mediated endocytosis in the newly designed biotin-tagged polysaccharide vesicles. The cellular uptake and intracellular localisation of the dextran vesicles $V_{DOX.HCl}$ and $V_{BIOTIN+DOX.HCl}$ was monitored by the confocal (CLSM) microscopy. Biotin conjugated and non-conjugated dextran vesicles were treated in these two different cell lines by varying the incubation time from 30 minutes to 360 minutes (6 hours). The images in the figure 3.17 a showed the cellular uptake of $V_{BIOTIN+DOX.HCl}$ vesicles with increasing incubation time. It is very clear from the images that the red fluorescence intensity from DOX.HCl gradually increased with the incubation time indicating that more drugs are taken up by the cells over a period of time. The fluorescence intensity from the images almost saturated at 6 hours. The images for non-biotin conjugated vesicles $V_{DOX.HCl}$ showed increment in the fluorescence intensity with incubation time (see Figure 3.17 b); however, the intensities of DOX emission were relatively low compared to the biotin conjugated vesicles. Free DOX.HCl was used as control and the cellular uptake images were recorded for 30, 120 and 360 minutes incubation. The free DOX uptake was relatively poor when compared to their delivery from biotin-conjugated vesicles. The cellular uptake images for free doxorubicin are showed in figure 3.18.

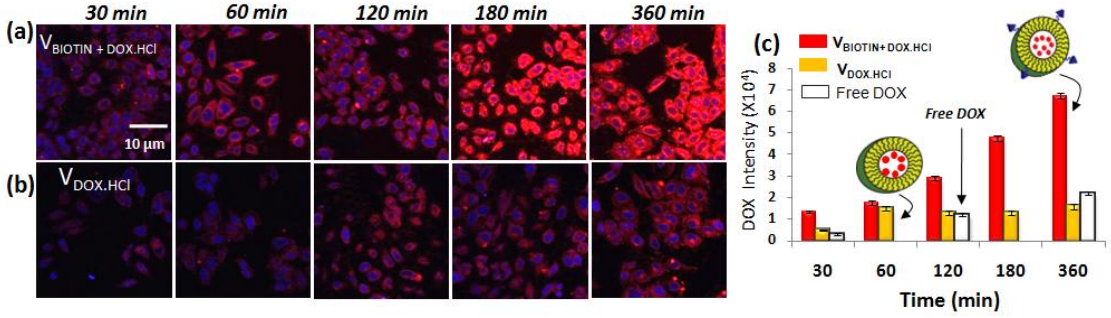

Figure 3.17: *Confocal microscopic images of $V_{BIOTIN+DOX.HCl}$ (a) and $V_{DOX.HCl}$ (b) in HeLa Cells at various incubation time, The plot showing the corrected total cell fluorescence of DOX estimated from the confocal images in the right side panels (a and b) for various incubation time in HeLa cell line (c).*

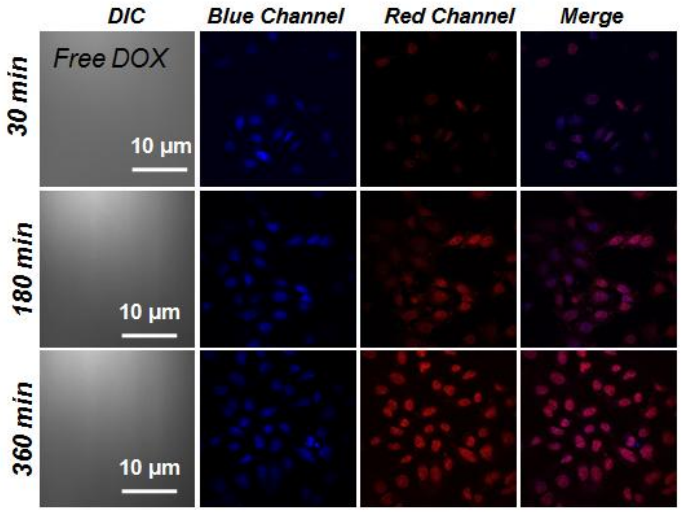

Figure 3.18: *Confocal microscopic images of free DOX.HCl in HeLa Cells at various incubation time, The concentration of DOX was maintained as 2 µg/mL.*

The DOX intensity in each panel in figure 3.17 a (for biotin-conjugate vesicles), figure 3.17 b (biotin free vesicles) and free DOX figure 3.18 in HeLa cell lines was determined by image J software and plotted and shown in Figure 3.19 c for quantification and comparison. A similar approach was carried for each panel in Figure 3.19 a (for biotin-conjugate vesicles) and figure 3.19 b (biotin free vesicles) in WT-MEF cell lines as shown in Figure 3.19 c. The plots in Figure 3.17 c and 3.19 c provide direct information on the uptake of the above vesicles in these two different cell lines which are

significantly different in the amount of membrane receptor concentration [8,9,1]In figure 3.17 c, it can be seen that there is 3 fold more uptake of DOX in case of $V_{BIOTIN+DOX.HCl}$ vesicles as compared to the $V_{DOX.HCl}$ vesicles in HeLa cell lines. The results revealed that in case of $V_{BIOTIN+DOX.HCl}$, the cellular internalization of drugs was significantly higher than $V_{DOX.HCl}$ proving that the biotin conjugation in the dextran vesicles indeed enhanced the DOX concentration at tumour cells. The healthy cells (WT-MEF cell line in Figure 3.19) do not over express the biotin receptors; thus, the cellular uptake by the biotin-functionalized vesicles and biotin-free vesicles do not show much difference in their cellular uptake. This is further evident from the comparison of the uptake by the biotin-functionalized vesicles in Figures 3.17 a (in HeLa) and 3.19 a (in WT-MEF) that the former one showed significant uptake compared to the latter.

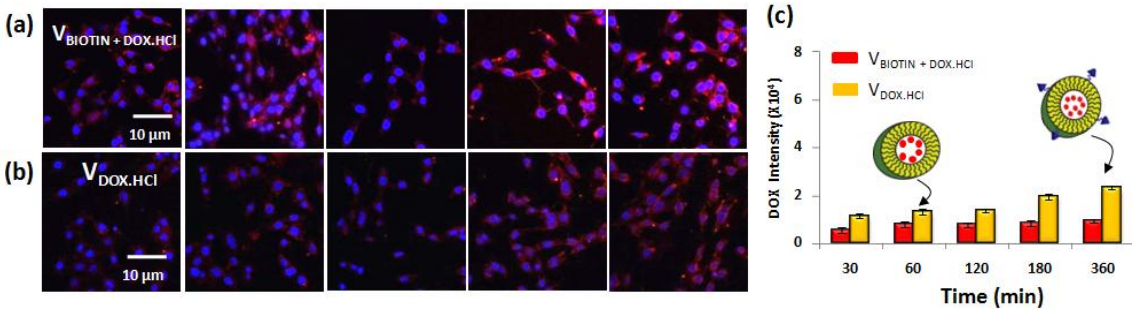

Figure 3.19: *Confocal microscopic images of* $V_{BIOTIN+DOX.HCl}$ *(a) and* $V_{DOX.HCl}$ *(b) in WTMEF cells at different time intervals. The plot showing the corrected total cell fluorescence of DOX estimated from the confocal images in the right side panels (d and e) for various incubation time in WTMEF cell line (c). The concentration of the DOX.HCl was maintained as 2 µg/mL and the various incubation times are shown in the panel.*

A similar experiment was carried out for $V_{BIOTIN+DOX.HCl}$ and $V_{DOX.HCl}$ in normal cell line (WT-MEF) and the images are showed in figures 3.19 d and 3.19 e. Both $V_{BIOTIN+DOXHCl}$ and $V_{DOX.HCl}$ did not so much increment in the cellular uptake with increasing the incubation period. This data was further supported by the plot of DOX intensity versus incubation time in Figure 3.19 f. The comparison of HeLa and WT-MEF cell lines data revealed that the cancer cells have preferential uptake for Biotin conjugated dextran vesicles (V_{BIOTIN}) compared to biotin free vesicles (V). This observation is further supported by the enhanced cell killing by the dextran vesicles in HeLa when compared to WT-MEF cells (see Figures 3.15 b and d). The lyso-tracker experiments indicated that the dextran vesicles were readily digested by both cell lines at

the intracellular level; thus, the difference in the cellular uptake (see Figures 3.17) and cytotoxicity effect (see Figure 3.15) among HeLa and WT-MEF cells is attributed to the difference in receptor-mediated uptake. The enhanced uptake of $V_{BIOTIN+DOX.HCl}$ in HeLa cells is attributed to the enhanced receptor-mediated endocytosis process. It is important to mention that the esterase enzyme concentrations could be similar in both WT-MEF and cancer cells for biodegradation; however, the higher receptor-mediated uptake in cancer cells allowed more uptake of biotin-targeted nanovesicles (see Figure 3.17). Thus, the selectivity accomplished in cancer cell is assisted by receptor mediated endocytosis process for increasing the drug payload in cancer cells (see Figure 3.17). The higher accumulation of drug carrier in cancer cells enabled enhanced cell killing in cancer cells compared to WT-MEF cells. Thus, the selectivity is accomplished in the present design by merging both intracellular biodegradation along with receptor-mediated endocytosis. To validate the receptor-assisted cellular uptake observation in confocal image, time-dependent flow cytometry analysis (uses live cell counting) was carried out for free DOX, V_{DOX}, and $V_{BIOTIN+DOX.HCl}$ in HeLa cell line. In figure 3.20 a, the $V_{BIOTIN+DOX.HCl}$ and $V_{DOX.HCl}$ were found to exhibit almost 1.5 and 2.0 times, respectively, higher uptake than free DOX. Based on the incubation time dependent flow cytometry data in Figure 3.20 b further indicates that the DOX was taken up by the cells in higher quantity with increase in the incubation time. The plot of DOX intensity versus incubation time (see Figure 3.20 c) further validates this observation. The comparison of data at 9 hours incubation for biotin-conjugated dextran vesicles and biotin free dextran vesicles further established the enhanced uptake of $V_{BIOTIN+DOX.HCl}$ in HeLa cell line. The above results directly evidence that the biotin-conjugated dextran vesicles are excellent nano-carriers for anticancer drugs like DOX.HCl to selectively target cancer cells compared to WT-MEF cells. *In vivo* data is further required to support the receptor-mediated approach for long-term application in cancer therapy. Nevertheless, the present manuscript has demonstrated the receptor-mediated endocytosis process in polymer vesicle and the proof-of-concept is successfully demonstrated in cancer cell lines.

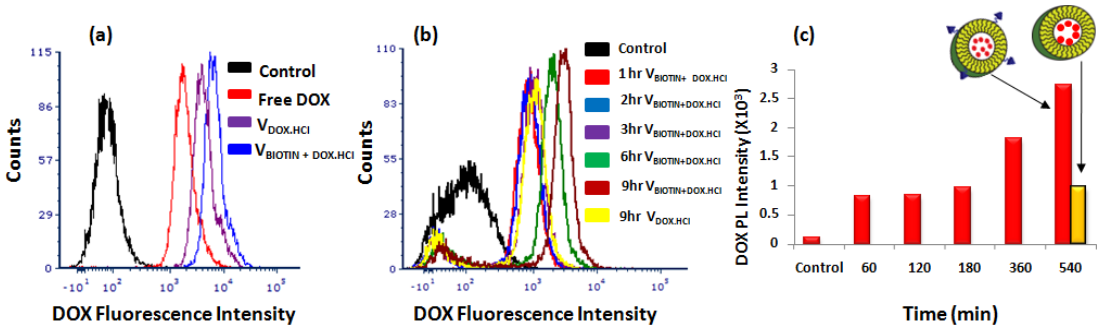

***Figure 3.20**: Histogram showing the cellular uptake by flow cytometry analysis for free DOX.HCl, $V_{DOX.HCl}$ and $V_{BIOTIN+DOX.HCl}$ at 9h incubation (a), Flow cytometry plots for $V_{DOX.HCl}$ and $V_{BIOTIN+DOX.HCl}$ at various incubation time (b), The plot of DOX intensity against incubation time estimated from figures a and b and shown in bar diagram (c). The concentration of the DOX.HCl was maintained as 2 µg/mL and 10000 cells were counted for each experiment.*

3.3.6 Evidence for Receptor-mediated Endocytosis

Three control experiments were carried out to support the receptor-mediated cellular uptake in HeLa cell lines and they are: (i) cellular uptake studies of dextran vesicles in biotin pre-treated cancer cells, (ii) cellular uptake of dextran vesicles at low temperature by supressing the regular endocytosis process, and (iii) time-dependent cytotoxicty assay. To study the biotin-receptor mediated endocytosis of dextran vesicles; cellular uptake experiment was carried out in HeLa cells at 37 ºC using biotin pre-treatment. HeLa cells were pre-treated with 2 mM biotin for 1 h[65-66]. The pre-treated cells and control cells (without biotin pre-treatment) were subjected to $V_{DOX.HCl}$ and $V_{BIOTIN+DOX.HCL}$ and incubated for 4 hours at 37 °C. The schematics of receptor mediated endocytosis and how the addition of free biotin blocks the receptors and reduces the uptake is showed in figure 3.21a.Confocal microscope images in figure 3.21 b showed the uptake of DOX from $V_{BIOTIN+DOX.HCl}$ in biotin-pre-treated HeLa cells. The biotin pre-treatment in the HeLa cells were carried out to block all the receptors with free biotin; hence one would anticipate that the biotin-functionalized vesicles uptake in cells will be reduced due to the non-availability of the receptors on the cell membranes.

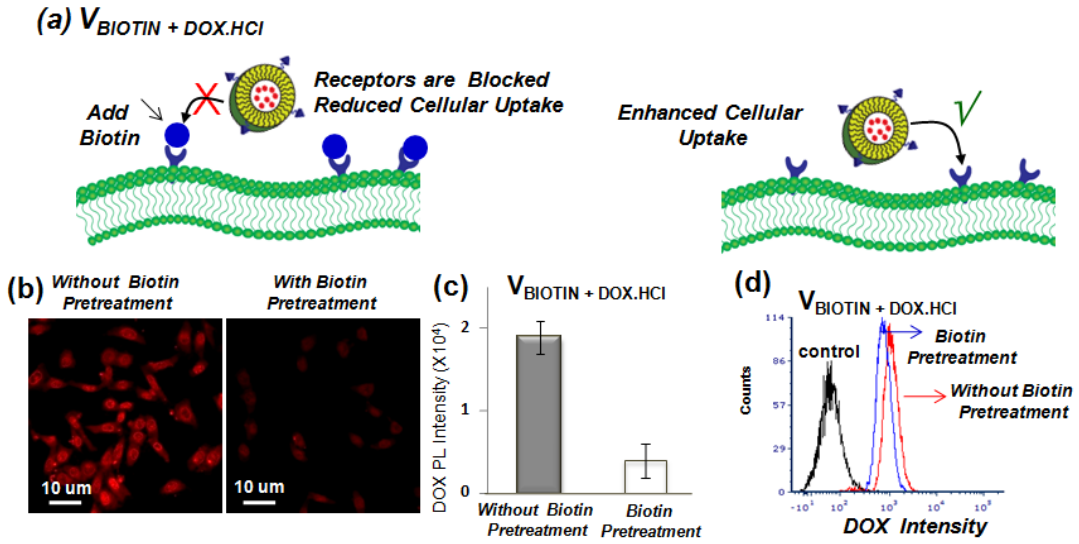

Figure 3.21: *Schematics of receptor mediated endocytosis process (a), Confocal images showing the cellular uptake of* $V_{BIOTIN+DOX.HCl,}$ *in HeLa cells with or without biotin pre-treatment (b), Corrected total cell fluorescence of DOX determined from images and plotted in bar diagram for* $V_{BIOTIN+DOX.HCl}$ *in HeLa cells(c), Flow cytometry plots showing the cellular uptake of* $V_{BIOTIN+\ DOX.HCl}$ *in HeLa cells with or without biotin pre-treatment (d). For biotin pre-treatment, the cells were initially exposed to 2 mM biotin for 1h and then 2 μg/mL DOX. HCl and incubated for 4h.*

The comparison of the uptake of the biotin-functionalized vesicles in HeLa cells indeed showed lower uptake in the biotin pre-treated cells due to the non-availability of receptors (see Figure 3.21 a). This control experiment validates the concept of receptor-mediated endocytosis in the polysaccharide vesicles. DOX florescence intensity was estimated using image J software and shown in figure 3.21 c. The biotin-tagged vesicles $V_{BIOTIN+DOX.HCl}$ showed four-fold better uptake in normal cells compared to biotin pre-treated cells. Further, this observation was validated by flow cytometry analysis (see figure 3.21 d) with biotin pre-treated and normal HeLa cells. The results in flow cytometry plots in figure 3.21 d showed relatively more uptake of $V_{BIOTIN+DOX.HCl}$ by HeLa cells without biotin pre-treatment. Similar experiment was carried out for $V_{DOX.HCl}$ vesicles and images are given in figure 3.22. In figure 3.22 a, the DOX internalization from $V_{DOX.HCl}$ did not show much difference between HeLa cells irrespective of their exposure to biotin pre-treatment or not. This observation was also validated by DOX intensity plot and flow cytometry data in figures 3.22 b and 3.22 c.

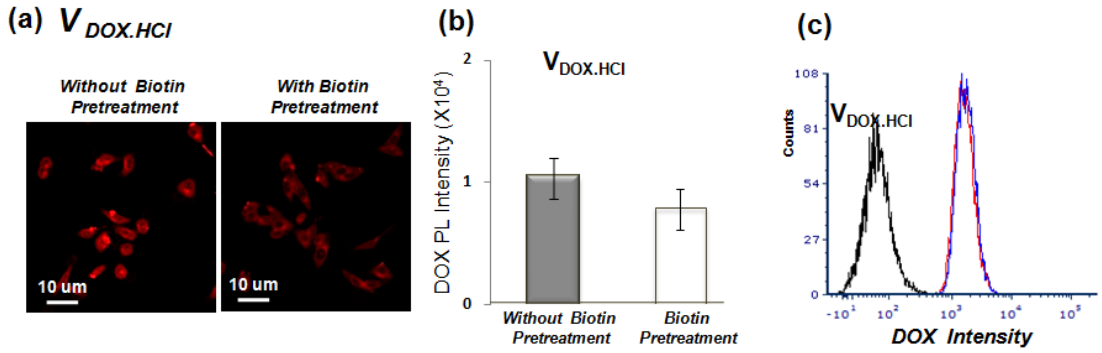

Figure 3.22: *Confocal images showing the cellular uptake of $V_{DOX.HCl,}$ in HeLa cells with or without biotin pre-treatment (a), Corrected total cell fluorescence of DOX determined from images and plotted in bar diagram for $V_{DOX.HCl}$ in HeLa cells (b), Flow cytometry plots showing the cellular uptake of $V_{DOX.HCl}$ in HeLa cells with or without biotin pre-treatment (c).*

From the above discussion, it is evident that these biotin conjugated dextran vesicles can be very good candidates for targeted drug delivery in cancer cells. The cellular internalization of the foreign materials like nano-objects through endocytosis is an active transportation process and hence it is an energy-dependent process. The cellular uptake experiments at lower temperature would reduce or inactivate the endocytosis process and thereby reduce the uptake of the nano-carriers.[67-68] To evaluate the role of the temperature on the dextran nanovesicles internalisation in cells, temperature dependent cellular uptake experiment was carried out in HeLa cells at 4 °C and 37 °C. The HeLa cells were incubated with $V_{DOX.HCl}$ and $V_{BIOTIN+DOX.HCl}$ at 4º C and 37 °C for 30 minutes and subjected to imaging using confocal microscope. At 37 °C, the cellular uptake of $V_{BIOTIN+DOX.HCl}$ was two times better than $V_{DOX.HCl}$ which supported the enhancement in the endocytosis of biotin-tagged vesicles (see Figure 3.23). The uptake of $V_{DOX.HCl}$ was found to be almost similar in both temperatuers indicating that the biotin free vesicles do not have impact towards the receptor mediated uptake process. The uptake of $V_{BIOTIN+DOX.HCl}$ was found to reduce almost half at 4 °C indicating that the receptor-mediated endocytosis primarily occurred under physiological temperature at 37 °C.

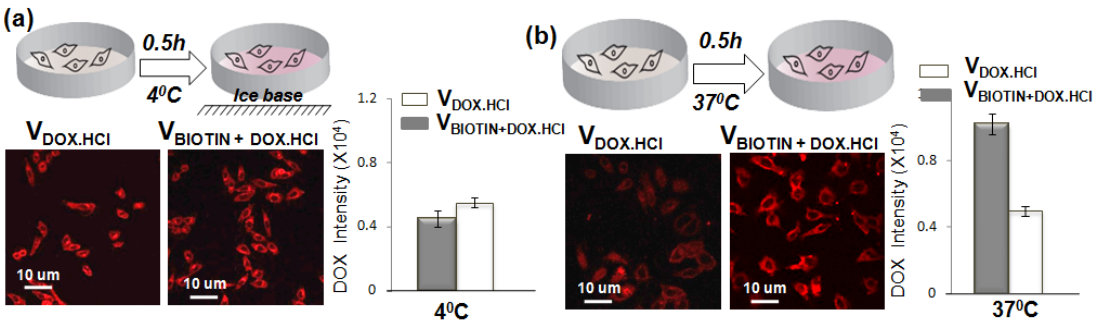

Figure 3.23: *Cellular uptake of dextran vesicles $V_{DOX.HCl}$ and $V_{BIOTIN+DOX.HCl}$, and the plot of corrected total cell fluorescence of DOX Intensity at 4 ºC as incubation temperature (a), Cellular uptake of dextran vesicles $V_{DOX.HCl}$ and $V_{BIOTIN+DOX.HCl}$ and plot of corrected total cell fluorescence of DOX Intensity at 37 ºC as incubation temperature (b). HeLa cells are treated with 2 μg/mL of DOX concentration and incubated for 30 minutes.*

The time-dependent cellular uptake studies (in Figure 3.18 and 3.19), flow cytometry analysis (in Figure 3.20) and the biotin pre-treatment experiment (in Figure 3.21 and 3.22) and temperature dependent endocytosis process (in Figure 3.23) supported the receptor-mediated drug administration in cancer cells. Since there is no significant difference between the HeLa and WT-MEF cells in terms of GSH and esterase enzyme concentration; one would anticipate similar intracellular digestion of the nano-vesicles. Thus, the difference in the cancer cell growth inhibition should arise from significant difference in their receptor-mediated drug accumulation or uptake. To validate this concept, time-dependent cytotoxicity studies were carried out for DOX concentration of 0.8 μg/mL (based on data in Figure 3.15 b) and subjecting the cells for MTT assay at various time intervals as shown in figure 3.24 a. In figure 3.24 b, the IC_{50} value (for 50 % cell killing) was attained at 12 h by biotin-tagged vesicles $V_{BIOTIN+DOX.HCl}$ in cancer (HeLa) cell. This value was thrice much faster compared to free DOX (36 hours) and *and* $V_{DOX.HCl}$ (more than 48 hours) in HeLa cell lines. In WT-MEF cells (see Figure 3.24 c), the free DOX killing was much faster (< 36 hours) compared to both biotin-tagged and biotin free dextran vesicles (more than 48 hours). The higher uptake of the nano-carriers results in the better cell killing due to the increase in the drug concentration. This is further evident from the comparison of the time dependent MTT assay in Figure 3.24 a and time dependent cellular uptake in figure 3.20. The biotin conjugated vesicles showed enhanced uptake which further reflected on their cytotoxicity trend in suppression of cell

growth in HeLa cell line. Thus the receptor-medicated endocytosis and their influence on cell growth inhibition are validated by these time dependent MTT and uptake studies.

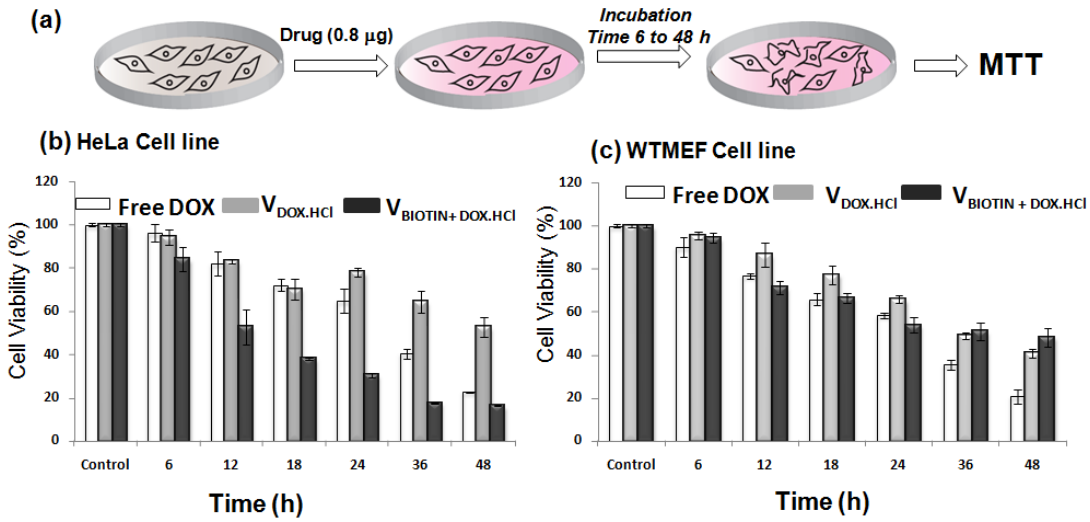

Figure 3.24: *(a) Schematics showing the time dependent MTT experiment. (b) Histogram showing the cytotoxicities for free DOX, $V_{DOX.HCl}$ and $V_{BIOTIN+DOX.HCl}$ in HeLa cells at various incubation time intervals. (c) Histogram showing the cytotoxicities for free DOX, $V_{DOX.HCl}$ and $V_{BIOTIN+DOX.HCl}$ in WTMEF cells at various incubation time intervals.*

This experiment suggetsed that the biotin-tagged vesicles $V_{BIOTIN+DOX.HCl}$ provided two advantages; (i) it achieves faster rate of cell growth inhibition in cancer cells owing to its targeting ability, and (ii) it is also relatively less toxic to the WT-MEF cells. These control experiments validate the targeting ability of the biotin-tagged dextran vesicles in HeLa cell lines. In the present investigation, the approach is demonstrated exclusively for DOX.HCl delivery in HeLa cells; however, the concept is not restricted only to this example and it may be applied to large number of other cancer cells that are over expressed in biotin-receptors. Further, the dextran vesicles are capable of loading both water soluble and water insoluble drugs; thus, the approach can be in principle expanded to variety of other anticancer drugs.

3.4 Conclusion

In summary, biotin-conjugated dextran vesicles were made with multi-stimuli-responsiveness and employed them for receptor-mediated endocytosis to enhance the uptake of water soluble anticancer drug doxorubicin-hydrochloride in cancer cell lines. Renewable resource hydrophobic unit consisting of glutathione-responsive disulfide bond and enzymatic-biodegrabale aliphatic ester linkage was tailor made and conjugated along with biotin on the dextran backbone to yield amphiphilic dextran. The amphiphilic dextran self-assembled into 180 ± 20 nm vesicular nano-assemblies in aqueous medium and the size and morphology of the vesicles was characterized by dynamic light scattering, electron and atomic force microscopes. The binding ability of biotin-tagged dextran vesicle with streptavidin like receptors in the cancer cell membrane was confirmed by Avidin-HABA binding assay. The biotin-tagged vesicles showed affinity up to 25 nM towards the membrane protein indicating their excellent capability to selectively target the biotin receptors over expressed cancer cells. The dextran vesicle provided appropriate geometry to encapsulate water soluble doxorubicin-hydrochloride at the core of the vesicles. Under the intracellular stimuli such as GSH and lysosomal esterase enzymes, the vesicles ruptured to release the drug in 60 and 90 %, respectively. The combination of both GSH and esterase together accomplished 100 % drug release at the intracellular conditions. The intracellular lysosomal degradation of these dextran vesicles was confirmed by lysosomal tracker experiments using confocal microscope. Enhanced cellular uptake of the biotin-conjugated vesicles was proven by time dependent cellular uptake studies which were validated by confocal microscopy imaging and flow cytometry analysis. Receptor mediated endocytosis mechanism was supported by control experiments such as endocytosis at lower temperature, endocytosis with biotin pre-treated cervical (HeLa) cell lines, and time dependent MTT assay and flow cytometry. All these results provide direct evidence for the targeting ability of biotin conjugated dextran vesicles in drug delivery. Based on the above observations, it can be concluded that the newly designed dextran vesicles are promising candidates for targeted delivery of anticancer drugs. Currently, the research work is focussed in this direction to explore the polysaccharide vesicles as targeted drug delivery vehicles to achieve better therapeutic efficacy in cancer.

References:

1. Ghang, Y. J.; Schramm, M. P.; Zhang, F.; Acey, R. A.; David, C. N.; Wilson, E. H.; Wang, Y.; Cheng, Q,; Hooley, R. J. *J. Am. Chem. Soc.* **2013**, *135*, 7090-7093.
2. Yue, T,; Zhang,X. *ACS Nano*, **2012**, *6*, 3196-3205.
3. Zhong, Y.; Meng, F.; Deng, C.; Zhong, Z. *Biomacromolecules*, **2014**, *15*, 1955-1969.
4. Vacha, R.; Martinez-Veracoechea, F. J.; Frenkel, D. *Nano. Lett.* **2011**, *11*, 5391-5395.
5. Nguyen, D.X.; Bos, P.D.; Massague, J. *Nat. Rev. Cancer*, **2009**, *9*, 274-284.
6. Nie, F.; Yang, J.; Wen, S.; An, Y. L.; Ding, J.; Ju, S. H.; Zhao, Z.; Chen, H. J.; Peng, X. G.; T. C. Wong, S.; Zhao, H.; Teng, G. J. *Cancer*, **2012**, *118*, 5198-5207.
7. Neman, J.; Termini, J.; Wilczynski, S.; Vaidehi, N.; Choy, C.; Kowolik, C. M.' Li, H.; Hambrecht, A. C.; Roberts, E. Jandial, R. *Proc. Natl. Acad. Sci.* **2014** , 111, 984-989.
8. Liu, W.; Samanta, S.K.; Smith, B. D.; Isaacs, L. *Chem. Soc. Rev.* **2017**, *46*, 2391-2407.
9. Chen, S.; Zhao, X.; Chen, J.; Chen, J.; Kuznetsova, L.; Wong, S. S.; Ojima, I. *Bioconjugate. Chem.* **2010**, *21*, 979-987.
10. Yang, Z.; Lee, J. H.; Jeon, H. M.; Han. J.H.; Park, N.; He, Y.; Lee, H.; Hong, K.S.; Kang, C.; Kim, J.S. *J. Am. Chem. Soc.* **2013**, *135*, 11657-11662.
11. Barz, M.; Canal, F.; Koynov, K.; Zentel. R.; Vecent, M. J. *Biomacromolecules*, **2010**, *11*, 2274-2282.
12. Poh, S.; Putt, K.S.; Low, P.S. *Biomacromolecules*, **2017**, *18*, 3082-3088.
13. Zhao, F.; Yin, H.; Zhang, Z.; Li, J. *Biomacromolecules*, **2013**, *14*, 476-484.
14. Zhu, Y.; Zhang, J.; Meng, F.; Deng, C.; Cheng, R.; Feijen, J.; Zhong, Z. *ACS Appl. Mater. Interfaces.* **2017**, *9*, 35651-35663.
15. Daniels, T. R.; Bernabeu, E.; Rodriguez, J. A.; Patel. S.; Kozmann, M.; Chiapetta, D. A.; Holler, E.; Ljubimova, J. Y.; Helguera, G.; Penichet, M. L. *Biochimica et Biophysica Acta,* **2012**, *1820*, 291-317.
16. Sun, Q.; Qian, J.; Tian, H.; Duan, L.; Zhang, W. *Chem. Comm.* **2014**, *50*, 8518-8521.
17. Ren, W. X.; Han, J.; Uhm, S.; Jang, Y. J.; Kang, C.; Kim, J. H.; Kim, J. S. *Chem. Comm.* **2015**, *51*, 10403-10418.
18. Maiti, S.; Park, N.; Han, J. H.; Jeon, H. M.; Lee, J. H.; Bhuniya, S.; Kang, C.; Kim, J. S. *J. Am. Chem. Soc*. **2013**, *135*, 4567-4572.
19. Qi, K.; Ma, Q.; Remsen, E. E.; Clark, C. C.; Jr.; Wooley, K. L. *J. Am. Chem. Soc.* **2004**, *126*, 6599-6607.
20. Wang, J. T.; Wang, L.; Ji, X.; Liu, L.; Zhao, H. *Macromolecules*, **2017**, *50*, 2284-2295.
21. Singh, Y.; Durga RaoViswanadham, K.K.; Jajoriya, A.K.; Meher, J.G.; Raval, K.; Jaiswal, S.; Dewangan, J.; Bora, H. K.; Rath, S. K.; Lal, J. *Mol. Pharmaceutics.* **2017**, *14*, 2749-2765.

22. Pramanik, A. K.; Siddikuzzuman.; Palaniumuthu, D.; Somasundaram, K.; Samuelson, A. G. *Bioconjugate. Chem.* **2016**, *27*, 2874-2885.
23. Wong Shi Kam, N.; Jessop, T. C.; Wender, P. A.; Dai, H. *J. Am. Chem. Soc.* **2004**, *126*, 6850-6851.
24. Matsumura, Y.; Maeda, H. *Cancer Res.* **1986,** *46*, 6387−6392.
25. Maeda, H. *Bioconjugate Chem.* **2010,** *21*, 797−802.
26. Balchandran, V. S.; Jadhav, S.R.; Vemula, K.V.; John, G. *Chem. Soc. Rev.* **2013**, *42*, 427-438.
27. Ulery, B. D.; Nair, L.S.; Larencin, C. T. *J. Polym. Sci. B: Polymer Physics.* **2011**, *49*, 832-864.
28. Mizarphy, S.; Peer, D.; *Chem. Soc. Rev*. **2012**, *41*, 2623-2640.
29. Basu, A.; Kunduru, K.R.; Abtew, E.; Domb, A. J. *Chem.* **2015**, *26*, 1396-1412.
30. Feng, A.; Yuan, J. *Macromol. Rapid. Commun.* **2014**, *35*, 767-779.
31. Wen, Y.; Oh, J. K. *Macromol. Rapid. Commun.* **2014**, *35*, 1819-1832.
32. Allen, M. J.; Leaderach, A.; Reilly, P. J.; Mason, R. J. *Biochemistry.* **2001**, *40*, 7789-7798.
33. Hoai, N. T.; Sasaki, A.; Sasaki, M.; Kaga, H.; Kakuchi, T.; Satoh, T. *Biomacromolecules.* **2011,** *12*, 1891-1899.
34. Lemarchand, C.; Gref, R.; Passirani, C.; GArcion, E.; Petri, B.; Muller, R.; Constantini, D.; Couvreur, P. *Biomaterials.* **2006**, *27*, 108-118.
35. Zhang, A.; Zhang, Z.; Shi, F.; Xiao, C.; Ding, J.; Zhuang, X.; HE, C.; Chen, L.; Chen, X. *Macromol. Biosci.* **2013**, *13*, 1249-1258.
36. Li, Y. Z.; Liu, Z. Z.; Cheng, R.; Meng, F.; Cui, J. H.; JI, S. J.; Zhong, Z. *Angew. Chem. Int. Ed.* **2009**, *48*, 9914-9918.
37. Luo, G.F.; Xu, X. D.; Zhang, J.; Yang, J.; Gong, Y.H.; Lei, Q.; Jia, H. Z.;Li, C.; Zhuo, R.X.; Zhang, X. Z *ACS. Appl. Mater. Interfaces.* **2012**, *4*, 5317-5324.
38. Singh Chandel, A. K.; Nutan, B.; Raval,I. H.; Jewrajka, S. K. *Biomacromolecules* **2018**, *19*, 1142-1153.
39. Hu, Y.; Zhao, N.; Yu, B.; Liu, F.; Xu, F. J. *Nanoscale.* **2014**, *6*, 7560-7569.
40. Tsao, C. T.; Kievit, F. M.; Ravanpay, A.; Erickson, A. E.; JEensen, M. C.; Ellnbogen, R. G.; Zhang, M. *Biomacromolecules.* **2004**, *15*, 2656-2662.
41. Pramod, P. S.; Takamura, K.; Chaphekar, S.; Balasubramanian, N.; Jayakannan, M. *Biomacromolecules* **2012**, *13*, 3627−3640.
42. Wang, S.; Wang, H.; Liu, Z.; Wang, L.; Wang, X.; Su, L.; Chang, J. *Nanoscale*, **2014**, *6*, 7635-7642.
43. Wang, S.; Zhang, S.; Liu, J.; Su, L.; Wang, H.; Chang, J. *ACS Appl. Mater. Interfaces.* **2014**, *6*, 10706-10713.
44. Pramod, P. S.; Shah R.; Jayakannan, M. *Nanoscale*, **2015**, *7*, 6636-6652.
45. Pramod, P. S.; Deshpande, N. U.; Jayakannan, M. *J. Phys. Chem. B* **2015**, *119*, 10511-10523.
46. Pramod, P. S.; Shah R.; Chaphekar, S.; Balasubramanian, N.; Jayakannan, M. *Nanoscale* **2014**, *6*, 11841-11855.
47. Deshpande, N. U.; Jayakannan, M. *Biomacromolecules.* **2017**, *18*, 113-126.
48. Curcio, M.; Fernandez, B. B.; Gomez, L. D.; Concheiro, A.; Alvarez-Lorenzo, C. *Bioconjugate. Chem.* **2015**, *26*, 1900-1907.
49. Saxena, S.; Jayakannan, M. *Biomacromolecules.* **2018**, *17*, 2594-2609.

50. Aluri, R.; Jayakanna, M. *Biomacromolecules.* **2017**, *18*, 189-200.
51. Kashyap, S.; Jayakannan, M. *J. Phy. Chem. B* **2012**, *116*, 9820-9831.
52. Kashyap, S.; Jayakannan, M. *J. Mater. Chem. B* **2014**, *2*, 4142-4152.
53. Houga, C. M.; Giermanska, J.; Lecommandoux, S. B.; Borsali, R.;Taton, D.; Gnanou, Y.; Le eins, J.-F. O. *Biomacromolecules* **2009**, *10*,32−40.
54. Burchard, W. Adv. Polym. Sci. **1983**, 48, 1−124.
55. Wilhelm, S.; Anthony J.; Dai, T.Q.; Ohta, S.; Audet, J.; Dvorak,H.F.; Chan, C.W., Warren. *Nat. Rev. Mater.* **2016**, *1*, 1-12.
56. Ennen, F.; Boye, S.; Lederer, A.; Cernescu, M.; Komber, H.; Brutschy, B.; Voit, B.; Appelhans, D. *Polym. Chem.* **2014**, *5*, 1323-1339.
57. Jia, Z.; Liu, J.; Boyer, C.; Davis, T, P.; Bulmus, V. *Biomacromolecules.* **2009,** *10*, 3253-3258.
58. H. I. Okur, J. Kherb and P. S. Cremer. *J. Am. Chem. Soc.*, **2013**, *135*, 5062–5067.
59. Kashyap, S.; Jayakannan, M. *J. Mater. Chem. B* **2015**, *3*, 1957-1967.
60. Sun, H.; Cheng, R.; Deng, C.; Meng, F.; Dias, A. A.; Hendriks,M.; Feijen, J.; Zhong, Z. *Biomacromolecules***, 2015**, *16*, 597-605.
61. Surnar, B.; Jayakannan, M. *Biomacromolecules*, **2016**, *17*, 4075-4085.
62. Mohammad A. K.; Reineke, J. *Mol. Pharmaceutics.* **2013**, *10*, 2183-2189.
63. Lim, J. P.; Glesson, P. A. *Immunol. Cel. Biol*. **2011**, *89*, 836-843.
64. Anas, A.; Okuda, T.; Kawashima, N.; Nakayama, K.; Itoh, T.; Ishikawa, M.; Biju, V. *ACS Nano*. **2009**, *3*, 2419-2429.
65. Lv, L.; Liu, C.; Chen, C.; Yu, X.; Chen, G,; Shi, Y.; Qin, F.; Ou, J.; Qiu, K.; Li, G. *Oncotarget.* **2015**, *7*, 32184-32199.
66. Droumaguet, B. L.; Nicolas, J.; Brambilla, D.; Mura, S.; Maksimenko, A.; Kimpe, L. D.; Salvati, E.; Zona, C.; Airoldi, C.; Canovi, M.; Gobbi, M.; Noiray, M.; Ferla, B. L.; Nicotra, F.; Scheper, W.; Flore, O.; MAsserini, M.; Andrieux, K.; Couvreur, P. *ACS Nano.* **2012**, *6*, 5866-5879.
67. Zeng, X.; Zhang, Y.; Nystrom, A. *Biomacromolecules.* **2012**, *13*, 3814-3822.
68. Wang, H. Y.; Hua, X. W.; Jia, H. R.; Liu, P.; Gu, N.; Chen, Z.; Wu, F. G. *J. Mater. Chem. B.* **2016**, *4*, 834-843.

Chapter-4

AIE Fluorophore Tagged Theranostic Polysaccharide Vesicles for Cancer Treatment

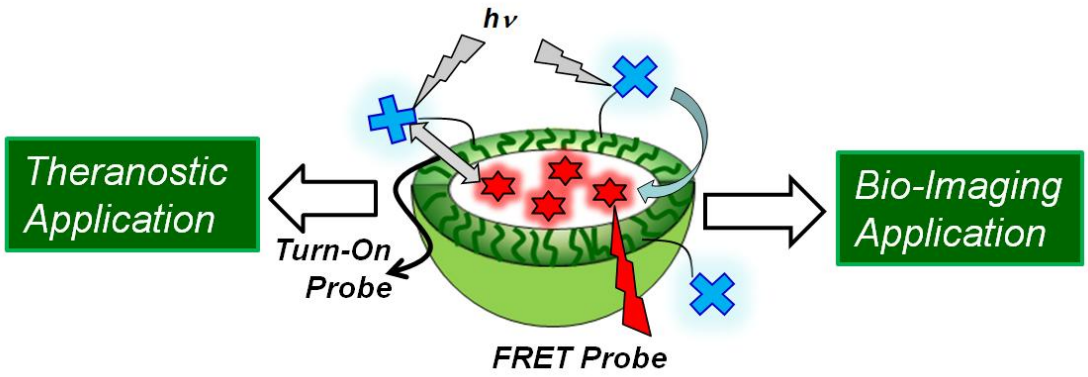

Abstract

Enzyme responsive fluorescent polysaccharide vesicle were designed and developed as "Turn ON" probe and for bio-imaging purpose in cancer cells. To do so, a polysaccharide dextran backbone was decorated with a special aggregation induced emissive (AIE) fluorophore tetraphenylethene (TPE) along with vesicular director hydrophobic source pentadecyl phenol (PDP). These dextran-PDP-TPE derivatives are nonfluorescent in nature when dissolved in organic solvents where as gives blue colour emission in aqueous medium. These derivatives when dispersed in water, produces vesicular structures which are subsequently used encapsulation of different water soluble and water insoluble drug and dye molecules. When these vesicles are loaded with doxorubicin drug molecule, owing to the spectral overlap and confined geometrical arrangement showed excellent fluorescence resonance energy transfer (FRET) phenomenon. This energy transfer from TPE (Donor) to the DOX molecules (acceptor) resulted in emission quenching due to the aggregation caused quenching (ACQ) effect shown by a doxorubicin. Hence, at physiological conditions these vesicles are in fluorescence off state whereas upon enzyme action, their fluorescence was regained thus, acting as a "Turn ON" probe for doxorubicin delivery to the cancer cells. This property of vesicles was studied in human breast cancer MCF 7 cells and their intracellular enzyme responsive was successfully demonstrated. Furthermore, these vesicles were loaded with three different red colure dyes namely rhodamin-B (RHB), Nile red (NR) and rose Bengal. There photophysical studies proved an efficient FRET phenomenon between TPE and these fluorophore. Time correlated single photon counting studies (TCSPC) proved the co-existence of these fluorophore within FRET distance. Intracellular FRET mechanism of these vesicles was studied in MCF 7 cells and proved that these vesicles can be used for bioimaging application. Further these designed vesicleswere modified with acid functionality to produce blue luminescent acid functionalised polysaccharide vesicles. These vesicles were used for cisplatin (effective anticancer drug) conjugation and real time monitoring of drug release in MCF 7 cells. These fluorescent polysaccharide vesicles can be used as theranostics for drug delivery application in cancer cells.

4.1Introduction

Fluorophore-tagged polymer have emerged as unique theronastic nano-carriers and provided single platform to study both internalization of macromolecular carriers through imaging protocols and simultaneous delivery of drugs/genes in cancer treatment[1-4]. Optical chromophores were anchored on the wide range of scaffold such as micelles[5-8], vesicles[9-12], nanoparticles[13], dendrimers[14], and block copolymers[5-12], etc and steady state emission, confocal microscopic bio-imaging was established both in vitro and in vivo. Two-photon fluorescence emission[15-18], fluorescence life-time imaging[19,20], single photon imaging[21], and fluorescence resonance energy transfer (FRET)[22,23] are some of the advanced imaging-cum-spectroscopic tools that are recently accessible to study the real-time dynamics of nano-carriers under physiological environments. The fluorescent-tagged nano-carriers are non-destructive vectors and function as non-invasive visualization tools[1-4]; thus, they could be readily excreted from the body after the prescribed function without causing any damage to internal organs or the site of the action. Some of these non-invasive fluorescence techniques are shown in Figure 4.1.

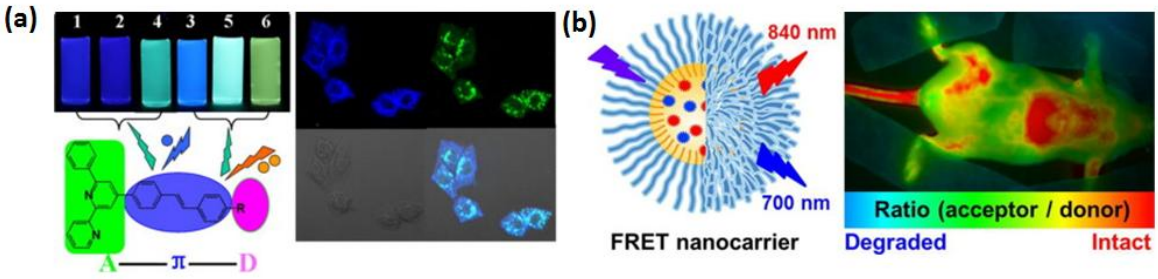

Figure 4.1: *A diagram showing the use of single photon, double photon (a) and FRET (b) techniques used for bioimaging application. Adopted from Dyes and pigments 2014, 109, 42-53 and J. Contrl. Rel. 2016, 236, 57-67.*

Among the fluorescent-imaging tools, FRET-assisted phenomenon is particularly important because it can provide few vital information like: (i) stability of the nanocarriers under the extracellular environment[24], (ii) receptor-mediated endocytosis in targeted delivery at the cellular membrane interface[25], (iii) insight into the intracellular transportation of nanocarriers[26], (iv) real-time release profiles of the loaded cargoes, and (v) direct visualization of the nano-carriers at the site of action[27], etc. FRET occurs within the close vicinity of donor-acceptor chromophores in nano-domains (Forster distance ≤

50 Å); hence, the observation of undisturbed occurrence of FRET (**Turn-On**) typically established the stability of the nano-carriers under circulation (or storage) till the time of particular action[24-27]. In the event of delivery of the cargoes under stimuli-responsiveness, the nano-carriers eventually lost the association of donor-acceptor chromophores with in the ≤ 50 Å confinement which makes the FRET " Turn-Off". This establishes the role of the FRET nano-carriers and also provides opportunity to study the particular biological event under the physiological conditions[28]. For instance, the receptor-mediated endocytosis could be traced by the Turn-On or Turn-Off FRET process at the periphery of the membrane depending upon the association between the receptor-ligand interactions[29]. FRET based nanocarriers found potential application in understanding the variety of other biological processes in the intracellular medium such as protein-protein interaction[30], protein folding at physiological[31] condition, enzyme-substrate interactions[32], DNA transitions from duplex to qudraplex[33-35], etc. and suitable examples for these processes are shown in Figure 4.2.

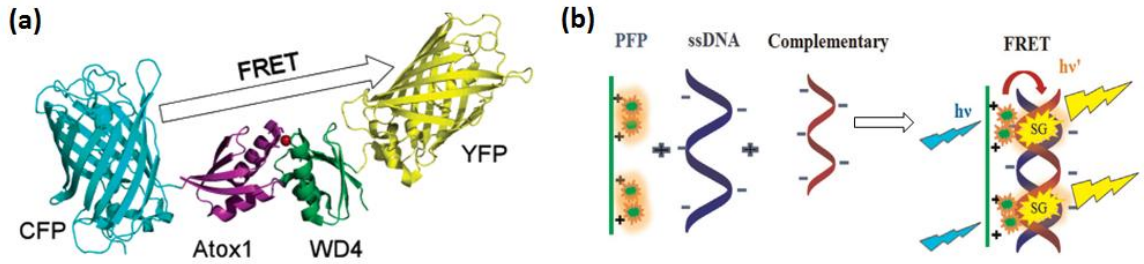

Figure 4.2: *A diagram showing the protein-protein interaction (a) and DNA duplex formation (b) monitored through a FRET phenomenon. Adopted from Dongen et al. J. Am. Chem. Soc. 2006, 128, 10754-10762 and Zhou et al. Biosensors and Bioelectronics. 2015, 65, 103-107.*

Recently a novel class of fluorophore molecules was discovered by Tang and co-workers that works on the principle of aggregation induced emission (AIE) in aqueous phase[36]. AIE offers new opportunities compared to traditional luminescent molecules that are largely experienced aggregation-caused quenching via aromatic π-stack interactions in their micro or nano-aggregates in the aqueous phase. On the other hand, the excitation energy is predominately used for radiative decay component rather than structural reorganization which is largely facilitated by the strong aggregation in the AIE

chromophores. As result, the AIE provide additional advantage to directly infer on the self-assembly aspects of the nano-scaffolds compared to their isolated form[37]. For instance, the formation of new aggregates enhanced the emission characteristics and "Turn-on" the probe compared to their isolated chains (Turn-off). This endows the drug delivering nano-carriers to be fluorescent in nature in aqueous medium which is most desirable especially for anticancer drug delivery application of the anticancer drugs that are non-fluorescent in nature like paclitaxel and cisplatin, etc[38]. The structure and mechanism of aggregation induced emission[39] is showed in figure 4.3.

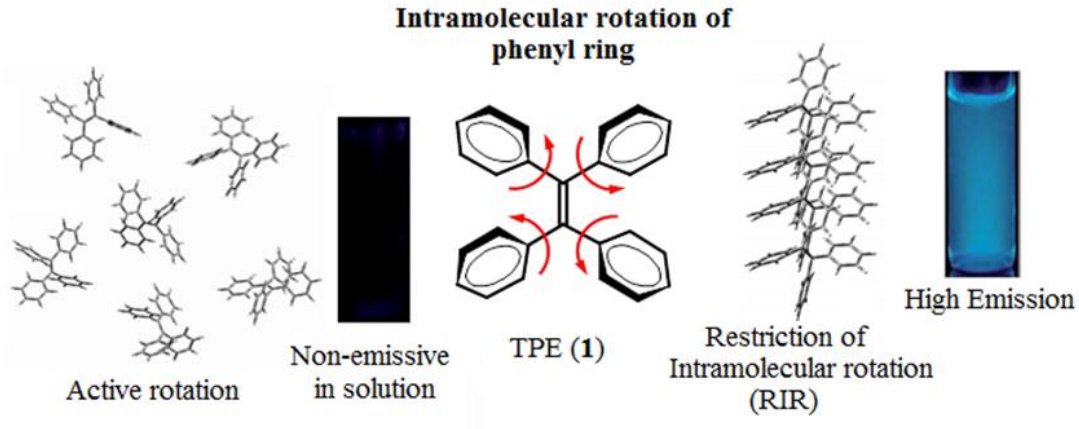

Figure 4.3: *A diagram showing the structure of tetraphenylethene an AIE probe and the mechanism of aggregation induced emission. Adopted from La et al. ACS Appl. Mater. Interfaces. 2018, 10, 12189-12216.*

Conjugation of the AIE Fluorophore in drug delivery vehicles provides an opportunity to develop unique theranostic systems (drug delivery + diagnostic) which allows the real-time tracking of the drug release along with bio-imaging[40]. Inspired from these discovery a number of drug delivery vectors ranging from small molecules and polymeric systems have been reported in the literature. Small molecules based AIE probes have been made and extensively used for diverse application in biomedical fields such as probing the DNA sequencing, apoptosis imaging, for biomarker detection, protein sensing, membrane tracking, studying enzyme substrate interaction, mitochondria tracking, glucose sensing, image guided chemotherapy etc[41]. In a quest of developing better theranostics system, number of AIE conjugated polymeric drug delivery systems were developed and used for anticancer drug delivery application. Mu et al. reported the synthesis of tetraphenylethylene (TPE), a AIE fluorophore conjugated *poly(N-*

isopropylacrylamide) polymer and showed its application for long term cellular imaging[14]. Hu et al. reported the redox responsive amphiphilic block copolymer of aspartic acid and 2-methacryloyloxyethylphosphorylcholine. This TPE-SS-PLAsp-*block*-PMPC copolymer could self-assemble into micellar structures[42]. These micelles were used for DOX encapsulation and delivery of doxorubicin. Stability and release study of DOX encapsulated micelles were carried out and proved redox responsive cleavage of the micelles. Further *invitro* cytotoxicity and *invivo* antitumor efficacy was carried which showed enhanced efficacy compared to free drug. Diagram in the figure 4.4 depicts the polymer structure, self assembly and their further cellular uptake.

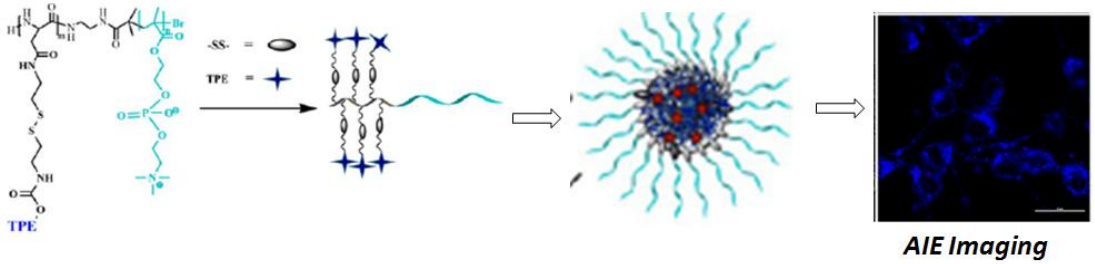

Figure 4.4: *A diagram showing structure of TPE-SS-PLAsp-b-PMPC polymer, schematics of self assembly and their GSH responsive intracellular drug release. Adopted from Hu et al. Bioconjugate Chemistry 2018, 29, 1897-1910.*

Zhang et al. synthesized multiarm star polymer using polystyrene-*b*-polyethylene and polyethylene-*b*-polycaprolactone and showed thermo responsive fluorescence characteristics of the polymers[43]. Wang et al. also showed the synthesis of thermo responsive *poly(N-isopropylacrylamide)* polymer and its potential application for long term imaging in HeLa cells[44]. Jiang et al. reported the formation polyplex micelles using polyethyleneimine, polyethylene glycol and TPE molecules and showed their application for efficient gene promotion in tumours at cancer site[45]. Wu and co-workers reported the synthesis of PEG-POSS-TPE polymer which self assembles into vesicular self assembled used for doxorubicin delivery to the cancer cells. Herein they showed effective FRET phenomenon between TPE and doxorubicin. Doxorubicin is a DNA intercalating anticancer drug and shows good absorbance spectral overlap with emission spectrum of TPE for effective energy transfer[46.] TPE conjugated polysaccharides nano-vectors that are responsive to the different stimuli present at tumour microenvironment are also

reported. Wang et al. synthesized pH responsive TPE-dextran micelles and used for doxorubicin delivery to the cancer cell to achieve better cancer cell ablation[47]. Tang and co-workers modified the chitosan backbone with TPE to produce chitosan-TPE conjugate. This conjugate was non fluorescent in nature in dissolved state and fluoresces when aggregated. The cellular trafficking of these chitosan-TPE conjugate was studied in cervical cancer HeLa cells and it has been observed that it enables the cell tracing as long as 15 passage number. These results proved its potential application for long term cell imaging in cancer cells[48]. The structure of chitosan-TPE conjugate and cell images are showed in figure 4.5. Liang and co-workers made quaternary ammonium modified TPE molecule and they have used this molecule in combination with hyaluronic acid to achieve cytotoxic effects in the cancer cells[49].

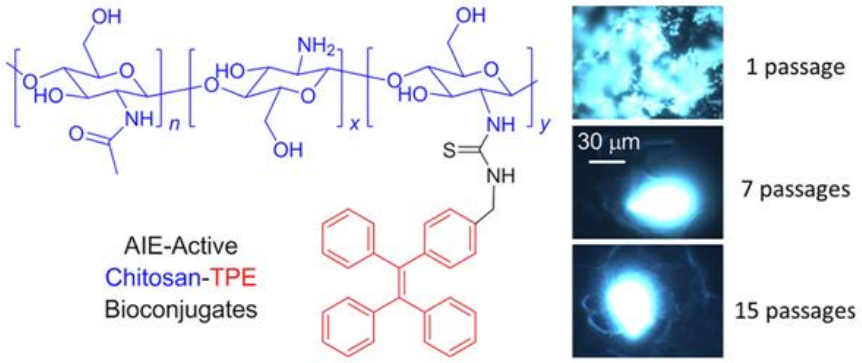

Figure 4.5: *A diagram showing the structure of chitosan-TPE conjugate and their cellular tracing in cervical cancer HeLa cells. Adopted from Wang et al. J. Am. Chem. Soc. 2013, 135, 8238-8245.*

Polymersomes or polymer vesicles are synthetically challenging to make but are very useful for drug delivery application. These vesicular assemblies are Charecterized by hydrophobic bilayer and a hydrophilic core which provides an additional advantage of loading the water soluble and water insoluble drug / dye molecules in this pockets[50-54]. Hence, polymersomes based on these aggregation induced emission property are synthetically challenging to make but will be a very good carrier for real time monitoring of the drug delivery process. Thus to make TPE based synthetic polymersomes, Huo et al. synthesized a series of TPE conjugated diblock copolymers and showed the importance of polymerization induced self assembly (PISA) and its effect on fluorescence property of AIE fluorophore[55]. These polymers showed a micelle to vesicle

transformation of the self assembled structures. The apmphiphilic polymer structure and their morphological transformation are showed in figure 4.6. He et al. reported the synthesis of poly (tetraphenylethene) polymer and AIE property is achieved by complexation with crown ethers[56]. These polymers showed a morphological transition from micelle to vesicles with increase in the respective fluorescence property. Zhao et al. reported the synthesis of several diblock copolymers from ring opening metathesis polymerisation and showed the pH responsive morphological transformation[57]. In another attempt stang and co-workers reported the synthesis of four armed amphiphilic copolymer which incorporates the fluorescent TPE metallocycle[58]. This polymer showed the formation of self assembled polymersomes which further have been used for doxorubicin delivery in HeLa cells. Several other crosslinked fluorescent vesicles based on small molecules such as myristoylcholine chloride, TPE bile acid conjugates, and Pyridine N-oxide derivative with TPE etc are also reported but all of these examples are explored in self assembly perspective and not for drug delivery application.

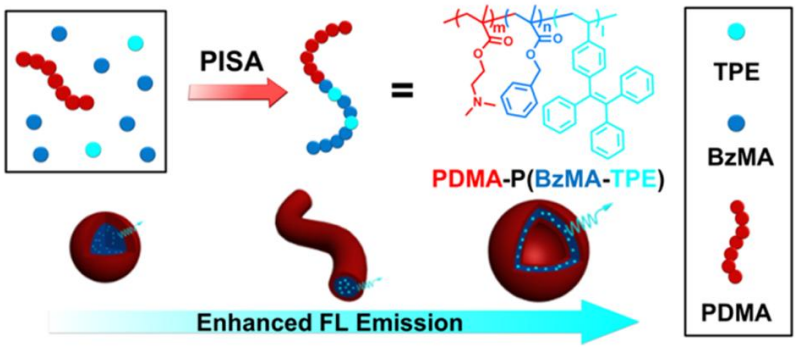

Figure 4.6: *A diagram showing the structure of polymer and morphological transformation from micelle to vesicles. Adopted from Huo et al. Macromolecules, 2017, 50, 1126-1133.*

Hence it has been observed that though the TPE based fluorescent self assembled structures (polymersomes) are reported in the literature, but have not been explored much for drug delivery application. Moreover these assemblies were made from the synthetic polymers which are mostly nonbiodegradable and hence limit their application in biomedical field. Thus at this point it is important to make nanocarriers (polymersomes) which can be used for the drug delivery as well as real time monitoring of the drug release profile. To accomplish this goal, herein we synthesized novel fluorescent

polysaccharide vesicles using naturally occurring resources. We have reported a dextran based vesicles by carefully modifying the hydrophilic dextran backbone using pentadecyl phenol, a hydrophobic molecule obtained from cashew nut shell liquid. These vesicles have been used for camptothecin delivery to the human breast cancer cells[50]. These vesicles also were used for understanding the endocytosis process in caveolae null (resembles non-cancerous cells) and caveolae positive (resembles cancer cells).Interestingly, it has been found that these vesicles were taken up better by the cancer cells as compared to the non-cancerous cells[51]. Acid functionalized dextran vesicles were also used for delivery of triple antagonistic drugs cisplatin, doxorubicin and camptothecin from a single polymer dose[54]. Recently biotin tagged dextran vesicles were made and proof of concept of targeted drug delivery of doxorubicin was showed in HeLa cells[59].

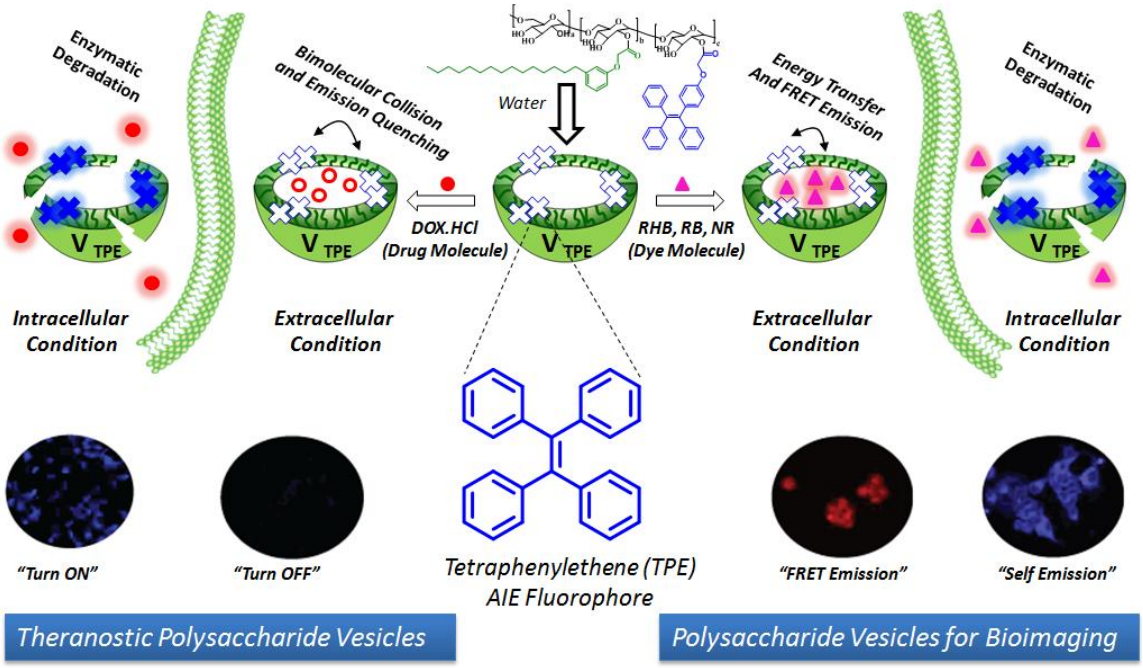

Figure 4.7: *Novel fluorescent polysaccharide vesicles as "Turn On" probe for doxorubicin delivery in breast cancer cells and for bioimaging in cancer cells.*

In the present report, the dextran backbone was carefully modified using the hydrophobic molecule which is necessary for vesicular morphology formation and small amount of tetraphenylethylene (TPE, AIE Fluorophore) was also conjugated to make the these derivatives luminescent in nature. It has been observed that a small modification on

the dextran backbone using TPE acid did not alter its vesicular assembly. When these derivatives were dispersed in aqueous medium, it showed formation of uniform sized blue fluorescent nanovesicles which were confirmed by different microscopic techniques such as Atomic Force Microscopy (AFM), Field Emission Scanning Electron Microscope (FESEM) and Transmission Electron Microscope (TEM). Since these blue colored vesicles are Charecterized with a hydrophobic layer and hydrophilic core, they have been used for loading the drug/dye molecules which are red luminescent in nature. A red luminescent doxorubicin hydrochloride, hydrophilic anticancer drug molecule was chosen for loading in these blue luminescent vesicles. This produces a luminescent DOX loaded vesicles as $V_{TPEDOX.}$ Since doxorubicin and TPE are known to be a very good FRET pair, their detailed photophysical studies have been done and a fluorescent "Turn ON" probe for doxorubicin delivery to human breast cancer cells were made for the first time using natural resources. The loading of different water soluble dye molecules such as rhodaminB and rosebengal and water insoluble nile red produces three different vesicles as V_{TPERHB}, V_{TPERB} and V_{TPENR} respectively. These dye loaded vesicles were also showed very good FRET phenomenon and these can be used for bioimaging in cancer cells. Cisplatin a widely used anticancer drug, being effective it shows severe side effects because of the limitation of real time tracking of the drug molecules in the tumour environment. To address this issue, these luminescent vesicles were also modified with acid functionality and used for delivery and real time tracking of the non fluorescent cisplatin anticancer drug. In nut shell, fluorescent polysaccharide nanovesicles were made delivery and real time tracking of the anticancer drugs and loading different dyes these vesicles were made available for bioimaging application in the biomedical field. The novel concept of these fluorescent polysaccharide vesicles is shown in figure 4.7.

4.2 Experimental Section

4.2.1 Materials: Benzophenone, 4-hydroxy benzophenone, Zinc powder, titanium tetrachloride, 3-Pentadecylphenol (PDP), Ethyl chloro acetate, succinic anhydride, triethylamine (TEA), dextran (mol. Wt 6000), dicyclohexylcarbodiimide (DCC), 4-dimethylamino pyridine (DMAP), N-hydroxy succinamide, triethyl amine, doxorubicin hydrochloride (DOX), cisplatin, Glutathione, dextran (6000 MW), rhodamin-B, rosebengal, nilered, tertiary butanol, trifluoro acetic acid (TFA), dimethylsulfoxide (DMSO)and horse liver esterase enzyme were purchased from Aldrich chemicals. NaOH and all other necessary reagents and solvents were purchased locally and purified following the standard procedures.PDP acid and tertiary butyl ester of succinic acid showed in synthetic schemes were made by following the procedure reported in our earlier reports.

4.2.2 General Procedures: NMR spectra were recorded using a 400 MHz Jeol and 100-MHz Bruker NMR spectrometer using $CDCl_3$ or DMSOd6 containing a small amount of TMS as an internal standard. The electronic spectra were recorded using Perkin-Elmer Lambda 45 UV−visible, and a Fluorolog HORIBA JOBIN VYON fluorescence spectrophotometer. The size determination of the self assembled structures were carried out by dynamic light scattering (DLS), using a Nano ZS-90 apparatus utilizing a 633 nm red laser from Malvern instruments. The data shown here is mean of at least three independent measurements. Freshly cleaved mica surface was used for drop casting the samples for atomic force microscope (AFM)and recorded using Agilent instrument. The imaging was carried out in tapping mode using TAP-190AL-G50 probe from Budget sensors with a nominal spring constant of 48 N/m and resonance frequency of 190. TEM images were recorded using a Technai-300 instrument. Differential scanning calorimetry (DSC) measurements were performed on a TA Q20 differential scanning calorimeter (DSC) at heating and cooling rates of 5.0 °C/min. FE-SEM images were recorded using Zeiss Ultra Plus scanning electron microscope. The samples for FE-SEM analysis were prepared by drop casting on silicon wafers. For TEM Analysis, the samples were prepared by drop casting on copper grid. Confocal microscopic images were recorded using LSM10 Confocal Microscope.

4.2.3 Synthesis of 4-(1,2,2-triphenylvinyl)phenol (TPE-OH) (1): In 250 mL round bottom flask, benzophenone (10.0 g 55 mmol), 4-hydroxy benzophenone (10.5 g, 53 mmol), zinc powder (9.25 g, 142 mmol) were dissolved in 100 mL of dry THF at 0 ºC with N2 purging. The reaction mixture was stirred for 0.5 h and then titanium tetrachloride (12.50 g 66 mmol) was added drop wise at temperature below 10 ºC and then reaction mixture was reflux for 12 h. After reaction mixture is cooled to room temperature, THF is evaporated under pressure and then 100 mL of dilute hydrochloric acid (0.1 N) was added and product was extracted using ethyl acetate, dried over sodium sulphate. The crude product was purified over 100-200 mesh silica gel column using 5-15 % ethyl acetate: pet ether solvent system. Yield 6.0 g (32 %).^{1}H NMR (400 MHz, $CDCl_3$) δ ppm: 4.76 (s, 1 H, Ar-OH) 6.54 - 6.60 (m, 2 H) 6.88 - 6.94 (m, 2 H) 7.01 - 7.08 (m, 6 H) 7.08 - 7.15 (m, 9 H).^{13}C NMR (100 MHz, $CDCl_3$)δ ppm: 76.69 (s, 1 C) 77.32 (s, 1 C) 114.56 (s, 1 C) 126.24 (s, 1 C) 126.35 (s, 1 C) 127.58 (s, 1 C) 127.69 (s, 1 C) 131.31 (s, 1 C) 131.34 (s, 1 C) 132.71 (s, 1 C) 136.33 (s, 1 C) 140.14 (s, 1 C) 140.39 (s, 1 C) 143.86 (s, 1 C) 143.96 (s, 1 C) 153.95 (s, 1 C). MALDI-TOF: (MW: 348.15) m/z: 371.09 ($M+Na^+$).HR-MS (ESI+): m/z [M + H+] Calculated for $C_{26}H_{20}O$ [M+], 348.1600; found, 348.1516.

4.2.4 Synthesis of Ethyl 2-(4-(1,2,2-triphenylvinyl)phenoxy)acetate (TPE- Ester) (2):TPE-OH (5.0 g, 15 mmol), K_2CO_3 (2.97 g, 22 mmol) were dissolved in 80.0 mL of acetonitrile and stirred at 80 ºC for 0.5 h. Reaction mixture was cooled to room temperature and ethyl chloro acetate (2.39 g, 15 mmol) was added drop wise and then reaction continued at 90 ºC for 12 h. Then reaction mixture was cooled to room temperature, K_2 CO_3 was separated by filtration, acetonitrile was concentrated under reduced pressure and product was extracted using ethyl acetate and dried over sodium sulphate. Crude product was purified by using 100-200 mesh silica gel column using 3-5 % ethyl acetate: pet ether solvent system.Yield 4.0 g (65 %).^{1}H NMR (400 MHz, $CDCl_3$) δ ppm:1.30 (t, 3 H) 4.28 (q, 2 H) 4.56 (s, 2 H) 6.67 (m, 2 H) 6.97 (m, 2 H) 7.01 - 7.08 (m, 6 H) 7.08 - 7.18 (m, 9 H).^{13}C NMR (100 MHz, $CDCl_3$)δ ppm:14.12 (s, 1 C) 61.27 (s, 1 C) 65.29 (s, 1 C) 76.69 (s, 1 C) 77.32 (s, 1 C) 113.74 (s, 1 C) 126.26 (s, 1 C) 126.36 (s, 1 C) 127.56 (s, 1 C) 127.68 (s, 1 C) 131.26 (s, 1 C) 131.32 (s, 1 C) 132.52 (s, 1 C) 137.11 (s, 1 C) 140.20 (s, 1 C) 140.36 (s, 1 C) 143.72 (s, 1 C) 143.78 (s, 1 C) 143.82 (s, 1 C)

156.25 (s, 1 C) 168.84 (s, 1 C).MALDI-TOF: (MW: 434.19) m/z : 473.09 ($M + K^+$). HR-MS (ESI+): m/z [M + H+] Calculated for $C_{30}H_{26}O_3$ [M+], 435.1978; found, 435.199.

4.2.5 Synthesis of 2-(4-(1,2,2-triphenylvinyl)phenoxy)acetic acid (TPE-Acid) (3):TPE-Ester (4.0 g, 9.2 mmol), KOH (1.55 g, 28 mmol) were dissolved in 50 mL of dioxane and reaction mixture was reflux for 6 h. after reaction mixture was cooled to room temperature, dioxane was concentrated under reduced pressure and the solid compound was dissolved in water, pH is maintained 6.0 using dilute hydrochloric acid (0.1 N) and product is extracted using ethyl acetate. Crude product is purified by passing over 100-200 mesh silica gel column using 20-40 % ethyl acetate: pet ether solvent system. Yield 3.72 g (99 %).^{1}H NMR (400 MHz, $CDCl_3$) δ ppm:4.63 (s, 2 H) 6.64 - 6.70 (m, 2 H) 6.95 - 7.00 (m, 2 H) 7.01 - 7.07 (m, 6 H) 7.08 - 7.17 (m, 9 H).^{13}C NMR (100 MHz, $CDCl_3$)δ ppm: 64.35 (s, 1 C) 76.36 (s, 1 C) 76.68 (s, 1 C) 113.42 (s, 1 C) 125.99 (s, 1 C) 126.03 (s, 1 C) 126.09 (s, 1 C) 127.27 (s, 1 C) 127.30 (s, 1 C) 127.40 (s, 1 C) 130.95 (s, 1 C) 130.99 (s, 1 C) 132.34 (s, 1 C) 137.25 (s, 1 C) 139.74 (s, 1 C) 140.24 (s, 1 C) 143.34 (s, 1 C) 143.40 (s, 1 C) 143.43 (s, 1 C) 155.46 (s, 1 C) 173.79 (s, 1 C).MALDI-TOF: (MW: 406.16) m/z : 445.06 ($M + K^+$).HR-MS (ESI+): m/z [M + H+] Calculated for $C_{28}H_{22}O_3$ [M+], 406.1600; found, 406.1572.

4.2.6 Synthesis of PDP and TPE substituted dextran derivative (DEX-PDP-TPE): In 100.0 mL round bottom flask, dextran (1.0 g, 6.10 mmol), PDP Acid (0.56 g, 1.55 mmol), and TPE-Acid (0.15 g, 0.37 mmol) were dissolved in 25.0 mL of dry DMSO and the reaction mixture was purged with nitrogen for 0.5 h. Meanwhile dimethyl amino pyridine (DMAP) (0.19 g, 1.55 mmol) and dicyclohexyl carbodiimide (DCC) (1.33 g, 6.45 mmol) were dissolved in dry DMSO separately and added to the reaction mixture and continued the reaction for 24 h at 37ºC. After 24 h, formed dicyclohexyl urea was separated by filtration, DMSO was evaporated by Vacuum distillation and the product is precipitated in methanol. Obtained product was purified thrice by reprecipitation technique using DMSO as a good solvent and methanol as bad solvent. Yield 0.70 g (48 %).^{1}H NMR (400 MHz, DMSOd6) δ ppm:δ 7.14-6.99 ppm (m, 10H, Ar−H), 6.98-6.95 ppm (m, 6H, Ar−H),6.88-6.86 ppm (t, 2H, Ar−H), 6.71-6.68 ppm (m, 5H, Ar−H) 4.63

ppm (s, dextran anomeric proton), 4.47, 4.82, 4.88 ppm(s, hydroxyl of dextran),3.14−3.69 ppm (dextran glucosidic protons), 2.49 ppm (2H, Ar−CH_2), 1.48 ppm (2H,Ar−CH_2−CH_2), 1.18−0.80 ppm(aliphatic protons).

4.2.7 Synthesis of PDP, TPE and Succinic acid substituted dextran derivative (DEX-PDP-TPE-SA): In 100.0 mL round bottom flask, oven dried dextran (1.0 g , 6.10 mmol), PDP Acid (0.56 g, 1.55 mmol), tertiary butyl ester of succinic acid (0.54 g, 3.10 mmol) and TPE-Acid (0.15 g, 0.37 mmol) were dissolved in 25.0 mL of dry DMSO and the reaction mixture was purged with nitrogen for 0.5 h. Meanwhile dimethyl amino pyridine (DMAP) (0.19 g , 1.55 mmol) and dicyclohexyl carbodiimide (DCC) (1.33 g, 6.45 mmol) were dissolved in dry DMSO separately and added to the reaction mixture and continued the reaction for 24 h at 37ºC. After 24 h, formed dicyclohexyl urea was separated by filtration, DMSO was evaporated by vacuum distillation and the product is precipitated in methanol. Obtained product was purified thrice by reprecipitation technique using DMSO as a good solvent and methanol as bad solvent. Yield 0.80 g (58 %).^{1}H NMR (400 MHz, DMSOd6) δ ppm :δ 7.14-6.99 ppm (m, 10H, Ar−H), 6.98-6.95 ppm (m, 6H, Ar−H),6.88-6.86 ppm (t, 2H, Ar−H), 6.71-6.68 ppm (m, 5H, Ar−H) 4.63 ppm (s, dextran anomeric proton), 4.47, 4.82, 4.88 ppm(s, hydroxyl of dextran),3.14−3.69 ppm (dextran glucosidic protons)2.6-2.5 ppm (m,4H)methylene protons of SA, 2.49 ppm (2H, Ar−CH_2), 1.48 ppm (2H,Ar−CH_2−CH_2), 1.34 ppm (s, 9H), tert- butyl, 1.18−0.80 ppm(aliphatic protons).

The t-butyl ester unit was de-protected in the above product using trifluoro acetic acid. In 25.0 mL round bottom flask, the above dextran derivative (0.5 g, 1.58 mmol) was dissolved in 5.0 mL of DMSO and trifluoro acetic acid (1.20 mL,15 mmol) was added dropwise and stirred the reaction mixture for 4 h at 37ºC. After removing the TFA and DMSO under reduced pressure, obtained viscous liquid was poured in methanol (100.0 mL) and the product was separated by filtration. Obtained product was finally purified by dialyzing against milli-q water for 24 h. The obtained solution was then lyophilized and used for further experiments. Yield 0.35 g (80.0 %) ^{1}H NMR (400 MHz, DMSOd6) δ ppm :δ 7.14-6.99 ppm (m, 10H, Ar−H), 6.98-6.95 ppm (m, 6H, Ar−H),6.88-6.86 ppm (t, 2H, Ar−H), 6.71-6.68 ppm (m, 5H, Ar−H) 4.63 ppm (s, dextran anomeric proton), 4.47, 4.82, 4.88 ppm(s, hydroxyl of dextran), 3.14−3.69 ppm (dextran glucosidic protons)2.6-

2.5 ppm (m,4H)methylene protons of SA, 2.49 ppm (2H, Ar−CH_2), 1.48 ppm (2H,Ar−CH_2−CH_2), tert- butyl, 1.18−0.80 ppm(aliphatic protons).

4.2.8 Synthesis of aquated cisplatin $[Pt(NH_3)_2(OH_2)_2]^{2+}$Complex: The cisplatin aqua complex was synthesized following the procedure mentioned in our earlier report.[54]Accordingly,cisplatin20.0 mg (0.066 mmol, 1equiv) was dissolved in 20.0 mL of H_2O. To this solution, 22.5 mg (0.132 mmol, 2 equiv) of silver nitrate was added with continuous stirring at 37 °C for 24 h in dark. The produced milky white silver chloride precipitate confirmed the formation cisplatin aqua complex. The precipitate was then removed by centrifugation followed by filtration using a 0.45 μm filter. The obtained solution was then lyophilized to get light green colored powder which was stored at 4 °C.

4.2.9 Synthesis DEX-PDP-SA+Cisplatin Conjugate: 20.0 mg of dextran polymer compound (8) was dissolved in 4 mL of milli-q water and 200 uL of aqueous NaOH solution was added to it and stirred for 0.5 h at 37 ^oC .To the above polymer solution cisplatin aqua complex (3.4 mg, 0.012 mmol) was stirred for another 48 hours at 37 ^oC in the dark. The solution was then dialyzed (MWCO=3500) against large amount of milli-q water for 24 h with periodically changing water to remove unwanted and unencapsulated impurities. The solution from the dialysis bag was filtered through 0.4 μm filter, lyophilized and stored at 4 °C. FT-IR (KBr, cm−1): 3300, 2920, 2880, 1660, 1560, 1395, 1360, 1090, 1050, 930, 830 and 548.

The drug loading efficiency (DLE) and drug loading content (DLC) were determined by using OPD colorimetric assay as described in our earlier report.

4.2.10 DOX encapsulation in dextran derivatives: 20.0 mg of fluorescent dextran polymer compound and 0.2 mg of doxorubicin hydrochloride molecule were dissolved in 2.0 mL of DMSO and stirred for 10 minutes. To the above solution 2.0 mL of milli-q water was added dropwise and the resulting solution was stirred for 12 h in the dark. The solution was then transfeered to dialysis bag (MWCO 3500) and dialysed against milli-q water for 48 h. The water from the reservoir was changed priodically to remove the

unencapsulated molecules.After 48 h , the obtained solution is filtered through 0.45 u whatman filter paper, lyophilised and stored at 4^{o}C. The amount of DOX loaded in the polymer was determined using lambert beers law using the molar extinction coefficient as 11500L mol^{-1} cm^{-1}.The drug loading content (DLC) and drug loading efficiency (DLE) were calculated following the equation mentioned in second chapter and they were found to be 1.8 % and 60 % respectively.

A similar procedure was adopted to encapsulate doxorubicin hydrochloride in cisplatin conjugated fluorescent dextran polymer.

4.2.11 Dye encapsulation in dextran derivatives: 20.0 mg of fluorescent dextran polymer compound and 0.2 mg of rhodamin B dye molecule were dissolved in 2.0 mL of DMSO and stirred for 10 minutes. To the above solution 2.0 mL of milli-q water was added dropwise and the resulting solution was stirred for 12 h in the dark. The solution was then transferred to dialysis bag (MWCO 3500) and dialysed against milli-q water for 48 h. The water from the reservoir was changed periodically to remove the unencapsulated molecules. After 48 h, the obtained solution is filtered through 0.45 u whattman filter paper, lyophilised and stored at 4^{o}C. The amount of DOX loaded in the polymer was determined using lambert beers law using the molar extinction coefficient as 11500L mol^{-1} cm^{-1}.The drug loading content and drug loading efficiency were calculated following the equation mentioned in second chapter. A similar protocol was followed for nile red and rose Bengal encapsulation. The dye loading contents (DLC) and dye loading efficiencies (DLE) for these three dyes were found to be 1.5 % and 65 % for V_{RB}, 1.8 % and 55 % for V_{RHB} and 1.2 % and 45 % for V_{NR}, respectively.

4.2.11 *In Vitro* Drug release studies for Cisplatin: Cisplatin release from cisplatin conjugated fluorescent dextran vesicles was carried out using dialysis method at physiological condition.typically 3.0 mg of cisplatin conjugated dextran vesicles were taken in a dialysis bag (in 3 mL) and they were immersed in 10 mL beaker and dialyzed at 37 °C with constant stirring. 0.4 mL of dialysate was taken out at specific time intervals and replaced with equal volume of fresh phosphate buffer saline (PBS) solution. The amount of cisplatin released in each aliquot was calculated by OPD colorimetric assay using absorption spectroscopy.[54]The percentage cumulative release was calculted

using the equation asCumulative release (%) = C_n x V_o / m x 100, where C_n is amount of loaded cisplatin in n^{th} sample, V_o is total volume and m is total amount loaded in vesicles. For esterase assisted release studies 10 units of esterase enzyme was used, followed the same protocol as mentioned above.

4.2.12 *In Vitro* Drug Release Studies for DOX.HCL: *In vitro* doxorubicin released from the fluorescent dextran vesicles was monitored using dialysis method as mentioned in second chapter. Typically 3.0 mg of DOX loaded dextran vesicles were taken in dialysis bag (MWCO 3500) in immersed in 10.0 mL of PBS at 37°C. To determine the dox concentration in the dialysate , 3.0 mL of dialysate was withdrawn periodically and absorbance was measrued to calculated the amount of dox released. The percent cumulative release was calculated following the equation. A similar protocol was followed to monitor the esterase enzyme action on the dox release.

Cumulative Release = amount of drug release at time t/ total amount of drug taken in dialysis tube *100

4.2.13 Photophysics and FRET Studies: All the absorption and emission experiments were carried out keeping the optical density of TPE fluorophore as 0.1. TPE chromophore was excited at 340 nm and DOX was excited at 480 nm. The other dyes like rhodamin B , nile red and rose Bengal were excited at 554 , 560 and 527 nm respectively. For Emission measurement the slit width was kept as 2 and it was held constant for all the measurements. For TCSPC lifetime studies nano-LED source with wavelength 340 nm for exciting TPE chromophores was used, and their lifetime decay was obtained at emission maxima of 460 nm. These decays were fitted by using DAS6 software.

4.2.14 Cell Viability Assay and Cellular imaging: A cell viability assay was performed in MCF 7 and HeLa cells using the tetrazolium salt, 3-4,5 dimethylthiazol-2,5-diphenyl tetrazolium bromide (MTT) to compare the cytotoxicities of free drug and drug loaded vesicles.1000 cells per well were seeded in 96 well plate in 100 μL of complete DMEM and allowed to adhere for 16 h. Different concentrations of the free drug and drug encapsulated vesicles were then added to the cells and incubated for another 72 h. Thereafter the media was aspirated and 100 μL of freshly prepared MTT solution (0.5 mg/ mL in complete media) was added and incubated for another 4h at 37 °C. The formed formazan crystals were dissolved in 100 μL of DMSO and the absorbance was immediately measured using varioscan micro plate reader at 570 nm. The data represents the mean value from at least three independent measurements. The relative percentage values, with respect to control, were calculated and plotted against the concentration. To envision the intracellular fate of free drug and drug loaded vesicles, cells were seeded at a density of 10^5 cells per well on 6 well-plates containing 2.0 mL of complete DMEM medium and incubated at 37 °C for 16 h. After 16 h, media was aspirated and cells were feeded with 2.0 mL media having required concentration of the compounds. After incubating for 9 h, the media was removed and cells were washed using 1X PBS two times following the permeablisation using 4.0 % paraformaldehyde solution. After staining cells with necessary dyes, cover slips were mounted on slides using Fluoromount™ mounting medium (Southern Biotech) and dried overnight at room temperature in the dark. The cells were imaged using a confocal microscope using the λ = 405 nm (blue channel) and λ = 560 nm (red channel) lasers. Image J software was used for processing the images.

4.3 Result and Discussion

4.3.1 Synthesis of TPE-tagged dextran

To make fluorescent dextran conjugates, a aggregation induced emissive (AIE) fluorophore molecule tetraphenylethene (TPE) was chosen and synthesized using McMurry coupling reaction as shown in scheme 4.1.Benzophenone and 4-hydroxy benzophenone were coupled using $TiCl_4$ and zinc powder to obtain compound (1). This compound (1) was then further alkylated using ethyl chloro acetate to get the compound (2) (see scheme 1) which upon hydrolysis produced compound (3). The compound (3) and PDP acid were then anchored on to the dextran backbone in one pot esterification reaction to obtain modified dextran derivative DEX-PDP-TPE.

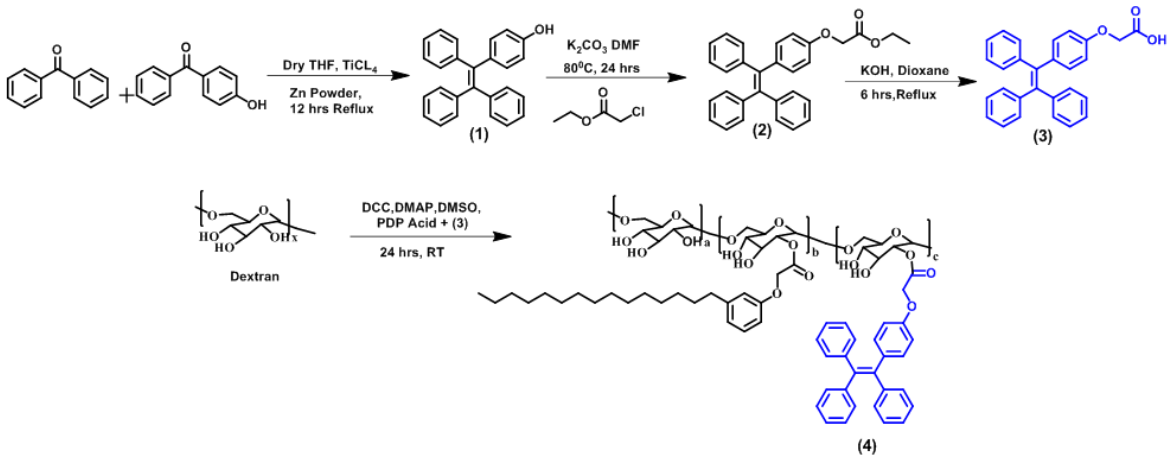

Scheme 4.1: *Synthesis of PDP acid and TPE acid substituted amphiphilic fluorescent dextran derivative.*

The substitution of these molecules on the dextran backbone was confirmed by proton NMR spectra as shown in the figure 4.8. The proton NMR spectrum of the individual acids (PDP acid and TPE Acid,) are shown in figure 4.8 a, b and the respective peaks are assigned alphabetically. The substitution of acid (3) on dextran backbone was confirmed by deshielding of proton f in figure 4.8 b to downfield region. This deshielding was attributed to the fact that when these acids were coupled onto the dextran backbone, the aromatic protons in the vicinity of the acid group are getting deshield due to the esterification reaction. This observation proved that the substitution of the acid has occurred on the dextran backbone.

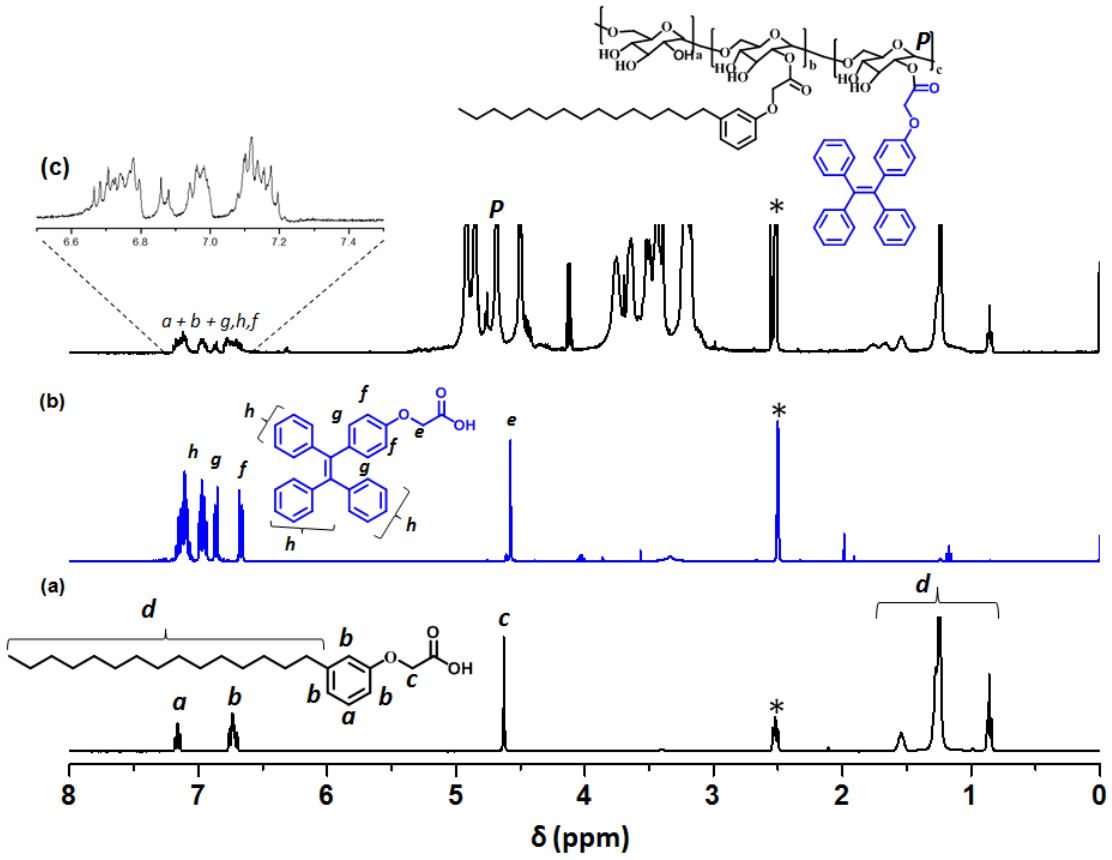

Figure 4.8: *^{1}H NMR spectra for PDP Acid (a), TPE acid (b) and PDP and TPE acid substituted dextran derivatives (c) taken in DMSOd6. The protons peaks are assigned alphabetically and showed in the spectrum.*

Degree of substitution on the dextran backbone was calculated by comparing the integration values of anomeric proton (proton' P') of dextran with one of the proton in each acid. So for compound (3), the integration value of proton 'g,h,f' is compared with proton'P' and the degree of substitution was obtained as 2%. Similarly for PDP acid, the integration value of proton 'a' is compared with proton'P' and degree of substitution was obtained as 5%.It was studied in our earlier report that if the degree of substitution exceeds more than 20 %, the dextran derivatives becomes insoluble in aqueous medium and hence the dextran backbone was modified carefully by optimising the equivalents of acids and the degree of substitution was kept constant as mentioned above.

4.3.2 Aqueous Self-assembly and AIE

The newly designed dextran derivatives were conjugated with a hydrophobic unit pentadecylphenol (PDP) which produces an apmhiphilicity in the current design. Based on our earlier studies, it was observed that these hydrophobic units form a bilayer sheet in aqueous medium which subsequently folds to form a vesicular type of self assemble structures. In a current design, similar kind of morphology was expected to form which forces tetraphenylethene (TPE) molecules to be in the aggregated state in the layer of the vesicles and produces fluorescent vesicles. The schematics showed in figure 4.9a depicts the formation of bilayer structures of these dextran derivatives in aqueous medium. Self assembly of these dextran derivatives were then facilitated by dialysing the solution against milli-Q water for 48 hours. The photograph of the dialyzed sample in vial showed in figure 4.9b clearly indicated that these assemblies are dispersible in water and produces a blue colour upon exposing to UV light.

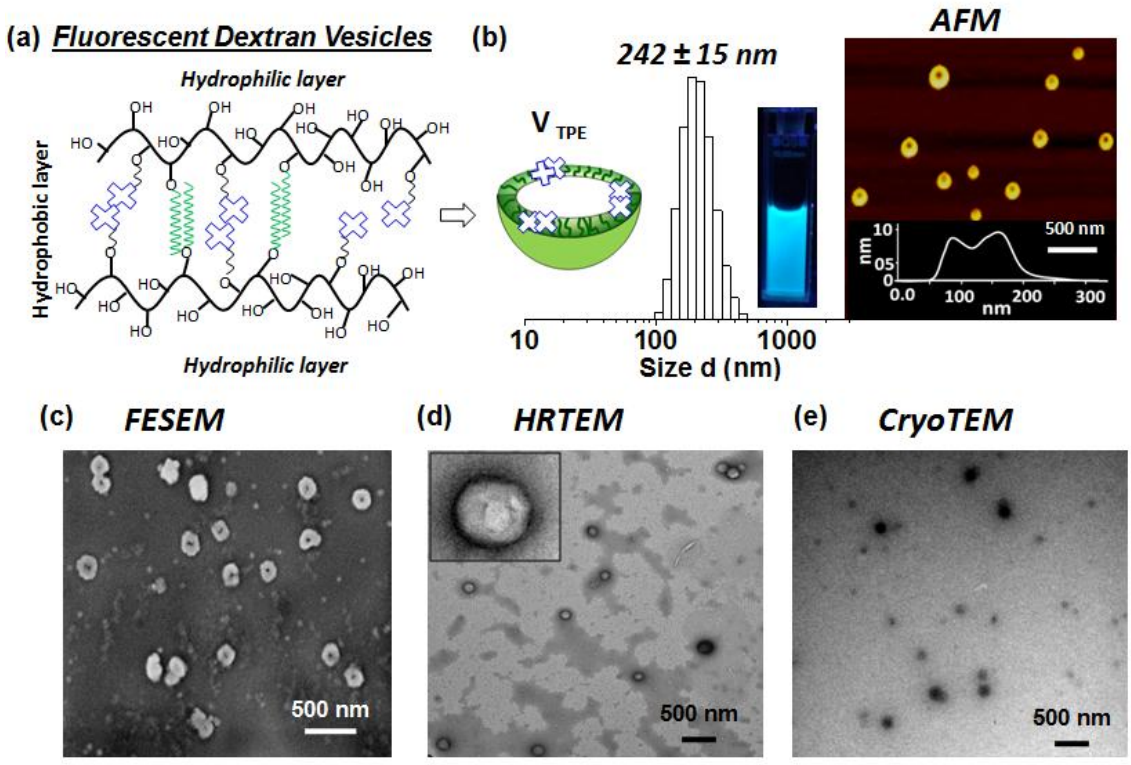

Figure 4.9: *Schematics showing mechanism of vesicle formation for dextran derivatives (a), DLS and AFM images for V_{TPE} (b) FESEM image for V_{TPE} (c) HRTEM morphology of V_{TPE} (inset diagram shows the distinct core and layer of vesicles) (d) and Cryo TEM morphology of V_{TPE} (f).*

The size of these nanoassemblies were determined using dynamic light scattering (DLS) technique, which showed monomodal distribution with size of around 250 ± 20 nm (see figure 4.9b). The vesicular nature of these nanoassemblies was confirmed by different microscopic techniques such as atomic force microscopy (AFM), transmission electron microscopy (TEM) and field emission scanning electron microscopy (FESEM). The images obtained in AFM technique are showed in figure 4.9b, It depicts the formation of donut shaped morphology which typically corresponds to the vesicular geometry of the self assemble structures. Furthermore, the height profile obtained from the AFM image (see figure 4.9b) showed a two hump profile which clearly indicates that the inner core of the self assemble structures is soft which is generally observed in the case of vesicles. The FESEM morphology in figure 4.9c showed a distinct core and layer features in these spherical nano-objects which validate the results obtained from AFM technique. These nano-objects when subjected for HRTEM analysis, which validates the formation of distinct core and layer in the nanostructures (see figure 4.9d).The cryo TEM analysis of these vesicles showed the formation of spherical objects having sizes around 230 ± 20 nm as shown in figure 4.9f. From all the observation discussed above it was obvious that the formed nanoassemblies are vesicular in nature which has a distinct hydrophilic core and a hydrophobic layer. Thus, they are a potential candidates for delivering the different anticancer drugs which otherwise are difficult owing to their poor water solubility. The TPE-tagged fluorescent dextran nanovesicles here are referred as "V_{TPE}"in all further discussion. The aggregation behaviour of newly designed TPE-tagged dextran derivative is was studied in water:DMSO solvent combination. As can be seen from figure 4.10 a , the absorbance of V_{TPE} does not change much with respect to the water: DMSO solvent combination. When these fluorescent dextran derivatives were dissolved in dimethylsulfoxide, they do not form any kind of self-assembled nanostructures; hence, the TPE fluorophore molecules are in non aggregated states and do not fluoresce, as shown in figure 4.10b. When these derivatives were dissolved in water, amphiphilicity in the dextran backbone forces them to self assemble in nanovesicles which brings the TPE fluorophore in the aggregated state and causing these structures to produce blue fluorescence (see Figure 4.9a).

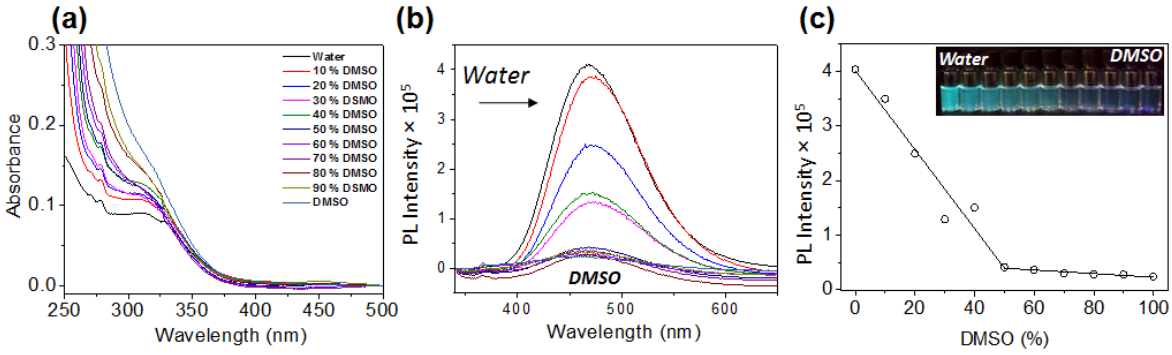

Figure 4.10: *Absorbtion spectrum of V_{TPE} in water: DMSO combination (a) emission spectrum of V_{TPE} in different solvent combinations of water: DMSO (b), and plot of percent of DMSO in solvent combination vs emission intensity for V_{TPE}(c).*

A solvent dependent fluorescence measurement of these dextran derivatives was carried out in different water:DMSO solvent combination and showed in figure 4.10 d. From the plot it can be seen that the fluorescence of these derivatives was getting quenched with increasing the amount of DMSO solvent, proving the fact that the florescence property of these molecules is dependent upon aggregation. When the DMSO solvent percentage was plotted against the fluorescence intensity, it was observed that even up to 50 % DMSO combination, these derivatives showed a good fluorescence as shown in photographs of the vials in figure 4.10c. From this observation it was revealed that, the aggregation of these vesicles were driven by a solvent and hence in water these vesicles showed prominent blue fluorescence where as in DMSO they become non fluorescent in nature. The aggregation phenomenon showed by the dextran derivatives was a concentration dependent process and hence it was important to determine the critical concentration needed to form aggregates. Formation of these aggregates was schematically showed in figure 4.11a and to determine the critical aggregation concentration (CAC) of these dextran derivatives, a concentration dependent fluorescence measurement in aqueous medium was carried out and shown in figure 4.11b, from the plot it was clear that; as the concentration decreases from 1.0 mg/mL to 0.01mg/mL, the fluorescence intensity was gradually decreased and becomes non fluorescent in nature at 0.01mg/mL.

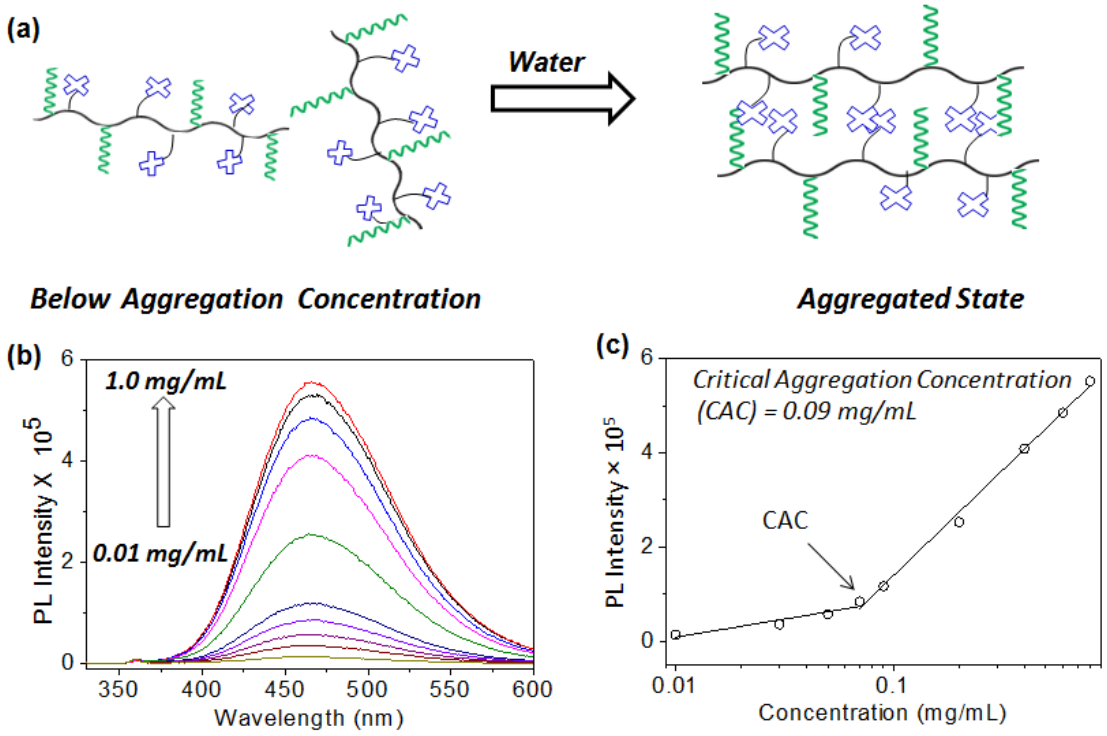

Figure 4.11: *Schematics showing mechanism of concentration dependent aggregate formation for V_{TPE} (a), A plot of concentration dependent emission intensity forV_{TPE} (b), and plot of concentration vs emission intensity for V_{TPE} (c).*

When the concentration of these dextran derivatives were plotted against fluorescence intensity (see Figure 4.11c), a break point was observed at a concentration of 0.09mg/mL suggesting that in a current design TPE molecules are aggregation responsive and minimum aggregation concentration was obtained as 0.09mg/mL. From this experiment it can be concluded that the aggregation behaviour of the dextran derivative was driven by a self assembly process and a minimum aggregation concentration is needed to make these derivatives fluorescent in nature. The stability of these derivatives at physiological conditions was also studied by recording fluorescence spectrum at different temperatures ranging from 25^0C to 70^0C by an interval of 5^0C as showed in figure 4.12.The schematics were drawn and showed in figure 4.12a, which explains the probable self assembly of these derivatives at different temperatures. The plot in figure 4.12b shows the florescence spectrum of these derivatives at different

temperatures and when fluorescence intensity was plotted against temperature (see Figure 4.12c) it was found that these derivatives are very stable up to 45^0C further increase in temperature causes the fluorescence quenching and it becomes non-fluorescent at 70^0C.

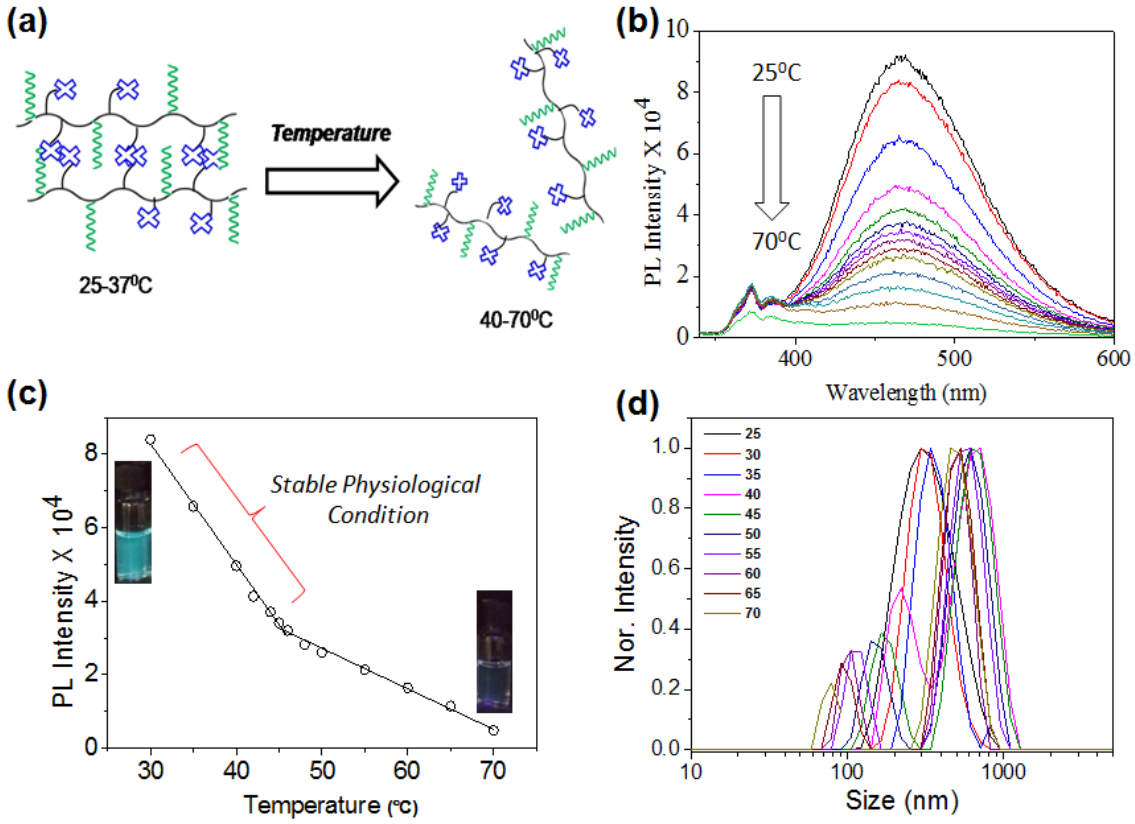

Figure 4.12: *Schematics showing effect of temperature on aggregate formation for V_{TPE} (a), A plot of temperature dependent emission intensity for V_{TPE} (b), plot of temperature vs emission intensity for V_{TPE} (c) and temperature dependent DLS plot for V_{TPE} (d).*

From the plot shown in figure 4.12c it can be seen that these fluorescent dextran derivatives were stable at physiological temperature and can be used for biological studies. The effect of temperature on the AIE property of these assemblies were also validated by doing temperature dependent dynamic light scattering (DLS) experiment, wherein the size measurement was done at various temperature ranging from 25^0C to 70^0C and the results are showed in figure4.12d. When the size of the nanoassemblies was plotted against temperature it was very clear that the nano-assemblies showed a monomodal size distribution of 200 ± 20 nm up to 40^0C. As the temperature increases

from 40^0C to 70^0C, the nanoassemblies showed a multimodal size distribution having sizes ranging from 300 nm to 1µm which proved that the self assembly of the nanoassemblies was getting disturbed. From all the above experiments it can be concluded that the aggregation induced emission property of the dextran nano-aggregates not only dependent on the concentration but also dependent on the temperature and solvent composition. These experiments helped in understanding the in-depth knowledge of the aggregation induced emission property and the factors affecting the property.

4.3.3. TPE-DOX "Turn-On" and "Turn-Off" Bioprobes

The tailor-made dextran vesicle was loaded with water-soluble anticancer drug doxorubicin hydrochloride (DOX.HCl) through dialysis method. The photograph of the vial showed in figure 4.13a proves the DOX loading in these dextran vesicles and its size was found to be 249± 20 nm. The vesicular nature of these assemblies was also examined using AFM and FESEM techniques and images are showed in figure 4.13b. From the AFM and FESEM images it was confirmed that these assemblies are vesicular in nature and loading the anticancer drug does not alter the self assembly of these structures. These DOX.HCl loaded vesicles were referred as "$V_{TPE\text{-}DOX}$" for all the further discussion.

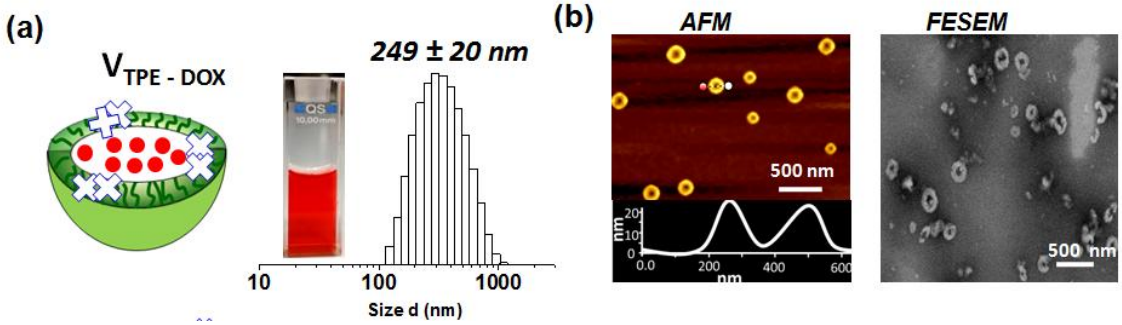

Figure 4.13: Schematics showing DOX.HCl loading in V_{TPE} vesicles, DLS histogram showing the size of V_{TPEDOX} (a), AFM and FESEM images for $V_{TPE\text{-}DOX}$ dual loaded vesicles (b).

The drug loading content (DLC) and drug loading efficiency (DLE) of $V_{TPE\text{-}DOX}$ was found to be 1.8 % and 60 %. A control non-fluorescent DOX.HCl loaded vesicle ("V_{DOX}", as reported in chapters 2 and 3)was used as a control. The dextran derivatives were engineered by conjugating the PDP units through aliphatic ester linkages; thus, their

responsiveness to intracellular enzymes in vitro disassembles these vesicles to deliver the DOX. To monitor the disassembly process, an *invitro* release studies were in the presence of 10U horse esterase enzyme and the releases of the drug molecule was monitored using UV absorption spectroscopy. For better understanding, schematics are showed in figure 4.14a which explains the disassembly of these vesicles and how the drug was getting release from the core of the vesicles. A control release experiment was also carried out in the absence of esterase enzyme and the stability of these vesicles was monitored for 48 hours. The cumulative drug release was plotted against the time and showed in figure 4.14b which conveys that 95 % of the DOX.HCl was released in the presence of enzyme proving the enzyme triggered disassembly of the present design. It was also observed that, in PBS alone at pH 7.4, these vesicles exhibited 20-30 % leaching. From the above results it can be concluded that the current design not only can load the anticancer drug DOX.HCL but also can deliver it at intracellular conditions.

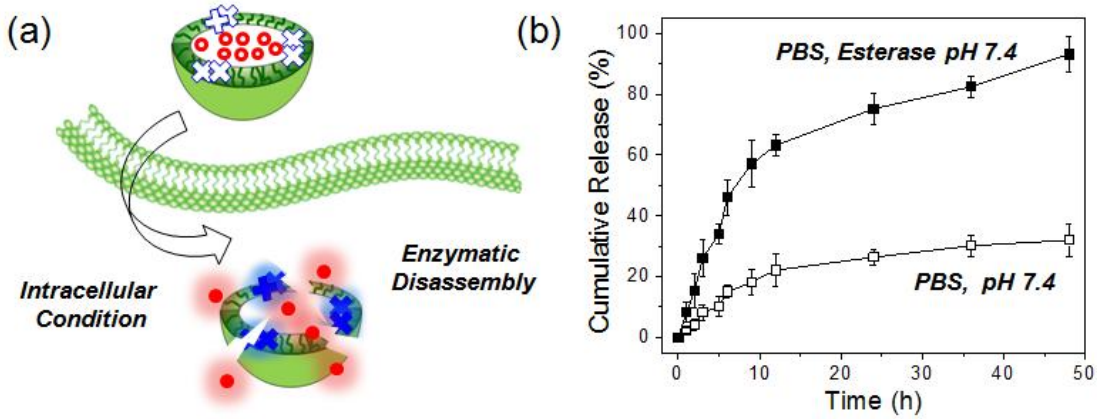

Figure 4.14: *Schematics showing the cellular uptake of* $V_{TPE\text{-}DOX}$ *and subsequent enzymatic cleavage (a), a plot showing the drug release profile in PBS pH 7.4 and in the presence of 10U horse liver esterase enzyme (b).*

The $V_{TPE\text{-}DOX}$ has two different optical chromophores with distinct photo physical characteristics in the UV to visible region. Thus, one would expect the occurrence of two photo physical phenomena among these two fluorophores: (i) fluorescence resonance energy transfer (FRET) between TPE donor and DOX acceptor, and/or (ii) aggregation caused quenching (ACQ) of TPE+DOX together. The advantages of the present system are that the enzyme-responsive dextran vesicular nano-assemblies could take advantages

of the above photo physical phenomena to construct very useful fluorescent turn-On or Turn-Off bio-probes for medical diagnostics. For instance, the enzymatic-biodegradation of ACQ vesicles would lead to Turn-Off to turn-On intracellular fluorescent probe and FRET phenomenon would provide Turn-On to Turn-Off intracellular FRET probe. Both theses probes are equally important for bio-imaging and diagnostics in medical research like in cancer. These two concepts are schematically shown in Figure 4.15.

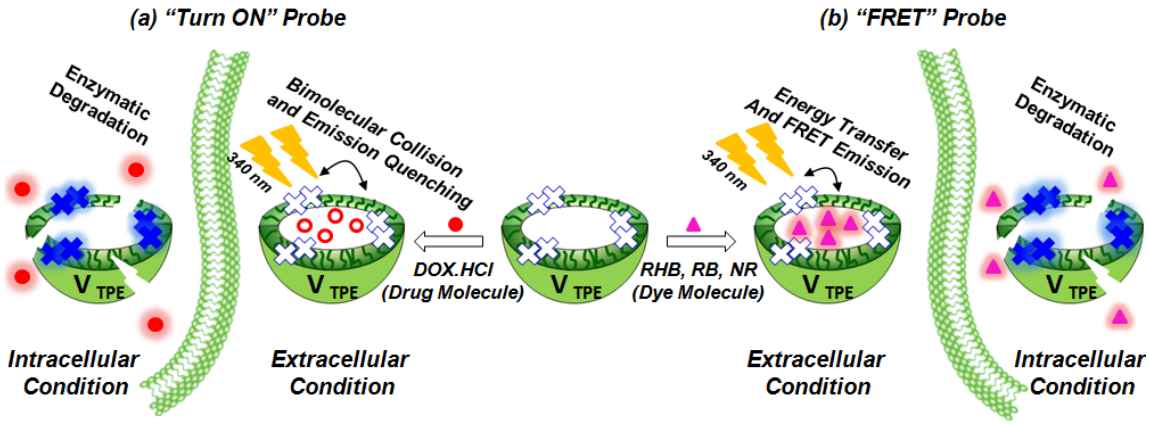

Figure 4.15: *A schematics showing the mechanism of energy transfer for "Turn ON" probe (a) and for FRET based bioimaging probe (b).*

TPE has absorption maxima in the UV-region at 340 nm and upon photo excitation it emits blue-fluorescent light with peak maxima at 460 nm. On the other hand, the anticancer drug DOX has absorption and emission maxima at 480 and 560 nm, respectively. In figure 4.16 a, The TPE emission spectrum exhibits excellent overlap with DOX absorbance spectrum and the overlap integral is estimated to be 92 %.To understand the fluorescence response in polysaccharide nanovesicles, the absorption and fluorescence spectra of V_{TPE}, V_{DOX} and $V_{TPE\text{-}DOX}$ were recorded and showed in the figures 4.16 b and 4.16 c. The concentration of the TPE and encapsulated DOX were maintained as OD= 0.1 and OD= 0.03 in all three systems. Upon photo excitation at λ_{ex} = 340 nm (TPE absorption maxima), the V_{TPE} showed strong emission at 470 nm with respect to the occurrence of AIE in the aqueous medium (see Figure 4.17c).At this excitation wavelength, two interesting trend were observed in $V_{TPE\text{-}DOX}$: (i) the AIE- blue emission from TPE chromophore was completely quenched in the presence of DOX, and (ii) there is DOX emission indicating that there is no significant energy transfer from TPE

to DOX (DOX has residual emission at this excitation wavelength, see the figure inset). At DOX excitation (λ_{ex} = 480 nm),V_{DOX} exhibited strong red-luminance's at 550 nm; however, $V_{TPE\text{-}DOX}$ did not show any substantial emission from the encapsulated DOX molecules in the TPE conjugated dextran vesicles. This implies that the self-emission of the DOX chromophores were also quenched in the presence of TPE in the dextran vesicular assemblies. This selective photo excitation experiments validate that the self-emission of both TPE and DOX were completely suppressed in their company of each other. The resultant turn-Off of the fluorescence in the vesicular nano-assemblies is attributed to the strong bi-molecular aggregation induced quenching as shown in Figure 4.16c. This trend is similar to the observation reported in other polymer nano-carriers such as block copolymer micelles, etc.

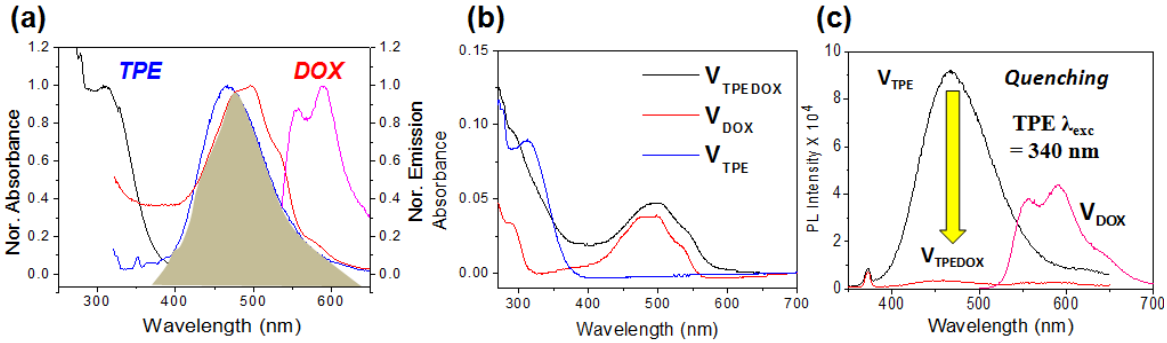

Figure 4.16: *A plot showing the spectral overlap between emission spectrum of TPE and absorbtion spectrum of DOX.HCl (a), A absorbance plot for V_{TPE}, V_{DOX}, $V_{TPE\text{-}DOX}$ (b) and A emission plot showing the emission intensity of V_{TPE}, V_{DOX} and $V_{TPE\text{-}DOX}$ vesicles (c).*

The unique advantages of the fluorescent "turn-Off" polysaccharide vesicular system is that it could be readily turn-On exclusively in the intracellular levels by the lysosomal enzymes. The enzymes could readily biodegrade the aliphatic ester linkages that connecting the hydrophilic dextran and hydrophobic PDP units. This results in the disassembly of the nano-vesicle and isolates the TPE-DOX chromophores from bi-molecular quenching and turn into bright luminescent turn-On probes. As result, bright blue-emission form TPE and red-emission form DOX could be readily monitored. This Turn-Off to Turn-On phenomena provide three direct observations: (i) the turn-Off state confirmed the stability of the vesicular system in the extracellular level, (ii) turn-On state confirmed the vesicular disassembly and drug release at the intracellular level, and (iii)

further the turn-On provide new opportunity to monitor the real-time drug-release kinetics. To test these concepts, the $V_{TPE\text{-}DOX}$ is tested for its enzyme triggered disassembly process using horse liver esterase enzyme in *invitro* conditions. A Schematics of $V_{TPE\text{-}DOX}$ vesicles showing the stability and degradation at extracellular and intracellular condition was showed in figure 4.17 a.

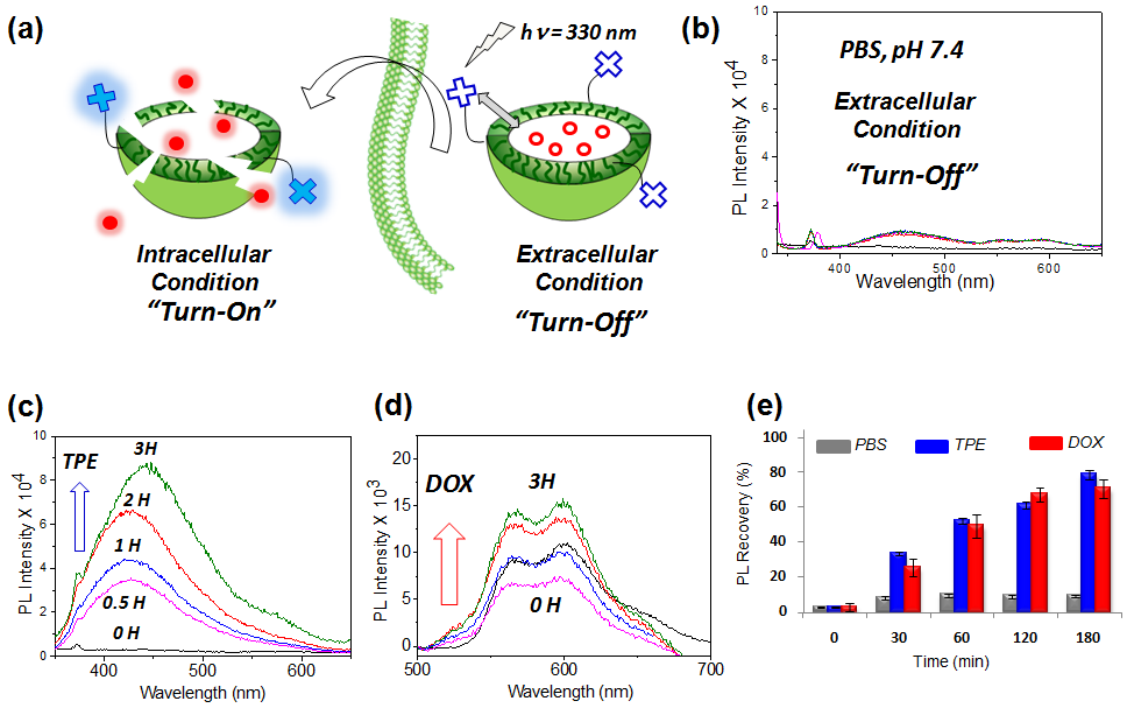

Figure 4.17: *Schematics of $V_{TPE\text{-}DOX}$ vesicles showing the stability and degradation at extracellular and intracellular condition (a), An emission spectrum of $V_{TPE\text{-}DOX}$ showing the stability of vesicles in PBS pH 7.4 (b), A emission spectrum of V_{TPEDOX} vesicles showing the emission recovery of TPE in the presence of esterase enzyme PBS pH 7.4 (c), A emission spectrum of V_{TPEDOX} vesicles showing the emission recovery of DOX in the presence of esterase enzyme PBS pH 7.4 (d) and a plot of time Vs emission recovery for $V_{TPE\text{-}DOX}$ vesicles in the presence and absence of esterase enzyme (e). 1 mg of esterase enzyme has been used for carrying the enzyme assisted disassembly studies of $V_{TPE\text{-}DOX}$ vesicles.*

In PBS at pH 7.4, the $V_{TPE\text{-}DOX}$ was found to be very stable and retained its turn-off state (see figure 4.17 b). The stability of the $V_{TPE\text{-}DOX}$ was also tested in liposomal pH = 5.0 and in FBS. The stability was also tested by continuously monitoring $V_{TPE\text{-}DOX}$ in PBS by measuring their size distribution in dynamic light scattering. All these experiments confirmed that the turn-off state in $V_{TPE\text{-}DOX}$ was found to be retained for more than 48 h. The real-time drug release under the enzymatic-degradation of the

nanovesicles $V_{TPE\text{-}DOX}$ was studied by steady-state fluorescence spectroscopy recovery by incubating the sample in the presence of esterase enzyme in PBS at pH= 7.4. The time-dependent emission spectra were recorded by exciting the samples at both TPE and DOX excitation wavelengths and shown in Figure 4.17 c and d. It is very obvious from the spectra that upon enzymatic-degradation, the probes became turn-On and the self-emission from TPE and DOX emerges in significant intensities. The bar-diagram in Figure 4.17 e quantifies the enzyme-responsive turn-On in $V_{TPE\text{-}DOX}$ system. It was found that the emission intensities of TPE and DOX were enhanced almost 6-8 folds which is very significant for bio-imaging application in cancer cells. From the above discussion it was obvious that the overall emission quenching was attributed to the bimolecular collision of the two fluorophores and it is completely driven by self assembly process. The enzyme action could disturb the self assembly and fluorophores regained their emission properties. Now to understand the role of DMSO solvent on the self assembly of these vesicles, a absorbance and emission of $V_{TPE\text{-}DOX}$ and free DOX were recorded in DMSO (10%): Water (90%) solvent combination and showed in figure 4.18 a and b. The optical density of TPE chromophore in $V_{TPE\text{-}DOX}$ was kept constant as 0.1 as can be seen from the absorbance spectrum (see figure 4.18 a).

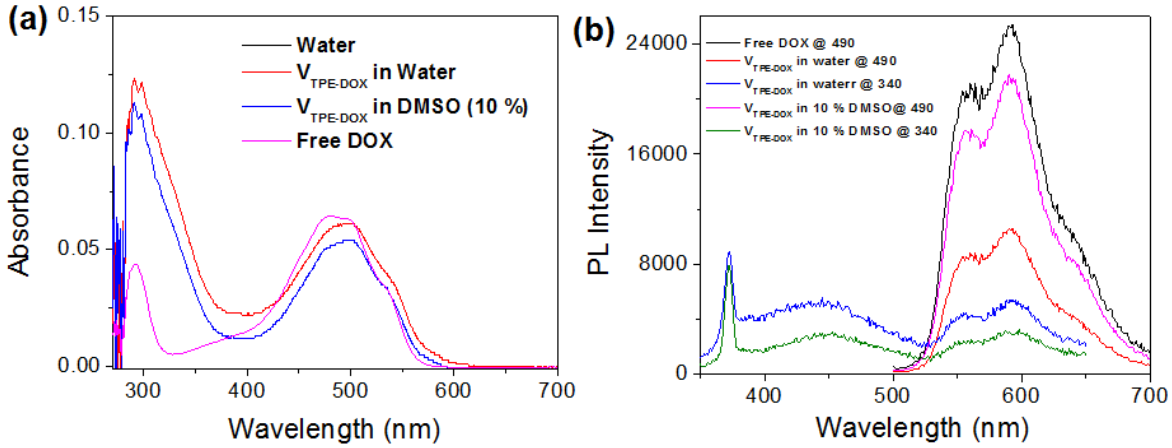

Figure 4.18: *An absorbance spectrum of $V_{TPE\text{-}DOX}$ and free DOX (a) and emission spectrum of $V_{TPE\text{-}DOX}$ and free DOX at different excitation wavelength as mentioned in the spectrum (b). The measurements are done in water and DMSO (10%): Water (90%) solvent combination.*

Moreover the presence of small fraction of DMSO solvent did not induce any effect on the absorbance spectrum. When the emission (excited at both 340 and 490 nm)

was recorded for $V_{TPE\text{-}DOX}$ solution in water, the quenching of the fluorescence of both the fluorophores was observed as seen in the earlier cases (see figure 4.18 b). When the similar emission measurement for $V_{TPE\text{-}DOX}$ was carried out in the presence of small fraction of DMSO (10 %) solvent, the DOX fluorescence (excited at 490 nm) was drastically increased by three folds as compared to the emission measured in case of water alone (see figure 4.18 b). This recovered intensity of DOX chromophore is equal to the intensity of free DOX (see figure 4.18 b). This indeed confirms that the DOX intensity was quenched by bimolecular collision of the two fluorophores and small change in self assembly could hamper the quenching process and helps in regaining the emission property. This observation supports the fact that presence of small amount of DMSO solvent could impart a great effect on self assembly of the self assembly of the vesicles. It has been observed that the TPE chromophore has not regained its emission property during the course of measurement and this attributed to the fact that aggregation of TPE is a thermodynamically driven process which may take some more time to regain the emission property. This control experiment validated the results obtained by steady-state fluorescence spectroscopy recovery method. Together all these experiments proved that these nanovesicles are very stable at extracellular condition and retains its turn OFF state while becoming turn ON probe at the intracellular condition. To prove the transportation and biodegradation $V_{TPE\text{-}DOX}$ in the lysosomal compartments, cellular uptake studies were performed in breast cancer cell line (MCF 7). It is important to know the cytotoxicity of polymeric nanovesicles and hence these polysaccharide vesicles were treated with human breast cancer cells (MCF 7) at varying concentrations ranging from 1 to 300 µg/mL and their cytotoxic effect was studied by standard MTT assay. The data for cytotoxicity for V_{TPE} was shown in figure 4.19 a, where they were found not to be toxic to the cells at a concentration of 300 µg/mL. The concentration used for drug delivery application lies much below the above tested concentration and these nanovesicles can be very good candidates for theranostics application. Similarly DOX.HCl loaded nanovesicles were treated with human breast cancer cells (MCF 7) and the toxicity plot was showed in figure 4.19 b. From the plot it was seen that the V_{TPEDOX} and free DOX. HCl showed almost similar killing at 72 hours of incubation time. Though V_{TPEDOX} and

free DOX.HCl showed a similar killing, V_{TPEDOX} has an advantage of being used as theranostic in cancer drug delivery application.

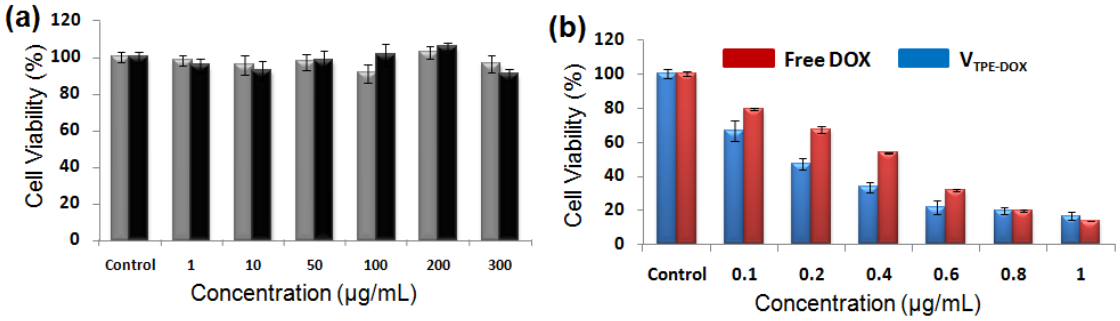

***Figure 4.19**: plot showing the cytotoxicity of V_{TPE} vesicles in human breast cancer MCF 7 cells (a) and a plot showing the cytotoxicity of V_{TPEDOX} and free DOX in MCF 7 Cells (b).*

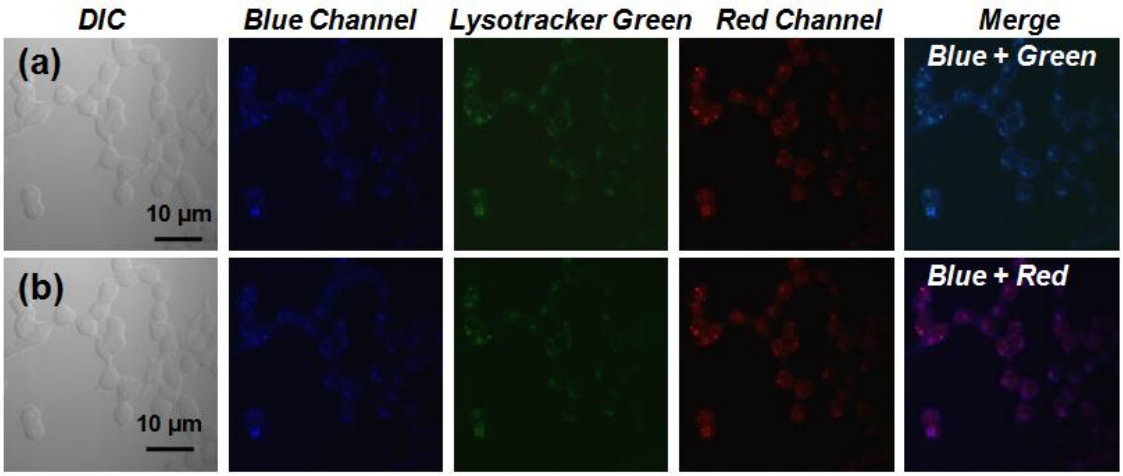

***Figure 4.20**: A panel showing live cell confocal microscope images for V_{TPEDOX} vesicles where the lysosomes were stained with Lysotracker green DND-26 (a) Blue emission from TPE was observed in Blue channel, the red emission from DOX was observed in red channel and merged image showed in first panel is the overlapping of blue and green channel giving the cyan colour (a) and merged image in second panel is the overlapping of blue and red channel giving magenta colour (b) The cells were incubated with 2 µg/mL concentration of DOX for 3hours.*

The vesicular nano-assemblies are expected accumulate and break in the enzyme rich lysosomal compartment of the cell. To visualise the lysosomal colocalization of vesicles, the breast cancer cells are stained using lysotracker green, and the cells are treated with $V_{TPE\text{-}DOX}$ for 3hrs prior to confocal microscopy imaging. The cyan colour of merged image in the first panel in figure 4.20 a proves the colocalization of blue colour

of TPE and green colour of lysotracker DND-26 confirming the digestion of these vesicles in the enzyme rich lysosomal compartment of the cells. Similarly the magenta colour of the merged image in the second panel in figure 4.20 b proves the colocalization of blue colour of TPE and red colour of DOX confirming the DOX release from the nanovesicles. The presence of magenta colour in the cytoplasm and the red colour in the perinuclear region confirmed the DOX release and subsequent accumulation at the nucleus of the cells. Based on the earlier discussion it is obvious that these vesicles are very stable at the extracellular conditions and regain their emission property only upon disassembly or degradation of the nanovesicles. From the results obtained in the cellular uptake studies tit was confirmed the appearance of the blue and red colour in the intracellular compartments is the clear indication of the intracellular disintegration of the nanovesicles. Thus, this experiment proved the potential of these nanovesicles as turn ON probe for doxorubicin delivery to the cancer cells.The schematics were drawn to explain the extracellular stability as "Turn OFF" state and intracellular "Turn ON" property of the $V_{TPE\text{-}DOX}$ vesicles and are showed in figure 4.21 a. Now to understand the performance of intracellular enzymes on the "Turn OFF" state of the nanovesicles, the breast cancer cells were treated with $V_{TPE\text{-}DOX}$ (2.0 µg/mL of DOX.HCl) and cells were incubated at different time ranging from 0 minutes to 180 minutes. Subsequently cells were fixed and imaged using confocal microscopy and the images at different time points are showed in the figure 4.21b. The first panel represents the DIC images; second panel represents the blue channel with the emission coming from the TPE molecule and a third panel represents the red channel with emission coming from the DOX.HCl molecules. From images for 0 minutes and 30 minutes it was confirmed that initially the nanovesicles V_{TPEDOX} was in "Turn OFF" state with increasing the time of incubation, there was a gradual increase in the emission intensity of both the fluorophores TPE and DOX.HCl respectively. This recovery in the emission of the fluorophore indeed proved that there was no crosstalk between the two fluorophore after being enzymatically disassemble. When the fluorescence intensity for both fluorophores were plotted against time and showed in figure 4.21c, it was observed that in three hours of incubation time there was a complete emission recovery from the fluorophores and now they are being apart from each other. From the above results it can be concluded that the current design

has a potential to be a "Turn ON" probe from a "Turn OFF" probe which differs these nanovesicles from other fluorescent drug delivery systems.

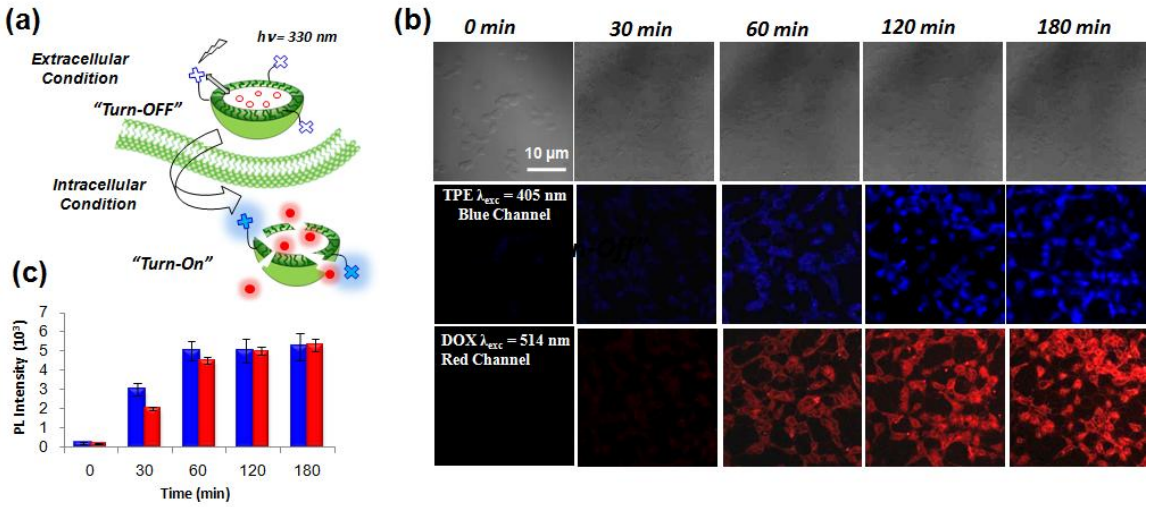

Figure 4.21: *A schematics showing extracellular stability "Turn OFF" and intracellular "Turn ON" of $V_{TPE\text{-}DOX}$ vesicles (a), a panel showing the confocal microscopy images taken at different time intervals for $V_{TPE\text{-}DOX}$ vesicles (b) and a bar plot of emission intensity of TPE and DOX vs time (c). The MCF 7 cells were treated with 2 µg/mL concentration of V_{TPEDOX} vesicles and incubated for respective time intervals.*

4.3.4 TPE-Polysaccharide vesicle FRET Probes

Fluorescent polymer nano-carriers which work on the principle of fluorescence resonance energy transfer (FRET) are gaining much interest since it offers a direct real time monitoring of drug release profile. FRET is emerging as important bio-imaging tools for studying the different biological processes such as protein -protein interactions, tumour imaging, drug release kinetics, enzyme activity etc. Such types of drug delivery systems are difficult to make owing to their tedious synthesis and choice of appropriate pair of chromophores which can show FRET phenomenon. TPE-tagged polysaccharide vesicles are tested for FRET probe construction. For this purpose, different water soluble and water insoluble fluorophore dyes were loaded in the vesicular assembles by dialysis method. Three different red emissive dyes namely rhodamin-B (RHB), rosebengal (RB) and Nilered (NR) were chosen to load in these vesicles. These three different dyes are diverse in their physical properties like RHB and RB is water soluble and NR is water insoluble. The selection of these dyes (acceptors) were done based on their spectral

overlap with the donor molecule i.e. tetraphenylethene (TPE). A spectrum which shows the overlap of emission spectrum of donor and the absorbance spectrum of acceptor molecules were shown in figure 4.22a. From the spectra it was observed that these pair showed a good to moderate spectral overlap and the fluorescence energy transfer phenomenon would be expected to happen between them. A very important criterion for a FRET phenomenon to happen is to bring these chromophores in close proximity and it was achieved by loading these dyes in the polysaccharide vesicles wherein the donor molecule was covalently conjugated to polymer backbone. For better understanding, a general energy level diagram explaining the energy transfer mechanism and schematics of the vesicles loaded with dye molecules dictating the process of the energy transfer was showed in figure 4.22b. Considering the entire important criterion, these dyes were loaded in these fluorescent vesicles and their size was measured using the dynamic light scattering technique followed by the morphology confirmation by using the atomic force microscopy (AFM) technique. The size of the rosebengal ($V_{TPE\text{-}RB}$) loaded vesicles was found to be 180 ± 20 nm and the vesicular geometry was confirmed by AFM technique (see figure 4.22c). Similarly the sizes for rhodamin b ($V_{TPE\text{-}RHB}$) loaded vesicles and Nilered ($V_{TPE\text{-}NR}$) loaded vesicles were found to be 200 ± 20 and 190 ± 15 nm respectively. Their vesicular nature of morphology was also confirmed using the AFM technique (see figure 4.22 d and e). Photographs of the vials showed in figure 4.22 c to e indicates that these vesicle solutions were very transparent and produced very stable encapsulation for further application. The dye loading contents (DLC) and dye loading efficiencies (DLE) for these three dyes were found to be 1.5 % and 65 % for V_{RB}, 1.8 % and 55 % for V_{RHB} and 1.2 % and 45 % for V_{NR}, respectively. The emission of V_{TPE} and $V_{TPE\text{-}RB}$ was measured at TPE excitation at 330 nm. V_{TPE} showed significant AIE at 460 nm whereas the TPE emission was quenched 90 % in the presence of RB in $V_{TPE\text{-}RB}$. Additionally, the $V_{TPE\text{-}RB}$ showed FRET emission corresponding to the RB at 554 nm followed by the excitation energy transfer from TPE to RB in the vesicular nano-assemblies. Similar fluorescence measurement was done for V_{TPERHB} and V_{TPENR} nanovesicles and the results obtained are showed in figure 4.23b and c. From the figure 4.23 b it was observed that the emission of TPE molecule was quenched by 50% and new emission corresponding to RHB was appeared at 564 nm. V_{TPENR}, there was 30 %

quenching in TPE emission and also new peak appeared at 630 nm corresponding to Nilered emission (see figure 4.23 c).

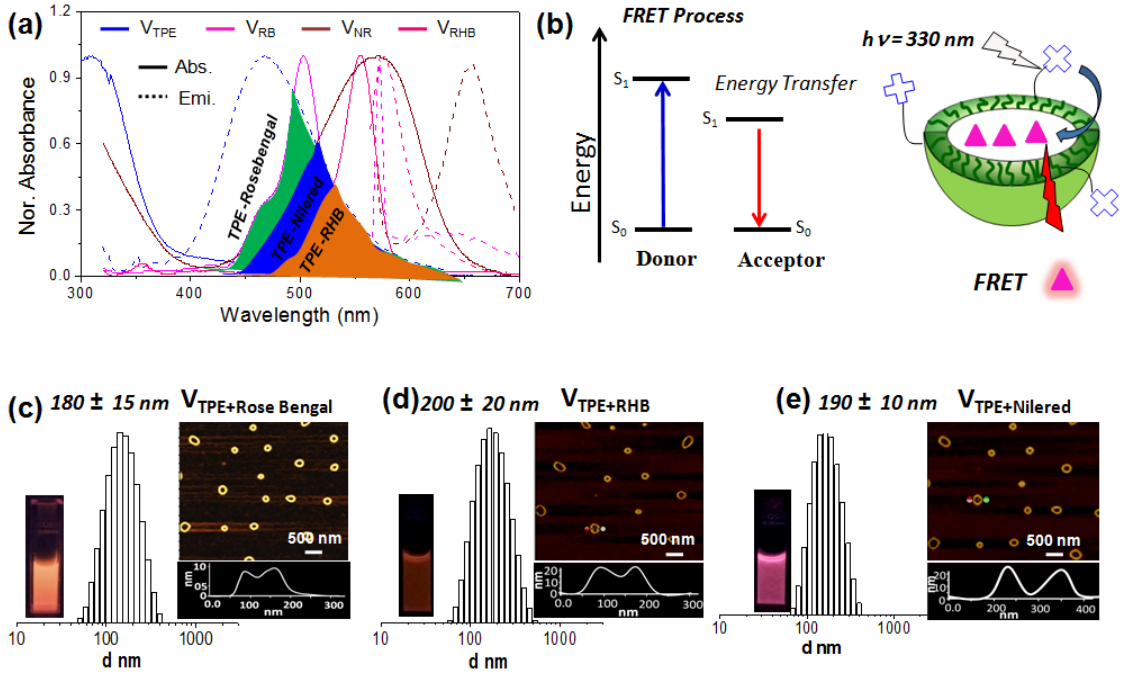

Figure 4.22: *A spectrum showing the spectral overlap of emission of TPE and absorbance of rosebengal, rhodamin B and nilered (a), a general energy level diagram explaining the mechanism of energy transfer from donor to acceptor molecule with schematics of vesicles showing the energy transfer in dye loaded TPE vesicles(b), DLS histogram and AFM morphology for V_{TPERB} vesicles (c), DLS histogram and AFM morphology for V_{TPERHB} vesicles (d) and DLS histogram and AFM morphology for V_{TPENR} vesicle (e). The concentration used for DLS and AFM measurements is 0.1 mg/mL.*

This appearance of new peak was a clear indication of the energy transfer phenomenon. Similarly in case of Further to confirm the effect of these dye molecule on the excited state lifetime of the TPE molecule, a lifetime measurement studies were carried out in PBS pH 7.4 and showed in figure 4.15 d. From the spectrum the lifetime for TPE was observe as 1.12ns but when these vesicles were loaded with rosebengal, then lifetime of TPE molecule was dropdown to 0.32 ns. This effect of other fluorophore on the lifetime of donor molecules proves that there was some energy transfer phenomenon was occurred. Lifetime measurements were also carried out for V_{TPERHB} and V_{TPENR} nanovesicles and it was found that there was decrease in the life time of donor molecule in the presence of acceptor molecule. These lifetimes were showed in figure 4.15 e and f

and lifetime for TPE in the presence of RHB was found to be 0.54 ns and in the presence of Nilered was found to be 0.22 ns. The FRET efficiencies and foster distance were calculated using the formulae given below:

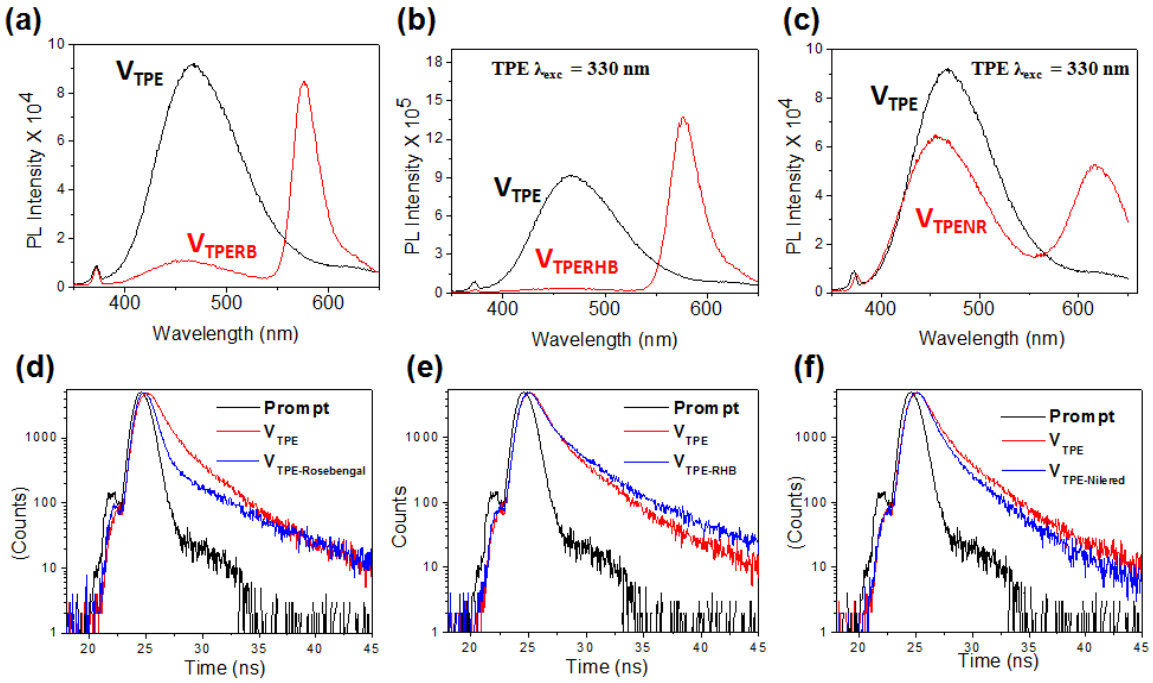

Figure 4.23: *A emission spectrum of V_{TPE} and V_{TPERB} (a), A lifetime measurement plot for V_{TPE} and V_{TPERB} (b) A emission spectrum of V_{TPE} and V_{TPERHB} (c), A lifetime measurement plot for V_{TPE} and V_{TPERHB} (d) A emission spectrum of V_{TPE} and V_{TPENR} (e), A lifetime measurement plot for V_{TPE} and V_{TPENR} (f).*

The energy transfer and FRET distance was calculated using the equation:

$$E_{FRET} = (R_0^6) / [R_0^6 + R^6] \ldots. (1)$$

Where, EFRET = energy transfer, R0 = distance at which energy transfer between donor and acceptor is 50% and is called Forster distance, and R is FRET distance between the given pair of donor and acceptor. R0 can be determined using the following:

$$R_0 = [8.79 \times 10^{-5} (\kappa^2 \eta^{-4} Q_D J(\lambda))]^{1/6} \ldots. (2)$$

where κ2 is the angle between the dipole moments of donor and acceptor, QD is the quantum yield of donor, η is refractive index of the medium and J(λ), the overlap integral form the emission spectrum of donor with t he absorption spectrum of acceptor is given as;

$$J(\lambda) = \int_0^{\infty} F_D(\lambda)\mathcal{E}_A(\lambda)\,\lambda^4\,d\lambda \ldots\ldots (3)$$

where F_D is the corrected fluorescence intensity of donor and $\mathcal{E}A(\lambda)$ is the molar extinction coefficient of the acceptor.

E_{FRET} is determined from the fluorescence life of donor molecule as follows:

$$E = 1-[\tau_{DA}/\tau_D] \ldots. (4)$$

where τ_D is the average fluorescence lifetime of donor in absence of acceptor and τ_{DA} is the average fluorescence lifetime of donor in presence of acceptor.

The overlap integrals and Forster distance (R_0) were computationally determined using the programme written by Hink et al.

Table 4.1 : *A table showing the foster distance (R_0), lifetime of donor (τ_D) , lifetime of donor in the presence of acceptor (τ_{DA}) , FRET efficiencies (E_{FRET}) and actual distance between two fluororphores (R) for V_{TPE}, V_{TPERB}, V_{TPERHB} and V_{TPENR} vesicles respectively.*

System	**J(λ) (M^{-1} cm^{-1} nm^4)**	**R_0 (Å)**	**τ_D (ns)**	**τ_{DA} (ns)**	**E_{FRET}**	**R (Å)**
V_{TPE}	-----	-----	1.12	-----	-----	-----
$V_{TPE\text{-}ROSEBENGAL}$	4.35×10^{14}	15.38	1.12	0.32	0.7142	13.16
$V_{TPE\text{-}RHB}$	5.56×10^{14}	23.52	1.12	0.73	0.5483	22.75
$V_{TPE\text{-}NILERED}$	1.05×10^{15}	26.15	1.12	0.87	0.223	32.30

From the values in the table 4.1 it was seen that the FRET efficiency were found to be best for V_{TPERB} pair (72 %) and also the foster distances (15.38 Å) matches very well with the distance between two chromophores (13.16 Å). Similarly, the foster distance and the distance between two chromophores for V_{TPERHB} and V_{TPENR} were calculated and mentioned in the table 4.1. It has been observed that the FRET efficiencies for V_{TPERHB} and V_{TPENR} are found to be very low as compared to V_{TPERB}. One of the reasons for these low FRET efficiencies can be attributed to the fact that the spectral overlap between these chromophores is very low and deviation from the theoretical foster distances (see table 4.1). One of the important observations to be made in these FRET pairs was that the amount of TPE emission quenching was different in each case and that

is what makes these FRET pairs special on their own. From all the results discussed above it was revealed that these FRET pairs have different FRET efficiencies and can be used for the bioimaging in the cancer cells.

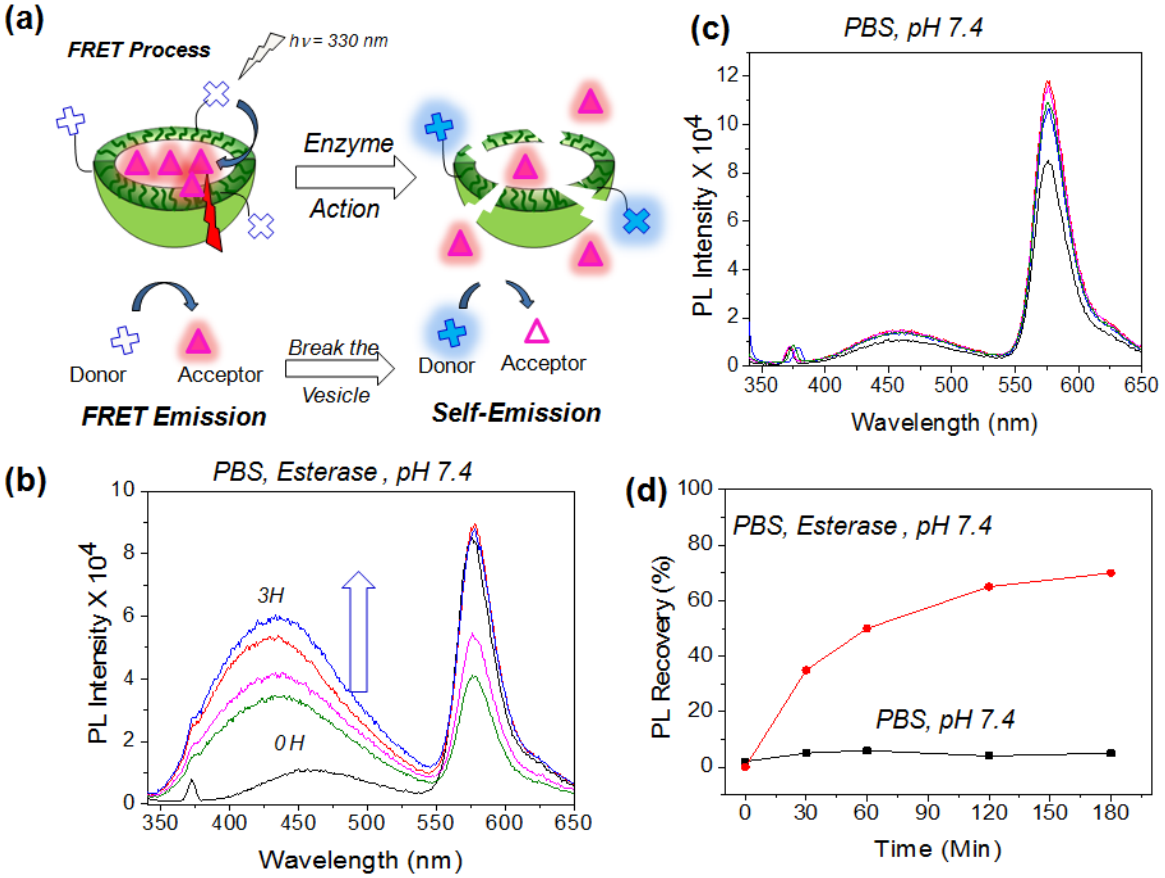

Figure 4.24: *Schematics of the vesicles V_{TPERB} showing the energy transfer and subsequent enzymatic disassembly process (a), a emission plot showing the emission recovery of TPE emission in the presence of esterase enzyme (b), a emission plot showing the stability of V_{TPERB} vesicle in PBS pH 7.4 (c) and a plot of emission recovery vs time for TPE emission recovery from VTPERB vesicles.*

The enzyme responsiveness of one of the dye loaded nanovesicles was studied using horse liver esterase and the schematics showed in figure 4.24a explains the stability and the enzyme responsive behaviour of the dye loaded nanovesicles (V_{TPERB}). Schematic in figure 4.24 depicts the process of energy transfer from TPE and to rosebengal in nanovesicles and their enzymatic disassembly. When distance between these two

chromophores was increased by means of enzymatic disassembly, the percent of FRET FRET emission decreases. To understand this enzymatic disassembly in *invitro* condition, these vesicles were treated with 1U of esterase enzyme and the change in emission intensity was monitored over a period of time (0-180 minutes). The decrease in the emission intensity was observed which was showed in figure 4.16 b. From the plot in figure 4.24 d, it has been observed that the TPE could regain its emission property in three hours as the distance between two chromophores was increased. The stability of these VTPERB vesicles were checked in PBS pH 7.4 and it was found that at physiological conditions these nanovesicles were stable and do not showed any diverse effect on the FRET phenomenon. These regain in the emission property of the TPE in the presence and absence of enzymes was plotted against the time and showed in figure 4.24d. From the plot it was found that esterase enzyme indeed helps in disassembling the nanovesicles as a result, the FRET emission was decreased and the individual emissions were recovered. The similar kind of disassembly was expected to happen in V_{TPERHB} and V_{TPENR} systems as the nanovesicles used for loading these two dyes are same and hence the enzyme responsive experiment was not done for the these two nanovesicles. From all the results discussed above it was revealed that these nanovesicles are enzyme responsive and their FRET emission vanishes upon the enzymatic disassembly.

One of the important challenges for any polymeric fluorescent probe based on FRET mechanism was to see the similar kind of energy transfer in the intracellular condition. To examine this FRET mechanism in the human breast cancer (MCF 7) cells, the cells were treated with V_{TPERB} having 2 µg/mL concentration of the rosebengal and incubated for two different time periods as 15 minutes and 180 minutes. This time points were selected based on the cellular uptake experiment explained earlier in this chapter. After this time point's cells were immediately fixed and imaged using the confocal microscopy. The cellular images are shown in figure 4.25. The first panel in the figure represents the cellular uptake for 15 minutes of incubation time wherein strong red emission was observed when excited at TPE excitation source (340 nm). This red emission coming at TPE excitation source was attributed to the energy transfer phenomenon between TPE and rose bengal. This observation validates the results obtained in *invitro* condition that the energy from TPE molecule was used by the

rosebengal and it was showing the FRET emission. This observation was further supported by the magenta colour of the merged image in first panel of figure 4.25. This magenta colour is colocalization of the blue colour coming from the TPE chromophore and the red emission coming from the rose bengal dye. In this experiment a negligible amount of blue colour has been observed due to the partial excitation of the TPE chromophores in the intracellular compartment.

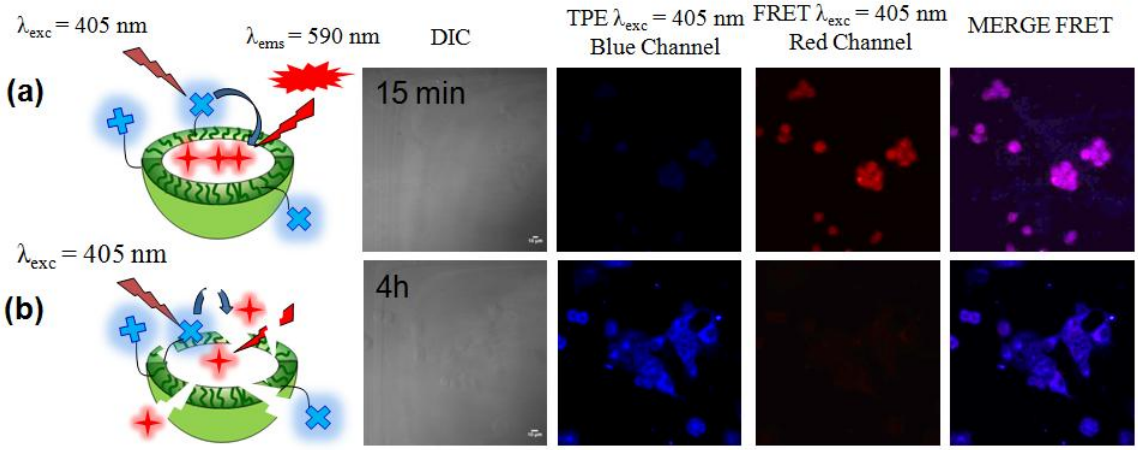

Figure 4.25: *A panel showing the confocal microscopic images for VTPERB vesicles for 15 minutes time point (a) and for 4 hours time point (b). MCF 7 cells were treated with 2µg/mL concentration rosebengal from* V_{TPERB} *vesicles and the excitation and emission windows were selected as shown in the images.*

The second panel in the figure 4.25 showed the cellular uptake at 4 hours of incubation time wherein a strong blue emission was observed when excited using the TPE excitation source (340 nm). At the similar excitation source, a very light red coloured emission was observed from the rose bengal dye suggesting that the these two chromophores are not in contact and FRET emission has vanished. This observation suggests that, at intracellular conditions the enzymes are active and the enzymatic disassembly could happen in three hours of incubation time. The results discussed here were validates all the observations described above and as anticipated, the enzymatic disassembly indeed helping to regain the individual emission properties of the fluorophores. Together all these results proved that the fluorescent polysaccharide vesicles can be a very good candidate for bioimaging in medical field. From the results

discussed above it has been observed that these polysaccharide nanovesicles are so unique in nature that they can act as a theranostics as well as bioimaging probes for anticancer drug delivery application. The encapsulation of the anticancer drug doxorubicin hydrochloride in these polysaccharide vesicles induces the special arrangement of these chromophores for the energy transfer mechanism. This energy transfer was attributed to the spectral overlap of the chromophores but bimolecular collision and formation of "Turn ON" probes makes these polysaccharide vesicles different than the other FRET based fluorescent probes reported in the literature. Further loading of different red colour dyes and occurrence of the FRET phenomenon makes these vesicles useful for bioimaging application. This has been showed for the first time that same polysaccharide vesicles can act as dual visualisation tool depending upon the selection of acceptor chromophore molecules. Since the formed assemblies are vesicular in nature this approach can be extended to the encapsulation of different water soluble or insoluble drug or dye molecules. Thus a unique polysaccharide carrier was designed and developed which could be a very good candidate for the biomedical application.

4.3.5 Cisplatin-Stitched Fluorescent Polysaccharide Prodrug

Functional handle on the polymer backbone provides an opportunity for conjugation of drug or targeting moieties on the polymer backbone. Herein the acid functionalised fluorescent polysaccharide vesicles were made and used for chemical conjugation of the cisplatin drug which can be delivered to the cancer cells. Since cisplatin is non fluorescent drug, the newly designed polysaccharide vesicles are decorated with a fluorophore moiety which makes the tracking of the cisplatin drug possible which otherwise was very difficult task.To achieve this goal, functional fluorescent polysaccharide vesicles were synthesised by coupling PDP acid, TPE acid and tertiary butyl ester of succinic acid to the dextran backbone in one pot reaction using the DCC/DMAP coupling via aliphatic ester linkages as described in chapter 2. The synthetic scheme is showed in scheme 4.2 The degree of substitution for PDP acid and TPE acid on the dextran backbone were calculated as discussed in the first portion of the chapter and were kept constant as 5% and 2% respectively. The NMR spectrum for

tertiary butyl ester of succinic acid was showed in figure 4.26 a and respective protons are assigned alphabetically in the spectrum. The NMR spectrum for newly designed dextran derivative was showed in figure 4.26 b. The degree of substitution for acid group was calculated as described in chapter 2 and kept constant as 20 %.

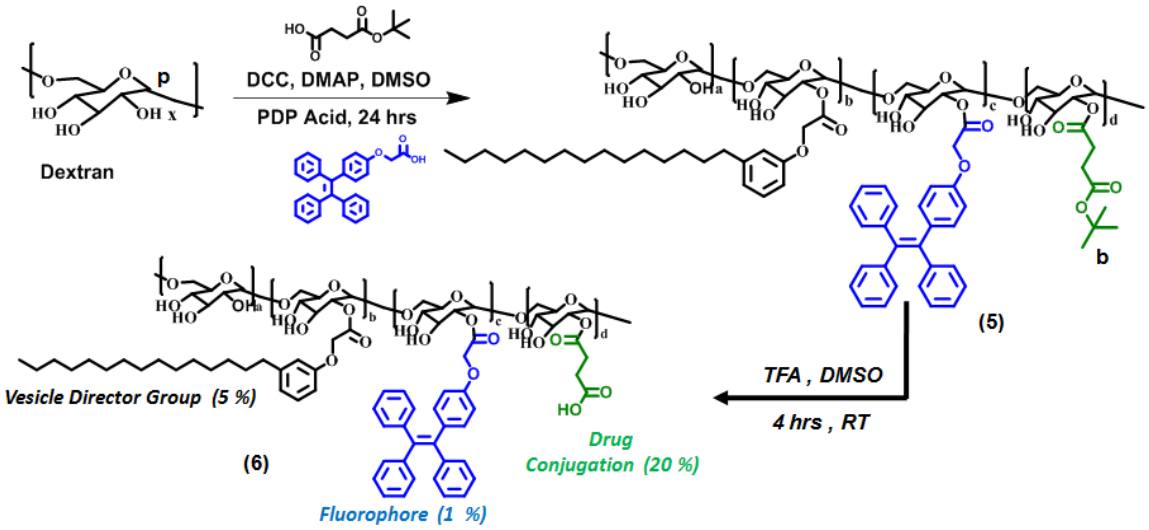

Scheme 4.2: *A chemical route for the synthesis of acid functionalized polysaccharide derivatives.*

The tertiary butyl group of these newly designed dextran derivatives were deprotected using the trifluoroacetic acid and deprotection was confirmed by disappearance of the tertiary butyl proton from the spectrum. These yielded a fluorescent acid functionalised dextran derivative was purified by a dialysis procedure and used for further application.

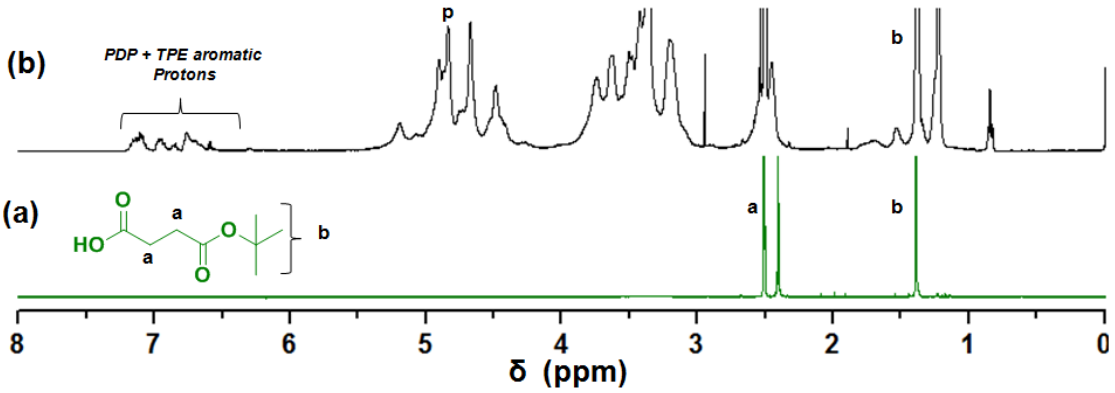

Figure 4.26: *^{1}H NMR spectrum for tertiary butyl ester of succinic acid (a), newly substituted dextran derivatives (b).*

To conjugate the cisplatin drug on polysaccharide backbone, cisplatin aqua complex was made by treating cisplatin with silver nitrate in water for 24 hours in dark. This aqua complex was then treated with acid functionalized polysaccharide derivatives in basic condition. The reaction for aqua complex formation and stitching of cisplatin to the polymer backbone was shown schematically in figure 4.27 a. The aqueous behaviour of these cisplatin stitched polysaccharide derivatives were studied by a dialysis method and the size of the nanoobjects were measured by dynamic light scattering (DLS) technique which showed a monomodal distribution of size around 224 ± 15 nm. The photograph of the vial showed in figure a represents a blue colored transparent aqueous solution of cisplatin stitched vesicles. Further the morphology of these nanoobjects was studied using AFM and FESEM techniques and showed in figure 4.27b, which confirmed the formation of vesicular self assembly from these derivatives. The sizes of the vesicles from AFM and FESEM were found to be 200 ± 20 nm and 210 ± 20 nm which are matching with sizes obtained from the DLS measurement. These polysaccharide vesicles are so unique in nature that even after cisplatin stitching they retain their vesicular morphology features like their non cisplatin stitched counterparts discussed in the first portion of the chapter. This observation proves that even after cisplatin stitched vesicles still holds the ability of loading and delivering the water soluble / insoluble drug/ dye molecules and can be used for theranostics application.

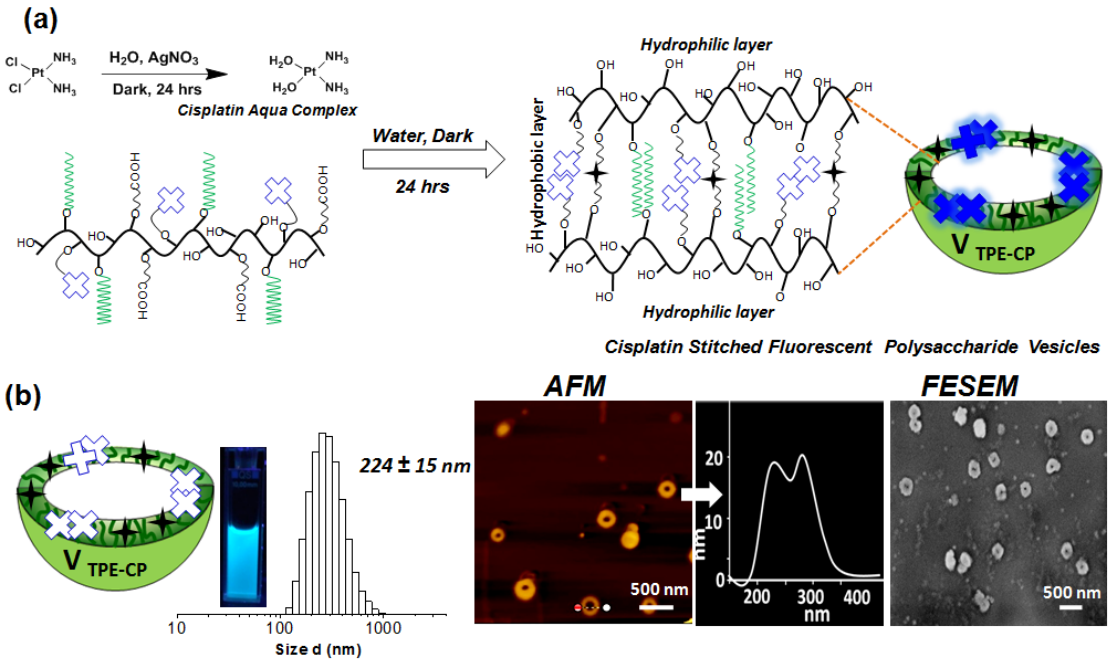

Figure 4.27: *Schematics showing the cisplatin conjugation to acid functionalised fluorescent dextran derivatives (a), schematics of cisplatin stitched vesicles, DLS histogram, AFM and FESEM image for* $V_{TPECP.}$

The cisplatin stitching onto the polymer backbone was confirmed by two different techniques as FT-IR and orthophenylenediamine (OPD) colorimetric assay. Firstly, in the FT-IR spectrum (showed in figure 4.28) of acid functionalized polysaccharide derivatives, where dextran has carboxyl functional group as well as ester functional group showed a distinct peak at 1740 cm^{-1} corresponding to ester –C=O peak. Upon cisplatin complexation these derivatives displayed a discrete stretching band at 1650 cm^{-1} with respect to Pt-O-C=O stretching frequency of carboxylic acid functional group. Additionally, a distinct peak at around 480 cm^{-1} corresponding to the Pt–O (metal alkoxide) bond stretching was clearly appeared in the cisplatin stitched derivatives.This results from FT-IR technique proved that cisplatin conjugation has been successfully done. To calculate the drug loading content (DLC), OPD assay has been done wherein the cisplatin stitched derivatives were treated orthophenylenediamine solution in dimethylformamide and allowed the reaction to happen at 80^0C for two hours. Upon the OPD complexation with cisplatin, it formed OPD-cisplatin adduct which was confirmed by a strong absorption peak at 706nm. Using the lambert-beers law the amount of cisplatin stitched on the polymer backbone was calculated and the drug loading content

was found to be 9.5 %. The detailed procedure and formulas used for calculation are given in experimental section of the chapter. This cisplatin stitched polysaccharide vesicles are refereed as V_{TPECP} in all further discussions.

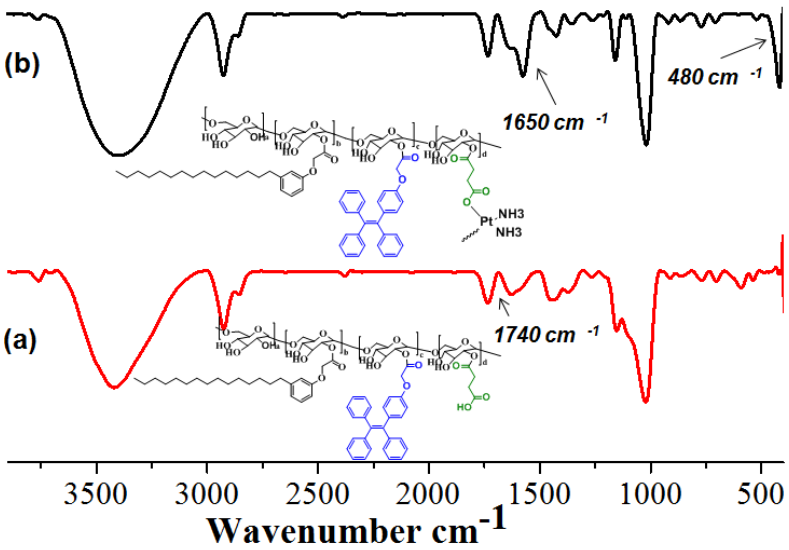

Figure 4.29: *FT-IR spectrum for acid functionalised dextran vesicles V_{TPE} (a) and for cisplatin stitched dextran vesicles V_{TPECP} (b).*

Since cisplatin stitching to the polymer backbone was done via the ester bonds, it was important to study the effect of the enzyme activity on these vesicles. Hence enzyme-responsive release of the cisplatin from these vesicles were investigated in pH = 7.4 at 37 °C. The schematics showed in the figure 4.30 a explains the enzymatic cleavage of the nanovesicles and release of the cisplatin drug. The *in vitro* kinetics were performed both in the presence of 10 U of esterase enzyme and in the absence of enzyme and their release profiles are shown in figure 4.30 b. The amount of the cisplatin released was monitored by OPD colorimetric assay and the details are given in the experimental section. In from figure 4.30b, it was observed that these cisplatin stitched vesicles showed a good stability with only 20 % of drug leaching. These drug leaching was attributed to the effect of different anions present in the phosphate buffer saline which could be releasing the drug. When these vesicles were treated with 10U of esterase enzyme, the enzyme triggered the release of the drug and almost 90 % of the drug release was observed in 48 hours. These experiment proved that the release of the cisplatin drug can

be triggered using the esterase enzyme and the same effect was expected to happen in the intracellular medium. Hence these using these fluorescent polysaccharide vesicles cisplatin can not only be delivered to the intracellular medium but tracking of the drug could also be possible.

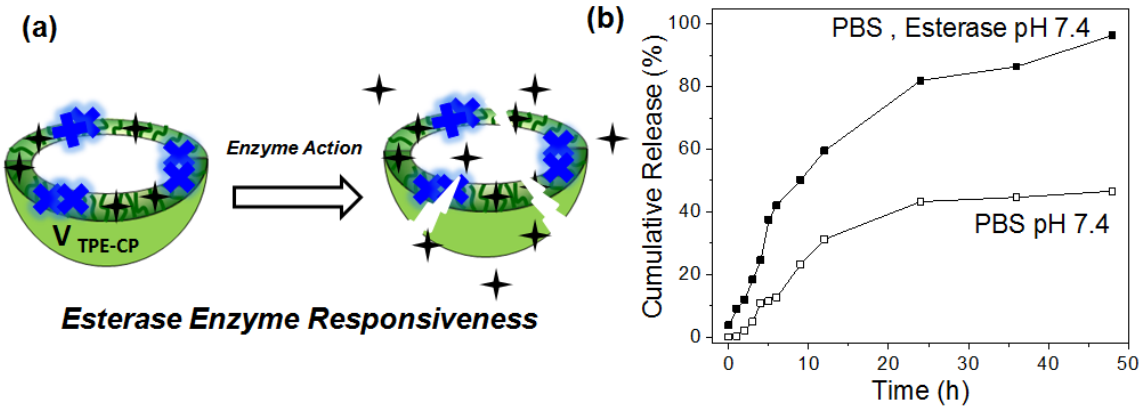

Figure 4.30: *Schematics of the cisplatin stitched vesicles and their enzymatic degradation (a) and plot of cumulative cisplatin release profile from V_{TPECP} in PBS pH 7.4 and in presence of esterase enzyme.(b)*

To evaluate the cytotoxic effect of the polysaccharide vesicles alone and cisplatin stitched vesicles (V_{TPECP}) on the human breast cancer MCF 7 cells, initially the cells were treated with polysaccharide vesicles alone with concentration ranging from 1 to 300 µg/mL and incubated for 72 hours and effect was studied using standard MTTT assay. The results are showed in figure 4.31a, and from the bar plot it was seen that these polysaccharide vesicles were not toxic to the cells upto the concentration of 300 µg/mL and hence proving the biocompatibility of the present design. Further to study the effect of the cisplatin stitched vesicles on the growth of MCF 7 cells, cells were treated with the cisplatin stitched vesicles and free cisplatin drug and incubated for 72 h and the results are showed in figure 4.31b . From the bar diagram in the figure 17b,it was observed that free cisplatin drug able to achieve only 60 % cell killing and the 40 % population was still alive even after 72 hours of incubation. This observation was attributed to the fact that when free cisplatin enters inside the cell, intracellular thiols attacks the cisplatin drug and the drug would be no longer active. The control experiment showing the detoxification of cisplatin by glutathione was done and discussed in chapter 2 and the same explanation holds true in the present case as well. On the other hand, the cisplatin

stitched polysaccharide vesicles could achieve almost 95 % of cell killing proving the fact that these vesicles are acting as shields against the detoxification of cisplatin from the intracellular thiols. Hence these polysaccharide vesicles are the best candidates to deliver the cisplatin drug in the breast cancer cells. Since the current design was decorated with fluorophore it provides an opportunity to track the drug release and to understand the fate of polymer drug carrier inside the cell. Hence the cellular uptake studies were carried out in the MCF 7 cells and the images are showed in figure 4.32. To understand the lysosomal degradation of these vesicles, lysosomes were stained using lyso tracker green and the images are showed in figure 4.32. The blue colour observed in the blue channel was the colour coming from the fluorescent nanovesicles and the green colour seen in the third image was colour coming from the lysosomes of the cells. Light yellow colour observed in merged images was the outcome of the overlap of these two channels (blue and green) which clearly indicates that these nanovesicles go through the lysosomes. Since these polysaccharide vesicles are designed with aliphatic ester linkages, these linkages are prone to cleave in the enzyme rich lysosomal compartment of the cells and the results obtained from the above experiment proves the lysosomal degradation of these vesicles. This lysosomal degradation of the vesicles helps in the cisplatin release which can be delivered to the nucleus. Hence these polysaccharide dextran vesicles were so unique for understanding drug release and intracellular tracking of cisplatin in breast cancer cells. These vesicles can be used for many other cancer cell lines as well but herein this chapter the studies were carried out only in breast cancer MCF 7 cells.

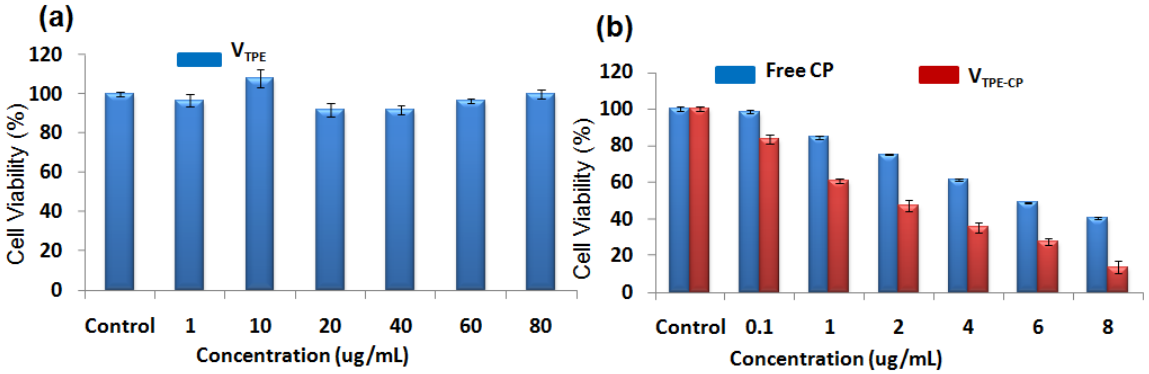

Figure 4.31: *A plot showing the cytotoxicity profile of acid functionalised fluorescent dextran vesicles to MCF 7 cells (a), a plot showing the cytotoxic effect of cisplatin stitched dextran vesicles* V_{TPECP} *and free cisplatin to human breast cancer MCF 7 cells (b).*

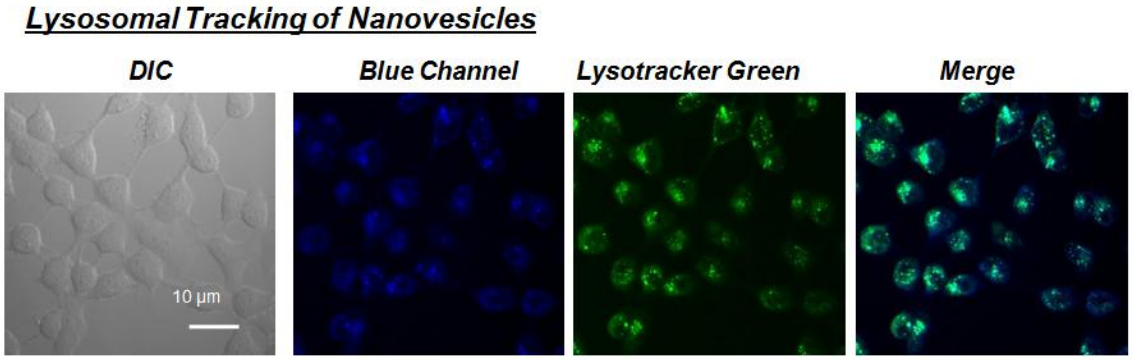

Figure 4.32: *A panel showing the live cell confocal microscopy images of V_{TPECP} in MCF7 cells. The cells were treated with 4 µg/mL concentration of VTPECP nanovesicles and incubated for 4 hours. The lysosomes are stained using Lysotracker green DND 26.*

Further these cisplatin stitched fluorescent vesicles were used for encapsulation of doxorubicin hydrochloride and the schematics showed in figure 4.33a explains the effective encapsulation of the drug molecules in these vesicles. The DOX loading to these cisplatin stitched fluorescent vesicles leads to energy transfer followed by bimolecular collision and quenching as discussed earlier in these chapter. This quenching process was not affected by the cisplatin stitching and these vesicles could able to take these two antagonistic drugs together in single nanocarrier vesicles. Moreover this vesicle provides the advantage of real time tracking and delivery of a non fluorescent cisplatin drug to the cancer cells. Doxorubicin loading to these cisplatin stitched vesicles produces a "Turn OFF" state nanocarriers which upon the enzymatic degradation or disassembly produces (see figure 4.33 a) a triple action polysaccharide vesicles for anticancer drug delivery application. The emission intensity of the V_{TPECP} and $V_{TPECPDOX}$ were measure and showed in figure 4.33 b. From the plot it was observed that the V_{TPECP} vesicles were nicely fluorescent in nature whereas the emission of TPE was completely quenched after DOX encapsulation. To assess the enzyme action on these vesicles, they were treated with 1U of horse liver esterase enzyme and the emission intensity was monitored over a period of time. From the plot given in figure 4.33 c it was clear that the TPE emission intensity was recovered from $V_{TPECPDOX}$ after the enzymatic disassembly.

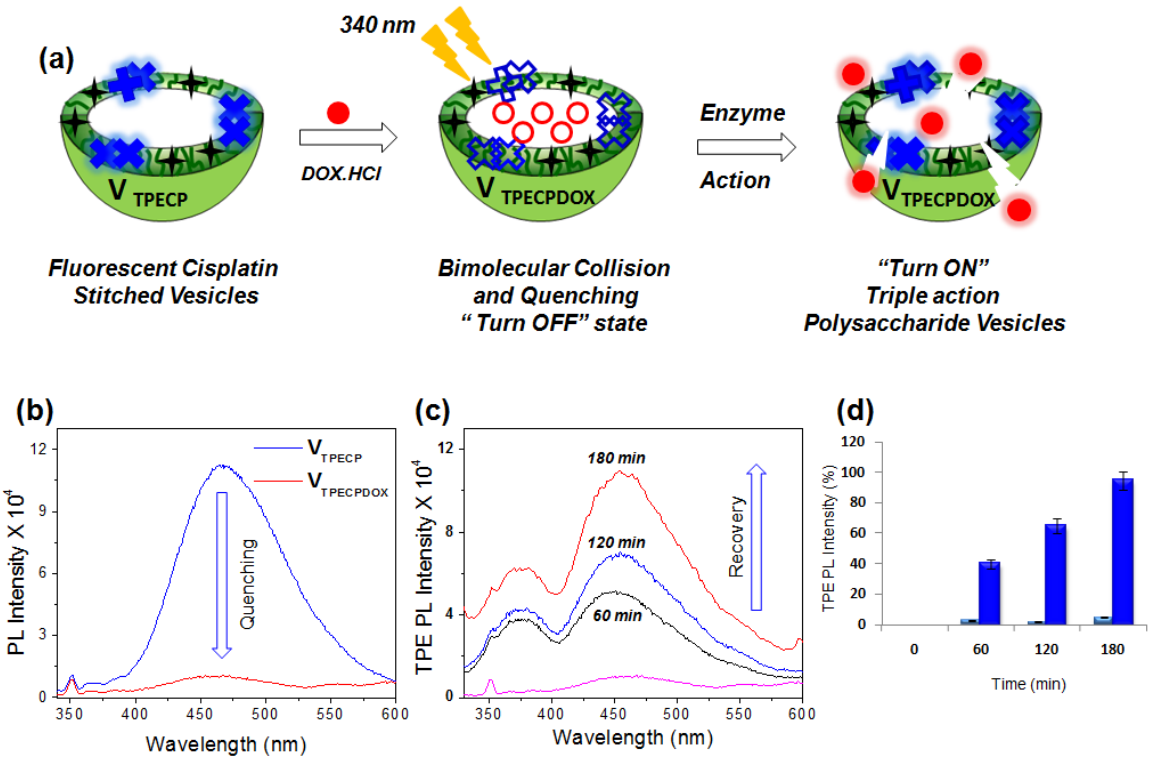

Figure 4.33: *A schematics explaining the DOX encapsulation to the cisplatin stitched polysaccharide vesicles and their intracellular enzyme degradation(a), A plot showing the emission intensity of V_{TPECP} and $V_{TPECPDOX}$ (b), A plot showing the emission intensity of $V_{TPECPDOX}$ recovered after the enzyme action (c) and a TPE emission intensity plot versus time (d)*

This TPE intensity was plotted against the time and showed in figure 4.33d, wherein it is seen that in three hours the TPE emission property was regained. From all these experiments it was confirmed that these polysaccharide are triple action in nature and can be used for i) for real time tracking and delivery of a nonfluorescent cisplatin drug, ii) for delivery of two antagonistic drugs together from single vesicles and iii) due to unique "Turn OFF" to "Turn ON" property can be a very good candidate in biomedical application. This type of triple action polymer nanocarriers were first time designed and developed for the delivery of anticancer drugs to the cancer cells. This approach can further be extended to the encapsulation of other pharmaceutically important molecules as well. Thus polysaccharide nanovesicles were developed for the first time for real time monitoring and delivery of cisplatin drug.

4.4 Conclusion

In conclusion, fluorescent polysaccharide vesicles were made as theranostics probe for doxorubicin delivery to breast cancer cells. Polysaccharide derivatives were constructed by substituting a pentadecyl phenol and AIE probe TPE on polymer backbone. There aqueous self assembly was studied and the formation of 200 ± 20 nm size vesicular architectures was confirmed by dynamic light scattering and various spectroscopic techniques such atomic force microscopy field emission electron scanning microscope etc respectively. Doxorubicin, an anticancer drug was encapsulated in these vesicles and their photo physical study proved fluorescence quenching of the both the fluorophore. The enzymatic disassembly of these vesicles was carried out in phosphate buffer saline and a fluorescence turn phenomenon was observed demonstrating its turn on behaviour upon the enzyme treatment. Intracellular DOX release and turn property was studied in breast cancer cells. Further different red coloured dyes were encapsulated in these vesicles and a efficient fluorescence resonance transfer phenomenon (FRET) was studied. TCSPC measurements were carried out and proved the existance of these chromophores in within a foster distance. Intracellular FRET mechanism and bioimaging was successfully demonstrated in MCF 7 cells and proof of concept for intracellular FRET based bio probes was established. Furthermore, acid functionalized blue luminescent vesicles were produced for cisplatin conjugation and their utility for real time monitoring of cisplatin drug release was showed in breast cancer cells. These cisplatin stiched vesicles were further used for doxorubicin encapsulation and triple action polysaccharide vesicles were made for real time monitoring of cisplatin delivery.

References

1. Lv, F.; Qiu, T.; Liu, L.; Ying, J.; Wang, S. *Small*, **2016**, 12, 696-705.
2. Duan, X.; Liu, L.; Feng, F.; Wang, S. *Acc. Chem. Res.* **2010**, *43*, 260-270.
3. Li, K.; Liu, B. *Polym. Chem.* **2010**, *1*, 252-259.
4. Liang, J.; Tang, B. Z.; Liu, B.; *Chem. Soc. Rev.* **2015**¸*44*, 2798-2811.
5. Chen, H.; Kim, S.; Wang,S.; Park, K.; Cheng, J-X. *PNAS***, 2008**, *105*, 6596-6601.
6. Cho, H.; Cho, C. S.; Indig, G. L.; Lavansanifar, A.; Vakili, M. R.; Kwon, G. S. *PLOS one***, 2014,** *9*,89968-89975.
7. Miura, Y.; Tsuji, A.B.; Sugyo, A.; Sudo, H.; Aoki, I.; Inubushi, M.; Yashiro, M.; Hirakawa, K.; Cabral, H.; Nishiyama, N.; Saga, T.; Kataoka, K. *ACS Biomater. Sci. Eng.* **2015**,*1*, 1067-1076.
8. Sun, X.; Wang, G.; Zhang, H.; Hu, S.; Liu, X.; Tang, J.; Shen, Y.; *ACS Nano***, 2018**, *12*, 6179-6192.
9. Dong, R.; Zhu, B.; Zhou, Y.; Yan, D.; Zhu, X. *Angew. Chem. Int. Ed.* **2012,** *51*, 11633-11637.
10. Zhu, A.; Miao, K.; Deng, Y.; Ke, H.; He, H.; Yang, T.; Guo, M.; Li, Y.; Guo, Z.; Wang, Y.; Yang, X.; Zhao, Y.; Chen, H. *ACS Nano***, 2015**, *9*, 7874-7885.
11. Chen, H, Jia, H.; Tham, H. P.; Qu, Q.; Xing, P.; Zhao, J.; Phua, S. Z. F.; Chen, G.; Zhao, Y. *ACS Appl. Mater. Interfaces.* **2017**, *9*, 23536-23543.
12. Gangadaran, P.; Li, X. J.; Kalimuthu, S.K.; Min, O. J.; Hong, C. M.; Rajendran, R. L.; Lee, H. W.; Zhu, L.; Baek, S. H.; Jeong, S. Y.; Lee, S-W.; Lee, J.; Ahn, B. C. Nat. Scietific Rep. 2018, 8, 13509 .
13. Chen, Y.; Han, H.; Tong, H.; Chen, T.; Wang, H.; Ji, J.; Jin, Q. *ACS Appl. Mater. Interfaces.* **2016**, *8*, 21185-21192.
14. Ma, H.; Qi, C.; Cheng, C.; Yang, Z.; Cao, H.; Yang, Z.; Tong, J.; Yao, X.; Lei, Z. *ACS Appl. Mater. Interfaces.* **2016**, *8*, 8341-8348.
15. Lv, Y.; Liu, M.; Zhnag, Y.; Wang, X.; Zhang, F.; Li, P.; Bao,W.; Wang, J.; Zhnag, Y.; Wei, W.; Ma, G.; Zhao, B.; Tian, Z. *ACS Nano***, 2018**, *12*, 1350-1358.
16. Zhu, M.; Zhang, J.; Zhou, Y.; Xing, P.; Gong, L.; Su, C.; Qi, D.; Du, H.; Bian, Y.; Jiang, J. *Inorg. Chem.*, **2018**, *57*, 11537-11542.

17. Cepraga, C.; Marotte, S.; Daoud, E. B.; Favier, A.; Lanoe, P. H.; Monnereau, C.; Baldeck, P.; Andraud, C.; Marvel, J.; Charreyre, M. T.; Leverrier, Y. *Biomacromolecules* **2017**, *18,* 4022-4033.
18. Yong, K. T.; Qian, J.; Roy, I.; Lee, H. H.; Bergey, E. J.; Pramposch, K. M.; He, S.; Swihart, M. P.; Maitra, A.; Prasad, P.N. *Nano Lett.* **2007,** *7,* 761-765.
19. Gershanov, S.; Michowiz, S.; Toledano, H.; Yahav, G.; Barinfeld, O.; Hirshberg, A.; Ben-Zvi, H.; Mircus, G.; Salmon-Divon, M.; Fixler, D.; Goldenberg-Cohen, N. *Nat. Sci. Rep.* **2017**, *7,*3648-3655.
20. Peng, X.; Yang, Z.; Wang, J.; Fan, J.; He, Y.; Song, F.; Wang, B.Sun, S.; Qu, J.; Qi, J.; Yan, M. *J. Am. Chem. Soc.* **2011**, *133,* 6626-6635.
21. Jin, F.; Xu, D-L.; Zhu, H-Z.; Yan, Y.; Zheng, J.; Zhang, J.; Zhou, H-P.; Wu, J-Y.; Tian, Y-P. *Dyes and Pigments* **2014**, *14*,
22. Bouchaala, R.; Mercier, L.; Andreiuk, B.; Mely, Y.; Vandamme, T.; Anton, N.; Goetz, J. G.; Klymchenko, A. S. *J. Control. Release.* **2016**, *236,* 37-67.
23. Saxena, S.; Jayakannan, M. *Biomacromolecules,* **2017**, *18,* 2594-2609.
24. Li, X.; Mu, J.; Liu, F.; Tan, E. W.P.; Khezri, B.; Webster, R. D.; Yeow, E. K.L.; Xing, B. *Bioconjugate Chem.* **2015,** *26,* 955-961.
25. Chen, J.; Zhong, W.; Tang, Y.; Wu, Z.; Li, Y.; Yi, P.; Jiang, J. M*acromolecules*, **2015**, *48,* 3500-3508.
26. Kikuchi, K. *Chem. Soc. Rev.* **2010**, *39,* 2048-2053.
27. Yuan, L.; Lein, W.; Zheng, K.; Zhu, A. S. *Acc. Chem. Res.* **2013**, *46,* 1462-1473.
28. Qin, L.; He, X.; Chen, L.; Zhang, Y. *ACS Appl. Mater. Interfaces.* **2015**, *7,* 5965-5971.
29. Yang, J.; Chen, H.; Vlahov, I. R.; Cheng, J-X.; Low, P. S. *PNAS* **2006**, *103*, 13872-13877.
30. Maity, H.; Reddy, G. *J. Am. Chem. Soc.* **2016**, *32,* 2609-2616.
31. Miyake-Stoner, S. J.; Miller, A. N.; Hammill, J. T.; Peeler, J. C.; Hess, K. R.; Mehl, R. A.; Brewer, S. H. *Biochemistry* **2009**, *48,* 5953-5962.
32. Lin, W.; Du, Y.; Zhu, Y.; Chen, X. *J. Am. Chem. Soc.* **2014**, *136,* 679-687.
33. He, F.; Tang, Y.; Yu, M.; Feng, F.; An, L.; Sun, H.; Wang, S.; Li, Y.; Zhu, D.; Bazan, G. C. *J. Am. Chem. Soc.* **2006**, *128,* 6764-6765.

34. van Dongen, E. M. W. M.; Dekkers, L. M.; Spijker, K.; Meizer, E. W.; Klomp, L. W. J.; Merkx, M. *J. Am. Chem. Soc.* **2006**, *128*, 10754-10762.
35. Zhou, R.; Xu, C.; Dong, J.; Wang, G. *Biosens. Bioelectron*, **2015**, *65*, 103-107.
36. Hong, Y.; Lam, J. W. Y.; Tang, B. Z. *Chem. Soc. Rev.* **2011**, *40*, 5361-5388.
37. Hong, Y.; Lam, J. W. Y.; Tang, B. Z. *Chem. Commun.* **2009**,4332-4353.
38. Yuan, Y.; Liu, B.; *Chem. Sci*. **2017**, *8*, 2537-2546.
39. La, D. D.; Bhosale, S. V.; Jones, L. A.; Bhosale, S. V. *ACS Appl. Mater. Interfaces*, **2018**, *10*, 12189-12216.
40. Shin, W. S.; Li, M-G.; Verwilst, P.; Li, J. H.; Chi, S-G.; Kim, J. S.; *Chem. Sci.* **2016**, *7*, 6050-6059.
41. Yuan, Y.; Kwok, R. T. K.; Feng, G.; Liang, J.; Geng, J.; Tang, B. H.; Liu, B. *Chem. Commun.* **2014**, *50*, 295-297.
42. Hu, J.; Zhuang, W.; Ma, B.; Su, X.; Yu, T.; Li, G.; Hu, Y.; Wang, Y. *Bioconjugate Chem.* **2018,** *29*, 1897-1910.
43. Zhang, Z.; Bilalis, P.; Zhang, H.; Gnanou, Y.; Hadjichristidis, N. *Macromolecules*, **2017**, *50*, 4217-4226.
44. Wang, Z.; Yong, T-Y, Wan, J.; Li, Z-H.; Zhao, H.; Zhao, Y.; Gan, L.; Yang, X-L.; Xu, H-B.; Zhang, C. *ACS Appl. Mater. Interfaces*, **2015**, *7*, 3423-3425.
45. Wwwwww
46. Wang, X.; Yang, Y.; Zhuang, Y.; Gao, P.; Yang, F.; Shen, H.; Guo, H.; Wu, D. *Biomacromolecules*, **2017**, *50*, 4217-4226.
47. Wang, H.; Liu, G.; Gao, H.; Wang, Y. *Polym. Chem.* **2015**, *6*, 4715-4718.
48. Wang, Z.; Chen, S.; Lam, J. W. Y.; Qin, W.; Kwok, R. T. K.; Xie, N.; Hu, Q.; Tang, B. H. *J. Am. Chem. Soc.* **2013**, *135*, 8238-8245.
49. Jiang, B-P.; Tan, X.; Shen, X-C.; Lei, W-Q.; Liang, W-Q.; Ji, S-C.; Liang, H. *ACS Macro Lett***, 2016**, *5*, 450-454.
50. Pramod, P. S.; Takamura, K.; Chaphekar, S.; Balasubramanian, N.; Jayakannan, M. *Biomacromolecules* **2012**, *13*, 3627−3640.
51. Pramod, P. S.; Shah R.; Jayakannan, M. *Nanoscale*, **2015**, *7*, 6636-6652.

Chapter-5

Polysaccharide Nanovesicles for Delivery of Aurora Kinase A Inhibitor to Breast Cancer Cells.

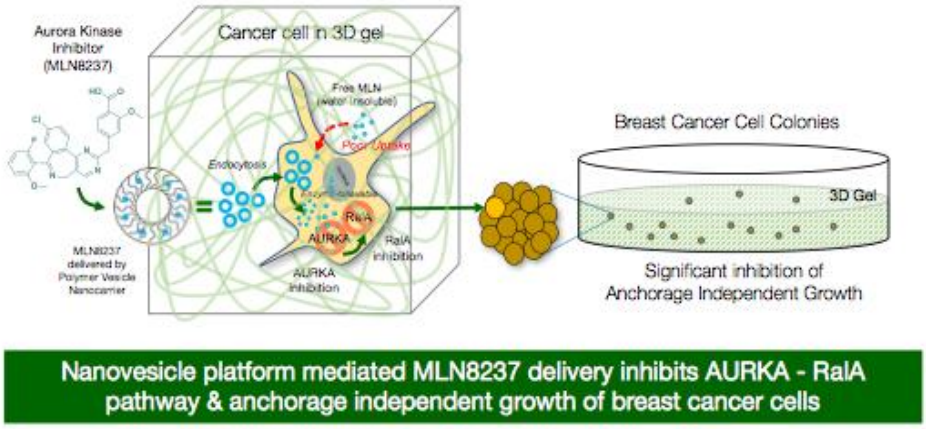

Nanovesicle platform mediated MLN8237 delivery inhibits AURKA - RalA pathway & anchorage independent growth of breast cancer cells

Abstract

The small GTPase RalA is a known mediator of anchorage-independent growth in cancers and differentially regulated by adhesion and Aurora Kinase A (AURKA). Inhibiting AURKA hence offers a means of specifically targeting RalA (over RalB) in cancer cells. MLN8237 (alisertib) is a known inhibitor of Aurora Kinases, its specificity for AURKA, however, is compromised by its poor solubility and transport across the cell membrane. A Polymer nanovesicle platform is used for the first time to deliver and differentially inhibit Aurora kinase A (AURKA) in cancer cells.For this purpose, polysaccharide nanovesicles made from amphiphilic dextran were used as nanocarriers to successfully administer MLN8237 (V_{MLN}) in cancer cells in 2D and 3D microenvironments. These nanovesicles (<200nm) carry the drug in their intermembrane space with up to 85% of it released by the action of esterase enzyme(s). Lysotracker experiments reveal the polymer nanovesicles localize in the lysosomal compartmentof the cell, where they are enzymatically targeted and MLN released in a controlled manner.Rhodamine-B fluorophore trapped in the nanovesicleshydrophilic core ($V_{MLN+RhB}$) allows us to visualize its uptake and localization in cells in a 2D and 3D microenvironment. In breast cancer, MCF-7 cells V_{MLN} inhibits AURKA significantly better than the free drug at low concentrations (0.02 to 0.04μM). This ensures that the drug in V_{MLN}at these concentrations can specifically inhibitup to 94% of endogenous AURKA without affecting AURKB. This targeting of AURKA causes the downstream differential inhibition of active RalA (but not RalB). Free MLN8237 at similar concentrations and conditions failed to affect RalA activation. V_{MLN} mediated inhibition of RalA, in turn, disrupts the anchorage-independent growth of MCF-7 cells supporting a role for the AURKA-RalA crosstalk in mediating the same. These studies not only identify the polysaccharide nanovesicle to be an improved way to efficiently deliver low concentrations of MLN8237 to inhibit AURKA but in doing so also help reveal a role for AURKA and its crosstalk with RalA in anchorage-independent growth of MCF-7 cells.

5.1 INTRODUCTION

Ras-like small GTPases RalA and RalB, as the name implies were first identified based on their sequence similarity to the HRas, KRas and NRas proteins. Human RalA and RalB although being 82% identical[1] are reported to play significant and divergent roles in normal and cancer phenotypes[2]. These isoforms diverge significantly in their C-terminal domain (50% identical) facilitating their differential post-translational modifications that further contribute to their distinct sub-cellular localization and function[3].RalB is critical for the survival of tumor cells and RalA is necessary for the anchorage-independent growth of cancer cells[4,5]. Anchorage-independent signaling and growth of cancer cells is a vital contributor to their tumor phenotype, regulating tumor cell invasion and metastasis[6]. Inhibiting RalA is hence an attractive method to target the tumorigenic potential of cancer cells. Small GTPases are inherently difficult to create effective drug candidates against[1].Ral isoforms with 82 % sequence identity are likely difficult to distinguished by an inhibitor[1]. A recently developed inhibitor forRal was also limited by its lack of specificity[7]. Being able to target an upstream regulator of RalGTPases that can differentially regulate their activation and function could not only allow to specifically target RalA vs RalB but could also become a tool to evaluate their differential involvement in cellular functions. Aurora Kinase A (AURKA) is one such regulator that can differentially phosphorylate and regulate RalA activity in cells[8]. AURKA phosphorylates RalA at Serine194 (a site missing in RalB) during mitosis and causes it's re-localization to the mitochondrial membrane where RalA through RalBP1 regulates mitochondrial fission[9]. AURKA belongs to the family of serine/threonine kinases that play crucial roles in mitotic entry and exit during cell division. Aurora Kinase A (AURKA) and Aurora Kinase B (AURKB) are structurally comparable[10], show 72% identity in their kinase domains and carry similar protein substrate preferences *in vitro.*[11, 12] *In vivo*, their unique substrate specificities and functions arise from their distinct cellular localization and discrete interactions with binding partners.[13-15]AURKA plays an important role in centrosome maturation, spindle assembly, meiotic maturation, and metaphase I spindle orientation.[14]AURKB is part of the chromosomal passenger complex (CPC)[16] and is critical for chromosome condensation, chromosome orientation on the mitotic spindle, and the spindle-assembly checkpoint (SAC) at the final stages of

cytokinesis. AURKA and AURKB activation are both regulated by their phosphorylation on the Threonine 288 (Thr288) and Threonine 232 (Thr232) residue respectively, in the activation loop.[17]

Aurora Kinases are also overexpressed and/or activated in a wide range of human cancers.[18, 19] AURKA is found to be overexpressed in primary breast tumors, colorectal cancers, and other cancer cell lines, including breast, ovarian, colon, prostate, neuroblastoma and cervical cell lines.[20-22]This has also been reported to be associated with a higher tumor grade and poor prognosis in hepatocellular carcinoma.[20] Preclinical studies have also demonstrated the oncogenic potential of AURKA activation as it promotes *in vitro* and *in vivo* transformation of rodent fibroblast cells, supporting the formation of multipolar mitotic spindles inducing genome instability.[23]Overexpression of Aurora kinase A in cancer cells also enhances oncogenic Ras-mediated transformation.[24]Ral GTPases are a major downstream effector of oncogenic Ras and vital to Ras-mediated transformation in breast, pancreatic, colon and other cancers.[25, 26]Downstream of Ras, RalA, and RalB can differentially regulate anchorage-independent growth and cell survival.[5, 27]Adhesion, we had discovered activates only RalA further supporting its role in anchorage-dependent signaling.[28,29]AURKA we also know differentially regulates RalA (but not RalB) and could contribute to Ras-dependent and independent Ral signaling in cancers. The presence and contribution of such an AURKA-RalA crosstalk in cancers and the possible role targeting this could have can be tested by specifically inhibiting AURKA in cancers.In the last two decades, several Aurora Kinase inhibitors have been identified and optimized through multiple-step organic synthesis.[30, 31]Majority of these inhibitors are heterocyclic polyaromatic molecules and hence poorly soluble or dispersible in an aqueous medium.[32] Their delivery across the cell membrane is hence poor, needing higher amounts to be administered to achieve necessary intracellular concentrations. At these higher concentrations, the specificity of many of these drugs is compromised [33]; hence, a new drug delivery protocol that would allow for a more efficient delivery of poorly water-soluble AURKA inhibitors could significantly help their bettertargeting of AURKA in cancer cells. Synthetic polymer nano-scaffolds are an emerging new class of drug vectors that could contribute to improving treatment efficacies in diseases like cancer.[34, 35]Among these drug carriers; polymer vesicles (or

polymersomes) are particularly interesting since they can deliver water-soluble and insoluble drugs in a single nanovesicles.[36-39]Liposomal nano-objects such as DOXIL and lipoplatin are among the important examples of vesicular nano-assemblies evaluated in clinical trials. These liposomal formulations are found to be excellent candidates for drug delivery; however, they are limited by their stability in blood with a half-life time of 12hours.[40-41] Further, the liposomal delivery systems also require additional protection, such as a layer of long-chain PEG to stabilize them against corona-effect induced by proteins in blood.[42-43]Synthetic polymer vesicles are an excellent alternative for liposomal systems in part due to their excellent stability in blood plasma and additional structure-tuneability for stimuli-responsive delivery and suitability for conjugation of drugs[36,47,48]. Polysaccharide vesicles also carry the added advantage of being made from a renewable resource and their interaction with cell surface lectins promoting their cell binding and uptake.[44-46]Polymer vesicles which are susceptible to cleavageat intracellular pH and by lysosomal enzymes have attained significant importance in cancer treatment.[47-50] Our earlier studies have established the use of a unique class of dextran (polysaccharide) nanovesicles to transport drugs such as cisplatin, doxorubicin, and camptothecin in breast and colon cancers.[51-54] These studies have also identified caveolin-1 lacking cancer cells (like breast cancer MCF-7 cells) to better uptake these dextran nano-vesicles.[54]

A detail literature survey has revealed that the polymer nano-carriers have not yet been explored for the delivery of MLN8237. This study hence presents one of the first examples of a polymer nano-carrier platform being used for the delivery of MLN8237 in cancer cells. MLN8237 encapsulation was attempted by our group in diverse polymer nano-assemblies such as polysaccharide vesicles, polycarprolactone di, and tri-block copolymer core-shells,[55-56]and L-amino acid based nanoparticles[57]. However, the poorly water-soluble nature of MLN meant it showed good encapsulation only in the dextran polysaccharide vesicles. The designing of this polysaccharide nanovesicles was also optimized in our group by systematically tuning the hydrophobic dextran backbone by multiple-step organic/polymer synthetic strategies[51-54].Thus the encapsulation of MLN8237 in the nanovesicle platform reported here is the outcome of almost a decade of work in this area by our research groups.The administration of MLN8237 using this vesicular nano-scaffold effectively causes ~8 fold increase in the inhibition of AURKA,

but not AURKB, targeting RalA (not RalB) to significantly inhibit anchorage-independent growth in breast cancer MCF-7 cells. The role of aurora linases in cell cycle regulation and the delivery of aurora kinase inhibitors using polymersomes is schematically shown in figure

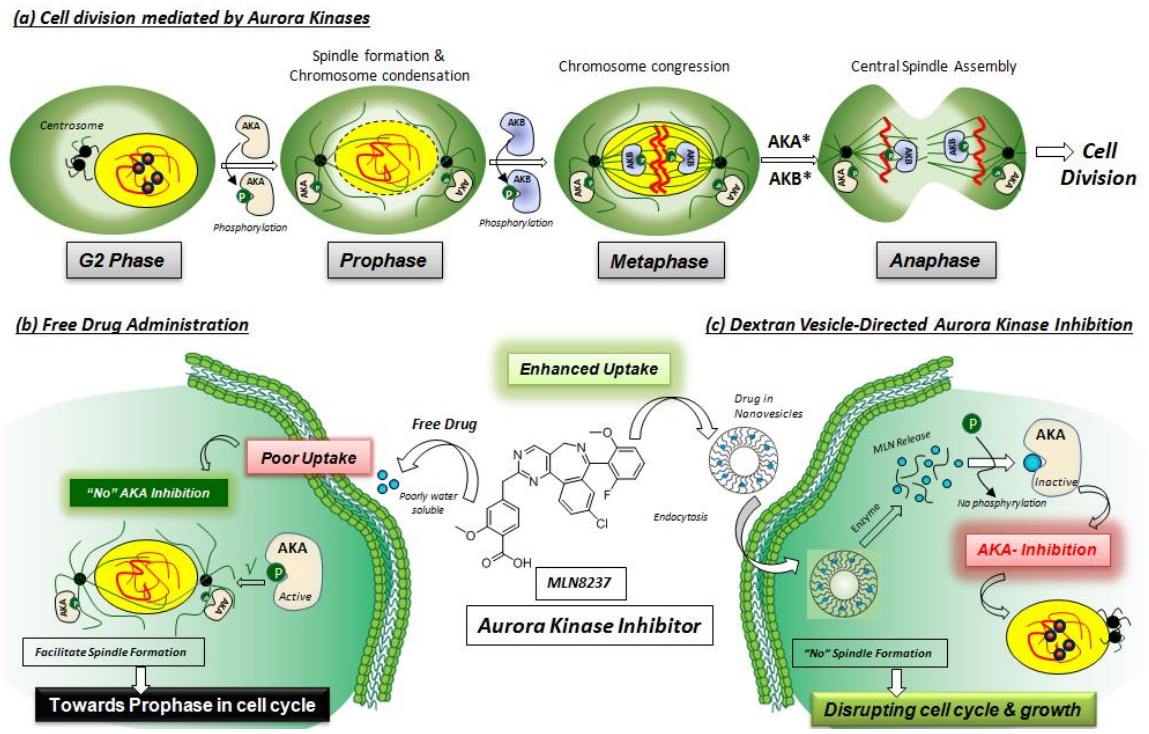

Figure 5.1: *Aurora kinases mediated regulation of cell division in cell cycle (a), Administration of MLN 8237 free drug (b) and Polysaccharide vesicular nano-carrier platform for enhanced drug uptake in cell and enzyme-responsive controlled releases of drugs for Aurora A inhibition and cell cycle arresting (c).*

5.2 EXPERIMENTAL SECTION

5.2.1 Materials: Dextran (6000 Mol. Wt), dicyclohexylcarbodiimide (DCC), dimethylamino pyridine (DMAP), ethylchloroacetate, Polyethyleneglycol (PEG) (4600 Mol. Wt), cisplatin and all the necessary reagents were purchased from Sigma Aldrich. Horse liver esterase was purchased from Sigma (Cat # 46069) and used as such. Alisertib (MLN8237) was purchased from Selleckchem chemicals. DMF and all the necessary solvents were purchased from Spectrochem laboratories. Anti-Phospho-Aurora A (Thr288)/Aurora B (Thr232)/Aurora C (Thr198) (Cat #2914) and anti-Aurora Kinase B (Cat #3094) antibodies were from Cell Signaling. Anti-Aurora Kinase A (Cat #610939) and Anti-RalA (Cat# 610221 clone 8) were purchased from BD Transduction Labs. Anti-RalB was from R&D labs (Cat# AF3204). Human Plasma fibronectin (Cat#F2006), Nocodazole (Cat # M1404), DMSO (Cat # D2438), DAPI (Cat# D9542) and Thiazolyl Blue Tetrazolium Bromide (MTT, Cat# M2128) were purchased from Sigma and Phalloidin-Alexa-488 (Cat# A12379) was from Molecular Probes (Invitrogen). Fluoromount-G used to mount cells for imaging was obtained from Southern Biotech(Cat# 0100-01). Glutathione sepharose beads used for Ral activity assay were from GE (Cat# 17075601). Crystal violet used for staining colonies in AIG assay was from Amresco (Cat# 0528).Collagen for doing 3D uptake studies was purchased from Corning (Cat# 354236). Carboxylic acid substituted 3-pentadecylphenol (PDP-acid) was synthesized following the procedure described in chapter 2.

5.2.2 General Methods: 400-MHz JEOL and Bruker NMR Spectrophotometer were used for ^{1}H and ^{13}C NMR Measurements. Absorption spectra were recorded using Perkin-Elmer Lambda 45 UV-Visible spectrophotometer. Dynamic light scattering (DLS) analysis was done by using a Nano ZS-90 apparatus utilizing 633 nm red laser (at 90 ° angle) from Malvern Instruments. Tapping mode atomic force microscope imaging was done by drop-casting the samples on mica surface using Agilent instruments. For TEM Analysis, the samples were prepared by drop casting on a copper grid.

5.2.3 Preparation of MLN8237 loaded drug Polysaccharide vesicles: Amphiphilic dextran (DEX-PDP) was synthesized using procedure described in chapter2 by

chemically conjugating carboxylic acid substituted 3-pentadecylphenol (PDP) hydrophobic unit on the hydrophilic dextran backbone (M_w= 6,000) by an enzyme-responsive aliphatic ester chemical linkage. The degree of substitution of PDP in dextran was kept at 5 %. To encapsulate MLN8237 in the polysaccharide (dextran) vesicles 20.0 mg of DEX-PDP and 0.20 mg of Alisertib MLN8237 were dissolved in 2.0 ml of DMSO and then 2.0 ml of Milli-Q water was added. The resulting solution was stirred for 12 hours in the dark and dialyzed (MWCO = 3500) against Milli-Q water for 48 hours to remove any unencapsulated drug. The resulting solution was filtered, lyophilized and stored at 4°C. This powder was reconstituted for use as needed. The drug loading content (DLC) and drug loading efficiencies (DLE) were determined by dissolving a known amount of lyophilized drug loaded sample in methanol and estimating its drug content by absorption spectroscopy. For this purpose, the molar extinction coefficient of MLN8237 was determined as 76500 L mol^{-1} cm^{-1} in methanol. The DLC and DLE were determined as 0.40 % and 56 % respectively.

DLC (%) = (weight of the drug in vesicles/weight of the drug-loaded vesicles) *100

DLE (%) = (weight of the drug in vesicles/weight of the drug in feed) *100

5.2.4 Preparation MLN8237 and Rhodamine B (Rh-B) loaded Polysaccharide vesicles ($V_{MLN+RhB}$): To encapsulate MLN8237 and Rh-B together in the dextran vesicles; 20.0 mg of DEX-PDP, 2.0 mg of Rh-B, and 0.20 mg of Alisertib MLN8237 was dissolved in 2.0 mL of DMSO and 2.0 mL of Milli-Q water added later. The resulting solution was stirred for 12 hours in dark and dialyzed using semi-permeable membrane (MWCO = 3500) against Milli-Q water for 48 hours to remove any unencapsulated drug. The resulting solution was filtered, lyophilized and stored at 4°C. The DLCs and DLEs were determined as 0.42% and 58% for MLN8237 and 1.4 % and 64 % for Rh-B, respectively.

5.2.5 *In vitro* drug release studies for MLN8237: 3.0 mg of MLN8237 loaded vesicles (V_{MLN}) or MLN8237 and Rhodamine-B dual loaded vesicles ($V_{MLN+RhB}$) were dissolved in 1 mL of PBS (pH 7.4) and placed in the dialysis tube. The tube was then immersed in 10 mL of PBS in a beaker incubated at 37° C. At fixed time intervals, 2 mL of media was

removed and replaced with fresh PBS. The absorbance of each aliquot taken out was measured and the amount of MLN8237 or Rh-B present was determined using Beer's law. For esterase assisted release studies same protocol was used with the addition of 10U of esterase.

5.2.6 Tissue culture: MCF-7 (human breast adenocarcinoma), A549 and Calu 1 cells were cultured in DMEM (Cat # 11995-065) supplemented with 5% (v/v) fetal bovine serum (FBS) (Cat # 26140-079) and 1% (v/v) penicillin-streptomycin (Cat # 15140-122) (all from Invitrogen) at 37°C under a 5% CO_2 humidified atmosphere. Cells were treated regularly with anti-mycoplasma agent sparfloxacin from Sigma (Cat # 56968) and when needed with mycozap from Lonza (Cat No #VZA-2011) to keep them mycoplasma free. Cells were detached using 0.05% trypsin (Cat # 25300-062) and seeded in 60mm dishes (Eppendorf) for all inhibition assays and in 6 well plates (Eppendorf) for uptake studies.

5.2.7 Cellular uptake of encapsulated MLN8237 (V_{MLN}) by confocal microscopy: MCF-7 cells seeded at a density of 1 x 10^5 cells on coverslips coated with 2µg/ml fibronectin in 6 well plates containing DMEM with 5% FBS and incubated at 37°C for 18hours. Cells were then incubated with the required concentration of the DEX loaded with MLN8237 and Rhodamine-B ($V_{MLN+RhB}$) for 48 hours, with or without nocodazole at a concentration of 10ng/ml (to activate Aurora Kinases). After 48 hours, the drug-containing medium was removed, cells were washed twice with PBS (1ml per wash) and fixed with 3.5% paraformaldehyde solution in PBS for 15mins at room temperature. They were then washed with PBS and stained with Phalloidin conjugated to Alexa 488 (Invitrogen) diluted 1:400 in 5% BSA solution in PBS for 45mins in dark. Excess dye was washed from cells, coverslips incubated with DAPI (0.05 mg/ml) for 2mins to stain the nucleus and finally mounted on slides using Fluoromount-G mounting medium (Southern Biotech). Slides were then dried overnight at room temperature in dark and imaged using an LSM780 multiphoton microscope with the λ 405 nm (blue channel), λ 568 (red channel) and λ 488 (green channel) lasers.

5.2.8 Stability of the dextran Nanovesiclesin serum using DLS Technique: To study the intracellular stability of the dextran vesicles, 0.1mg/mL concentration of the nanovesicles were made in phosphate buffer saline (PBS), Dulbecco's modified eagles medium (DMEM) with 5% Fetal Bovine Serum (FBS) and 5% Fetal bovine serum (FBS) alone, incubated at 37^0C for 24 h. The size of nanovesicles in these solutions was measured by DLS every hour for the initial 6h and then at 9h, 12h and 24 h respectively. The DLS data thus obtained was plotted using Origin 8.0 software and compared.

5.2.9 Treatment of cells using MLN8237 (MLN) and encapsulated MLN8237 (V_{MLN}) : 3 x 10^5 cells MCF-7 cells were seeded in 60mm dishes and allowed to attach for 24 hours. Cells were treated with 0.02µM or 0.04 µM MLN8237 as free drug or in the nanovesicle (V_{MLN}) for 24hours. 10ng/ml (33nM) nocodazole was simultaneously added to the cells with the drug for this period. Four untreated controls, a) cells without nocodazole and MLN8237, b) cells without nocodazole and with empty DEX scaffold (equivalent to highest amount DEX added with the encapsulated drug), c) cells with nocodazole and without MLN8237 and d) cells with nocodazole and empty DEX, were used in each experiment. When required, cells were similarly treated with MLN8237 or V_{MLN} without Nocodazole treatment. MLN8237 dissolved in DMSO (stock concentration 100uM) is diluted in DMEM with FBS and administered to cells at the required concentration. Controls described in inhibition studies are all cells treated with only DMSO at concentrations matching the highest amount used with the drug in that assay.

5.2.10 Cellular uptake of encapsulated MLN8237 ($V_{MLN+RhB}$) in 3D gels. MCF-7 cells growing in DMEM with 5% FBS were trypsinized and 2.5 x 10^5 cells were mixed with 1.5mg/ml Collagen diluted with PBS and polymerized using NaOH in glass bottom Lab-Tek chambers. The gel with cells was allowed to polymerize for 30mins at 37°C in a CO2 incubator and 400uL of DMEM containing 5% FBS with 5uM Rhodamine B encapsulated in DEX vesicle (V_{RhB}) or with MLN8237 ($V_{MLN+RhB}$). Cells were incubated for incubated for 3hours at 37°C and fixed with 3.5% paraformaldehyde solution in PBS for 15mins at room temperature. Cells were then imaged using LSM-710 anisotropy microscope with λ 568 (red channel) laser.

5.2.11 Deconvolution of Z stacks using Huygen's Professional Image analysis software. Z-stacks of V_{RhB} or $V_{MLN+RhB}$ labeled MCF-7 cells in 3D collagen gels were imaged using a confocal microscope as cross-section images collected as a Z stack 0.2um apart. All the images were processed and analyzed using the Huygens Professional software (version 16.10 825) (Scientific Volume Imaging, The Netherlands, http://svi.nl). Deconvolution of these z-stacks was done using their deconvolution add-on using the following settings: Iterations-30, Threshold-0.0001, Signal to Noise ratio (SNR)-20 and Background estimation radius – 1. Deconvoluted z-stacks were processed using the Maximum intensity projection (MIP) tool to render images with 15% threshold.

5.2.12 Co-localization of Nanovesicles with lysosomal markers: To evaluate the intracellular localization of the dextran nanovesicles, 25000 cells were seeded in a glass bottom four chamber slide and allowed to adhere for 16h. These cells were then incubated with the 4.2μM of V_{RhB} and $V_{MLN+RhB}$ for 4h. Cells were then washed thrice with 1X PBS and treated with 25nM of Lysotracker green DND-26 as described earlier [57]. Cells were then imaged using a laser confocal microscope and the overlap between rhodamine trapped in the nanovesicle and the lysotracker green compared.

5.2.13 Detection of Aurora Kinase Activity by western blotting: Following their 24hour or 48hour treatment (as required) cells were lysed in SDS-Laemmlis buffer, cell equivalent samples were resolved by SDS-PAGE and transferred to PVDF membrane. Blots were incubated with anti phospho-Aurora Kinase A/B/C or anti-Aurora Kinase A / anti- anti-Aurora Kinase B antibody respectively, followed by the appropriate secondary antibodies conjugated to HRP. Using Pierce ECL or PICO immuno-detection reagents (Thermo Scientific Cat # 32106, Cat # 34079 respectively) blots were developed in the LAS4000 detection system (Fujifilm-GE). Densitometric band analysis was done using the Image J software (NIH). Aurora Kinase activation was determined by calculating the ratio of phosphorylated Aurora Kinase to total Aurora Kinase band intensity and compared across treatments.

5.2.14 Ral activity Assay: For Ral activity post MLN8237 /BQU57 treatment, MCF-7 cells were treated with 0.02μM of free inhibitor (MLN) or nano-vesicle encapsulated

inhibitor (V_{MLN}) or BQU57 (5mM) for 48hours. Following the above treatments, cells were lysed and processed for Ral activity assay as described earlier(29). Blots were developed using the LAS4000 detection system (Fujifilm-GE) and densitometric band analysis done using Image J software (NIH). Percent active levels of RalA/RalB were determined as described earlier(29). Active RalA or active RalB levels under different treatment conditions were normalized to their respective control (CON).

5.2.15 Anchorage-independent growth assay: MCF-7 cells treated with 0.02μM of free inhibitor (MLN) or dextran encapsulated inhibitor (V_{MLN}) were trypsinized after 24 hours and 5000 cells mixed with 0.3% agar containing DMEM and layered on the top base of 0.5% agar per well in 6-well plates. Each of the control and inhibitor-treated cells was plated in duplicates. The agar was allowed to solidify and 1.5 ml of DMEM containing 5% FBS and 0.02μM MLN8237 (as free drug or nano-vesicle encapsulated inhibitor V_{MLN}) added. These dishes were maintained for 15days with their medium changed every three days. Freshly reconstituted free drug or V_{MLN} at the same used concentration were added to the medium during this change. A similar protocol was followed to study AIG of MCF-7 cells treated with 5μMBQU57 (Ral inhibitor). Colonies formed in agar at the end of the 15-day incubation were stained with 0.05% crystal violet dissolved in 20% ethanol for one hour at room temperature and destained by repeated washing with distilled water till stained colonies are clearly visible. The colonies were then imaged on Olympus MVXC10 microscope at 0.63X zoom in HDR mode and counted using particle analysis tool of Image J software.

5.2.16 Stastical Analysis of Data

Statistical analysis of data was done with the paired Student's T-test or when comparing to a normalized control with a single sample T-test using the Prism GraphPad analysis software.

5.3 Result and Discussion

5.3.1 Synthesis of dextran nanovesicles containing MLN8237 (V_{MLN})

The hydrophilic dextran was made amphiphilic by substituting its backbone with renewable hydrophobic unit 3-pentadecylphenol[58] (PDP) via aliphatic ester linkages which can be cleaved in the enzyme-rich intracellular lysosomal compartment.[51] The synthetic scheme and proton NMR of the dextran derivative is given in figure 5.2. The percent of PDP relative to the dextran backbone was kept constant at 5% to balance the amphiphilicity in the newly designed dextran derivative. The substituted dextran polymer was dialyzed against Milli-Q water and the obtained nanostructures were subjected to the dynamic light scattering (DLS), electronic microscopic techniques (TEM) and atomic force microscopy (AFM) technique (Figure 5.3).

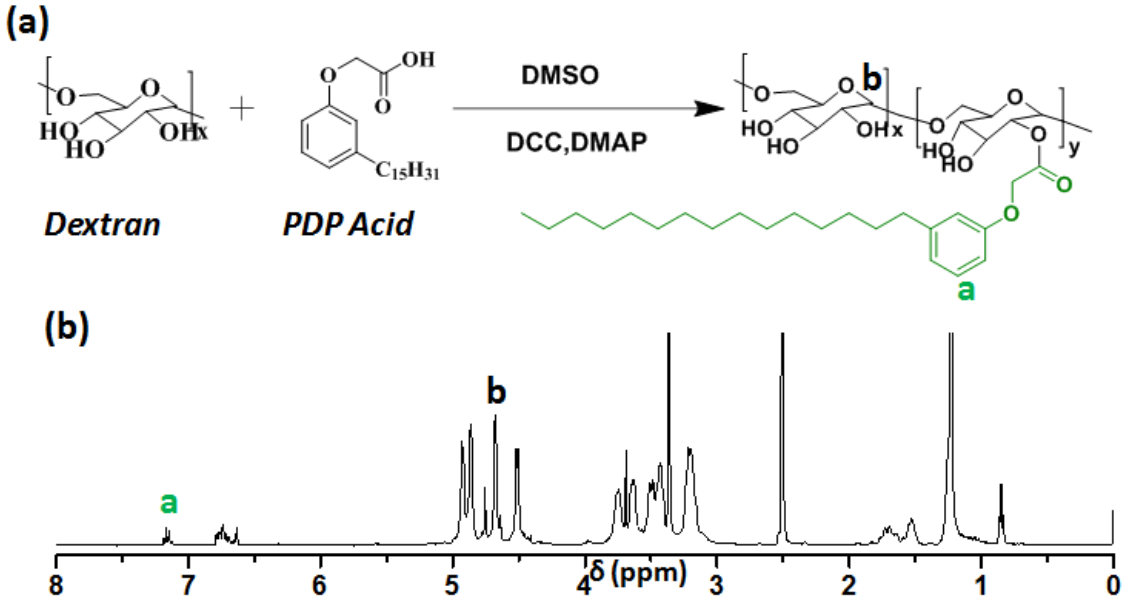

Figure 5.2: *A synthetic scheme for DEX-PDP derivative (a) and proton NMR for DEX-PDP (b).*

As shown in the Figure 5.3a, the aqueous polymer solution was completely transparent and DLS analysis of this solution revealed its mono-modal distribution corresponding to the size of 170 ± 10 nm. The formation of spherical nanostructures in an aqueous medium was confirmed by AFM analysis which shows a typical two hump height profile corresponding to their vesicular geometry (Figure 5.3a).

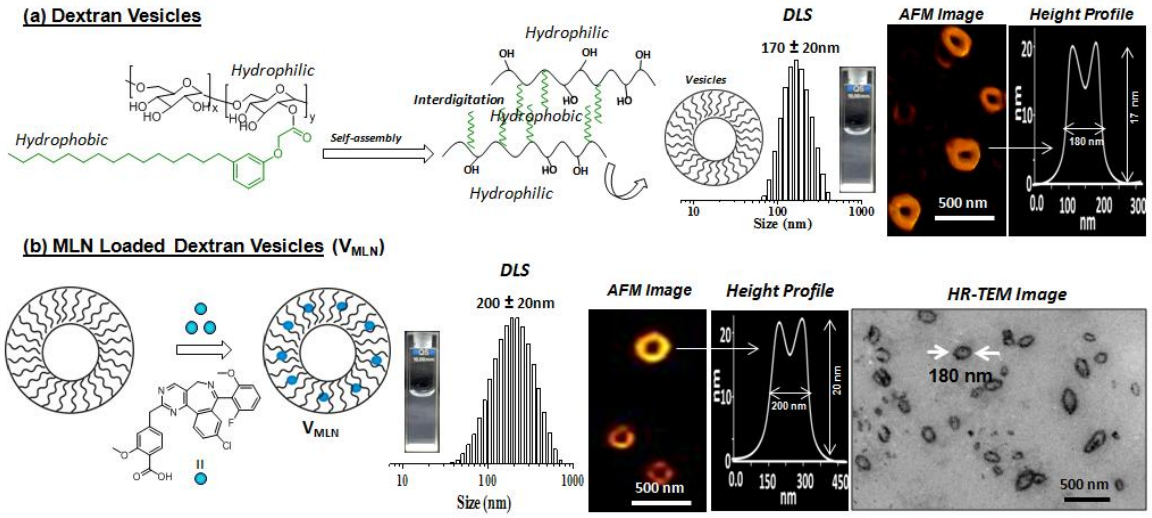

Figure 5.3 : *Schematics of the self-assembly of the newly designed dextran derivative, DLS histogram and AFM morphology of the nascent dextran vesicles (a), MLN 8237 loading to dextran vesicles(V_{MLN}), DLS histogram of V_{MLN}, AFM morphology of V_{MLN} and HR-TEM morphology of V_{MLN}. (Arrows mark the size and distinct layer and core of the vesicles) (b).*

To determine the hydrophobic layer thickness of the vesicles, large area AFM and HR TEM images were used as showed in figure 5.4 a and b. The single crystal X-ray structure of the hydrophobic part (PDP-unit) from our earlier studies revealed that the hydrophobic PDP units underwent inter-digitization to self-assemble the molecules in bi-layer structure.[54]The average thickness of the hydrophobic layer was estimated from the size distribution plot as 43±5 nm and 38±4 nm from AFM and TEM images, respectively (see figure 5.4 a and b). The average size of the hydrophobic layer was bigger than the single-layer thickness; thus, it may be assumed that the vesicles were constituted by multi-layer hydrophobic units.So as the modified dextran produces vesicles in the aqueous medium, its capability to encapsulate water insoluble Aurora kinase inhibitor MLN8237 (Alisertib) was tested by the dialysis method. The polymer and drug were dissolved in DMSO + Water and subjected to nano-precipitation, and then dialyzed against Milli-Q water for 48h using a semi-permeable membrane. The vial in Figure 1b shows vesicles loaded with the MLN8237 to be a clear solution suggesting enhanced aqueous solubility of the drug in the vesicular nano-scaffold. DLS histogram of the drug-loaded vesicles (Figure 5.3b) confirmed its mono-modal size distribution of 200 ± 20 nm. The AFM analysis of the MLN8237 loaded nano-objects revealed their vesicular

geometry (Figure 5.3b) to be comparable to the nascent dextran vesicles (Figure 5.3a) and unaffected by loading of the hydrophobic drug. HR-TEM microscopic analysis of these vesicles showed the existence of a distinct hydrophobic thin-layer separating their inner and outer walls in the nano-scaffold (Figure 5.3b). A controlled encapsulation experiment was done for MLN8237 in fully water soluble PEG-4600 sample to study the role of polymer formulation for MLN8237 stabilization in aqueous medium.

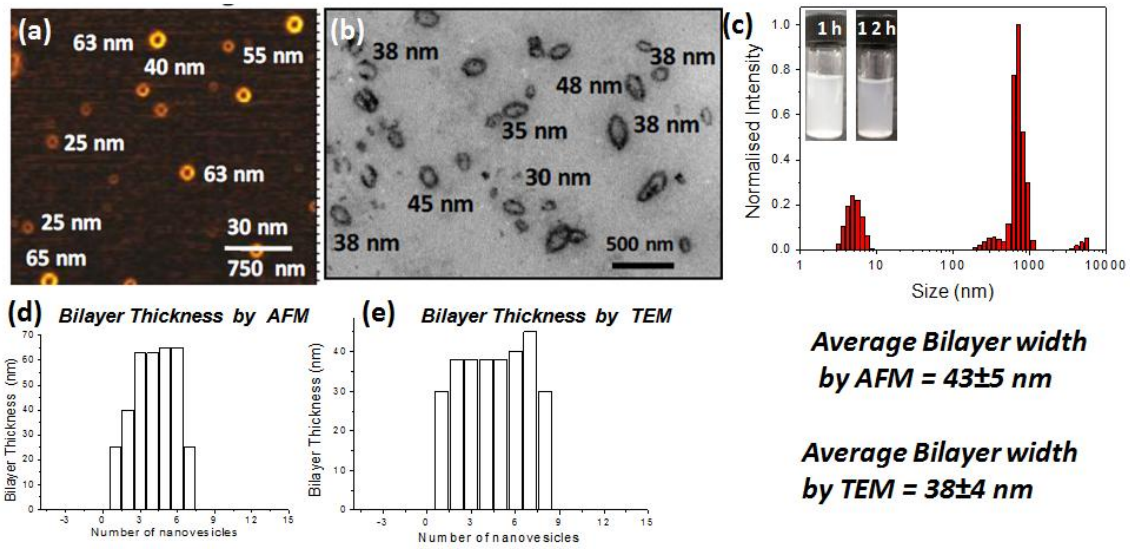

Figure 5.4: *A diagram showing large area AFM (a), and HRTEM image (b) for DEX-PDP nanovesicles, DLS histogram for MLN 8237 encapsulation to PEG 4600 (c). Inset photograph of vial showing the stabilization of MLN 8237 in PEG 4600 at 1 and 12 hour time interval, plot of bilayer thickness vs number of vesicles as determined by AFM (d) and plt of bilayer thickness vs number of vesicles as determined by TEM (e).*

MLN8237 was found to be precipitating from the polymer aqueous solution. DLS histograms of the trace amount of drug dispersed turbid polymer solution showed multi-model distribution with particle size in the range of 1.0 to 2.0 µM (see figure 5.4c) which is not suitable for cellular studies. This suggests that appropriate amphiphilicity in the polymer back bone is required to encapsulate MLN8237 in nano-carriers and stabilize them in aqueous medium. In the present study, this was accomplished by carefully choosing the renewable PDP hydrophobic unit and dextran hydrophilic backbone in polysaccharide vesicles to stabilize MLN8237. Together, these studies show the water-insoluble MLN8237 to be effectively loaded in the hydrophobic layer of the dextran

vesicles with a drug loading efficiency (DLE) of 56% and drug loading content (DLC) of 4.0 μg/mg/mL. This MLN8237 loaded dextran vesicle is hereafter referred to as $V_{MLN.}$

5.3.2 Enzyme-responsive release and cellular uptake of V_{MLN} in MCF-7 cells

The stability and release of MLN8237 from dextran nanovesicles were tested in-vitro by dialysis. In PBS pH 7.4 at 37°C (Figure 5.5a), V_{MLN} was found to bestable with<25%of the drug being released over 25 hours. As the dextran nanovesicle was made through the conjugation of a hydrophobic PDP subunit via a biodegradable aliphatic ester linkage (see figure 5.2); these vesicles show more than ~85% of MLN8237 to be released in the presence of 10U of esterase enzyme at pH 7.4 and 37°C (Figure 5.5 a). This mimics esterase concentrations reported in cytosols[59] and shown to be sufficient to cleave polysaccharide derivatives.[59]The schematics showed in figure 5.5b, explains the endocytosis of the dextran nanovesicles which ruptures in the presence of esterase enzyme to release MLN8237 in the intracellular medium. Studies by Xu et al, looking at esterase activity in 18 different types of tumors, showed their levels to be variable and elevated in breast, colon and liver cancers.[59] This would allow for better cleavage of the dextran nanovesicle in cancer cells further supporting the better release of MLN8237. Earlier computational docking studies from our lab have revealed the aliphatic chemical linkage connecting the hydrophilic dextran backbone and hydrophobic PDP tail to perfectly lock in the enzymatic pocket of the esterase enzyme.[61] Thus, cleavage of this aliphatic ester linkage will disturb the amphiphilicity in the scaffold, causing it to disassemble and hence release the drug (MLN8237). The stability of V_{MLN} and its enzyme-responsiveness were both investigated by DLS and the data is summarized in figure 5.6 a and b. Stability of the MLN loaded nanovesicle was tested in PBS, Dulbecco's modified Eagles medium (DMEM) with 5% FBS and 5% FBS alone. The MLN loaded nanovesicle was incubated at 37^0C in these conditionsand its stability tested by dynamic light scattering (DLS) analysis[57]. From the DLS plots in figure 5.6 c and d, it was very clear that sizes of the self-assembled nanovesicle structures were retained without any change up to 24h. This proves the dextran nanovesicles to be stable in the presence of serum allowing it to survive similar biological environments.In vitro drug release profiles of V_{MLN} (Figure 5.5 a) matched observed changes in the size and

organization of disassembled nanovesicles detected by dynamic light scattering (DLS), further confirming the breakdown of the nanovesicle. This release plots (Figures 5.5 a and figure 5.6 a and b); suggest that a similar action of esterase enzymes on V_{MLN} in cells could facilitate the slow and steady release of the drug. Upon exposure to esterase enzyme in PBS, the size of the nanovesicles changed from nano-meter to sub-micrometer range (see figure 5.6 a and b). This change is attributed to the cleavage of the aliphatic-ester linkage that connects the hydrophobic PDP unit on the dextran backbone, causing the disassembly of the nanovesicles. These disassembled nanovesicles affected the turbidity of the aqueous solution due to the partialsolubility of the PDP units in water.Together these results indicate the enzyme-mediated disassembly of dextran nanovesicles will support the gradual release of MLN8237. The resulting 3-pentadecylphenol and its carboxylic derivative, when tested for cellular cytotoxicity, were seen to be non-toxic to cells. The cytotoxicity plot is given in figure 5.6 f.

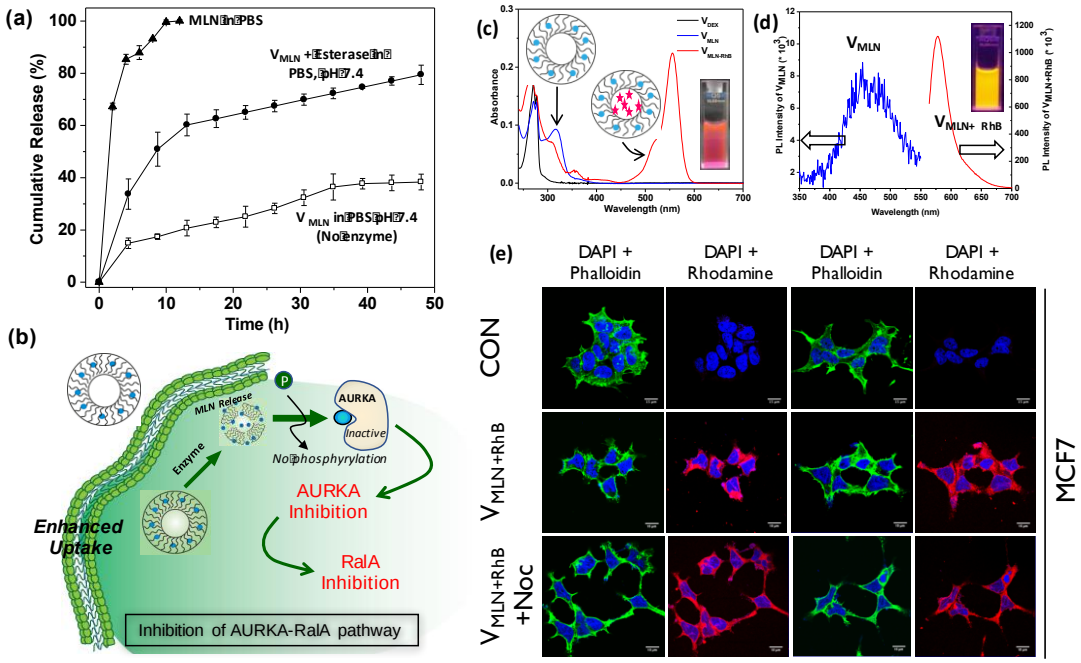

Figure 5.5:*(a) Cumulative release profile for free MLN and V_{MLN} in PBS in presence or absence of Esterase at pH 7.4, 37℃. (b) Schematic representation of enzyme responsiveness of V_{MLN} in the cell releasing MLN8237 to act on AURKA and inhibit RalA downstream. (c) Absorbance spectra of V_{MLN}, $V_{MLN+RhB}$, and V_{DEX}. (d) Emission spectra of V_{MLN} and $V_{MLN+RhB}$. (e) Uptake of DEX nano-vesicle with Rhodamine-B (1.37 µM) and MLN8237 (0.5 µM) ($V_{MLN+RhB}$) in absence or presence of 10ng/ml Nocodazole ($V_{MLN+RhB}$+ Noc) was visualized by confocal microscopy in MCF-7 cells treated for 48hours relative to untreated control (CON).*

Being able to specifically inhibit AURKA over AURKB has been the basis of designing inhibitors like MLN8237.[32,33]However, its poor solubility in water and reduced bioavailability doessuggestconcentrations needed for inhibiting AURKA could likely affect AURKB. We hence tested if the known differential uptake of V_{MLN} could support better delivery and inhibition of AURKA in cancer cells.

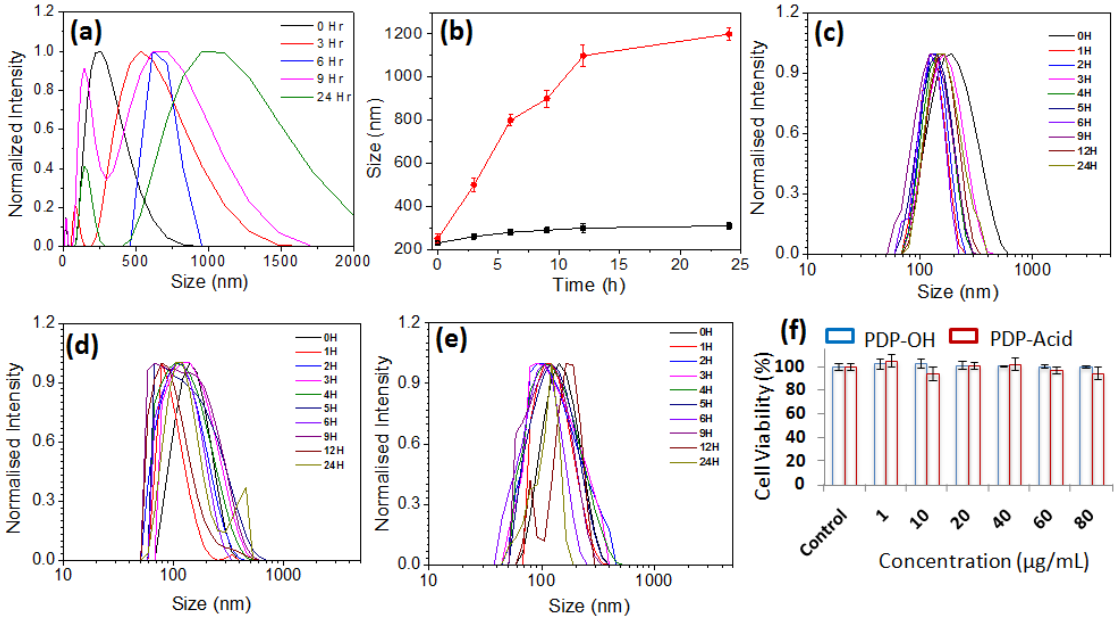

Figure 5.6: *A DLS histogram showing size of the nanovesicles (a), a plot of change in size of the nanovesicles with respect time (b), A DLS histogram showing the stability of the nanovesicles in PBS (c), in DMEM media (d), in FBS (e) and the cytotoxicity Plot of PDP-OH and PDP-Acid in MCF 7 cells (f).*

This was tested in breast cancer MCF-7 cells that overexpress Aurora Kinase A to induce their cancer stem cell-like properties.[62] AURKA in these cells is also seen to play an important role in invasion and MMP9 expression.[63] MCF-7 cells in our earlier studies were also seen to better take up the dextran nanovesicle, relative to normal fibroblasts.[54]As MLN8237 is not inherently fluorescent, visualization of its cellular uptake as V_{MLN} or its release in cells is not possible. A water-soluble fluorescent dye Rhodamine-B was hence loaded along with MLN8237 in the dextran vesicles by dialysis method.[51] These RhB and MLN containing vesicles are called $V_{MLN+RhB}$. The DLS histogram showed in figure 5.7a of these dual loaded vesicles also showed a mono-modal distribution corresponding to the size of 180±20 nm. Further, AFM images of $V_{MLN+RhB}$

(see figure 5.7c) confirmed their preservation of the vesicular geometry reported earlier in these dextran nanovesicles. The optical properties of the RhB loaded vesicles were tested by recording their absorbance and emission spectra (Figures 5.6 c and d). The absorbance spectrum confirmed absorbance peak maxima at λ 310nm and 550nm corresponding to MLN and RhB chromophores (Figure 5.6 c). The emission spectrum of V_{MLN} (Figure 2d) was found to be non-luminescent or weakly luminescent.The absorbance and emission spectra of free MLN8237 are recorded and provide in the SF-9. The absorbance maximum for MLN8237 was found to be λ300nm which was exactly the same as observedfor the MLN loaded nanovesicles. From the Absorbance and emission spectrum showed in figure 5.7 d and e it has been observed that MLN8237 did not show any significant emission; thus, confirming it to be a non-luminescent drug. On the other hand, the emission spectra of $V_{MLN+RhB}$ exhibited a strong red-luminescence with maxima at 580 nm (Figure 5.6d). When vials containing V_{MLN} and $V_{MLN+RhB}$ are imaged under UV light, V_{MLN} was seen to be weakly fluorescent while $V_{MLN+RhB}$ showed a strong red-orange coloured emission. This allows for $V_{MLN+RhB}$ to be used to visualize the cellular uptake of the drug-containing nanovesicle in breast cancer MCF-7 cells.

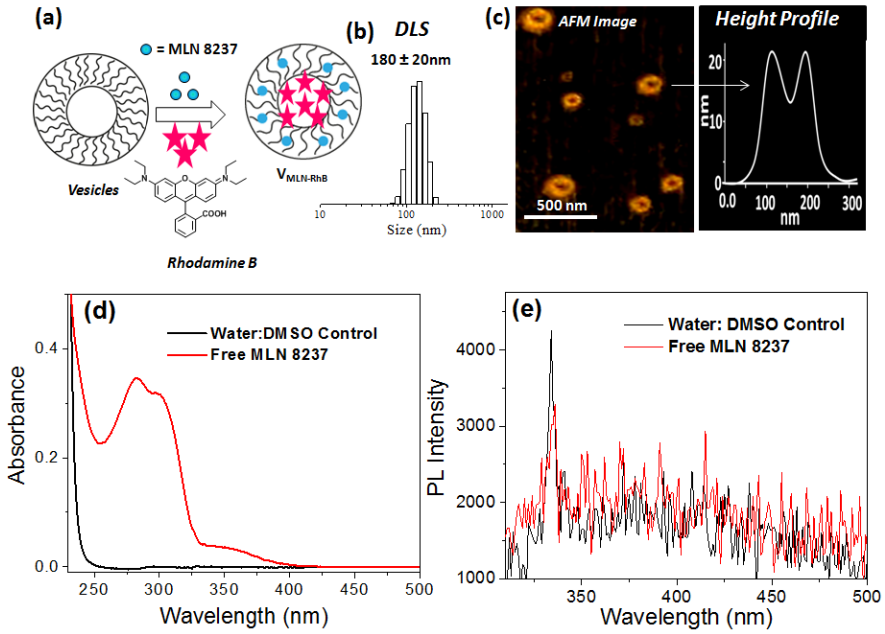

Figure 5.7: *Schemtaics of RHB and MLN 8237 encapsulation in dextran nanovesicles (a), DLS histogram for $V_{MLN+RHB}$ (b) and AFM images for $V_{MLN+RHB}$ (c), absorbance spectrum of free MLN (d) and emission spectrum of free MLN 8237.*

Considering MCF-7 cells were treated with nocodazole (33nM) to arrest cells in mitosis and activate Aurora kinases (Figure 5) we also tested their uptake of $V_{MLN+RhB}$ under these conditions. These revealed MCF7 cells show a robust endocytosis of $V_{MLN+RhB}$ unaffected by Nocodazole treatment (Figure 5.5 e). This could be explained by the fact that Nocodazole at <50nM concentrations have been reported to cause cell cycle arrest without significantly altering the microtubule network.[64-65] Phalloidin-stained actin cytoskeleton confirms the intracellular localization of $V_{MLN+RhB}$. Dextran nanovesicles with inbuilt aliphatic ester linkages are susceptible to cleavage in the intracellular lysosomal compartment.To trace the intracellular location of the nanovesicles, Rhodamine B loaded vesicles V_{RhB} and $V_{MLN+RhB}$ were colocalised with Lysotracker in live cells as described earlier [57].Lysosomes stained with 25nM of Lysotracker green DND-26 co-localized with V_{RhB} and $V_{MLN+RhB}$(Figure 5.9 - column 3). This does suggest the nanovesicle taken up by cells is co-localized extensively with lysosomes, which could be the site for its degradation by the enzyme-rich environment.

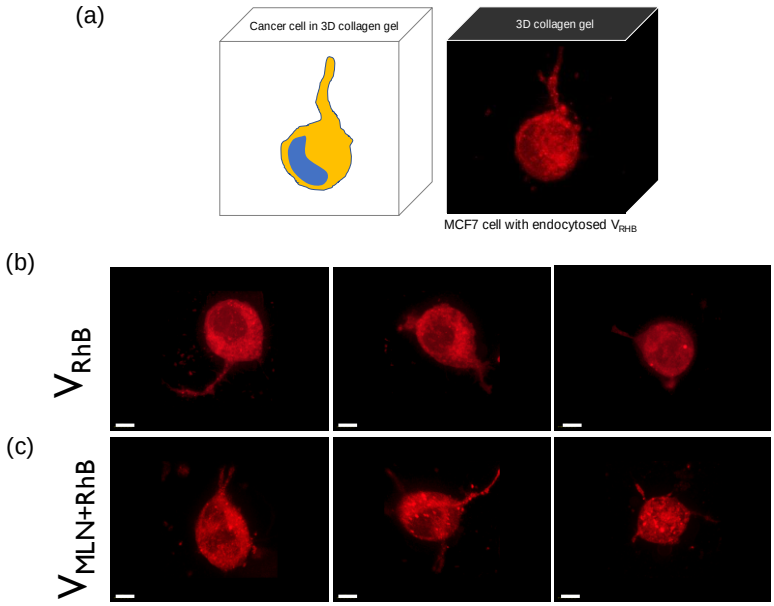

Figure 5.8: *Uptake of DEX encapsulated MLN8237 ($V_{MLN+RhB}$) by MCF-7 in 3D microenvironment: Uptake of DEX nano-vesicle with Rhodamine-B (5 µM) alone or Nano-vesicle with Rhodamine B(5µM) and MLN823(1.3µM). was visualized by confocal microscopy in MCF-7 cells treated for 3hours. Images shown are representative of two independent experiments that gave similar results(Scale bar 5µm).*

Together, they further support the enzyme responsiveness of the dextran scaffold. The uptake of $V_{MLN+RhB}$ was also tested in MCF-7 cells embedded in 3D collagen gels (Figure 5.8).

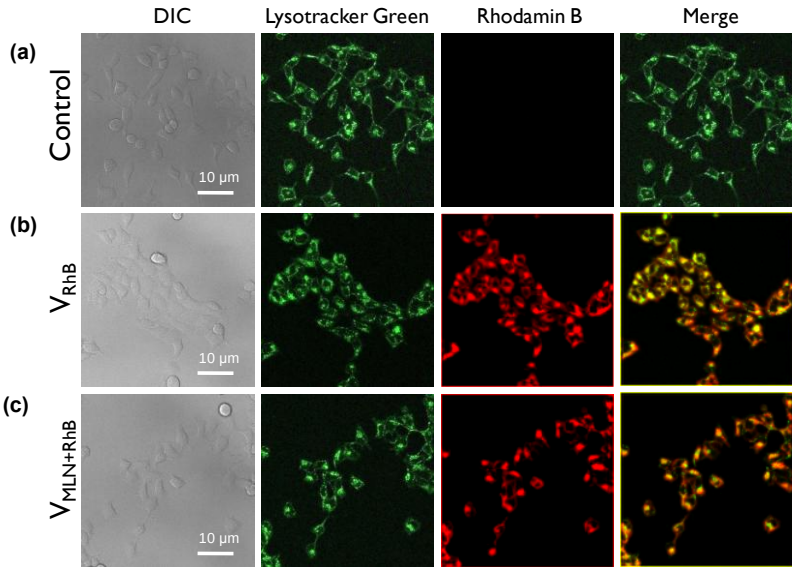

Figure 5.9*: Co-localization of Lysotracker DND-26 with $V_{MLN+RhB}$ Live cell Confocal Images in MCF-7 cells for (a) control, (b) V_{RhB} and (c) for $V_{MLN + RhB}$ (c)The excitation wavelength used for Lysotracker DND-26 and Rhodamine B are 488 nm and 561 nm respectively. The cells are treated with 2µg/ml(4.2µM) concentration of Rhodamine B and incubated for 4h then imaged using confocal microscopy.*

The endocytosis of these nanovesicles in 3D microenvironment was robust and could be visualized within 3 hours of treating the cells with the nano-vesicles. The endocytosed nanovesicles are seen to be distributed homogeneously throughout the cells even in the 3D microenvironment (Figure 5.8).

5.3.3 Inhibition of Aurora Kinases by V_{MLN} in MCF-7 cells

Basal AURKA and AURKB activation in cells, detected by their auto-phosphorylation on the Thr288 and Thr232 residues respectively[66], is low which makes evaluating the efficiency of its inhibition by V_{MLN} more difficult. We hence activated Aurora kinases (AURKA and AURKB) by arresting MCF-7 cells using nocodazole.[67] This causes up to a 2-fold increase in basal AURKA and AURKB activation (Figures 5.10 a and b). Nocodazole-treated MCF-7 cells incubated for 24hours with 0.02µM and

0.04μM free MLN8237 and V_{MLN}, showed inhibition of AURKA activation by V_{MLN} to be significantly better (~4 and ~8 fold respectively) than the free drug.

Comparing this inhibition suggests V_{MLN} could work as well as the free drug at less than half of its concentration. In these studies, the DEX nano-vesicle scaffold by itself only very marginally affected AURKA or AURKB activation (Figure 5.10 a and b). We further found V_{MLN} (at 0.02μM and 0.04μM) to significantly better inhibit AURKA over AURKB, unlike the free drug that comparably affected both (Figures 5.10 a and b). This confirms the nanovesicle mediated delivery of MLN8237 at low concentrations to indeed be more effective against AURKA in MCF-7 cells. We further evaluated the effect V_{MLN} has on inhibition of basal AURKA and AURKB activation (without nocodazole) in these cells.

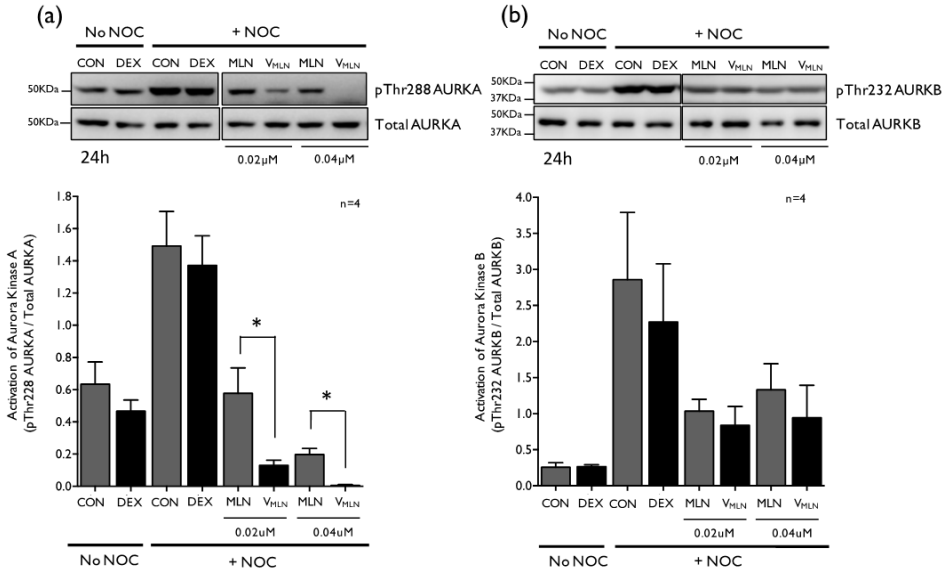

Figure 5.10: *Incubation of MCF-7 cells for 24hours with 10ng/ml of nocodazole causes an increase in AURKA and AURKB activation in DMSO treatedcontrol (CON) and dextran treated cells (DEX). Dextran nano-vesicle alone had no effect on basal AURKA or AURKB activity or its stimulation by nocodazole. Nocodazole-treated MCF-7 cells incubated for 24hours with 0.02μM and 0.04μM inhibitor MLN8237 as a free drug (MLN) and encapsulated in dextran nano-vesicles (V_{MLN}) show V_{MLN} to inhibit AURKA activation significantly better than the free drug (MLN8237) but inhibit AURKB comparably. Blots on top represent AURKA and AURKB activation detected by their auto-phosphorylation on the threonine 288residue (pThr288 AURKA) and threonine 232 residue (pThr232 AURKB), respectively and total AURKA/AURKB levels in cells. All samples shown in both blots were run together on the same gel. The graph represents the mean±SE of pThr288 AURKA/total AURKA and pThr232 AURKB/total AURKB ratio from four independent experiments. Statistical analysis was done using Paired Students T-Test and p values if significant are represented in the graph (* $p<0.05$).*

While needing higher western blot exposures for their detection, basal Aurora kinase activation in MCF-7 cells incubated with V_{MLN} (0.02μM) for 48 hours showed a ~94 % inhibition of AURKA activity, relative to control and DEX-treated cells (Figure 5.11). This is significantly better than the effect free MLN8237 has at the same concentration (~56% inhibition). V_{MLN} also did not affect AURKB activation, unlike the free drug (~ 28% inhibition) (Figure 5.11b). When increasing concentrations of MLN8237 and V_{MLN} were compared at 24hours, inhibition of AURKA (but not AURKB) was indeed better with V_{MLN} at lower concentrations. This makes V_{MLN} at the concentration and time used here (0.02μM and 48hours) a significantly more potent version of MLN8237.

5.3.4 V_{MLN} mediated anchorage-independent growth

Aurora Kinase A is known to phosphorylate and regulate the small GTPase RalA (but not RalB) during mitosis.[8] AURKA mediated phosphorylation of RalA is also seen to regulate its ability to transform cells and make them anchorage-independent.[68]MCF-7 cells overexpress AURKA and carry active RalA that could support their anchorage-independent growth. Hence it was obvious that V_{MLN} mediated specific inhibition of AURKA affects downstream activation of RalA (vs RalB) which further affects the anchorage-independent growth of MCF-7 cells.

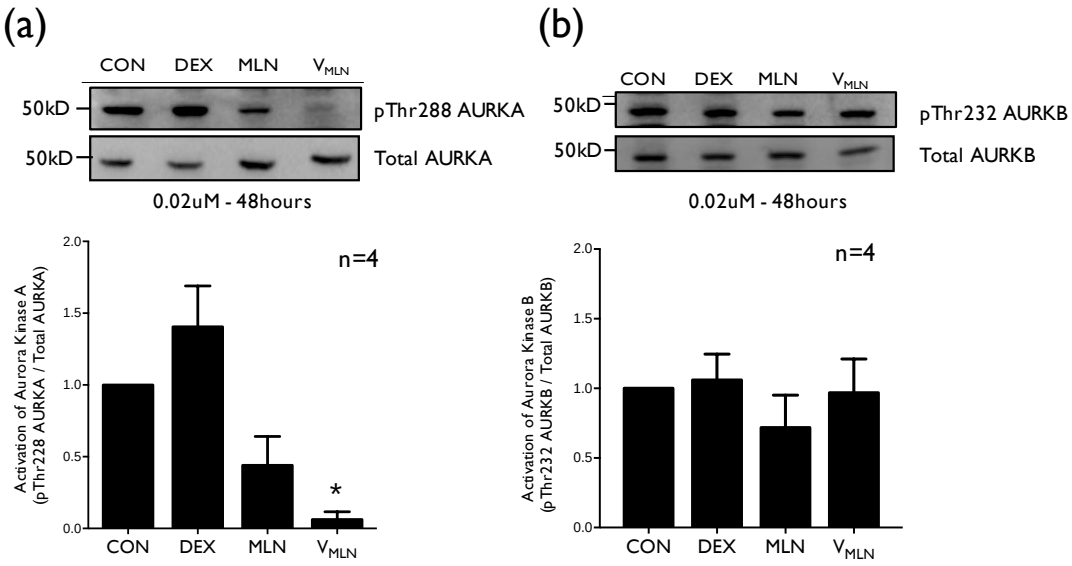

Figure 5.11: *V_{MLN} inhibits Aurora Kinase A without affecting Aurora Kinase B in MCF-7 cells. Incubation of MCF-7 cells for 48hours 0.02µM inhibitor MLN8237 as a free drug (MLN) and encapsulated in dextran nano-vesicles (V_{MLN}) show V_{MLN} to inhibit, (a) AURKA activation significantly better than the free drug (MLN8237). (b) At this concentration, V_{MLN} did not inhibit AURKB activity. Blots on top represent AURKA and AURKB activation detected by their autophosphorylation on the threonine 288 residue (pThr288 AURKA) and threonine 232 residue (pThr232 AURKB), respectively and total AURKA/AURKB levels in cells. All samples shown in both blots were run together on the same gel. The graph represents the mean±SE of pThr288 AURKA/total AURKA and pThr232 AURKB/total AURKB ratio from four independent experiments normalized to their respective DMSO treated control (CON). Statistical analysis was done using Single sample T-Test and p values if significant are represented in the graph (* $p<0.05$).*

From the above results, it has been observed that V_{MLN} could mediate RalA inhibition significantly which further decreases anchorage-independent growth (~38% decrease) of MCF-7 cells. The effect V_{MLN} has on the anchorage independent growth of the cancer cells was studies and showed in figure 5.12. Interestingly, free MLN8237 did not affect RalA activation or AIG at the same concentration of drug used in V_{MLN}. Together this not only establishes the ability of V_{MLN} to be a more effective inhibitor of AURKA but also uses the same to help us understand the role Aurora Kinase A plays in RalA mediated anchorage-independent growth of MCF-7 cells.

By encapsulating the Aurora Kinase inhibitor MLN8237 in dextran nanovesicles, we have been able to use the drug at significantly lower concentrations, which when coupled with the preferential uptake of nanovesicles in MCF-7 cells drives significantly better targeting of Aurora Kinase A. The preferential uptake of V_{MLN} in MCF-7 cells that lack caveolin-1 (relative to normal fibroblast)[54] suggests this might be mediated by non-caveolar endocytic pathways, supported by changes in membrane composition and/or organization that loss of caveolin-1 promotes.

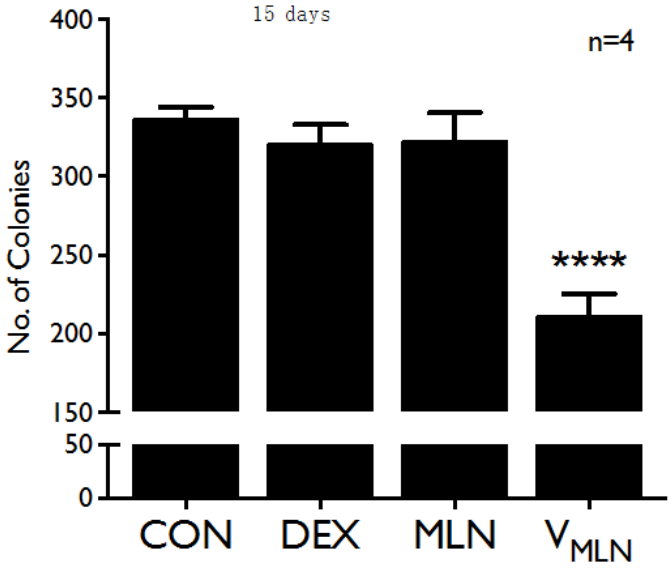

Figure 5.12: *A bar plot showing the effect VMLN has on the ancgorage independent growth of MCF 7 cells. Cells treated were embedded in the agarose gel and incubated for 15 days with DEX, MLN or V_{MLN} and colonies formed were studied and counted. The graph represents mean ± SE data from minimum three independent experiments.*

The stability of dextran nano-vesicles with rhodamine for up to 36hours[52] coupled with the fact that less than ~ 25% of the MLN8237 leaches out from V_{MLN} in the first 24 hours (see Figure 5.4a), suggests a significant amount of encapsulated drug is retained and carried into cells for extended periods of time. This could contribute to the ability of V_{MLN} to act over 48hours (in activity assays) and longer (15 days) in anchorage-independent growth studies in MCF-7 cells. The sensitivity dextran nanovesicles have to physiological levels of esterase[59, 60] that releases ~85% of the encapsulated drug, coupled

with the fact that multiple esterases are functional in MCF-7 cells[69] could further add to the effectiveness of V_{MLN} in these cells. The differential inhibition of Aurora Kinases is more apparent when we look at the effect V_{MLN} has on their basal activation in MCF-7 cells, inhibiting ~94% endogenous AURKA activity without affecting AURKB at all (Figure 5.10). This when compared to the free drug that inhibits AURKA (54%) and AURKB (28%) makes V_{MLN} more effective at these concentrations.

The fact that V_{MLN} can deliver this dramatically improved inhibitionfor AURKA over AURKB in cells, makes it a particularly relevant tool in understanding the differential role AURKA vs AURKB could have in cellular processes, like mitosis[70], migration[71], ciliary disassembly[72], centrosome amplification, aneuploidy and cell viability[73]. During mitosis AURKA inhibition using MLN8237 (500nM – 0.5μM) or AURKB inhibition using AZD 1152 (60nM – 0.06μM) can both disrupt CenpE phosphorylation to regulate chromosome alignment. At these concentrations, MLN8237 inhibits not only AURKA but also AURKB[33], which we have seen in our studies as well (data not shown). Treating cells with V_{MLN} will allow us to specifically inhibit AURKA directly helping discern its contribution relative to AURKB in such a cellular process.
Similarly, with AURKA known to differentially regulate RalA (but not RalB)[8], V_{MLN} mediated inhibition of AURKA can also act as an effective tool to test for an AURKA-RalA crosstalk in cellular pathways and cancers. In the absence of oncogenic Ras in MCF-7 cells, such an AURKA-RalA crosstalk we now discover effectively drives anchorage-independent growth. The ability of V_{MLN} to specifically inhibit RalA (but not RalB), unlike the free drug that affects neither, allows for us to detect such an AURKA-RalA crosstalk and test its effect on AIG. The Ral inhibitor, BQU57, while inhibiting RalA and RalB affects AIG comparable to V_{MLN}. This suggests RalA is the primary regulator of AIG in MCF-7 cells, with RalB not seen to affect RalA function. Having both inhibitors has now allowed us to determine the relative role RalA and RalB have along this pathway in a way that would not have been possible otherwise. AURKA mediated differential regulation of Ral is known to be through the phosphorylation of RalA on the Serine 194 residue, which affects its localization in cells.[74] The role RalA and RalB have along multiple pathways eg. downstream of integrin-mediated adhesion, is known to also be dependent on their localization (our unpublished data). V_{MLN} could now

provide a tool for us to evaluate the role AURKA dependent Ral localization and activation has along such pathways in normal and cancer cells. V_{MLN} nano-vesicles in specifically delivering MLN8237 and targeting Aurora Kinase A, overcome a major issue this inhibitor has faced in preclinical and clinical trials.[75] The stability and effectiveness of V_{MLN} in the above *in-vitro* studies raises the possibility of testing this nano-vesicle in animal tumor models.

5.3.5 Cisplatin Stitched and MLN 8237 Dual Drug Loaded Polysaccharide Vesicles:

The formed polysaccharide derivatives are vesicular in nature and hence provide an opportunity for dual drug loading to achieve better therapeutic efficacy from a single dose. Herein the results obtained from the V_{MLN} vesicles showed a very profound effect on the AIG growth of MCF 7 cells. It is also very well known fact that the MLN 8237 mediated aurora inhibition enhances the cisplatin induces the cell death in esophageal adenocarcinoma cells. Since in the present design we could specifically inhibit aurora kinase A at very low concentration (0.02μM) of inhibitor MLN 8237, combining this inhibitor with cisplatin drug could yield a better candidate to study the effect on AIG growth of the cancer cells. Hence cisplatin stitched vesicles discussed in chapter 2 have been used for the encapsulation of aurora inhibitor MLN 8237 to produce a V_{CPMLN} dual drug loaded polysaccharide vesicles. The schematics of the dual drug loaded vesicles ar showed in figure 5.13 a. The encapsulation studies and the morphological characterization of these dual loaded vesicles were carried out in the same way as discussed in the chapter 2, 3 and 4. The amount of cisplatin in these vesicles were carried out by OPD assay as discussed in chapter 2 and it was found to be 95μg/mg of the polymer. The amount of MLN 8237 in these vesicles was carried out by absorbtion spectroscopy and found to be 4.5μg/mg of the polymer. To study the cytotoxic effects of these dual drug loaded vesicle, two cisplatin resistant cell lines were selected namely A549 and Calu 1 cells. These cells were treated with free cisplatin and it was found that these cells are very resistant to cisplatin and does not showed a dell killing even at a concentration of 120 μg/mL (see figure 5.13 b and c) of cisplatin. This control experiment proves that the selection of these kinds of cells is important to understand the role of these two drugs have on growth of these cells.

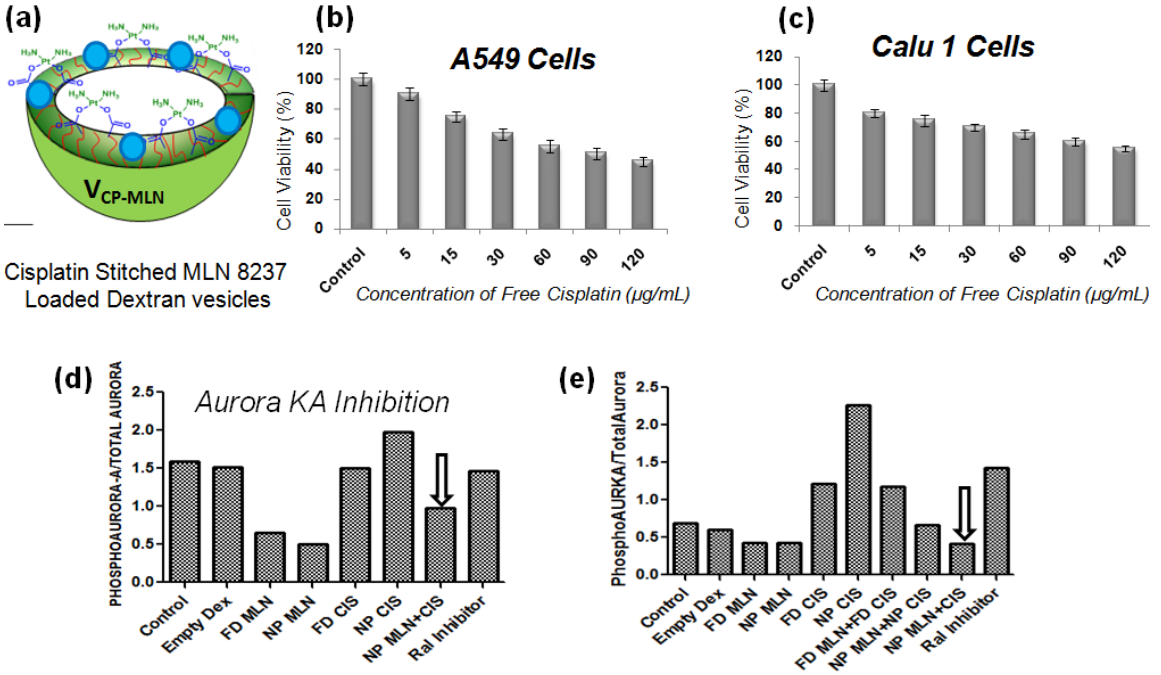

Figure 5.13: *Schematics of cisplatin stitched MLN 8237 dual drug loaded vesicles (a), A plot showing the cytotoxic effect of free cisplatin in A549 cells (b) and Calu 1 cells (c), the effect of V_{CPMLN} on aurora kinase inhibition along with other controls in A5499 cells (d) and in Calu1 Cells (e).The concentration of cisplatin and MLN 8237 used for this experiment was 2 and 0.04 µg/mL respectively.*

The effect of these dual drug loaded vesicles V_{CPMLN} on the aurora kinase inhibition of both the cell lines was studied by western blot analysis and the data is showed in figure 5.13 d and e. It has been observed that these dual drug loaded vesicles showed good to moderate inhibition of the aurora kinase A in both the cell lines. These results are almost similar to that has obtained from the V_{MLN} vesicles. Thus, it is important to monitor the effect of these vesicles on both cytotoxicity of the cells and aurora kinase inhibition. The experiments to investigate these effects are in progress and will be carried out as part of future project or by other juniors. The above discussed work will be the part of this thesis and other remaining work will be done by other colleagues who are continuing this work.

5.4 Conclusion

In conclusion, the present study highlights one of the first examples of a polymer nanovesicle being used for encapsulation and delivery of the Aurora Kinase A (AURKA) inhibitor MLN8237 to preferentially target AURKA and RalA downstream. This significantly inhibits the anchorage-independent growth of breast cancer cells. The polymer nanovesicleis constructed by modifying dextran with a renewable hydrophobic unit through analiphatic ester linkage. The dextran vesicles were self-assembled as < 200 nm nano-carriers, their morphological features confirmed by various microscopic techniques such as AFM and TEM. They were hence used for loading MLN8237 (V_{MLN}) with Rhodamine ($V_{MLN+RhB}$), their cellular internalization confirmed by confocal microscopy in 2D and 3D microenvironments. These nanovesicles could be degraded by enzymes in the intracellular lysosomal compartments. Lysotracker experiments further proved these vesicles to indeed be localized in lysosomes and digested by resident esterase enzymes to release the drug in a controlled manner.V_{MLN} thus allows for lower concentrations (0.02 to 0.04μM) of the drug to enter the cell and inhibit AURKA many fold better than free MLN8237. This effectiveness of the drug at low concentrations in the nanovesicle further supports better inhibition of AURKA over AURKB. This AURKA inhibition remarkably targets downstream RalA activation (but not RalB) suppressing the anchorage-independent growth of breast cancer cells embedded in 3D agarose gels. This establishes the presence of an AURKA–RalA crosstalk in breast cancer cells that controls their anchorage independence. These results make the dextran nano-vesicles effective candidates for delivering the poorly soluble MLN8237 to better target AURKA and its downstream signalling (through RalA) in cancers. Further this inhibitor MLN 8237 was encapsulated in cisplatin stitched vesicles to study the effect of both these drugs together have on the growth of the cancer cells. For this purpose, a cisplatin resistant cell lines were selected and it has been observed that these vesicles have a good to moderate effect on the aurora kinase inhibition even in the dual drug loaded case. Thus, it is has been observed that the encapsulation of other drug in these nanovesicles does not alter the activity of the MLN 8237 loaded vesicles.

5.5 References

1. Camonis, J. H., and White, M. A. *Trends Cell Biol*. **2005**, *15*, 327–332.
2. Gentry, L. R., Martin, T. D., Reiner, D. J., and Der, C. J *BBA – Mol. Cell Res*. **2014**, *1843*, 2976–2988.
3. Gentry, L. R., Nishimura, A., Cox, A. D., Martin, T. D., Tsygankov, D., Nishida, M., Elston, T. C., and Der, C. J. *J. Biol. Chem.***2015**, *290*, 22851–22861.
4. Chien, Y., and White, M. A. *EMBO reports*. **2003**, *4*, 800–806.
5. Bodemann, B. O., and White, M. A. *Nat. Rev. Cancer*. **2008**, *8*, 133–140.
6. Mori, S., Chang, J. T., Andrechek, E. R., Matsumura, N., Baba, T., Yao, G., Kim, J. W., Gatza, M., Murphy, S., and Nevins, J. R. *Oncogene*. **2009**, *28*, 2796–2805.
7. Yan, C., Liu, D., Li, L., Wempe, M. F., Guin, S., Khanna, M., Meier, J., Hoffman, B., Owens, C., Wysoczynski, C. L., Nitz, M. D., Knabe, W. E., Ahmed, M., Brautigan, D. L., Paschal, B. M., Schwartz, M. A., Jones, D. N. M., Ross, D., Meroueh, S. O., and Theodorescu, D *Nature*. **2014**, *515*, 443–447.
8. Lim, K. H., Brady, D. C., Kashatus, D. F., Ancrile, B. B., Der, C. J., Cox, A. D., and Counter, C. M. *Mol. Cell. Biol*. **2009**, *30*, 508–523.
9. Kashatus, D. F., Lim, K.-H., Brady, D. C., Pershing, N. L. K., Cox, A. D., and Counter, C. M. *Nat. Cell Biol*. **2011**, *13*, 1108–1115.
10. Vader, G., and Lens, S. M. A. *BBA - Rev Cancer*. **2008**, *1786*, 60–72.
11. Ohashi, S., Sakashita, G., Ban, R., Nagasawa, M., Matsuzaki, H., Murata, Y., Taniguchi, H., Shima, H., Furukawa, K., and Urano, T. *Oncogene*. **2006**, *25*, 7691–7702.
12. Ferrari, S., Marin, O., Pagano, M. A., Meggio, F., Hess, D., El-Shemerly, M., Krystyniak, A., and Pinna, L. A. *Biochem. J.***2005**, *390*, 293–302.
13. Carmena, M., and Earnshaw, W. C. *Nat. Rev. Mol. Cell Biol*. **2003**, *4*, 842–854.
14. Nikonova, A. S., Astsaturov, I., Serebriiskii, I. G., Dunbrack, R. L., and Golemis, E. A. *Mol. Life Sci.***2012,** *70*, 661–687.
15. Li, S., Deng, Z., Fu, J., Xu, C., Xin, G., Wu, Z., Luo, J., Wang, G., Zhang, S., Zhang, B., Zou, F., Jiang, Q., and Zhang, C. *J Biol Chem.***2015**, *290*, 17546–17558.
16. Bolton, M. A., Lan, W., Powers, S. E., McCleland, M. L., Kuang, J., and Stukenberg, P. T. *Mol. Biol. Cell*. **2002**, *13*, 3064–3077.
17. Yasui, Y., Urano, T., Kawajiri, A., Nagata, K. I., Tatsuka, M., Saya, H., Furukawa, K., Takahashi, T., Izawa, I., and Inagaki, M. *J Biol Chem.***2004**, *279*, 12997–13003.
18. Giet, R., Petretti, C., and Prigent, C. *Trends Cell Biol*. **2005**, *15*, 241–250.
19. Mehra, R., Serebriiskii, I. G., Burtness, B., Astsaturov, I., and Golemis, E. A. *Lancet Oncol*. **2013**, *14*, e425–e435.

20. Jeng, Y.-M., Peng, S.-Y., Lin, C.-Y., and Hsu, H.-C. *Clin.Cancer Res*. **2004**, *10*, 2065–2071.
21. Furukawa, T., Kanai, N., Shiwaku, H. O., Soga, N., Uehara, A., and Horii, A. *Oncogene*. **2006**, *25*, 4831–4839.
22. Katsha, A., Belkhiri, A., Goff, L., and El-Rifai, W. *Mol. Cancer*. **2015**, *14*, 21–13.
23. Jiang, Y., Zhang, Y., Lees, E., and Seghezzi, W. *Oncogene*. **2003**, *22*, 8293–8301.
24. Tseng, Y.-S., Lee, J.-C., Huang, C.-Y. F., and Liu, H.-S. *BMC Cancer*. **2009**, *9*, 21–12.
25. Neel, N. F., Martin, T. D., Stratford, J. K., Zand, T. P., Reiner, D. J., and Der, C. J. *Genes Cancer*. **2011**, *2*, 275–287.
26. Yu, Y., and Feig, L. A. *Oncogene*. **2002**, *21*, 7557–7568.
27. Feig, L. A. *Trends Cell Biol*. **2003**, *13*, 419–425.
28. Balasubramanian, N., Meier, J. A., Scott, D. W., Norambuena, A., White, M. A., and Schwartz, M. A. *Curr. Biol*. **2010**, *20*, 75–79.
29. Pawar, A., Meier, J. A., Dasgupta, A., Diwanji, N., Deshpande, N., Saxena, K., Buwa, N., Inchanalkar, S., Schwartz, M. A., and Balasubramanian, N. *Cell Signal*. **2016**, *28*, 1225–1236.
30. Yan, A., Wang, L., Xu, S., and Xu, J. *Drug Discov Today*. **2011**, *16*, 260–269.
31. Yan, C., Liu, D., Li, L., Wempe, M. F., Guin, S., Khanna, M., Meier, J., Hoffman, B., Owens, C., Wysoczynski, C. L., Nitz, M. D., Knabe, W. E., Ahmed, M., Brautigan, D. L., Paschal, B. M., Schwartz, M. A., Jones, D. N. M., Ross, D., Meroueh, S. O., and Theodorescu, D. *Nature*. **2014**, *515*, 443–447.
32. de Groot, C. O., Hsia, J. E., Anzola, J. V., Motamedi, A., Yoon, M., Wong, Y. L., Jenkins, D., Lee, H. J., Martinez, M. B., Davis, R. L., Gahman, T. C., Desai, A., and Shiau, A. K. A *Front Oncol*. **2015**, *5*, 285.
33. Sells, T. B., Chau, R., Ecsedy, J. A., Gershman, R. E., Hoar, K., Huck, J., Janowick, D. A., Kadambi, V. J., LeRoy, P. J., Stirling, M., Stroud, S. G., Vos, T. J., Weatherhead, G. S., Wysong, D. R., Zhang, M., Balani, S. K., Bolen, J. B., Manfredi, M. G., and Claiborne, C. F. *ACS Med ChemLett*. **2015**, *6*, 630–634.
34. Bearss, D. J. *SciTransl Med*. **2016**, *8*, 325fs4–325fs4.
35. Ashton, S., Song, Y. H., Nolan, J., Cadogan, E., Murray, J., Odedra, R., Foster, J., Hall, P. A., Low, S., Taylor, P., Ellston, R., Polanska, U. M., Wilson, J., Howes, C., Smith, A., Goodwin, R. J. A., Swales, J. G., Strittmatter, N., Takáts, Z., Nilsson, A., Andren, P., Trueman, D., Walker, M., Reimer, C. L., Troiano, G., Parsons, D., De Witt, D., Ashford, M., Hrkach, J., Zale, S., Jewsbury, P. J., and Barry, S. T. *SciTranslMed*. **2016**, *8*, 325ra17–325ra17.
36. Mizrahy, S., and Peer, D. *Chem. Soc. Rev.* **2012,** *41*, 2623–2640.
37. Rodríguez-Hernández, J., and Lecommandoux, S. *J. Am. Chem. Soc.* **2005**, *127*, 2026–2027.

38. Deng, Z., Qian, Y., Yu, Y., Liu, G., Hu, J., Zhang, G., and Liu, S. *J. Am. Chem. Soc.* **2016**, *138*, 10452–10466.
39. Li, Y., Liu, G., Wang, X., Hu, J., and Liu, S. *Angew. Chem. Int. Ed.***2015**, *128*, 1792–1796.
40. Barenholz, Y. *J. Control. Release,* **2012,** *160***,** 117-134.
41. Canta, A.; Chiorazzi, A.; Meregalli, C.; Oggioni, N.; Sala, B.; Crippa, L.; Avezza, F.; Foretieri, D.; Rotella, G.; Zucchetti, M.; Cavaletti, G. *Cancer Chemother. Pharmacol*, **2011**, *68*, 1001-1008.
42. Pozzi, D.; Colapicchioni, V.; Caracciolo, G.; Piovesana, S.; Capriotti, A.L.; Palchetti, S.; Grossi, S. D.; Ricciolo, A.; Amenitsch, H.; Logana, A. *Nanoscale*, **2014**, *6*, 2782-2792.
43. Palcchetti, S.; Colapicchioni, V.; Digiacomo, L.; Caracciolo, G.; Pozzi, D.; Capriotti, A. L.; Barbera, G. L.; Lagana, A. *Biochimica et BiophysicaActa*, **2016**, *1858*, 189-196.
44. Allen, M. J.; Leaderach, A.; Reilly, P. J.; Mason, R. J. *Biochemistry*.**2001**, *40*, 7789-7798.
45. Hoai, N. T.; Sasaki, A.; Sasaki, M.; Kaga, H.; Kakuchi, T.; Satoh, T. *Biomacromolecules.***2011,***12*, 1891-1899.
46. Lemarchand, C.; Gref, R.; Passirani, C.; GArcion, E.; Petri, B.; Muller, R.; Constantini, D.; Couvreur, P. *Biomaterials.***2006**, *27*, 108-118.

47. Jang, W.-S., Park, S. C., Reed, E. H., Dooley, K. P., Wheeler, S. F., Lee, D., and Hammer, D. A. *Soft Matter*. **2016**, *12*, 1014–1020
48. Feng, A., and Yuan, J. *Macromol Rapid Commun*. **2014**, *35*, 767–779.
49. Molla, R., M. , Rangadurai, P. ; Pavan, G., M. ; Thayumanavan, S. *Nanoscale*, **2015**, *7*, 3817-3837.
50. Azagarswamy, A., M. ; Sokkalingam, P. ; Thayumanavan S. *J. Am. Chem. Soc.***2009**, *131*, 14184-14185.
51. Pramod, P. S., Takamura, K., Chaphekar, S., Balasubramanian, N., and Jayakannan, M. *Biomacromolecules*. **2012**, *13*, 3627–3640.
52. Pramod, P. S., Shah, R., and Jayakannan, M. *Nanoscale*. 2015, **7**, 6636–6652.
53. Deshpande, N. U., and Jayakannan, M. *Biomacromolecules*. **2017**, *18*, 113–126.
54. Pramod, P. S., Shah, R., Chaphekar, S., Balasubramanian, N., and Jayakannan, M. *Nanoscale*. **2014**, *6*, 11841–11855.
55. Surnar, B.; Jayakannan, M. *Biomacromolecules*, **2016**, *17*, 4075-4085.
56. Surnar, B. ;Sharam, K.; Jayakannan, M. *Nanoscale*, **2015**, *7*, 17964-17979.
57. Saxena, S.; Jayakannan, M. *Biomacromolecules*, *2017*, *18*, 2594-2609.
58. Balchandran, S. V.; Jadhav, S.R.; Vemula, K.V.; John, G. *Chem. Soc. Rev.***2013**, *42*, 427-438.

59. Xu, G., Zhang, W., Ma, M. K., and McLeod, H. L. *Clin. Cancer Res*. **2002**, *8*, 2605–2611.
60. Alter, S. C., Metcalfe, D. D., Bradford, T. R., and Schwartz, L. B.. *Biochem. J*.**1987**, *248*, 821–827.
61. Pramod, P. S., Deshpande, N. U., and Jayakannan, M. *J. Phy. Chem. B*. **2015**, *119*, 10511–10523.
62. D'Assoro, A. B., liu, T., Quatraro, C., Amato, A., Opyrchal, M., Leontovich, A., Ikeda, Y., Ohmine, S., Lingle, W., Suman, V., Ecsedy, J., Iankov, I., Di Leonardo, A., Ayers-Inglers, J., Degnim, A., Billadeau, D., McCubrey, J., Ingle, J., Salisbury, J. L., and Galanis, E. *Oncogene*. **2014**, *33*, 599–610.
63. Noh, E.-M., Lee, Y.-R., Hong, O.-Y., Jung, S. H., Youn, H. J., and Kim, J.-S. *Oncol. Rep.***2015**, *34*, 803–810.
64. Vasquez, R. J., Howell, B., Yvon, A. M., Wadsworth, P., and Cassimeris, L. *MolBiol Cell*. **1997**, *8*, 973–985.
65. Jordan, M. A., Thrower, D., and Wilson, L. *J. Cell Sci*. **1992**, *102(Pt 3)*, 401–416.
66. Littlepage, L. E., Wu, H., Andresson, T., Deanehan, J. K., Amundadottir, L. T., and Ruderman, J. V. *Proc. Natl .Acad. Sci. USA,* **2002**, *99*, 15440–15445.
67. Rosner, M., Schipany, K., and Hengstschläger, M. *Nat Protoc*. **2013**, *8*, 602–626.
68. Wu, J. C., Chen, T. Y., Yu, C. T. R., Tsai, S. J., Hsu, J. M., Tang, M. J., Chou, C. K., Lin, W. J., Yuan, C. J., and Huang, C. Y. F. *J. Biol. Chem*. **2005**, *280*, 9013–9022.
69. Katz, J., Finlay, T. H., Banerjee, S., and Levitz, M. *J. Steroid Biochem.***1987**, *26*, 687–692.
70. Carmena, M., Ruchaud, S., and Earnshaw, W. C. *Curr. Opin. Cell Biol*. **2009**, *21* , 796–805.
71. Mahankali, M., Henkels, K. M., Speranza, F., and Gomez-Cambronero, J. *J. Cell Sci*. **2015**, *128*, 516–526.
72. Pugacheva, E. N., Jablonski, S. A., Hartman, T. R., Henske, E. P., and Golemis, E. A. *Cell*. **2007**, *129*, 1351–1363.
73. Fu, J., Bian, M., Jiang, Q., and Zhang, C. *Mol. Cancer Res*. **2007**, *5*, 1–10.
74. Lim, K. H., Brady, D. C., Kashatus, D. F., Ancrile, B. B., Der, C. J., Cox, A. D., and Counter, C. M. *Mol.Cell. Biol*. **2009**, *30*, 508–523.
75. Tayyar, Y., Jubair, L., Fallaha, S., and McMillan, N. A. J. *Crit. Rev. Oncol. Hematol*. **2017**, *119*, 59–65.

6.0 Overall Summary and Future Direction

This thesis work mainly focussed on the design and development of the new polysaccharide vesicles for bioimaging and drug delivery application in cancer treatment. For this purpose a biocompatible polysaccharide dextran was chosen and modified with a hydrophobic unit pentadecyl phenol obtained from cashew nut shell liquid. Along with these the polysaccharide backbone was also modified with functional handle and fluorophores which provides opportunity for drug conjugation. The structures chosen in the current study have been obtained from the natural resources and are biocompatible in nature. Hence, the newly designed polysaccharide vesicles are made from natural resources and are very useful for biomedical application.

Polysaccharide dextran was anchored with self-assembly directing renewable hydrophobic unit 3-pentadecylphenol (PDP) along with carboxyl functionality which enables the vesicle formation as well as cisplatin drug conjugation. The vesicles were found to retain their size and shape in the cisplatin-stitched form and also exhibited excellent encapsulation capability for water soluble DOX and water insoluble CPT in the core and layer, respectively. The cisplatin-polymer conjugate was stabilized by the dextran vesicular geometry against the GSH drug detoxification which was very crucial for the delivery of the drugs in the active form in the cytoplasm. The vesicles are very unique to load all three drugs together in single platform to produce triple drug loaded nano-carriers. This triple drug loaded vesicle exhibited excellent synergistic killing in breast cancer cells at nanogram concentration level which is very remarkable for future therapeutic applications.

Biotin-conjugated dextran vesicles were made with multi-stimuli-responsiveness and employed them for receptor-mediated endocytosis to enhance the uptake of water soluble anticancer drug doxorubicin-hydrochloride (DOX.HCl) in cancer cell lines. Renewable resource hydrophobic unit consisting of glutathione-responsive disulfide bond and enzymatic-biodegrabale aliphatic ester linkage was tailor made and conjugated along with biotin on the dextran backbone to yield amphiphilic dextran. These newly designed biotin tagged dextran vesicles showed a three to four fold higher uptake of DOX. HCL in

cancer (HeLa) cells compared to non cancerous WYTMEF cells. This type of biotin tagged vesicles is very important to enhance the drug concentration at the site of action in the cancer treatment.

Further fluorescent polysaccharide vesicles were made as "Turn ON" theranostics probe for doxorubicin delivery to breast cancer cells. Polysaccharide derivatives were constructed by substituting a pentadecyl phenol and AIE probe TPE on polymer backbone. These fluorescent vesicles were explored for encapsulation of different red coloured dyes which showed efficient fluorescence resonance transfer phenomenon (FRET). These dye loaded vesicles can be used for bioimaging application in the biomedical field. Furthermore, acid functionalized blue luminescent vesicles were produced for cisplatin conjugation and their utility for real time monitoring of cisplatin drug release was showed in breast cancer cells.

These polysaccharide nanovesicles were employed for encapsulation and delivery of the Aurora Kinase A (AURKA) inhibitor MLN8237 to preferentially target AURKA and RalA downstream. This significantly inhibits the anchorage-independent growth of breast cancer cells. These nanovesicles could effectively inhibit AURKA over AURKB at very low concentrations of the drug (0.02-0.04 μM). This AURKA inhibition remarkably targets downstream RalA activation (but not RalB) suppressing the anchorage-independent growth of breast cancer cells embedded in 3D agarose gels. Thus, these polysaccharide vesicles were found to be of various applications in the cancer treatment.

Future Direction

The current thesis work deals with the development of targeted and fluorescent multiresponsive polysaccharide vesicles by carefully modifying the polysaccharide backbone. So the targeting and fluorescence property was combined and a new polysaccharide derivative was developed for real time monitoring and delivery of non fluorescent drugs. Cisplatin is routinely used anticancer drug but its nonfluorescent nature limits its application. To deliver such non fluorescent drug and to achieve a site specific delivery of the drugs, a polysaccharide design was developed which consist of a biotin as a targeting ligand, tetraphenylethene as fluorophore and acid functionality which allows the conjugation of the cisplatin. Hence the newly designed polysaccharide derivatives are the ideal nanocarriers since they are equipped with all the necessary groups according to the Ringsdorf model of drug delivery systems for polymers. Moreover the formed derivatives after cisplatin stitching retain its vesicular nature and hence this approach can be extended for other drugs or dyes as well. Thus, this newly designed polysaccharide vesicles provides an opportunity to achieve better therapeutic effects from the drug molecules and the current work is going on in that direction.

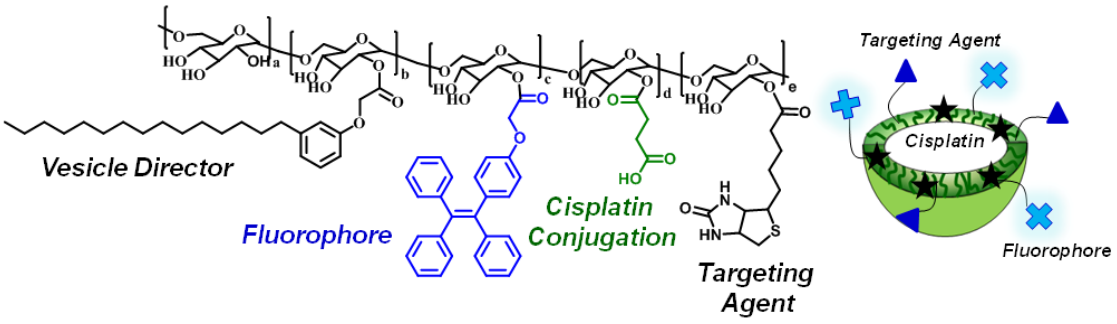

Since these formed polysaccharide derivatives are vesicular in nature, there application can be extended to encapsulation of different water soluble and water insoluble drugs or dyes and subsequently they can be used for delivery or bioimaging application. This vesicle also provides an opportunity for encapsulation of two different drugs or dyes in the same vesicles and brings them in close proximity where the effective energy transfer process can happen. Hence these vesicles are used for encapsulation of different dyes and

drugs and their self assembly studies have been carried out. Currently the cellular uptake and cytotoxicity studies of these drug and dye encapsulated vesicles is in progress.

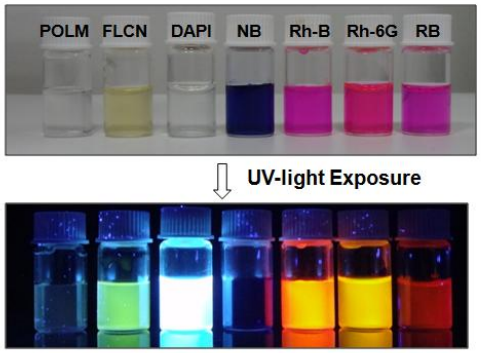

POLM = Polymer Alone FNCN= Fluoroscein, NB= Nile Blue, Rh-B= Rhodamin B, Rh6g= Rhodamin 6G, RB= Rose Bengal

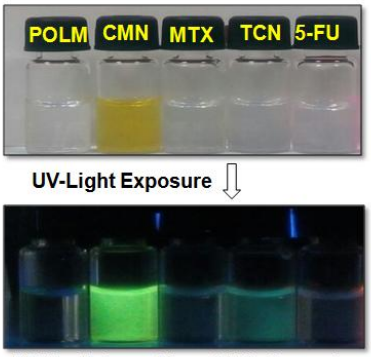

POLM = Polymer Alone, CMN= Curcumin, MTX= Methotrexate, TCN= Topotecan. HCL, 5FU= 5 Fluoro Uracil.

Thus, this polysaccharide vesicle can be used for diverse application and a potential to be a good nanocarriers to be used in biomedical application.

List of Publications

1. Deshpande, N. U.; Jayakannan, M. Biotin-Tagged Polysaccharide Vesicular Nanocarriers for Receptor-Mediated Anticancer Drug Delivery in Cancer Cells. **Biomacromolecules, 2018,** 19, 3572-3585.
2. Inchanalkar, S.*; Deshpande, N.U.*; Kasherwal, V.; Jayakannan, M.; Balasubramanian, N. Polymer Nanovesicle mediated delivery of MLN8237 preferentially inhibits Aurora Kinase A to target RalA and Anchorage-Independent Growth in Breast Cancer Cells. **Mol Pharmaceutics**, 2018, 15, 3046-3059. * Equal contribution
3. Deshpande, N. U.; Jayakannan, M. Cisplatin-Stitched Polysaccharide Vesicles for Synergistic Cancer Therapy of Triple Antagonistic Drugs. **Biomacromolecules**, **2017**, 18, 113- 126.
4. Pramod, P. S.; Nilesh, U. D.; Jayakannan, M. Real-time Drug Release Analysis of Enzyme and pH Responsive Polysaccharide Nano-vesicles, **J. Phys. Chem. B**. 2015, 119, 10511 - 10523. (not included in the thesis).
5. Deshpande, N. U.; Jayakannan, M., AIE Fluorophore Tagged Theranostic Polysaccharide Vesicles for Cancer Treatment. (Manuscript Under Preparation)
6. Deshpande, N. U.; Jayakannan, M., Biotin Tagged Fluorescent Polysaccharide Vesicles for Cisplatin Delivery to Breast cancer Cells. (Manuscript Under Preparation)
7. Deshpande, N.U.; Jayakannan, M. Multiple Drug/Dye Encapsulated Polysaccharide Vesicles for Drug Delivery and Bioimaging in Cancer Cells. (Manuscript Under Preparation)

Conferences and Symposia

1. Attended and presented poster at International Conference on Bioorganic Chemistry (ISBOC-10) Conference held at IISER Pune during 11th - 15th January 2015, Pune. Received best poster award in the conference.
2. Attended and presented poster at MACRO 2015 Conference held at IACS Kolkatta, India during 23rd - 26th January 2015.
3. Attended and presented poster at International Conference on Direct Digital Manufacturing and Polymers (ICDDMAP) Conference held at Karnataka University , Dharwad, India during 28th – 31st October 2015. Received best poster award in the conference.
4. Attended and presented poster at Peptide engineering meeting (PEM-10) Conference held at IISER Pune , Pune, India during 5th – 7th December 2015.
5. Attended and presented poster at MACRO 2017 Conference held at Thiruvananthapuram, India during 8th - 11th January 2017.
6. Attended and delivered Oral presentation at IUPAC-FAPS Polymer Congress meeting during 11th- 13th October 2017 at International Convention centre (ICC), Jeju, South Korea.
7. Attended and delivered Oral presentation at MACRO 2018 held at IISER, Pune India, during 19th- 22nd December 2018.
8.

Article Highlighted in Biomacromolecules

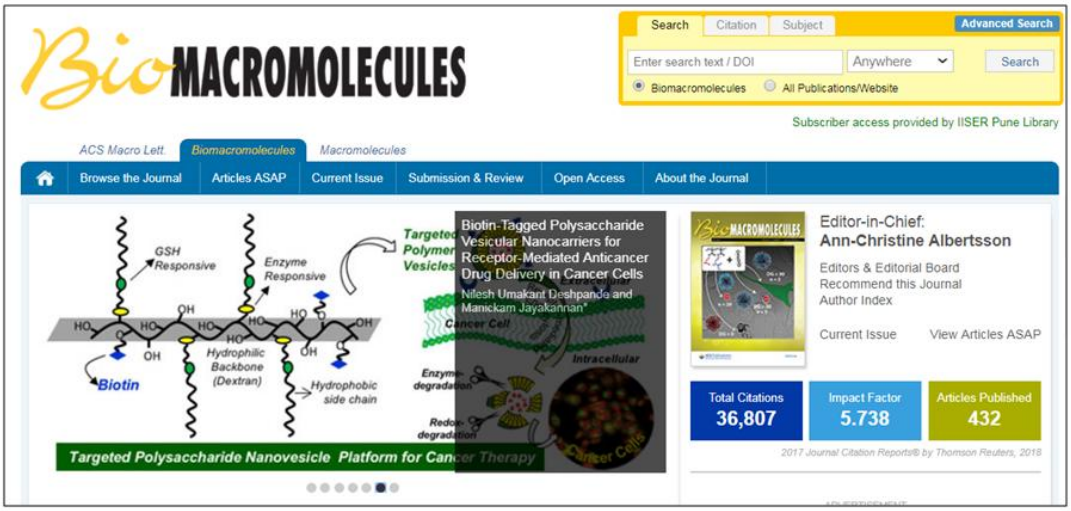

Chapter-2

Copyright Clearance Center RightsLink®

Home | Create Account | Help

ACS Publications Most Trusted. Most Cited. Most Read.

Title: Cisplatin-Stitched Polysaccharide Vesicles for Synergistic Cancer Therapy of Triple Antagonistic Drugs

Author: Nilesh Umakant Deshpande, Manickam Jayakannan

Publication: Biomacromolecules

Publisher: American Chemical Society

Date: Jan 1, 2017

Copyright © 2017, American Chemical Society

LOGIN

If you're a copyright.com user, you can login to RightsLink using your copyright.com credentials.

Already a RightsLink user or want to learn more?

PERMISSION/LICENSE IS GRANTED FOR YOUR ORDER AT NO CHARGE

This type of permission/license, instead of the standard Terms & Conditions, is sent to you because no fee is being charged for your order. Please note the following:

- Permission is granted for your request in both print and electronic formats, and translations.
- If figures and/or tables were requested, they may be adapted or used in part.
- Please print this page for your records and send a copy of it to your publisher/graduate school.
- Appropriate credit for the requested material should be given as follows: "Reprinted (adapted) with permission from (COMPLETE REFERENCE CITATION). Copyright (YEAR) American Chemical Society." Insert appropriate information in place of the capitalized words.
- One-time permission is granted only for the use specified in your request. No additional uses are granted (such as derivative works or other editions). For any other uses, please submit a new request.

Chapter-3

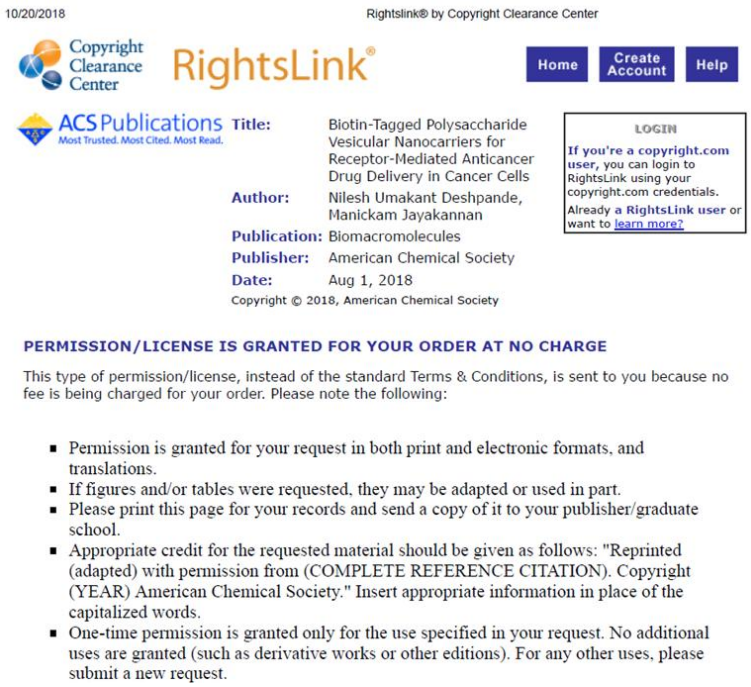

10/20/2018 Rightslink® by Copyright Clearance Center

Copyright Clearance Center RightsLink®

Home | Create Account | Help

ACS Publications Most Trusted. Most Cited. Most Read.

Title: Biotin-Tagged Polysaccharide Vesicular Nanocarriers for Receptor-Mediated Anticancer Drug Delivery in Cancer Cells

Author: Nilesh Umakant Deshpande, Manickam Jayakannan

Publication: Biomacromolecules

Publisher: American Chemical Society

Date: Aug 1, 2018

Copyright © 2018, American Chemical Society

LOGIN

If you're a copyright.com user, you can login to RightsLink using your copyright.com credentials.

Already a RightsLink user or want to learn more?

PERMISSION/LICENSE IS GRANTED FOR YOUR ORDER AT NO CHARGE

This type of permission/license, instead of the standard Terms & Conditions, is sent to you because no fee is being charged for your order. Please note the following:

- Permission is granted for your request in both print and electronic formats, and translations.
- If figures and/or tables were requested, they may be adapted or used in part.
- Please print this page for your records and send a copy of it to your publisher/graduate school.
- Appropriate credit for the requested material should be given as follows: "Reprinted (adapted) with permission from (COMPLETE REFERENCE CITATION). Copyright (YEAR) American Chemical Society." Insert appropriate information in place of the capitalized words.
- One-time permission is granted only for the use specified in your request. No additional uses are granted (such as derivative works or other editions). For any other uses, please submit a new request.

Chapter-5

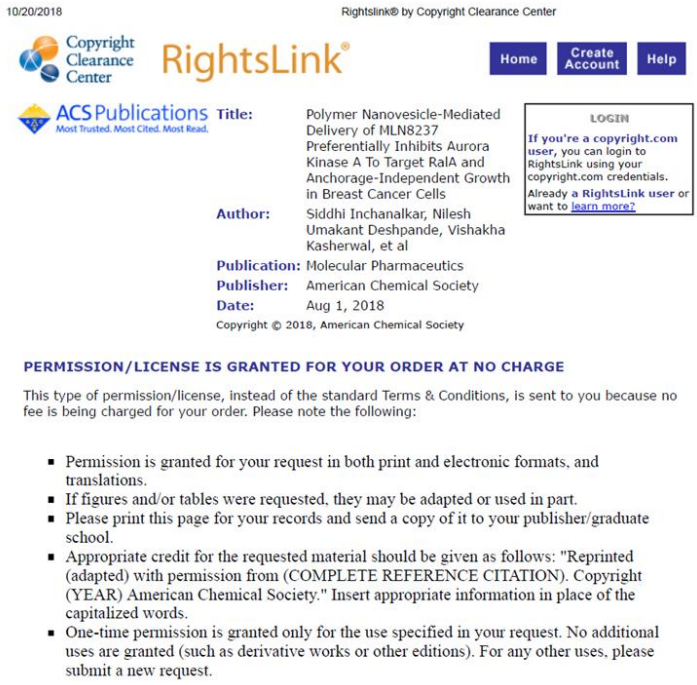

10/20/2018 Rightslink® by Copyright Clearance Center

Copyright Clearance Center RightsLink® Home Create Account Help

ACS Publications Most Trusted. Most Cited. Most Read.

Title: Polymer Nanovesicle-Mediated Delivery of MLN8237 Preferentially Inhibits Aurora Kinase A To Target RalA and Anchorage-Independent Growth in Breast Cancer Cells

Author: Siddhi Inchanalkar, Nilesh Umakant Deshpande, Vishakha Kasherwal, et al

Publication: Molecular Pharmaceutics

Publisher: American Chemical Society

Date: Aug 1, 2018

Copyright © 2018, American Chemical Society

LOGIN

If you're a copyright.com user, you can login to RightsLink using your copyright.com credentials.

Already a RightsLink user or want to learn more?

PERMISSION/LICENSE IS GRANTED FOR YOUR ORDER AT NO CHARGE

This type of permission/license, instead of the standard Terms & Conditions, is sent to you because no fee is being charged for your order. Please note the following:

- Permission is granted for your request in both print and electronic formats, and translations.
- If figures and/or tables were requested, they may be adapted or used in part.
- Please print this page for your records and send a copy of it to your publisher/graduate school.
- Appropriate credit for the requested material should be given as follows: "Reprinted (adapted) with permission from (COMPLETE REFERENCE CITATION). Copyright (YEAR) American Chemical Society." Insert appropriate information in place of the capitalized words.
- One-time permission is granted only for the use specified in your request. No additional uses are granted (such as derivative works or other editions). For any other uses, please submit a new request.

BioMACROMOLECULES

Article

pubs.acs.org/Biomac

Cisplatin-Stitched Polysaccharide Vesicles for Synergistic Cancer Therapy of Triple Antagonistic Drugs

Nilesh Umakant Deshpande and Manickam Jayakannan*

Department of Chemistry, Indian Institute of Science Education and Research (IISER)-Pune, Dr. Homi Bhabha Road, Pune-411008, Maharashtra, India

Supporting Information

ABSTRACT: New cisplatin-stitched polysaccharide vesicular nanocarrier is developed for combination therapy of three clinical important antagonistic drugs together to accomplish synergistic cancer therapy in breast cancer treatment. Carboxylic functionalized dextran was tailor-made for the chemical conjugation of cisplatin, and a renewable hydrophobic unit was anchored in the backbone to interdigitize the chains to self-assemble as cisplatin-stitched polysaccharide nanovesicles. Water-soluble DNA-intercalating drug doxorubicin·HCl (DOX) and water insoluble topoisomerase type I inhibitor drug camptothecin (CPT) were encapsulated in these vesicles to produce dual or triple drug-loaded vesicular nanocarrier. This unique cisplatin, DOX and CPT triple drug-loaded dextran vesicles were stable in aqueous medium, and the vesicular geometry acted as a shield for Pt-polymer drug conjugate against glutathione (GSH) detoxification under physiological conditions. Lysosomal enzymes ruptured the nanovesicle exclusively at the intracellular compartments to deliver the combination of all three drugs simultaneously to maximize the therapeutic efficacies. In vitro cytotoxicity studies revealed that free cisplatin was highly detoxified by the GSH in breast cancer cells, whereas the enhanced stability of Pt-stitched dextran vesicle against GSH facilitated ~99% cell killing in breast cancer cells. Combination therapy studies revealed that the free cisplatin, DOX, and CPT were found to be antagonistic to each other. Dual drug-loaded vesicles exhibited synergistic cancer cell killing while delivering these antagonistic drugs from a dextran vesicular platform. Remarkable synergistic cell killing was accomplished in cisplatin, DOX, and CPT triple drug-loaded vesicles at nanogram concentrations in breast cancer cells. The internalization of drugs and cellular uptake were confirmed by confocal microscope and flow cytometry analysis. The drugs were taken by the cancer cells in large amounts while delivering them from dextran vesicles compared to their free form. These spectacular results opened new opportunities for synergistic cancer therapy for GSH-overexpressed breast cancer using triple drug-loaded polysaccharide vesicular nanocarriers.

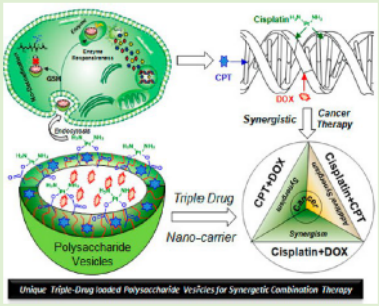

INTRODUCTION

Combination therapies are emerging as an important treatment protocol to overcome the Pt-drug resistance in breast and ovarian cancers at the second and third levels of chemotherapy to improve the patient compliance and survival against metastasis.[1,2] The inherent ability of breast cancer tissues to develop resistance against Pt-drugs directly associated with various biochemical processes including glutathione (GSH) overexpression, poor uptake of the anticancer drugs, DNA autorepair mechanism, and so on so forth.[3] Breast (also ovarian) cancer tissues are estimated to be overexpressed with glutathione (GSH, 20 mM) compared to normal tissues (1.0 mM);[4,5] as a result, the highly reactive Pt drugs were readily detoxified by the GSH through the formation of a stable Pt−S bond and excreted from the cytoplasm prior to their action at the nucleus.[6−8] The absence or low expression of CTR1 protein in the cell membrane was also responsible for the poor transportation of the Pt drug. The DNA autorepairing process at the Pt-guanine-N_7 position by NER proteins was also accounted for cell proliferation, increasing the chances of metastasis.[9] To overcome some of these limitations, combination therapy was developed for cisplatin (CP), along with DNA-specific drugs such as doxorubicin (DOX),[10−12] paclitaxel,[13−15] and so on. The cellular uptakes of the Pt drugs were improved using small molecular nanovectors[16−21] and polymeric nanocarriers[11−13,22−35] to accumulate them at the cancer tissues via enhanced permeability and retention (EPR) effect.[36−38] Polymer nanovesicles[39−44] (or polymersomes) and liposomes[45] are excellent choice for this purpose since they are capable of loading both water insoluble and water-soluble anticancer drugs simultaneously in the hydrophobic layer and hydrophilic core, respectively. Cisplatin-loaded liposomes were developed to enhance the membrane protein trafficking,[46] efficacy in triple negative breast cancer tumors,[47] and in glioma cells.[48] It was found that cisplatin encapsulation induced the usual rigidity in the liposome layers; however, they

Received: September 21, 2016
Revised: November 11, 2016
Published: November 22, 2016

DOI: 10.1021/acs.biomac.6b01411
Biomacromolecules 2017, 18, 113−126

Article

Cite This: Biomacromolecules 2018, 19, 3572−3585

pubs.acs.org/Biomac

Biotin-Tagged Polysaccharide Vesicular Nanocarriers for Receptor-Mediated Anticancer Drug Delivery in Cancer Cells

Nilesh Umakant Deshpande and Manickam Jayakannan*

Department of Chemistry, Indian Institute of Science Education and Research (IISER) Pune, Dr. Homi Bhabha Road, Pune 411008, Maharashtra, India

Supporting Information

ABSTRACT: Biotin-conjugated multistimuli-responsive polysaccharide vesicular nanocarriers are designed and developed, for the first time, to accomplish receptor-mediated endocytosis in cancer cells and to deliver anticancer drugs to intracellular compartments. For this purpose, a new renewable hydrophobic unit was custom designed with redox-degradable disulfide and enzyme-biodegradable aliphatic ester chemical linkages, and it was conjugated along with biotin on the dextran backbone. The dextran derivative self-assembled into nanovesicles of <200 nm in size, which were characterized by dynamic and static light scattering, electron, and atomic force microscopes. Avidin-HABA assay established the high affinity of biotin-tagged dextran vesicles toward membrane-receptors up to 25 nM concentration. Doxorubicin−hydrochloride (DOX.HCl)-loaded dextran vesicles exhibited stable formulation in phosphate-buffered saline (PBS) and fetal bovine serum (FBS). Redox-degradation by glutathione (GSH) showed 60% drug release, whereas lysosomal esterase enzyme enabled >98% drug release in 12 h. Confocal microscope and flow cytometry-assisted time-dependent cellular uptake studies revealed that the biotin-receptors overexpressed in cervical cancer cells (HeLa) exhibited larger drug accumulation through the receptor-assisted endocytosis process. This process enabled the delivery of higher amount of DOX and significantly enhanced the killing in cancer cells (HeLa) compared to wild-type mouse embryonic fibroblast cells (WT-MEF, normal cells). Control experiments such as biotin pretreatment in cancer cells and energy-suppressed cellular uptake at 4 °C further supported the occurrence of receptor-mediated endocytosis by the biotin-tagged polymer vesicles. This report provides first insights into the targeted polysaccharide vesicle platform, and the proof-of-concept is successfully demonstrated in biotin receptor-overexpressed cervical cancer cells.

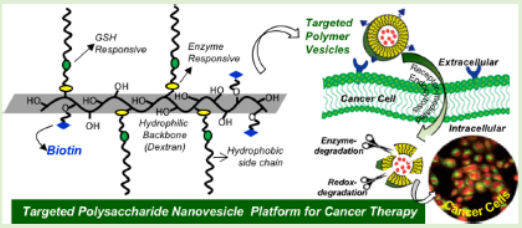

INTRODUCTION

Receptor-mediated endocytosis of nanocarriers is emerging as an important approach for targeted delivery of anticancer drugs or genes to cancer tissues under physiological conditions.[1−4] Cancer cells are overexpressed by a large number of signaling receptors for metastasis and also by enriching the nutrient supply to fast and uncontrolled cell growth.[5−7] These receptors exhibit high binding affinity toward targeting ligands such as biotin (vitamin B7),[8,9] folic acid[10−13], RGD peptide,[14] and tranSerrin,[15] etc. Nanoassemblies tagged with these targeting ligands enhance the delivery of payload at the cancer tissue site through receptor−ligand interaction.[3] Biotin is an excellent targeting ligand for streptavidin-type membrane proteins (avidin class of proteins) at the cell surface with high association constant[16] in the range of 10^{13} to 10^{15} M^{-1}. Various cancer cells such as cervical, breast, lung, and ovarian are overexpressed with biotin receptors.[17] Biotin-conjugated nanoassemblies from small molecules,[18] block copolymers,[19−21] dendrimers,[12] gold nanoparticles,[22] and carbon nanotubes,[23] etc. were explored for delivering chemotherapeutic agents. The polymer nanocarriers are particularly important since they have unique capability to passively selectively target the cancer tissue via enhanced permeability and retention effect (EPR).[24,25] Thus, the receptor-mediated endocytosis in macromolecular nanocarriers is an appropriate choice for both active and passive selective targeting of cancer tissues. Bioresource-based polymer nanocarriers have recently gained significant importance in the biomedical field.[26,27] Polysaccharide nanocarriers are unique bioresource systems due to their excellent biocompatibility associated with structural diversity,[28−31] and also possess a sugar-type macromolecular backbone for enhanced internalization via like−like interactions with lectins (carbohydrate-binding proteins) at the cell membrane.[32−34] Polysaccharide micelles,[35] nanoparticles,[36] capsules,[37] hydrogels,[38−40] and polymersomes (or vesicles)[28−31] were reported for drug and gene delivery. Among these nanocarriers; polysaccharide nanovesicles are very unique for delivering both water-soluble and water insoluble anticancer drugs from a single nanocarrier.[41] Earlier dextran vesicles using stearyl chains as hydrophobic units and

Received: May 25, 2018
Revised: June 14, 2018
Published: June 15, 2018

DOI: 10.1021/acs.biomac.8b00833
Biomacromolecules 2018, 19, 3572−3585

molecular pharmaceutics

Article

Cite This: Mol. Pharmaceutics 2018, 15, 3046−3059

Polymer Nanovesicle-Mediated Delivery of MLN8237 Preferentially Inhibits Aurora Kinase A To Target RalA and Anchorage-Independent Growth in Breast Cancer Cells

Siddhi Inchanalkar,[†,§] Nilesh Umakant Deshpande,[‡,§] Vishakha Kasherwal,[†] Manickam Jayakannan,[*,‡] and Nagaraj Balasubramanian[*,†]

[†]Department of Biology, [‡]Department of Chemistry, Indian Institute of Science Education and Research (IISER) Pune, Dr. Homi Bhabha Road, Pune 411008, Maharashtra, India

Supporting Information

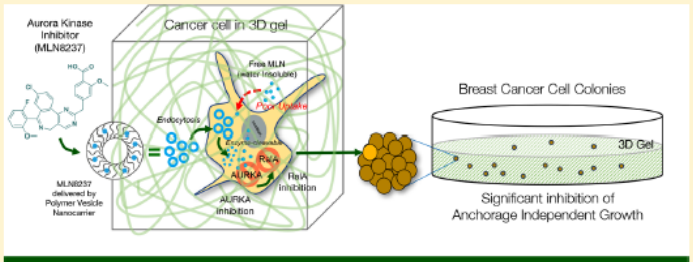

Nanovesicle platform mediated MLN8237 delivery inhibits AURKA - RalA pathway & anchorage independent growth of breast cancer cells

ABSTRACT: The small GTPase RalA is a known mediator of anchorage-independent growth in cancers and is differentially regulated by adhesion and aurora kinase A (AURKA). Hence, inhibiting AURKA offers a means of specifically targeting RalA (over RalB) in cancer cells. MLN8237 (alisertib) is a known inhibitor of aurora kinases; its specificity for AURKA, however, is compromised by its poor solubility and transport across the cell membrane. A polymer nanovesicle platform is used for the first time to deliver and differentially inhibit AURKA in cancer cells. For this purpose, polysaccharide nanovesicles made from amphiphilic dextran were used as nanocarriers to successfully administer MLN8237 (V_{MLN}) in cancer cells in 2D and 3D microenvironments. These nanovesicles (<200 nm) carry the drug in their intermembrane space with up to 85% of it released by the action of esterase enzyme(s). Lysotracker experiments reveal the polymer nanovesicles localize in the lysosomal compartment of the cell, where they are enzymatically targeted and MLN released in a controlled manner. Rhodamine B fluorophore trapped in the nanovesicles hydrophilic core ($V_{MLN+RhB}$) allows us to visualize its uptake and localization in cells in a 2D and 3D microenvironment. In breast cancer, MCF-7 cells V_{MLN} inhibits AURKA significantly better than the free drug at low concentrations (0.02−0.04 μM). This ensures that the drug in V_{MLN} at these concentrations can specifically inhibit up to 94% of endogenous AURKA without affecting AURKB. This targeting of AURKA causes the downstream differential inhibition of active RalA (but not RalB). Free MLN8237 at similar concentrations and conditions failed to affect RalA activation. V_{MLN}-mediated inhibition of RalA, in turn, disrupts the anchorage-independent growth of MCF-7 cells supporting a role for the AURKA−RalA crosstalk in mediating the same. These studies not only identify the polysaccharide nanovesicle to be an improved way to efficiently deliver low concentrations of MLN8237 to inhibit AURKA but, in doing so, also help reveal a role for AURKA and its crosstalk with RalA in anchorage-independent growth of MCF-7 cells.

KEYWORDS: *aurora kinase, AURKA, MLN8237, polymer nanovesicle, RalA, BQU57, anchorage-independent growth*

INTRODUCTION

Ras-like small GTPases RalA and RalB, as the name implies, were first identified based on their sequence similarity to the HRas, KRas, and NRas proteins. Human RalA and RalB, although being 82% identical,[1] are reported to play significant and divergent roles in normal and cancer phenotypes.[2] These isoforms diverge significantly in their C-terminal domain (50% identical), facilitating their differential post-translational modifications that further contribute to their distinct subcellular localization and function.[3] RalB is critical for the survival of tumor cells, and RalA is necessary for the anchorage-independent growth of cancer cells.[4,5] Anchorage-independent signaling and the growth of cancer cells are vital contributors to

Received: February 14, 2018
Revised: May 25, 2018
Accepted: June 4, 2018
Published: June 4, 2018

DOI: 10.1021/acs.molpharmaceut.8b00163
Mol. Pharmaceutics 2018, 15, 3046−3059

THE JOURNAL OF PHYSICAL CHEMISTRY B

Article

pubs.acs.org/JPCB

Real-Time Drug Release Analysis of Enzyme and pH Responsive Polysaccharide Nanovesicles

Poothayil Subash Pramod,[§] Nilesh Umakant Deshpande, and Manickam Jayakannan*

Department of Chemistry, Indian Institute of Science Education and Research (IISER)-Pune, Dr. Homi Bhabha Road, Pune 411008, Maharashtra, India

Supporting Information

ABSTRACT: The accurate estimation of drug release kinetics of polymeric vehicles is an indispensable prerequisite for the developments of successful drug carriers for cancer therapy. The present investigation reports the development of time-resolved fluorescence spectroscopic approach for the real-time release kinetics of fluorophore loaded polysaccharide vesicles that are potential vectors in cancer treatment. The polysaccharide vesicles were custom designed with appropriate enzyme and pH responsiveness and loaded with water-soluble biocompatible fluorophore Rhodamine B (Rh-B). The semi-permeable membrane dialysis method along with steady state absorbance spectroscopic technique was found to be inaccurate for the estimation of drug release. Time correlated single photon counting (TCSPC) technique was found to exhibit significant difference in excited state decay profiles and fluorescent lifetime of Rh-B in the free and polymer bound states. This enabled the establishment of real-time drug release protocols by TCSPC method for polysaccharide vesicles that are responsible to pH and enzyme with respect to intracellular compartments. Real-time analysis predicted the release kinetics 20−25% higher accuracy when compared to the dialysis method under in vitro conditions. Moreover, the ability of enzyme to cleave the polysaccharide vesicles was further validated by docking studies. The positioning of the molecules in active site of enzyme and the binding energy data were generated using AUTODOCK program to study the rupture of polysaccharide vesicles. This new TCSPC technique could be very useful for studying the drug release pattern of synthetic polymer vesicles loaded with Rh-B fluorophore.

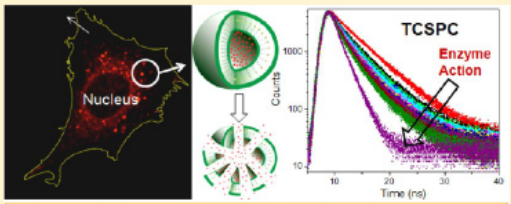

Real-time Drug Release Analysis of Polymer vesicles

INTRODUCTION

Tailor made polymeric structures have received tremendous attention in the recent past for controlled drug delivery in cancer treatment.[1,2] Self-organized polymeric structures such as micelles,[3] vesicles,[4] and nanoparticles[5,6] were found to undergo passive selectivity in cancer tissues through enhanced permeability and retention (EPR) effect.[7,8] Among all these assemblies, polymer vesicular assemblies are unique nano-scaffolds since they can be utilized for loading and delivering the combination of both hydrophilic and hydrophobic drugs.[9] Unlike the liposmes, the synthetic polymer vesicular drug carriers were found to be more stable under physiological conditions and in systemic circulation that are essential for the in vivo administration of drugs.[10] Cancer tissue or cancer related pathological inflammation is found to be overexpressed by enzyme, such as glutathione reductase[11] and esterase.[12,13] Enzyme responsive vesicles (or polymersomes) were developed to exploit the cancer tissue environment for selective and targeted delivery to cancer cells.[14,15] Nevertheless, there has been no effort taken until now to study the real-time drug release kinetics of enzyme responsive polymer vesicles to unlock the mechanism of enzyme action on the polymer backbone. Absorption spectroscopy analysis is routinely employed in combination with semipermeable membrane dialysis for the in vitro drug release kinetics.[16] Recent studies revealed that this approach had limitations due to the process by which the estimation of drug release analysis was performed.[17] Typically, the dialysis approach involved two steps: (i) the rupture of the polymer membrane and transportation of the loaded cargoes (or drugs) to the liquid medium inside the dialysis tube and (ii) transportation of the drug molecules from the dialysis tube to the outer reservoir by crossing the barrier of the dialysis membrane. These processes are rather different from the actual forces experienced by the polymer vesicles when they are administered in the cell in vitro or intravenous injection in vivo. As a consequence, most often the drug release kinetics profiles obtained from the dialysis method were found to be mismatched with the cellular cleavage of polymer nanoscaffolds.[17]

Reliable methods to calculate the in vitro drug release kinetics are necessary for establishing a good correlation between drug release capabilities and clinical effectiveness of formulation of synthetic polymer vesicles. Real-time analysis of drug release kinetics by in situ methods are very good protocols

Received: June 17, 2015
Revised: July 25, 2015
Published: August 3, 2015

DOI: 10.1021/acs.jpcb.5b05795
J. Phys. Chem. B 2015, 119, 10511−10523

Appendix

Chapter-2

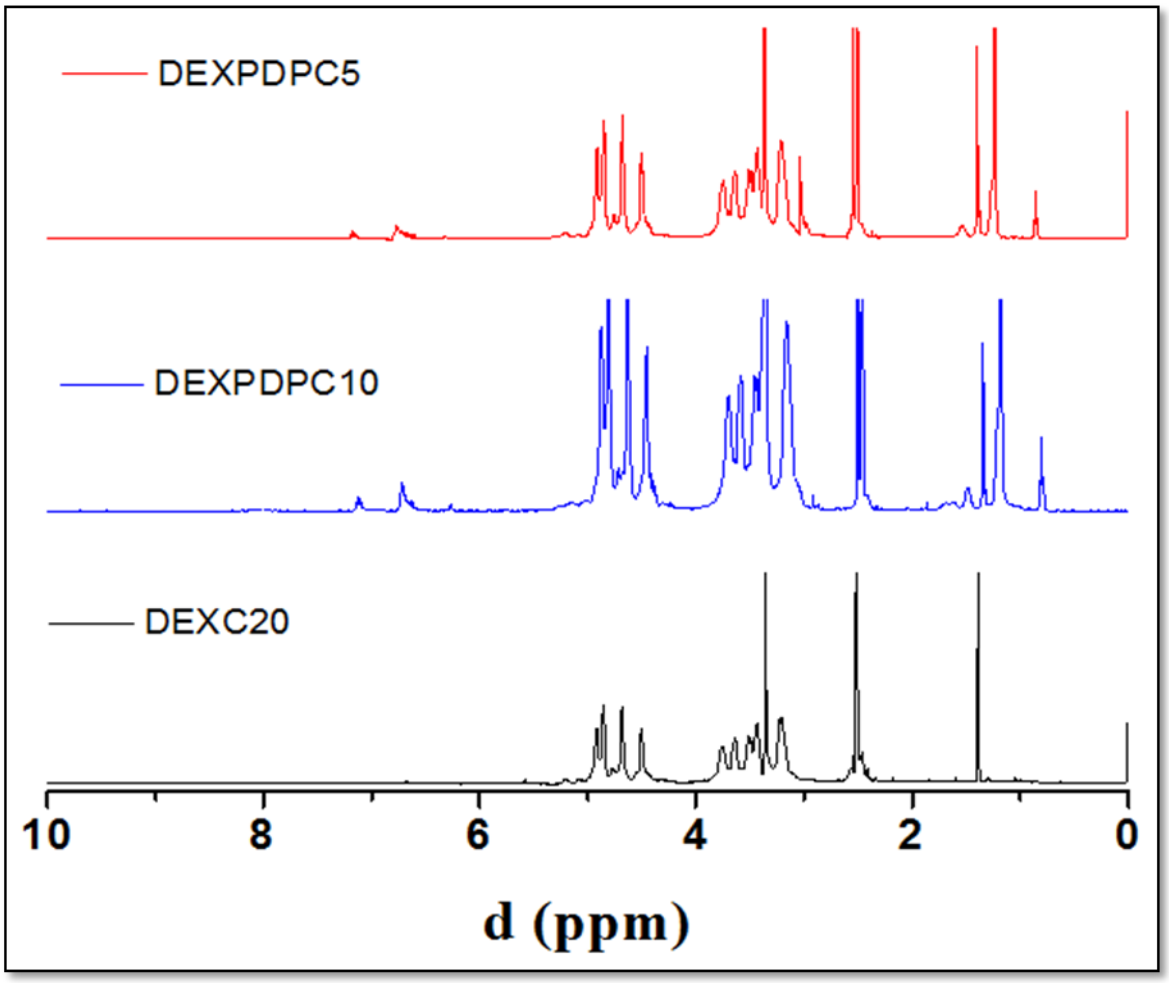

Figure 2.1: *^{1}H NMR for DEXPDPC5, DEXPDPC10, and DEXC20 protected with tertiary butyl group in DMSOd6.*

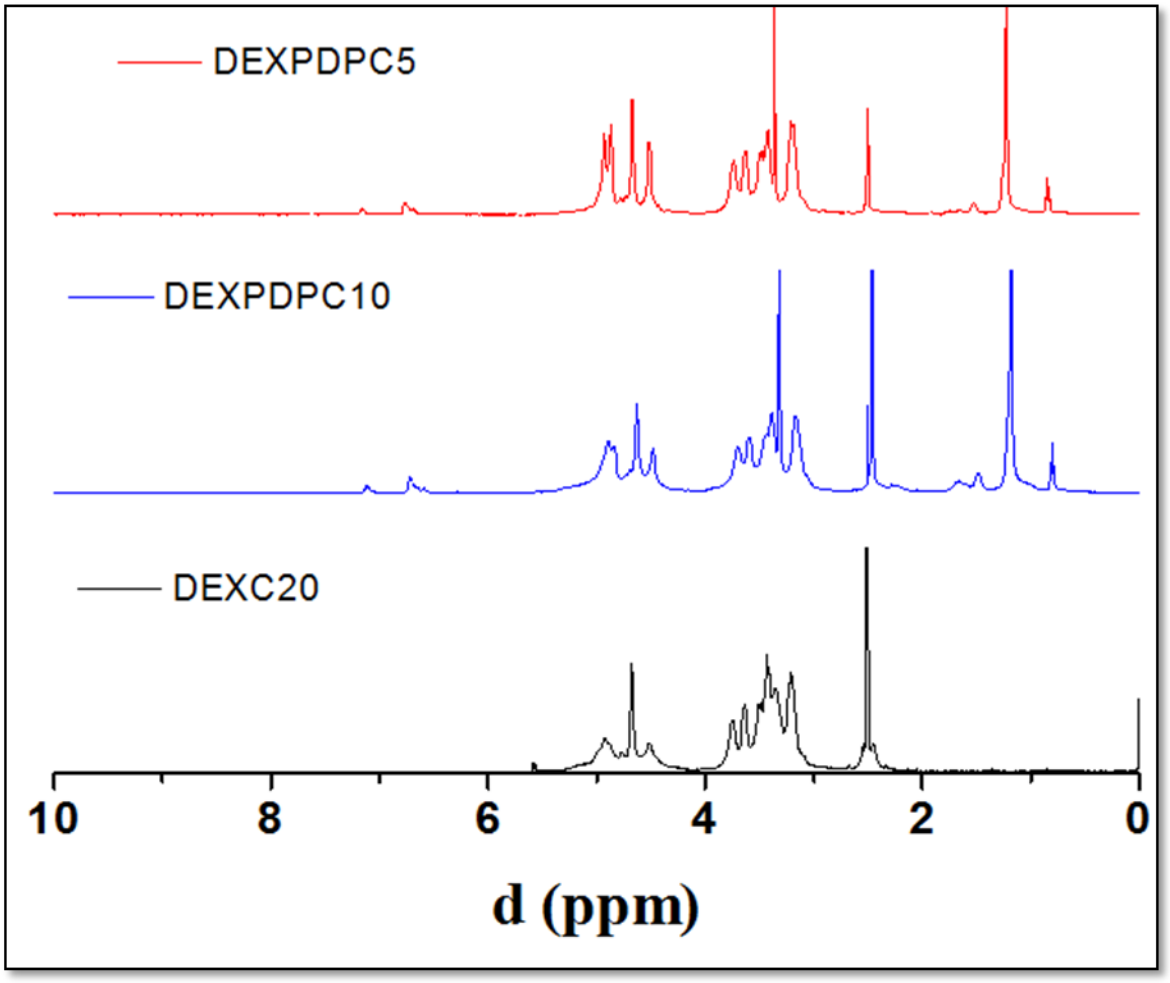

Figure 2.2: *^{1}H NMR for DEXPDPC5, DEXPDPC10 and DEXC20 in deprotected form. (Solvent: DMSOd6)*

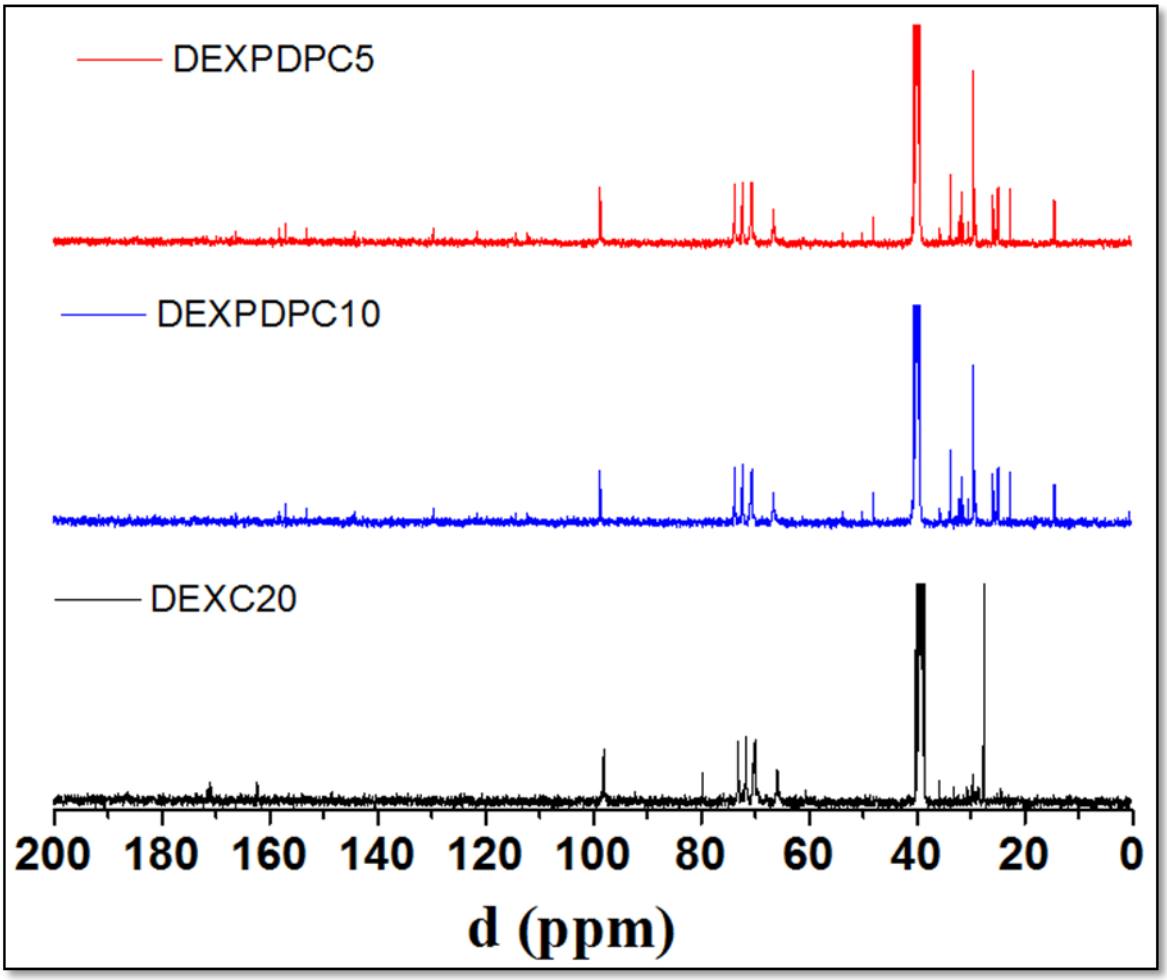

Figure 2.3: *^{13} C NMR of DEXPDPC5, DEXPDPC10 and DEXC20 having tertiary butyl group. (Solvent: DMSOd6)*

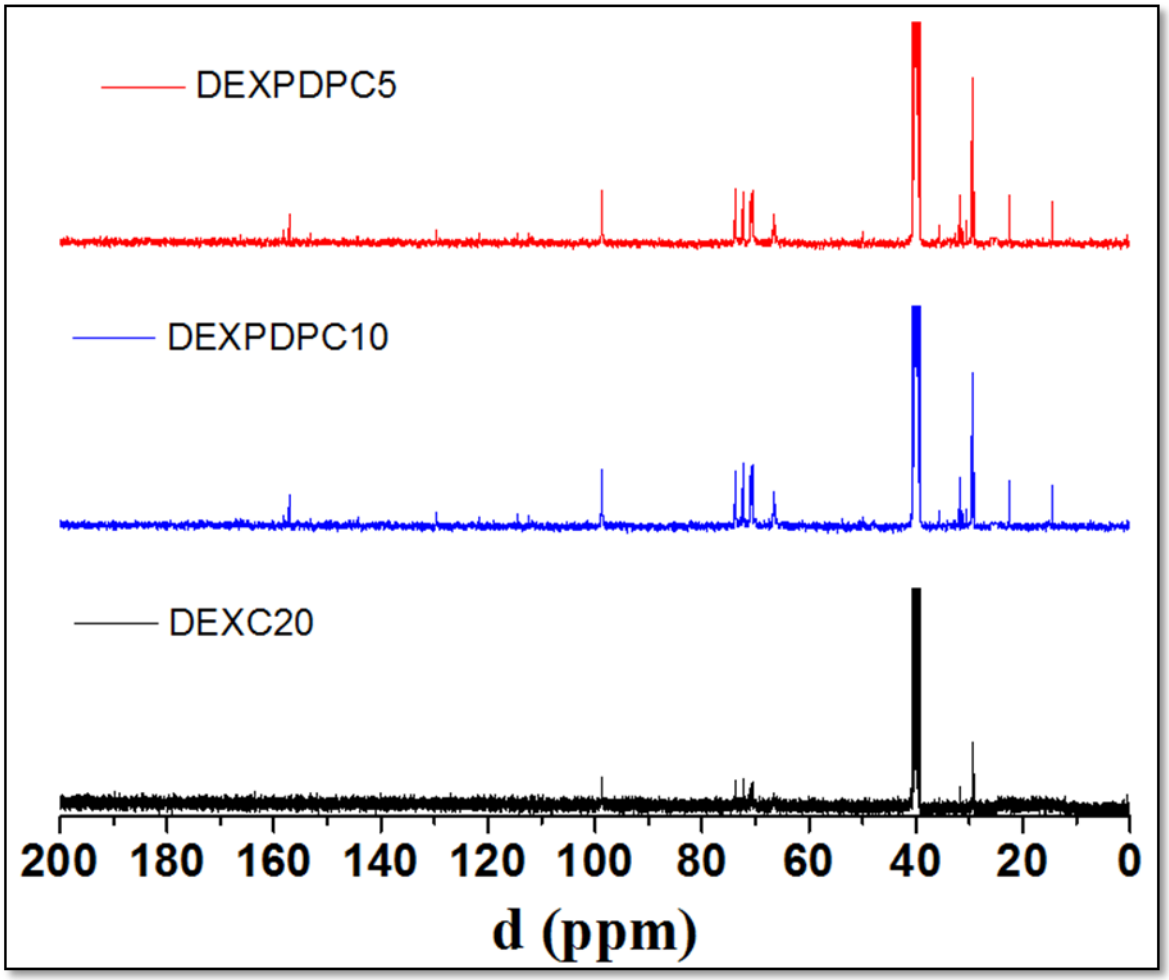

Figure 2.4: *^{13} C NMR of DEXPDPC5, DEXPDPC10 and DEXC20 in deprotected form (Solvent: DMSOd6)*

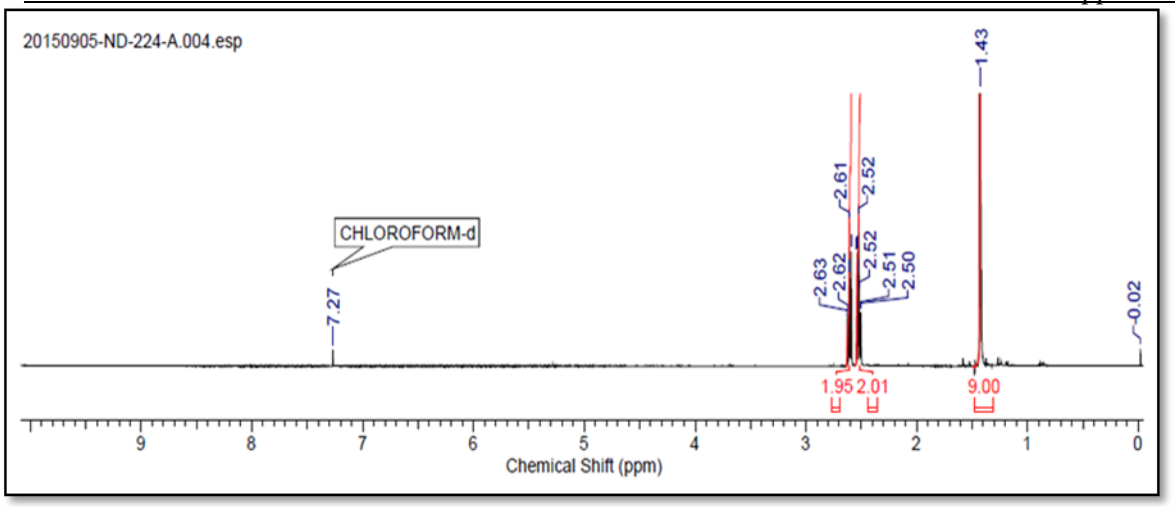

Figure 2.5: *^{1}H NMR of compound (3) 4-(tert-butoxy)-4-oxobutanoic acid (Solvent: CDCl3)*

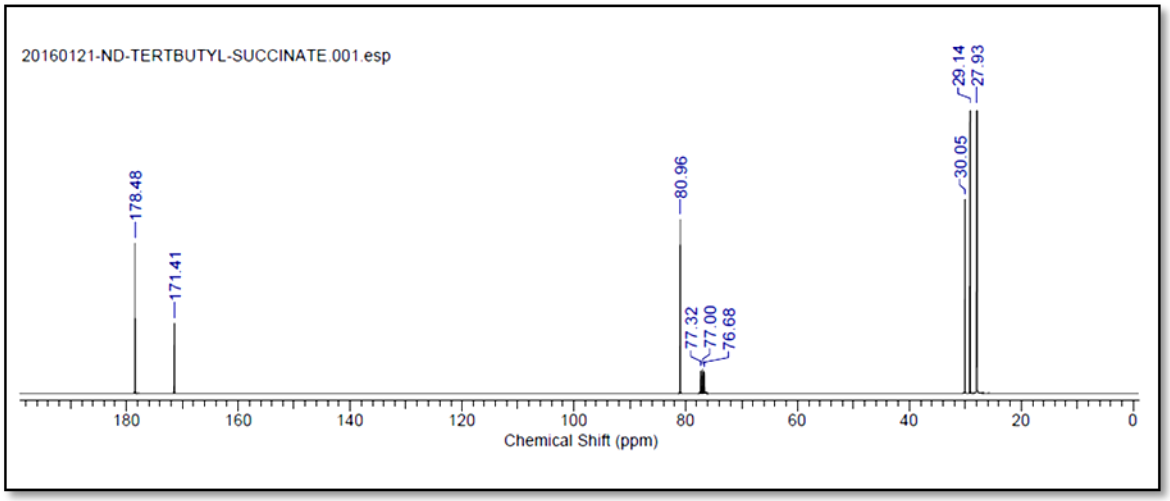

Figure 2.5 : *^{13}C NMR of compound (3) 4-(tert-butoxy)-4-oxobutanoic acid (Solvent : CDCl3)*

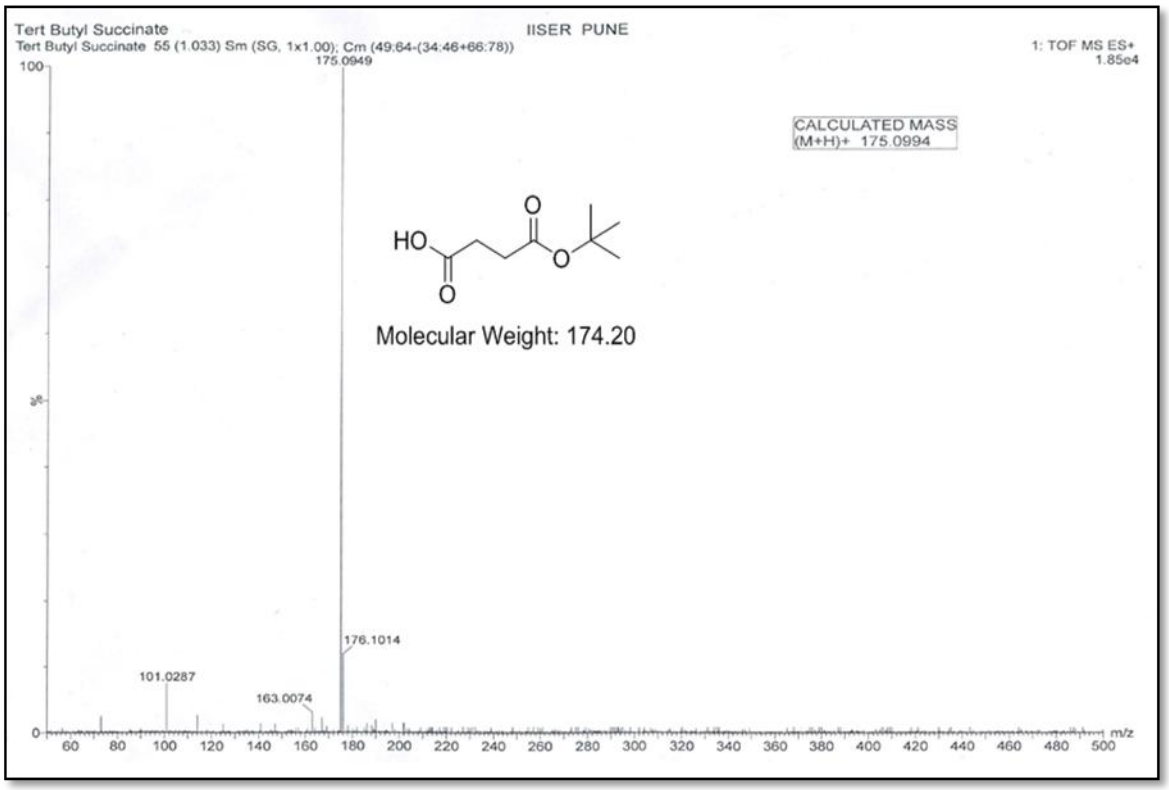

Figure 2.6: *HRMS of compound (3) 4-(tert-butoxy)-4-oxobutanoic acid*

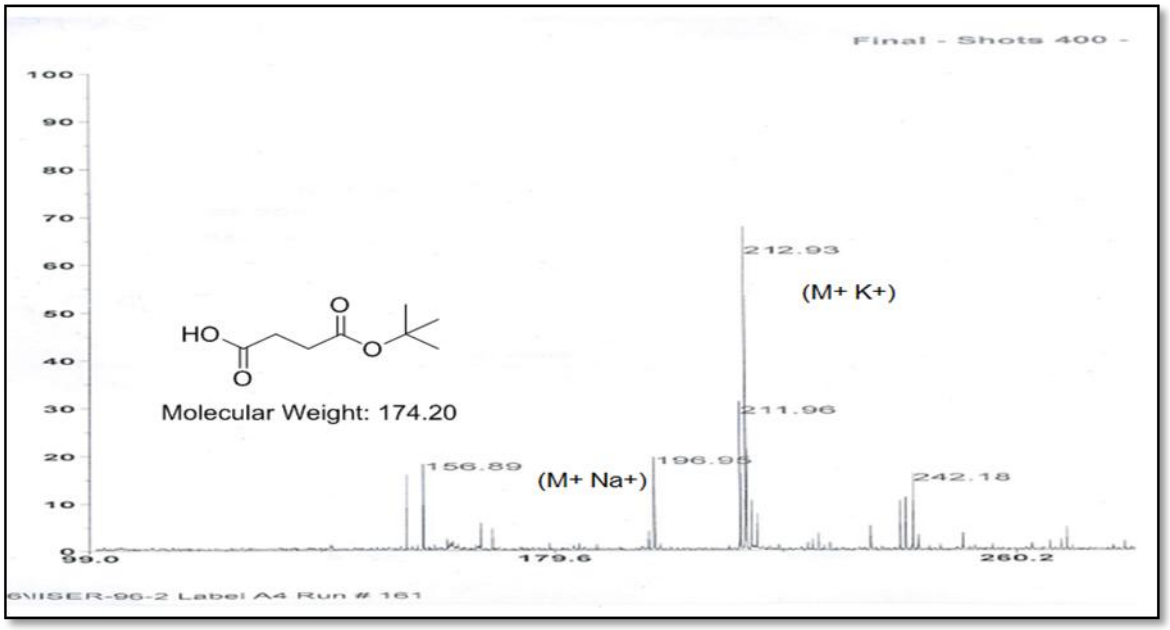

Figure 2.7: *MALDI-TOF spectrum of compound (3) 4-(tert-butoxy)-4-oxobutanoic acid*

Chapter- 3

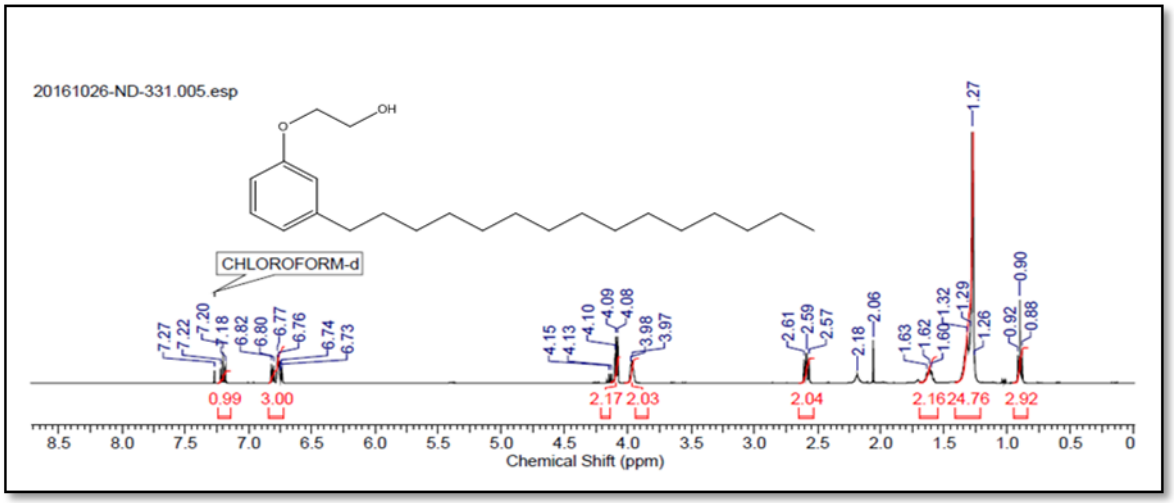

Figure 3.2: *^{1}H NMR spectrum of compound 1 in $CDCl_3$*

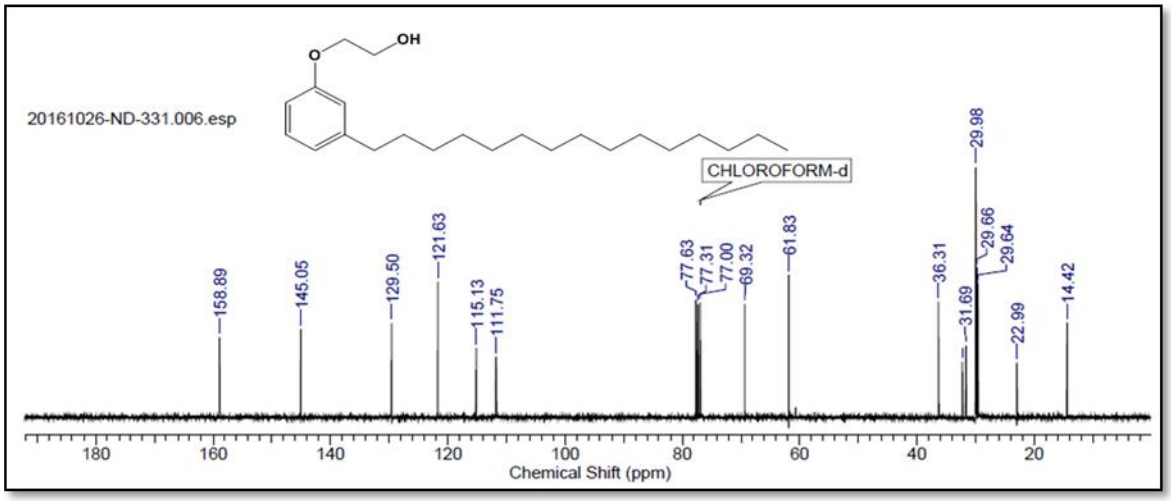

Figure 3.3: *^{13}Carbon NMR spectrum of compound 1 in $CDCl_3$*

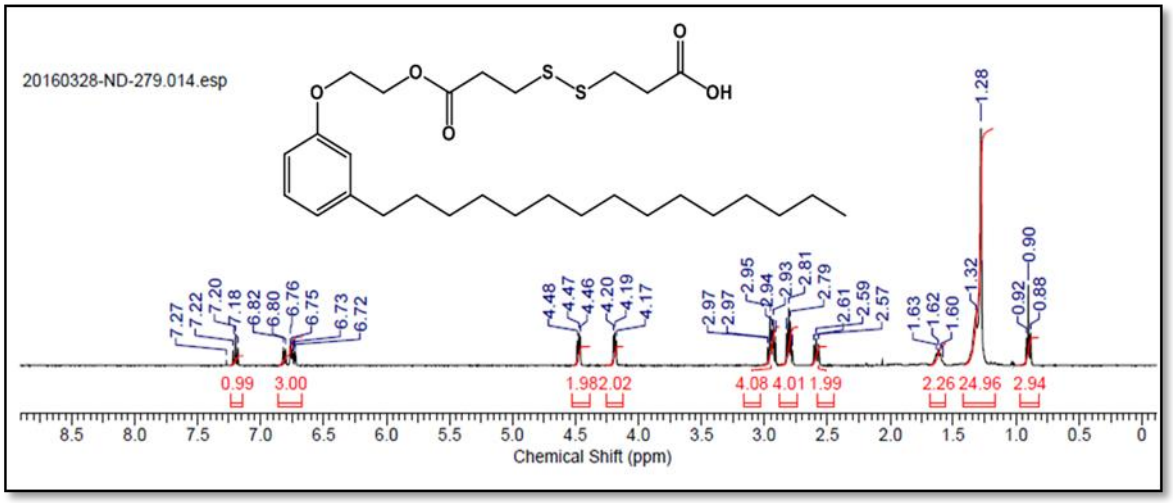

Figure 3.4: *^{1}H NMR spectrum of compound 2 (PDP-SS-Acid) in $CDCl_3$*

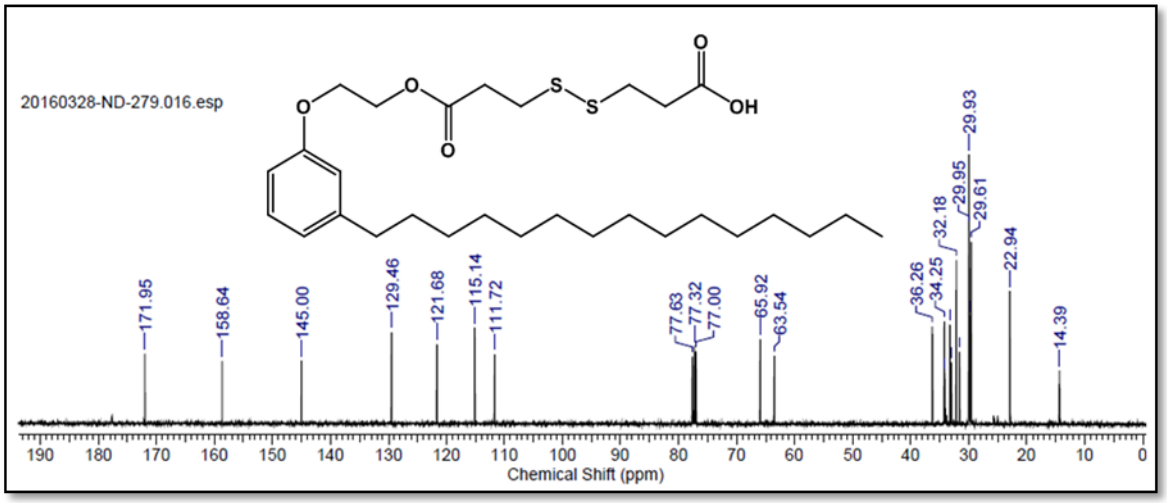

Figure 3.5: *^{13}Carbon NMR spectrum of compound 2 (PDP-SS-Acid)in $CDCl_3$*

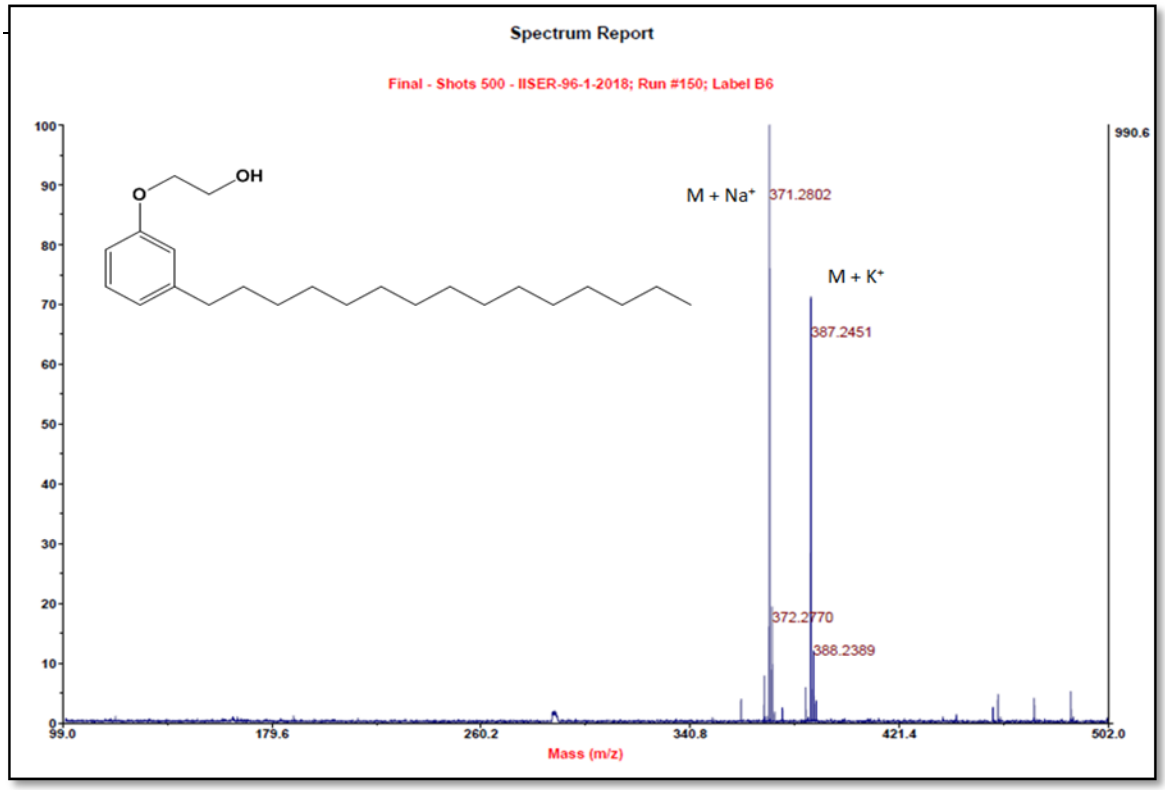

Figure 3.5: *MALDI-TOF spectrum of compound 1*

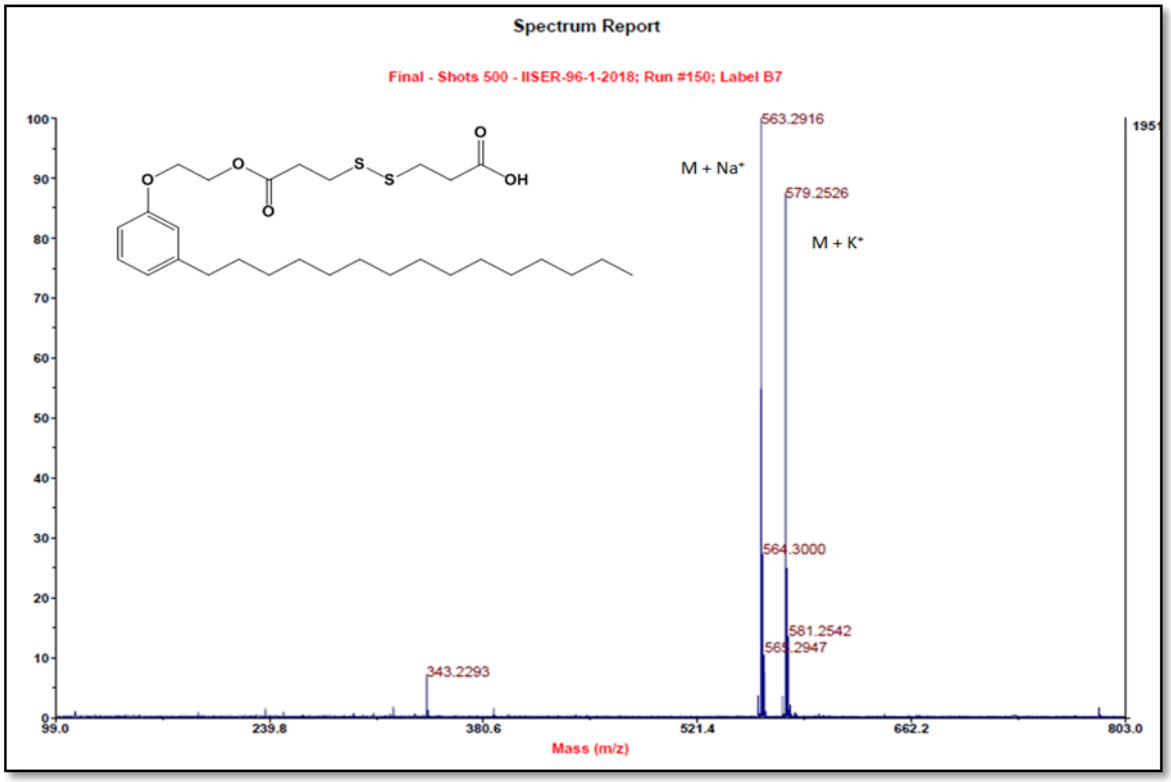

Figure 3.6: *MALDI-TOF Spectrum of compound 2 (PDP-SS-Acid)*

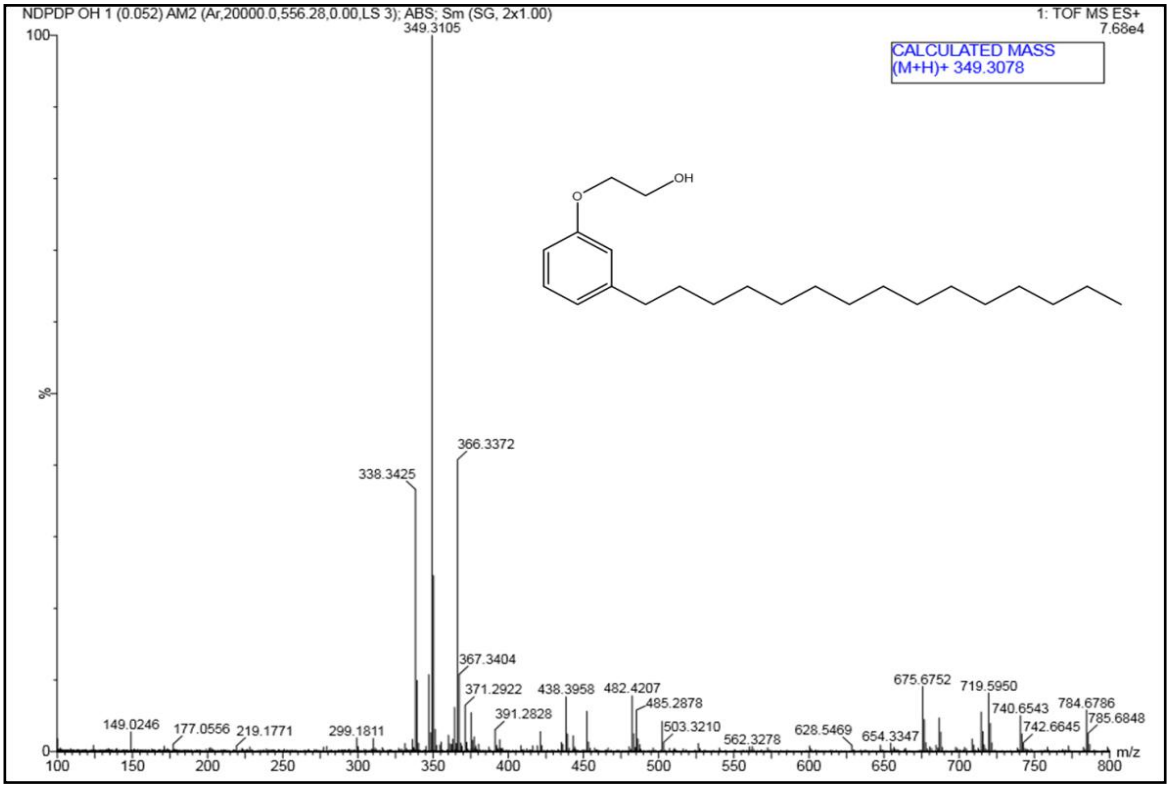

Figure 3.7: *HRMS spectrum of compound 1*

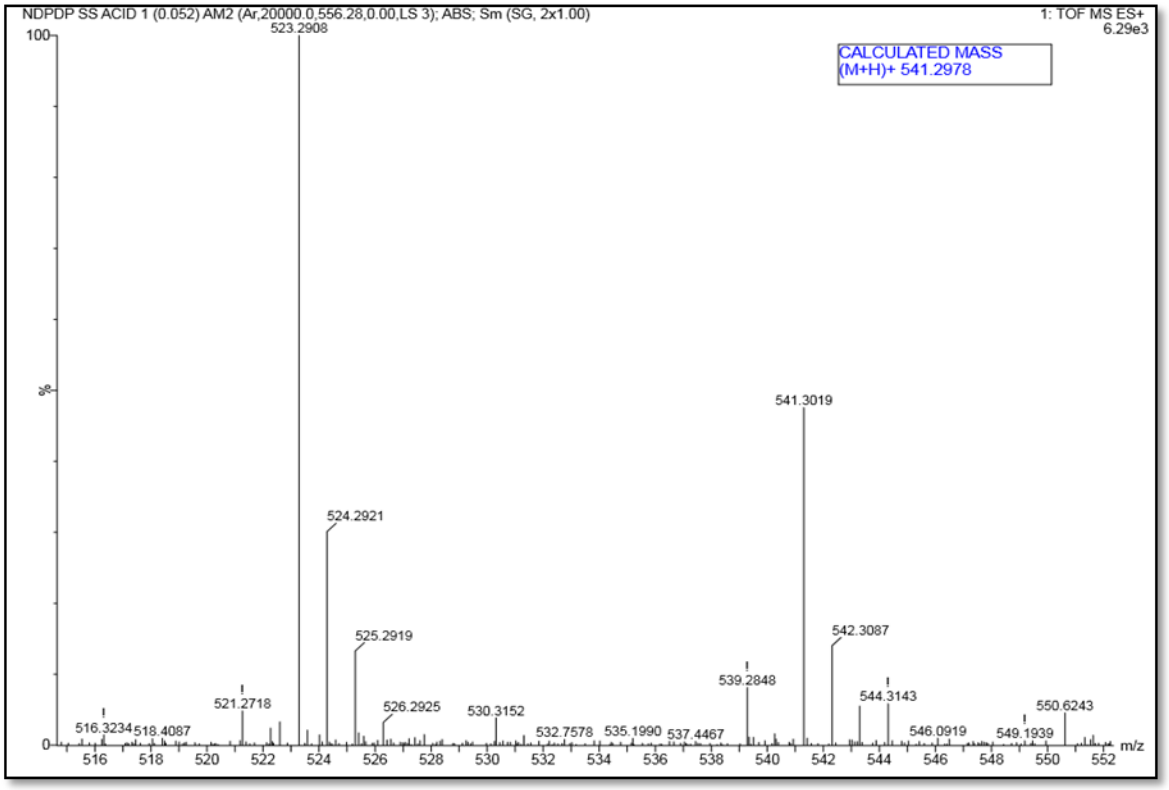

Figure 3.8: *HRMS spectrum of compound 2 (PDP-SS-Acid)*

Chapter-4

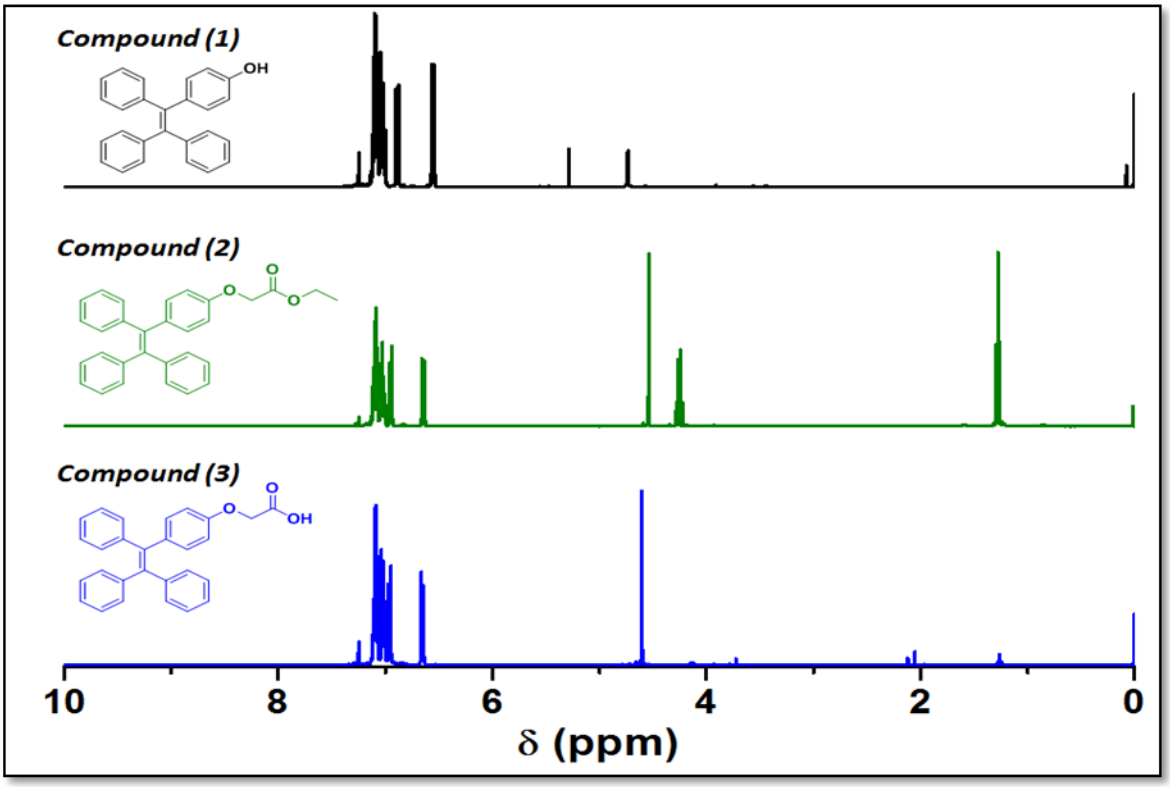

Figure 4.1: *^{1}H NMR for Compound (1), (2) and (3)*

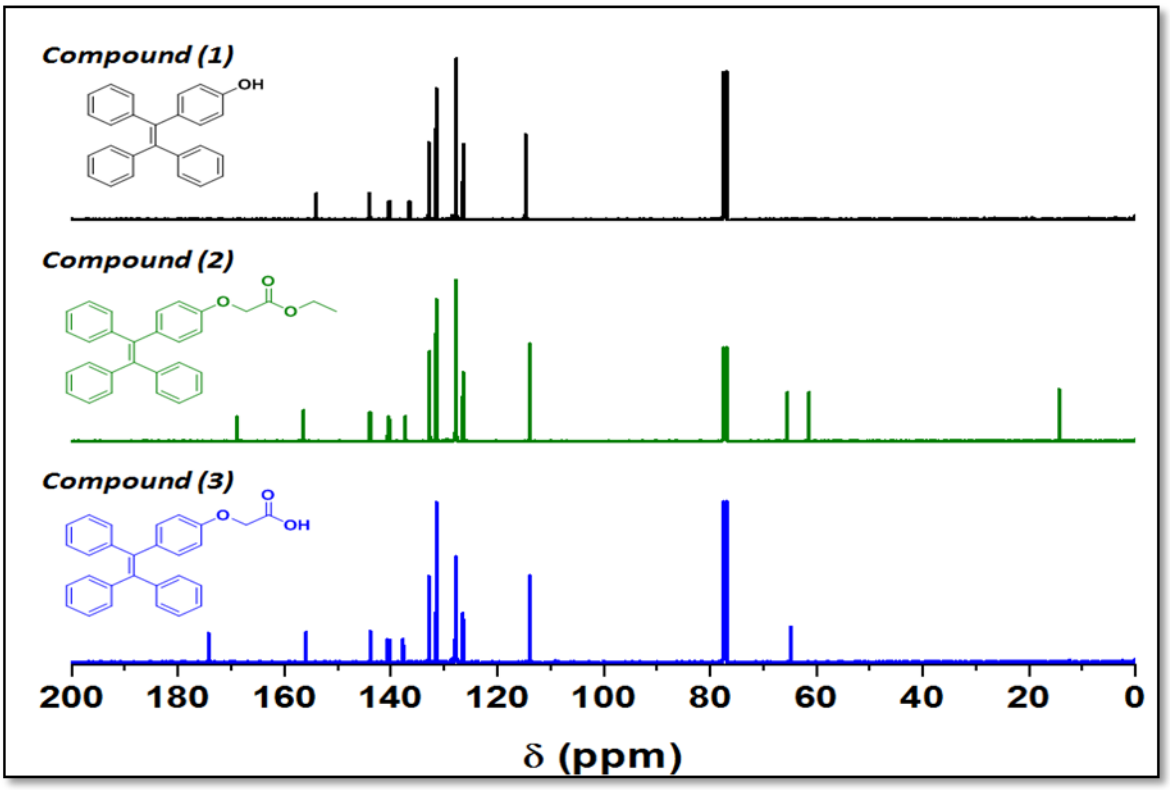

Figure 4.2: *^{13}C NMR for Compound (1), (2) and (3)*

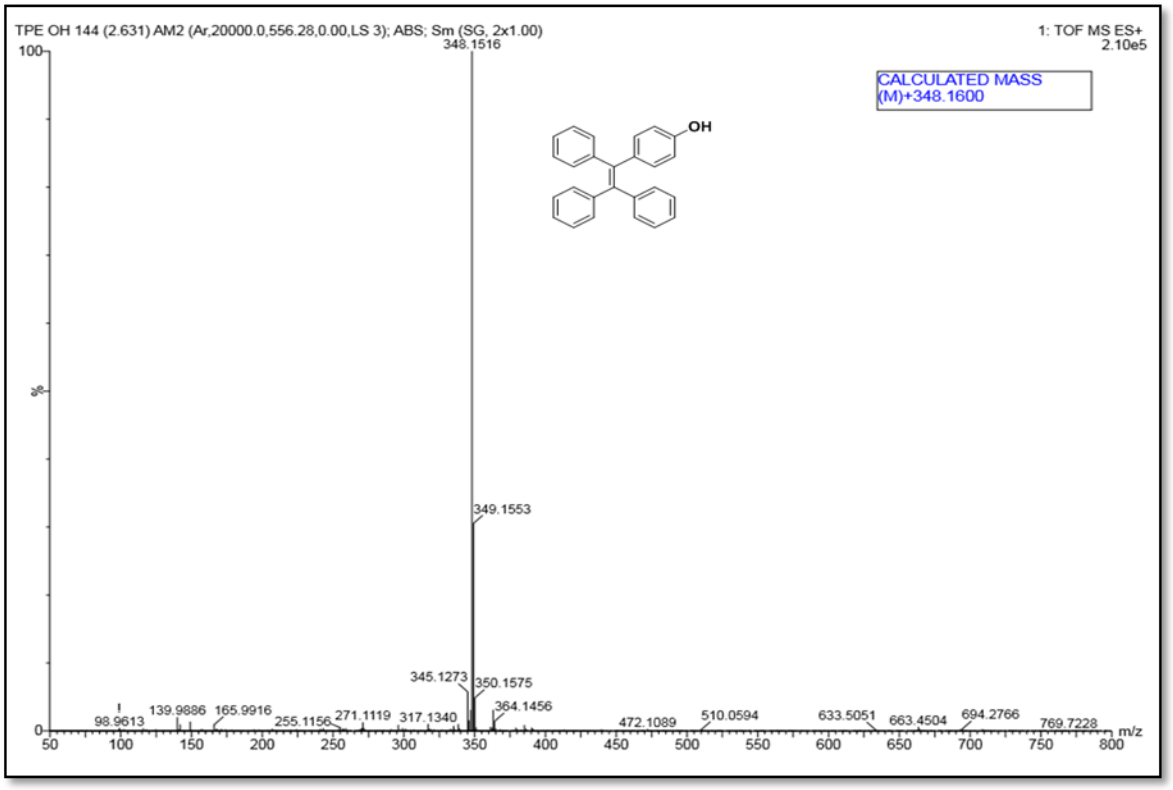

Figure 4.3: *HRMS for Compound (1)*

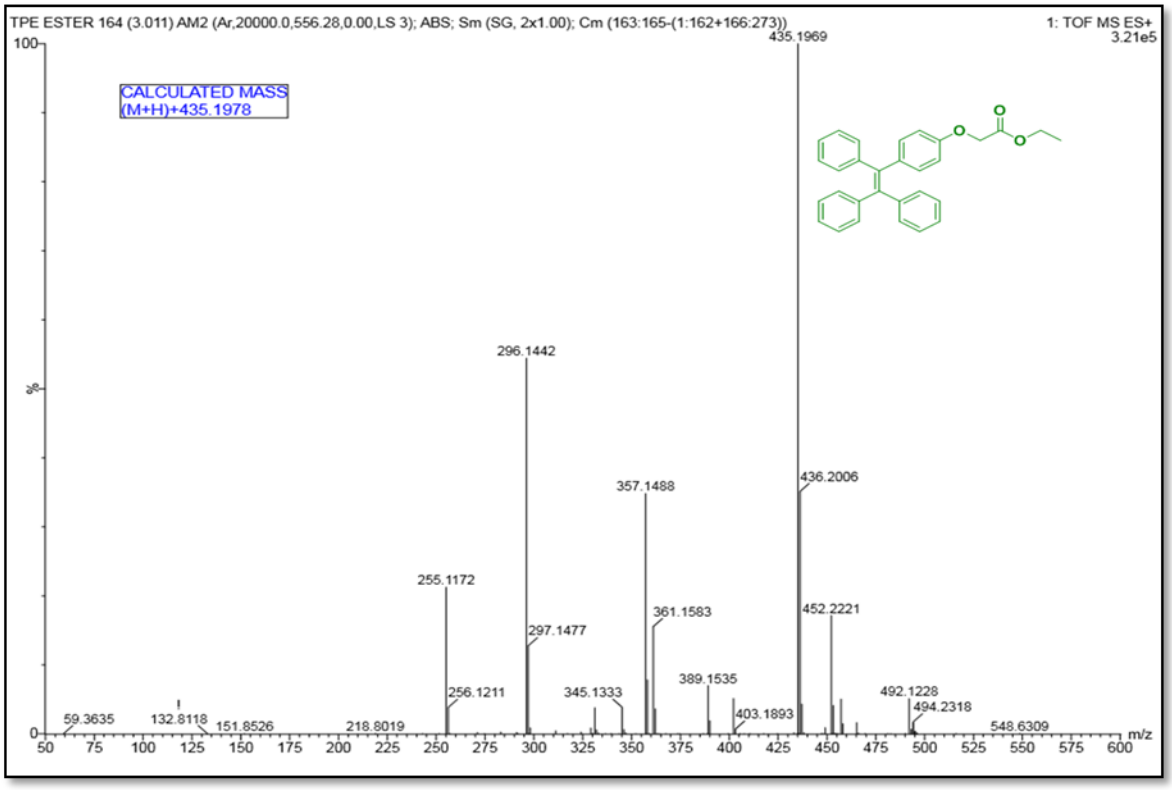

Figure 4.4: *HRMS for Compound (2)*

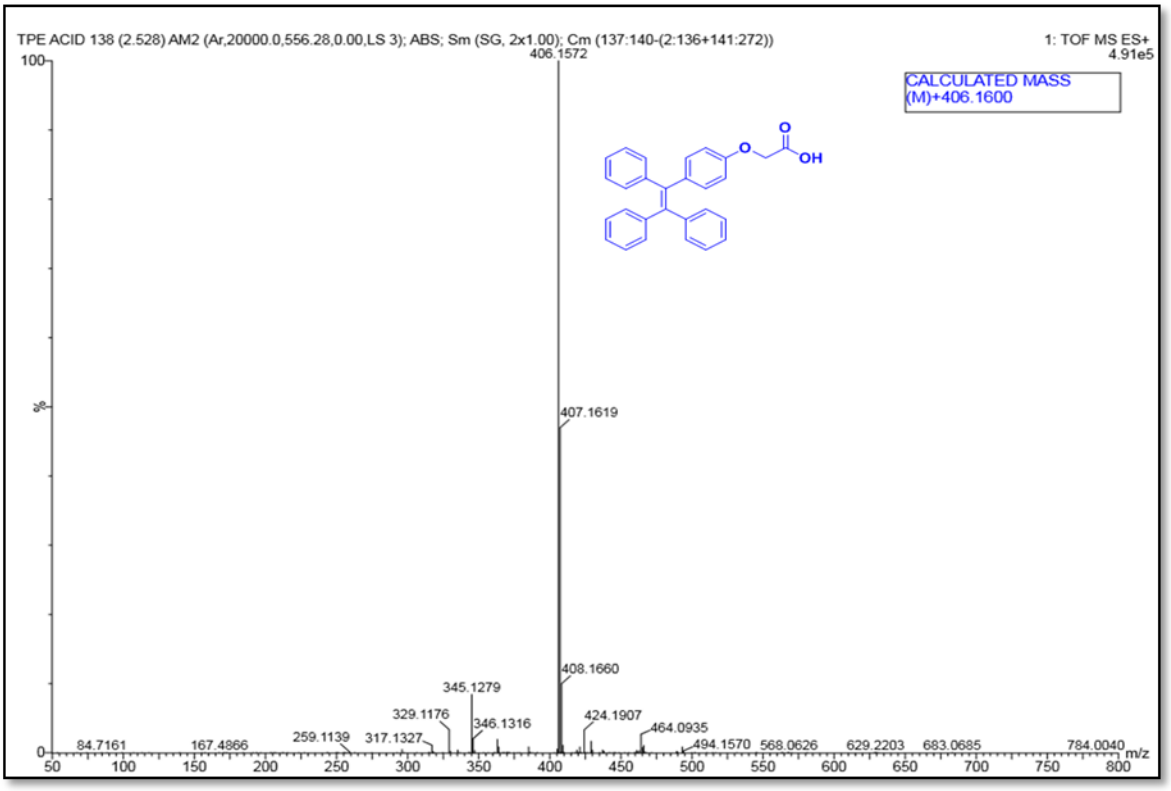

Figure 4.5: *HRMS for Compound (3)*

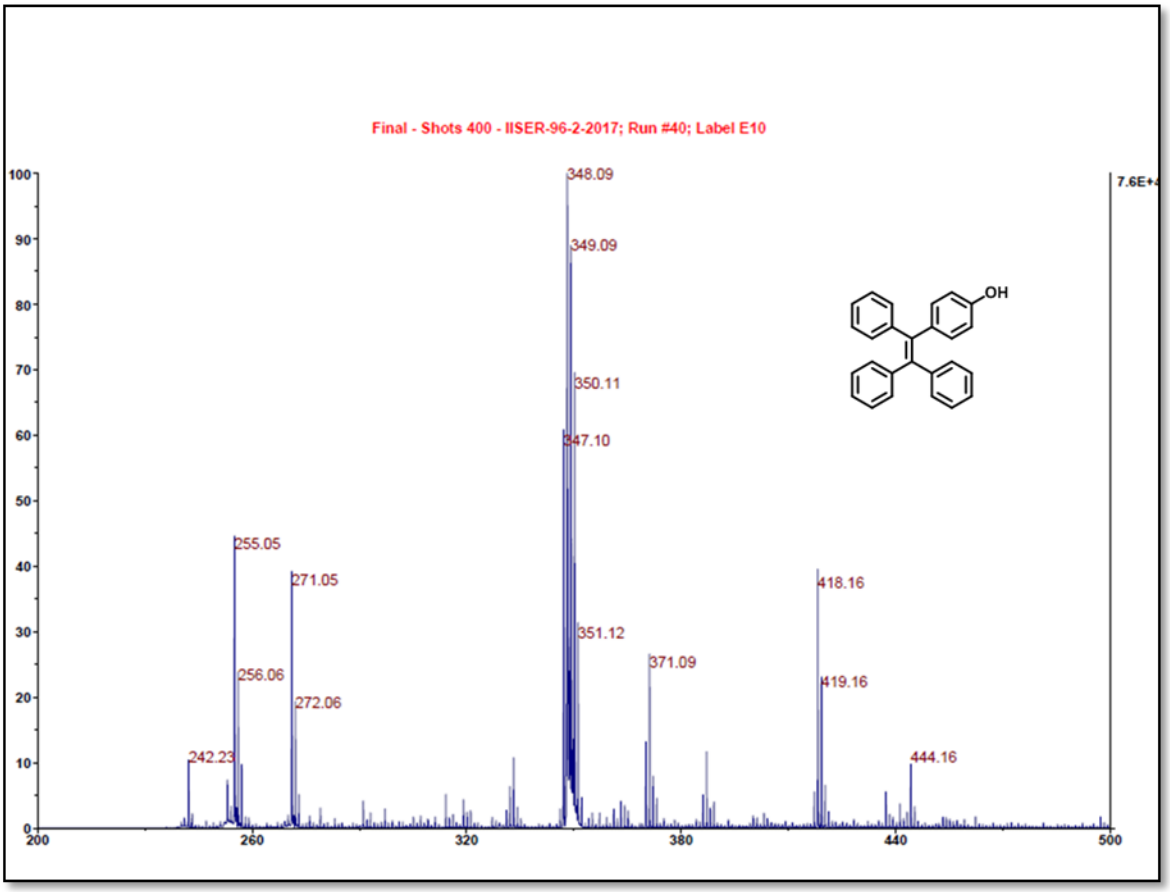

Figure 4.6: *MALDI-TOF spectrum of compound 1 (TPE-OH)*

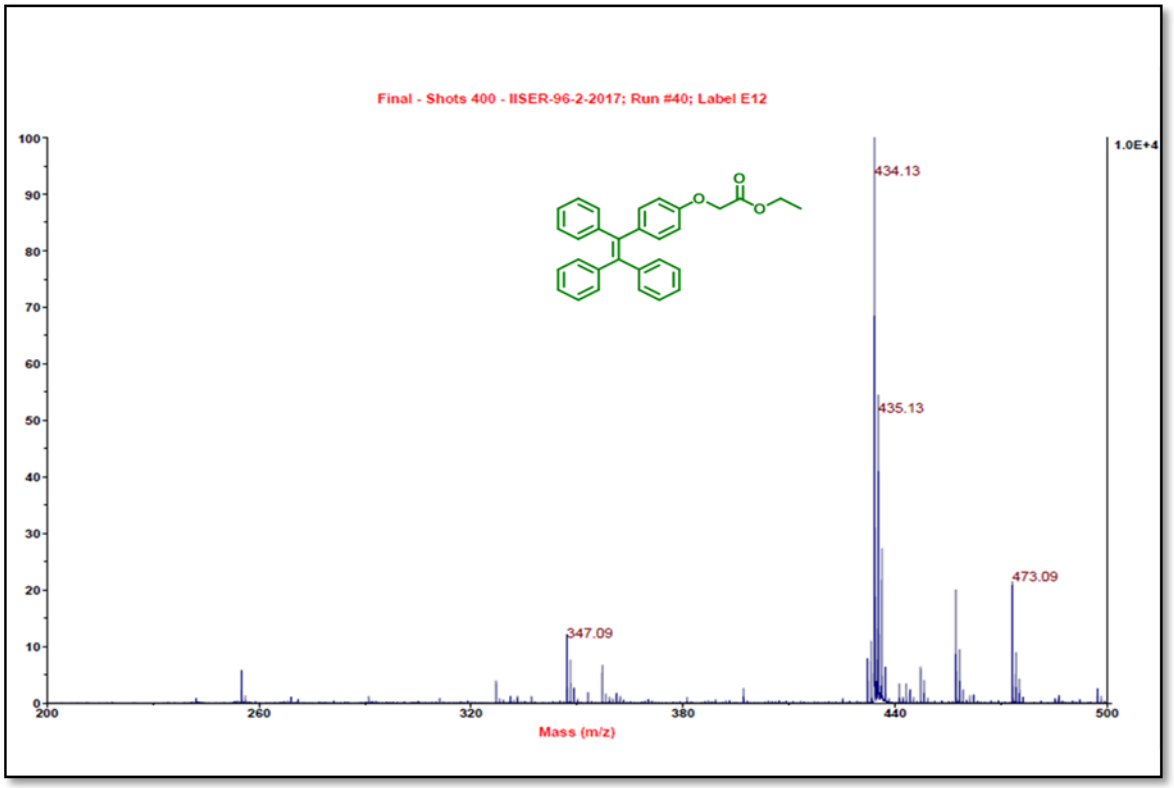

Figure 4.7: *MALDI-TOF spectrum of compound 2 (TPE-Ester)*

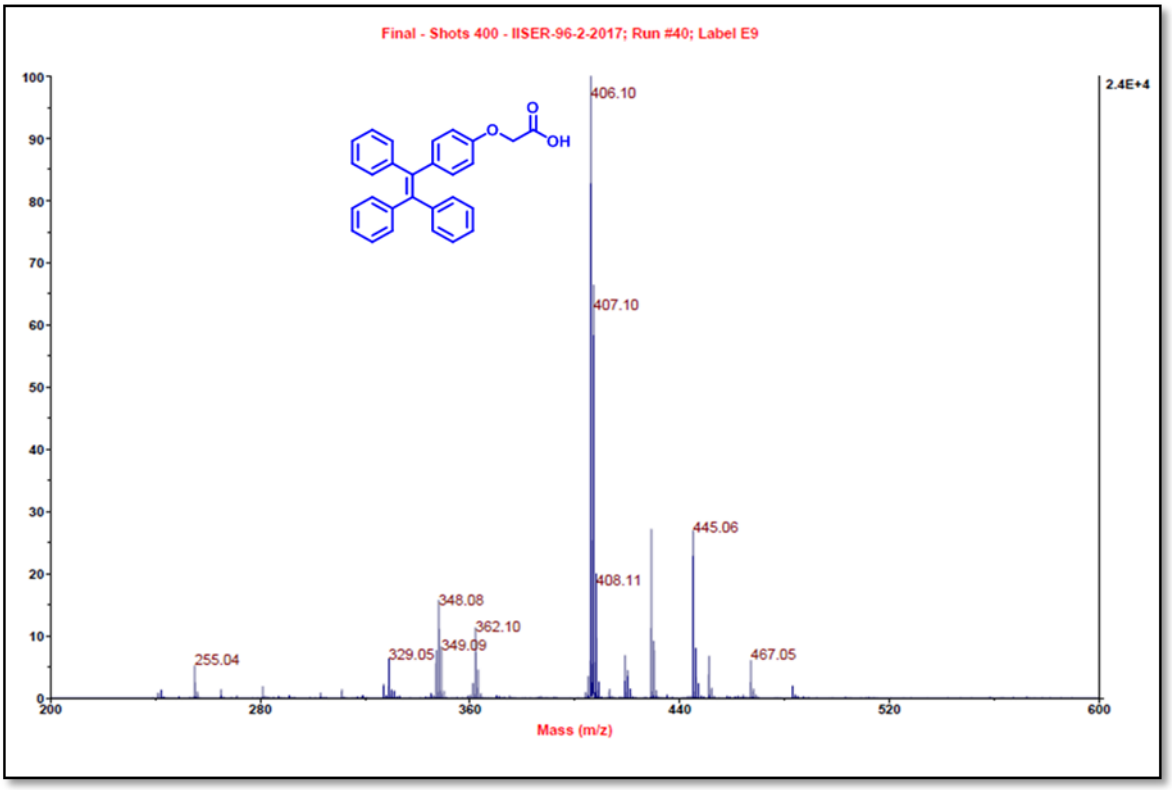

Figure 4.8: *MALDI-TOF spectrum of compound 3 (TPE-Acid)*